

INFORMATION TO USERS

This manuscript has been reproduced from the microfilm master. UMI films the text directly from the original or copy submitted. Thus, some thesis and dissertation copies are in typewriter face, while others may be from any type of computer printer.

The quality of this reproduction is dependent upon the quality of the copy submitted. Broken or indistinct print, colored or poor quality illustrations and photographs, print bleedthrough, substandard margins, and improper alignment can adversely affect reproduction.

In the unlikely event that the author did not send UMI a complete manuscript and there are missing pages, these will be noted. Also, if unauthorized copyright material had to be removed, a note will indicate the deletion.

Oversize materials (e.g., maps, drawings, charts) are reproduced by sectioning the original, beginning at the upper left-hand corner and continuing from left to right in equal sections with small overlaps.

Photographs included in the original manuscript have been reproduced xerographically in this copy. Higher quality 6" x 9" black and white photographic prints are available for any photographs or illustrations appearing in this copy for an additional charge. Contact UMI directly to order.

Bell & Howell Information and Learning
300 North Zeeb Road, Ann Arbor, MI 48106-1346 USA

UMI[®]
800-521-0600

UNIVERSITY OF OKLAHOMA
GRADUATE COLLEGE

A COUPLED MODEL FOR THE
PREDICTION OF FLUID AND RESERVOIR PROPERTIES FROM
MINIFRAC TESTS

A Dissertation
SUBMITTED TO THE GRADUATE FACULTY
in partial fulfillment of the requirements for the
degree of
Doctor of Philosophy

By
Ion N. Ispas
Norman, Oklahoma
1999

UMI Number: 9949712

UMI[®]

UMI Microform 9949712

Copyright 2000 by Bell & Howell Information and Learning Company.

All rights reserved. This microform edition is protected against
unauthorized copying under Title 17, United States Code.

Bell & Howell Information and Learning Company
300 North Zeeb Road
P.O. Box 1346
Ann Arbor, MI 48106-1346

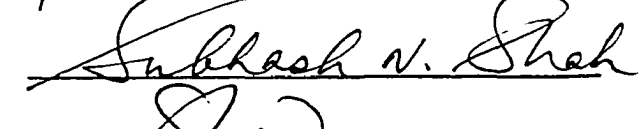
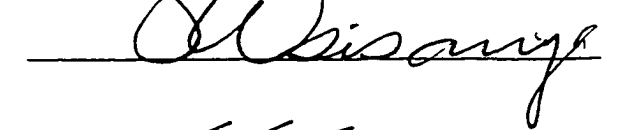
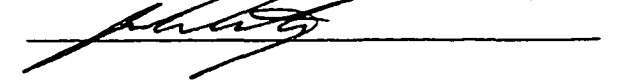
c Copyright by Ion N. Ispas 1999
All rights reserved

A COUPLED MODEL FOR THE
PREDICTION OF FLUID AND RESERVOIR PROPERTIES FROM
MINIFRAC TESTS

A Dissertation APPROVED FOR THE
SCHOOL OF PETROLEUM AND GEOLOGICAL ENGINEERING

BY



Subhash V. Shah




ACKNOWLEDGMENTS

Despite the fact that time is irreversible, there are occasions when certain events repeat in our lives, and thus changing their note of uniqueness. First of all I wish, with the occasion of this unique event in my life, to thank God from the bottom of my heart for His constant help and guidance. I also consider this a unique opportunity to express my sincere appreciation for each of the faculty members who has served on my committee and shared, in a professional manner, their expertise. For Dr. Djebbar Tiab, who, as a mentor and professor, has been the motivating force, and the main guide and advisor of my graduate study during the past five years. He has taught me to visualize the essence of research, problem solving, and teaching. For Dr. Subhash Shah, who exemplifies the fine years of experience. For Dr. Anuj Gupta who taught me the insights of formation evaluation and advanced reservoir engineering. For Dr. Samuel Osisanya who has been my first guide through the science of horizontal drilling technology. For Dr. John P. Castagna who led my steps through the fascinating teachings provided by reservoir characterization, AVO analysis, and seismic petrophysics.

I would also like to express my gratitude to the Department of Petroleum and Geological Engineering for their financial support which made my graduate study possible.

A very profound “Thank You” to my wife, Vilia, who stand by me all these years, and who through her patience and understanding was always a source of strength and optimism for me. I am also very thankful to my children, Adina Loredana, and Larisa who, with their lovely smiles and sincere hearts, are the joy of

my life. And finally, I thank my mother Mrs. Silvia Ispas and dedicate this work to the memory of my father, Mr. Nicolae S. Ispas.

TABLE OF CONTENTS

	Page
Acknowledgments.....	IV
Table of contents.....	VI
List of tables.....	X
List of figures.....	XII
Abstract.....	XVI
CHAPTER 1 - INTRODUCTION	1
1.1 Calibration treatments.....	1
1.2 Research objectives.....	9
CHAPTER 2 - CRITICAL REVIEW OF MINIFRAC MODELS.....	11
CHAPTER 3 - HYDRAULIC FRACTURING – THEORETICAL ASPECTS.....	56
3.1 Mechanics of fracturing.....	56
3.2 Fluid pressure profile.....	60
3.3 Constant height fracture models.....	62
CHAPTER 4	
A COUPLED MODEL FOR THE PREDICTION OF FLUID AND RESERVOIR PROPERTIES FROM MINIFRAC TESTS.....	70
4.1 Introduction	70
4.2 Fracturing fluid coefficient - Carter’s leak-off model.....	70
4.3 Improved pressure decline model (Pw-II)	84

4.4 Non-Newtonian behavior of the fracturing fluid.....	89
4.4.1 Fracture width equations for the basic 2D fracture geometries...	89
4.4.1.1 PKN width equation.....	91
4.4.1.2 KGD width equation.....	93
4.4.1.3 Radial width equation.....	93
4.4.2 Equivalent Newtonian viscosity.....	94
4.4.2.1 Modified maximum fracture width – PKN geometry.....	94
4.4.2.2 Modified maximum fracture width – KGD geometry.....	95
4.4.2.3 Modified maximum fracture width – Radial geometry.....	96
4.5 Spurt loss estimation.....	97
4.5.1 Material balance approach.....	98
4.5.1.1 Spurt loss approximation – PKN geometry.....	98
4.5.1.2 Spurt loss approximation – KGD geometry.....	99
4.5.1.3 Spurt loss approximation – Radial geometry.....	100
4.5.2 Laboratory measurements.....	101
4.5.3 Spurt loss from synergy analysis.....	103
4.5.4 Fracture half-length determination as a function of spurt loss – PKN.....	105
4.5.5 Fracture half-length determination as a function of spurt loss – KGD.....	105
4.5.6 Fracture half-length determination as a function of spurt loss – Radial.....	105

4.5.7 Spurt loss estimation by the use of a high pressure simulator	107
4.5.8 Spurt loss from empirical correlations	107
4.6 Pressure derivative model.....	108
4.7 Filtercake–reservoir flow leak-off model.....	110
CHAPTER 5 - METHODOLOGY AND COMPUTER PROGRAM	123
5.1 Methodology.....	123
5.1.1 PKN geometry.....	125
5.1.2 KGD geometry.....	128
5.1.3 Radial geometry.....	131
5.2 Computer program for the coupled model.....	133
CHAPTER 6 - APPLICATIONS AND SENSITIVITY ANALYSIS	136
6.1 Applications.....	136
6.1.1 Case M1.....	136
6.1.2 Case M2.....	141
6.1.3 Case M3.....	146
6.1.4 Case M4.....	151
6.1.5 Case M5.....	157
6.2 Sensitivity analysis.....	168
CHAPTER 7 - CONCLUSIONS AND RECOMMENDATIONS.....	170
7.1 Conclusions.....	170
7.2 Recommendations.....	172

Nomenclature.....	178
References.....	182
Appendix A.....	191
Modeling equations (pressure decline analysis).....	192
Appendix B.....	206
Modeling equations (Filter-cake – reservoir flow leak-off transient analysis).....	207
Appendix C.....	216
Applications-input and output data.....	217
Appendix D.....	284
Sensitivity analysis.....	285
Appendix E.....	289
Program flow - chart.....	290

LIST OF TABLES

Table	Page
Table C-1A - Input parameters - case M1.....	217
Table C-1B Fall off time - pressure data - case M1.....	218
Table C-1C G-function and diagnostic functions - case M1.....	221
Table C-1D Net pressure during injection - case M1.....	222
Table C-1E Synthesis of computed fluid and reservoir properties - case M1.....	222
Table C-2A - Input parameters - case M2.....	223
Table C-2B Fall off time - pressure data - case M2.....	224
Table C-2C G-function and diagnostic functions - case M2.....	226
Table C-2D Net pressure during injection - case M2.....	228
Table C-2E Synthesis of computed fluid and reservoir properties - case M2.....	230
Table C-3A - Input parameters - case M3.....	231
Table C-3B Fall off time - pressure data - case M3.....	232
Table C-3C G-function and diagnostic functions - case M3.....	239
Table C-3D Net pressure during injection - case M3.....	243
Table C-3E Synthesis of computed fluid and reservoir properties - case M3.....	245
Table C-4A - Input parameters - case M4.....	246
Table C-4B Fall off time - pressure data - case M4.....	247
Table C-4C G-function and diagnostic functions - case M4.....	248
Table C-4D Pressure derivative data – case M4.....	248

Table C-4E Synthesis of computed fluid and reservoir properties - case M4....	249
Table C-5A - Input parameters - case M5.....	250
Table C-5B Fall off time - pressure data - case M5.....	251
Table C-5C G-function and diagnostic functions - case M5.....	255
Table C-5D Net pressure during injection - case M5.....	258
Table C-5E Synthesis of computed fluid and reservoir properties - case M5....	259
Table C-5F Synthesis and comparison of computed fluid and reservoir properties by the old and new model – All cases.....	259
Table C-5G Evaluation of the leak-off coefficient obtained from pressure and Pressure derivative analysis.....	277

LIST OF FIGURES

Figure	Page
Fig. 1.1 Diagnostic from pressure decline data - Net pressure versus time.....	5
Fig. 1.2 Decline analysis- Net pressure versus	7
Fig. 1.3 Net pressure versus G-function	8
Fig. 2.1 – Schematic of fracture models.....	42
Fig. 2.2 - Schematic for areas and times used in derivations.....	43
Fig. 2.3 – Fluid efficiency from closure time.....	44
Fig. 2.4 – Pressure and flow in fracture for shut-in.....	45
Fig. 2.5 – Bottomhole pressure versus time.....	46
Fig. 2.6 – Illustration of fracture evolution as a family of confocal ellipses.....	46
Fig. 2.7 - Two dimensional fracture of unit height.....	47
Fig. 2.8 - G-function derivative plot.....	48
Fig. 2.9 - Pressure function derivative plot.....	49
Fig. 2.10 - Excess wellbore pressure vs GL function for stress contrast.....	50
Fig. 2.11 – Bottomhole pressure vs. square root of time, and time.....	51
Fig. 2.12 - Specialized plot.....	52
Fig. 2.13 - Effect of permeability on fluid leak-off.....	53
Fig. 2.14 – Plot for the determination of reservoir permeability.....	54
Fig. 2.15 – Plot for the determination of reservoir permeability.....	55
Fig. 3.1 – Horizontal section of a vertical wellbore under the action of in-	

situ stresses and hole pressure	63
Fig. 3.2 – Normal stress at fracture tip.....	64
Fig. 3.3 – Pore pressure profile (left) and elliptic coordinates (right).....	64
Fig. 3.4 - Downhole pressure profile.....	65
Fig. 3.5 - KGD constant height fracture model.....	66
Fig. 3.6 – The PKN constant height fracture model.....	67
Fig. 3.7 – Circular fracture with dry zone.....	68
Fig. 3.8 – Radial geometry- ratio of permeable to total surface area.....	69
Fig. 4.1 – Fluid loss characteristics.....	102
Fig. C-1 Injection and fall-off of a minifrac - case M1.....	260
Fig. C-2 Identification of closure from the fall-off of a minifrac - case M1.....	260
Fig. C-3 Net pressure versus time – case M1.....	261
Fig. C-4 G-function of a minifrac test – case M1.....	261
Fig. C-5 Filter cake –reservoir flow diagnostic plot – case M1.....	262
Fig. C-6 Injection and fall-off of a minifrac - case M2.....	262
Fig. C-7 Identification of closure from the fall-off of a minifrac - case M2.....	263
Fig. C-8 Net pressure versus time – case M2.....	263
Fig. C-9 G-function of a minifrac test – case M2.....	264
Fig. C-10 Filter cake –reservoir flow diagnostic plot – case M2.....	264
Fig. C-11 Injection and fall-off of a minifrac - case M3.....	265
Fig. C-12 Identification of closure from the fall-off of a minifrac - case M3...	265
Fig. C-13 Net pressure versus time – case M3.....	266

Fig. C-14 G-function of a minifrac test – case M3.....	266
Fig. C-15 Filter cake –reservoir flow diagnostic plot (significant noise)– case M3.....	267
Fig. C-16 Filter cake –reservoir flow diagnostic plot (data filtering)– case M3.....	267
Fig. C-17 Filter cake –reservoir flow diagnostic plot (after data filtering)– case M3.....	268
Fig. C-18 Fall-off of a minifrac test - case M4.....	268
Fig. C-19 Identification of closure from the fall-off of a minifrac - case M4...	269
Fig. C-20 G-function of a minifrac test - case M4.....	269
Fig. C-21 Filter cake –reservoir flow diagnostic plot - case M4.....	270
Fig. C-22 Pressure derivative - case M4.....	270
Fig. C-23 Fall-off of a minifrac test - case M4.....	271
Fig. C-24 Identification of closure from the fall-off of a minifrac - case M4...	271
Fig. C-25 Net pressure versus time – case M3.....	272
Fig. C-26 G-function of a minifrac test - case M4.....	272
Fig. C-27 Filter cake –reservoir flow diagnostic plot - case M4.....	273
Fig. C-28 Pressure derivative - case M1.....	273
Fig. C-29 Pressure derivative - case M2.....	274
Fig. C-30 Pressure derivative - case M3.....	274
Fig. C-31 Pressure derivative - case M4.....	275
Fig. C-32 Pressure derivative - case M5.....	275

Fig. C-33 Old filtercake – reservoir flow model - case M1.....	278
Fig. C-34 New filtercake – reservoir flow model - case M1.....	278
Fig. C-35 Old filtercake – reservoir flow model - case M2.....	279
Fig. C-36 New filtercake – reservoir flow model - case M2.....	279
Fig. C-37 Old filtercake – reservoir flow model - case M3.....	280
Fig. C-38 New filtercake – reservoir flow model - case M3.....	280
Fig. C-39 Old filtercake – reservoir flow model - case M4.....	281
Fig. C-40 New filtercake – reservoir flow model - case M4.....	281
Fig. C-41 Old filtercake – reservoir flow model - case M5.....	282
Fig. C-42 New filtercake – reservoir flow model - case M5.....	282
Fig. C-43 Dynamic fluid loss test.....	283
Fig. D-1 Fracture half-length – Poisson’s Ratio.....	285
Fig. D-2 Fracture half-length – Young’s Modulus.....	285
Fig. D-3 Leak-off coefficient – Young’s Modulus.....	286
Fig. D-4 Reservoir permeability – Young’s Modulus.....	286
Fig. D-5 Fracture width – fracture height	287
Fig. D-6 Reservoir permeability – fracture height.....	287
Fig. D-7 Reservoir permeability – initial reservoir pressure.....	288
Fig. D-8 Reservoir permeability – initial reservoir pressure.....	288
Computer program flow chart.....	290

ABSTRACT

One of the most significant contributors to the oil and gas industry as a primary means of well production increase, is the hydraulic fracturing treatment. In essence, more than a million of such treatment operations have been conducted on over 44 % of the drilled wells. Nowadays, the costs of these operations, applied for the stimulation of oil and gas wells, have significantly increased, along with the increase of treatment size, pump rates and pressures, varying from fifteen thousands to more than one million dollars per operation. Consequently, a correct calibration of such operations is very important, and to ensure this, mini-fracture treatments are used.

Many models, describing the mathematics and application of a mini-fracture have been developed. However, a significant number of assumptions limit their applicability, and consequently often times they can not be used successfully for the delineation of fluid and reservoir properties necessary for the calibration of the actual fracturing operation.

The present study presents a coupled model for the determination of fluid and reservoir properties, such as fracturing fluid efficiency, leak-off coefficient, fracture half-length, fracture width, spurt-loss coefficient, reservoir permeability and filter-cake resistance. In essence this model can be used for the analysis and interpretation of the fracturing fluid leak-off characteristics as well as the filter-cake reservoir flow based on pressure decline data from a minifrac test.

New equations for the analysis of fracturing fluid spurt loss and subsequent calculation of fracturing fluid and reservoir properties based on spurt loss, if identified, are introduced.

In addition, a new pressure derivative equation was derived and incorporated into the model. This is used as an alternate tool for the case in which classic minifrac analysis techniques fails to produce reasonable means of interpretation, which if used would result in unreliable fluid and reservoir properties sought from such a test.

A computer program was developed for the calculation of all parameters mentioned above and also to automatically curve-fit the main output and diagnostic plots of the model.

A step by step procedure is included and application of the model is demonstrated on real field data obtained from minifrac tests performed on several oil wells. The fluid and reservoir properties determined with this model, are verified by comparison with results obtained from post-fracture tests (i.e. build up, history matching).

Also, sensitivity analysis is performed, to enhance its applicability by indicating which parameters are playing a major role in the interpretation of a calibration treatment.

CHAPTER 1

INTRODUCTION

1.1 Calibration Treatments

Hydraulic fracturing plays a major role in the oil and gas industry. Often times we hear that by applying this stimulating treatments to oil and gas wells, reserves are being increased, when in essence that is not the case. Instead, with the help of the hydraulic fracturing treatments, we make existent reserves exploitable, producible and consequently add a significant number of barrels of oil and millions of cubic feet of gas from reserves that would have otherwise not been economical to develop and produce.

As a method of accelerating recovery, hydraulic fracturing requires a correct calibration of the actual treatment, which implies the prediction and determination of fluid and reservoir properties such as fluid efficiency, leak-off coefficient, spurt loss, fracture half-length, fracture width, reservoir permeability, in-situ stress, and filter-cake resistance. The dimensional and propagation characteristics of the hydraulic fracture constitute valuable information for a proper design of the fracturing treatments.

A calibration treatment is a special case of hydraulic fracturing, which is executed without proppant before the actual stimulation treatment. Calibration treatments are generally performed for critical stimulations or at the beginning of a field wide program. The main objective of the minifrac is to determine the hydraulic fracturing parameters necessary for the design of an effective fracture stimulation.

In essence, minifrac tests are composed of two basic injection tests, which are conducted to ensure a reliable fracture analysis, a stress test and calibration treatment¹. As far as the stress test is concerned, a step-rate injection procedure followed by flow-back or pressure decline analysis is used to determine the closure pressure which is equal to the minimum in-situ rock stress. Since all subsequent fracture analysis and proppant selection are using the closure pressure, it is very important that it be determined as accurately as possible.

Once the closure pressure is determined, a calibration test is performed. The test is conducted with the same fluid and at the same rate that will be used on the actual job. After the pumping period, following the shut-in, the pressure decline is monitored until closure is attained. The information obtained from the injection period is used for the identification of the fracture geometry, as shown by Nolte and Smith². The information is later used to determine which is the most appropriate model to use for the decline analysis, and also to diagnose the undesired occurrence of fissure opening and/or rapid height growth.

Fracture calibration, also known as minifrac, is used to help optimize the hydraulic fracture treatment design, since it provides critical information pertaining to the well to be treated. Minifrac pressure decline analysis, as presented by Nolte^{3,4,5}, first became popular in the 1980's and is used routinely today. An excellent review and detailed description of the theoretical framework and current application of fracture pressure analysis is presented by Nolte^{5,6}.

Numerous papers have been written on the subject of analyzing the pressure-decline data obtained from a calibration test, and a variety of theoretical models have

been developed and presented. They address the uncertainties derived from ideal assumptions employed in their derivation.

Minifrac test procedure and analysis have been the subject of considerable investigation and controversy, over the last eighteen years. In essence, despite the extensive work on the topic, and at least two international workshops⁷ on in-situ stress measurement, many uncertainties remain in the interpretation of hydraulic fracture injection tests. Several factors have been shown to influence the post shut-in, pressure decline behavior of vertical fractures, including: fluid injection rate, fluid rheology, reservoir permeability, fluid leak-off additives, fluid compressibility, fluid pressure, minimum horizontal in-situ stress, and the opening of natural fractures⁷.

Most minifrac analysis is based on Nolte's equations, in essence based on the material balance during fracturing and closure. His most recent published paper⁸ provides a technical frame work for adding after closure fracturing pressure-decline analysis, to the pre-treatment calibration testing sequence, that defines fracture geometry and fluid-loss characteristics.

The basic analysis of decline data, is based on assumptions that fluid loss depends on \sqrt{t} and it is independent of pressure. Also they consider the fracture area and closure pressure to be constants, and that the fluid is incompressible. However such assumptions, of the basic analysis employed for the interpretation of pressure-decline data, is seldom met in practice.

Consequently, although deviations from these assumptions have been considered previously, he proposed a method⁴ based on the consideration of the slope at strategic locations on the G-plot for pressure decline, in conjunction with available

information for the fluid and reservoir, standard well logs, pressure diagnostics, and treatment design improvements. In fact, a variety of pressure-time plots were prepared for the minifrac, using most of the commonly applied graphical techniques (i.e. pressure, log pressure or pressure derivative vs. square root of time, log time, Horner time, Nolte's time function (G-function), DeBree, etc.)

Shlyapobersky et al.⁹, described a new model for the design and interpretation of hydraulic fracturing treatments and minifrac tests, using the fracture overpressure measured at shut-in to determine the apparent field-scale fracture toughness of the fractured interval.

The Nolte-Shlyapobersky technique can be used for the determination of fluid efficiency, leak-off coefficient, fracture half-length, and fracture width. However, the model has limitations and thus it is not suitable, in most of the situations, for the following reasons:

Ideally, a plot of the net pressure versus the G-function should be a straight line, as shown in Fig. 1 (a). However, when analyzing field data, the plot, in most cases it is not a straight line, but rather a curve as shown in Figs. 1 (b) and Fig. 2. It is believed, that one of the main reasons for the deviation from its expected linear behavior, is the ratio of the spatial net pressure (Δp_f) to the wellbore net pressure (Δp), and known as β_N . A deviation from the ideal expected behavior, as shown in Nolte's analysis⁴, Figs. (1.1a and 1.2) can be explained by the occurrence of fracture geometry changes, unlike the opinion of other authors who consider the ratio of

spatial average to the wellbore net pressure, $\beta_N=1$ after shut in. If the net pressure in the fracture were the same at all points, then a value of $\beta_N=1$ would be valid.

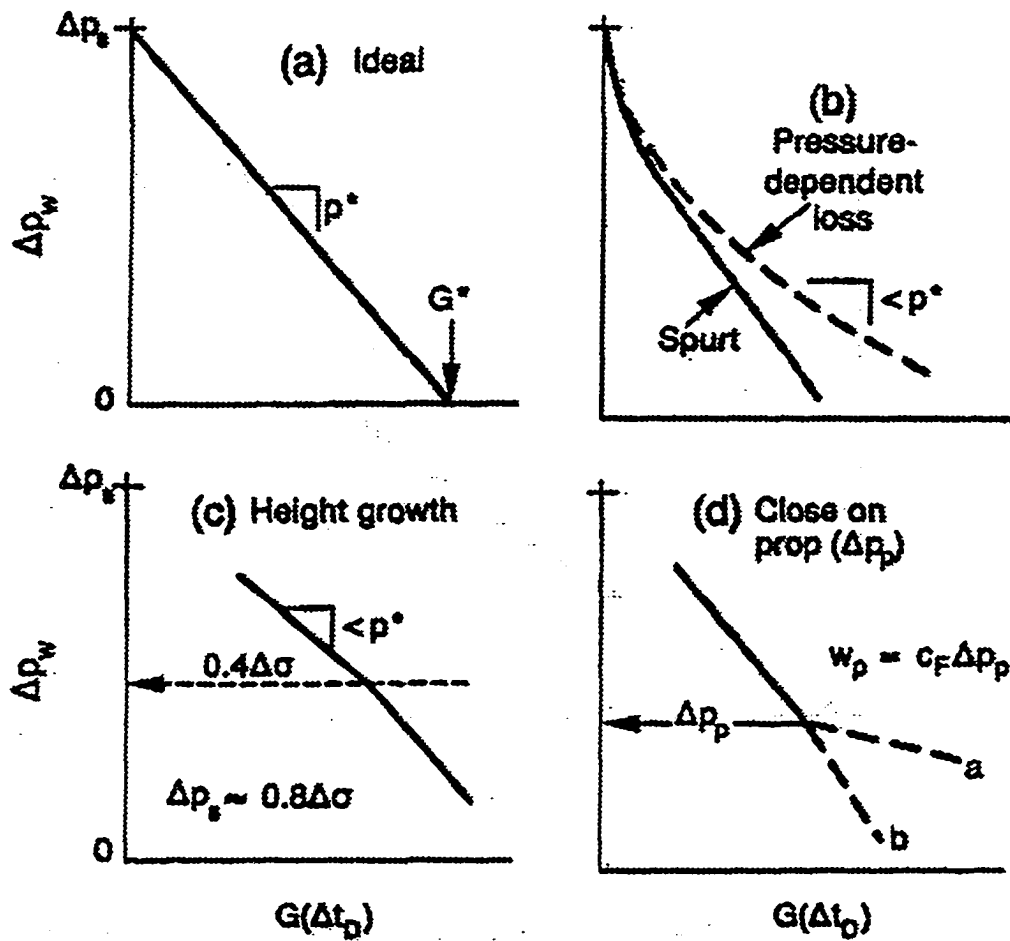


Fig. 1.1 Diagnostic from pressure decline data - Net pressure versus $G(\Delta t_D)$ (Adapted from Nolte et al.⁴)

However, Nolte^{3,4} showed that during and after pumping there is fluid flow from the wellbore region to the extremities of the fracture, and this generates a

pressure gradient until the fluid is completely lost in the formation. Figure 2.4 shows the simulated pressure and flow rate in a fracture both before and after shut-in³. In his study and analysis Nolte³ also shows that β_N prior and after pumping has different values due to flow rate and pressure gradient reduction in the entrance area of the fracture

Nolte^{4,6,10}, developed the equation of the dimensionless G-function as an integral for the lower and upper bounds (loss dominated and storage cases). When the model is solved with the aid of the hyper-geometrical function^{11,12}, $g(\Delta t_D, \alpha)$, both the dimensionless shut-in time, Δt_D , and the fracture area growth power law exponent, α , are simultaneously considered, and increased accuracy is expected. However a remarkable inconvenience can be generated if the plot of the fracture net pressure versus the G-function is a curve, and thus making difficult or unreliable the pressure decline analysis, Fig. 1.3. Consequently, other methods should be developed for the interpretation of fall-off data, when the classical approach does not lead to valid results.

In addition to that, the model does not consider the rheology of the polymer based fluid used to perform the calibration treatment of the well. Since a minifrac test uses an injection fluid with the same or similar properties, as the one used for the actual fracturing job, rheological properties and fluid behavior should be included.

Finally, the Nolte - Shlyapobersky fall-off analysis assumes that the spurt loss is zero, which in reality is expected to be approximately 80 % of the entire leak-off in wells located on reservoirs with high permeability.

Consequently, the parameters determined from the intercept and slope of this plots (i.e. fluid efficiency, η , leak-off coefficient, C_L , fracture half-length, x_f , for the PKN and KGD geometries, and R_f for the Penny Shape or radial geometry), and fracture width, w_f , are not always reliable.

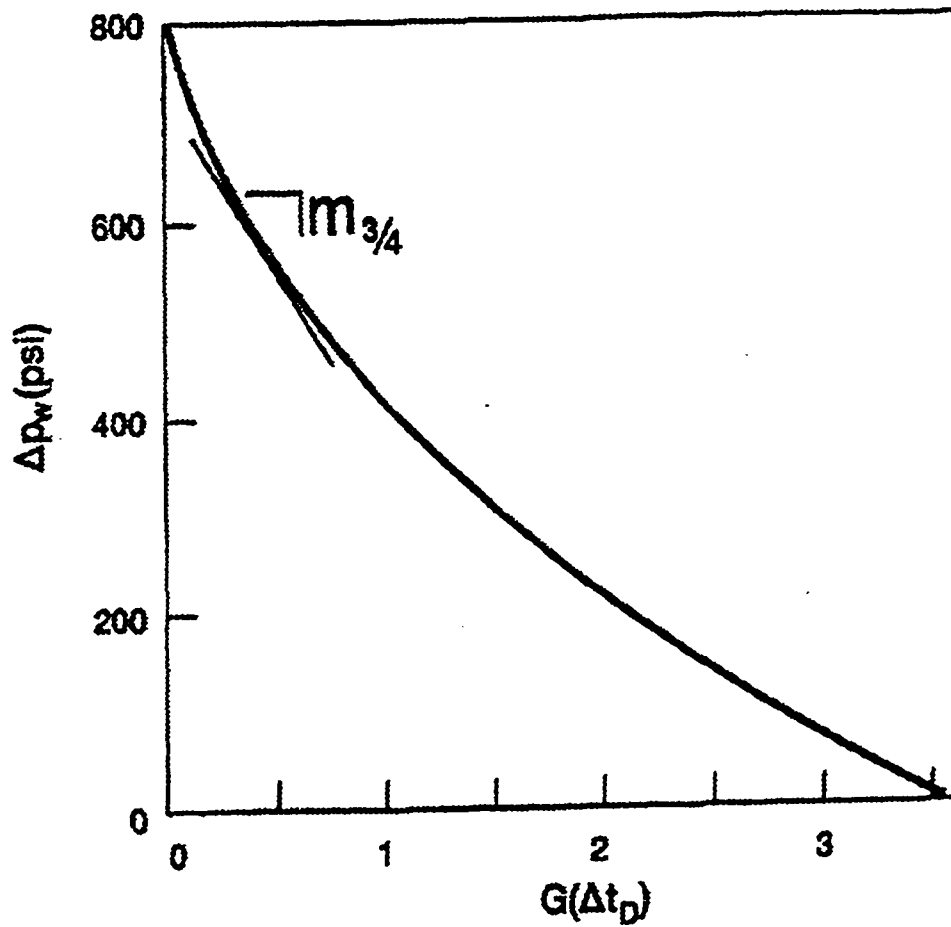


Fig. 1.2 Decline analysis- Net pressure versus $G(\Delta t_D)$
(Adapted from Nolte et al.⁴)

Mayerhofer et al.¹³, developed a model that considers the total pressure drop as a sum of pressure drops, Eq. (1.1), across the filter-cake, polymer invaded zone and the reservoir. The main output of the model consists of two parameters, the reservoir permeability and the filter-cake resistance.

$$\Delta p(t) = \Delta p_{face}(t) + \Delta p_{pivz}(t) + \Delta p_{res}(t) \dots\dots\dots(1.1)$$

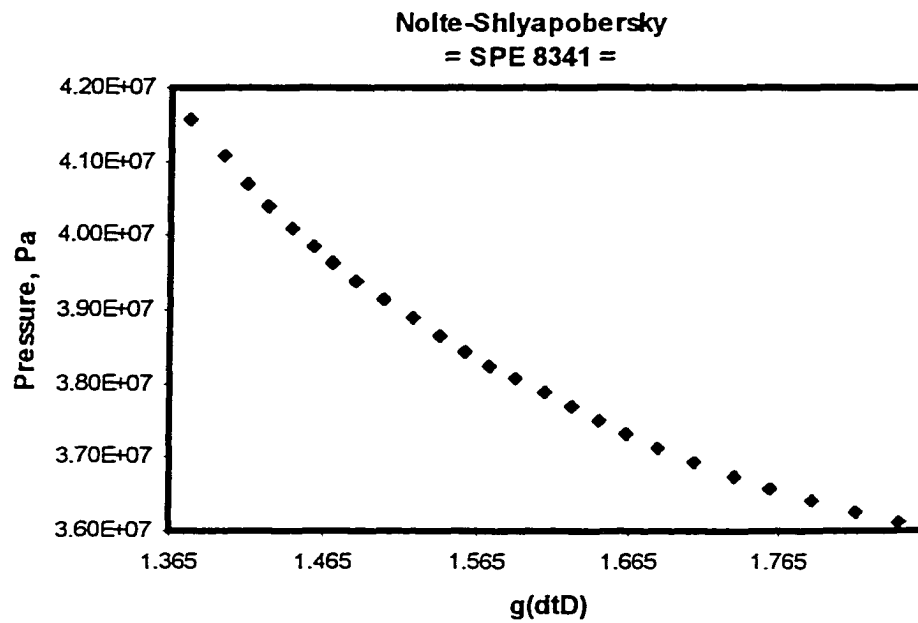


Fig. 1.3 Net pressure versus G-function of a case presented by Nolte¹⁴

The method can thus differentiate between the two major factors of the leak-off process: the filter-cake and the reservoir permeability. However, the method is sensitive to deviations from its assumptions^{13,15,16}, and therefore the analysis on the

same data sets as in the case of Nolte-Shlyapobersky's technique, indicates that not always a straight line is obtained. Also, often times, when the straight line is well defined, a negative intercept may occur. In this case the filter cake resistance delineated from the intercept has no meaning (i.e. negative energy), and thus the reservoir permeability obtained from the slope of the plot, after fitting a straight line through zero intercept, is unreliable, since in such a case, the method does not differentiate between the two parameters, and attributes the entire resistance to the reservoir permeability.

Biot¹⁷ presented a method based on Lagrange's equation, which in essence shows the balance between work expanded and work done in the propagation of a two dimensional crack. However he only developed it for the KGD geometry and does not consider the rheology of the fracturing fluid. Later on Lee¹⁸⁻²¹, incorporated his model into the pressure decline analysis. He considers the rheological properties but does not assume direct proportionality between the width of the created fracture and the pressure difference between instantaneous shut-in pressure and formation closure pressure.

1.2 Research Objectives

Research was undertaken to provide a more realistic and practical coupled model for the analysis of the pressure decline from minifrac tests, for the determination of the fluid and reservoir properties, as stated earlier in this chapter.

The objectives of this work are therefore:

1. To perform a critical review of the models available for the analysis of data sets, obtained from minifrac tests.
2. To present the essential theoretical aspects of the fracture propagation, stress analysis, and minifrac technique.
3. To develop a more realistic model for the prediction of the fluid and reservoir properties from minifrac tests.
4. To develop equations for the determination of fluid and reservoir properties from a minifrac test if the spurt loss is known.
5. To develop and include the pressure derivative, as an alternate method for the fall-off analysis and interpretation.
6. To develop a computer program for the efficient applicability of the model.
7. To apply the model to real field cases and thus assess its applicability .
8. To perform sensitivity analysis on all parameters used in the model, and thus identify which are the most critical and how significant is their impact on the modeling.

The objectives presented above are addressed individually in this work and collectively produce a coupled model for the prediction of fluid and reservoir properties from minifrac tests.

CHAPTER 2

CRITICAL REVIEW OF MINIFRAC MODELS

This chapter describes currently available models and methods of analysis of the fracture calibration treatments (minifrac), used to predict the fluid and reservoir properties.

Nolte^{2,22,23}, with his innovative ideas, started a new industry of minifrac test performance and analysis and accelerated the development of fracture technology in the 1980's. Initially he presented the basis for interpreting fracturing pressures, that permits identification of confined-height extension, uncontrolled height growth, and a critical pressure. The analysis of fracturing pressure during injection shows information of the nature of the fracture's growth (i.e. height confinement or growth, excessive fluid loss, or restricted extension). From pressure decline analysis, after fracturing, information on the fluid loss characteristics, fracture dimensions, fluid efficiency and fracture closure time and pressure can be obtained (Fig. 2.5).

The assumptions used by Nolte²³ are summarized bellow:

1. A continuous rate of fracture growth, Eq. (2.1), which requires a constant injection rate.
2. A continuous change of the ratio of fracture to fluid loss would not be violated by the subsequent penetration of an impermeable and higher - stress zone, generally the case for shale, for which both width and fluid loss would be relatively negligible.

3. Spurt loss, the opening and closing of natural fractures, and pressure dependent loss, are not explicitly considered.
4. Constant fracture area from shut-in of injection to fracture closure.

The main formulas derived, based on the above assumptions, are:

The rate of fluid loss¹² through an incremental area, $d\alpha$, at time, t , as shown in Fig. 2.2, and expressed by the Carter²⁴ relation is:

$$q_l = \frac{2C_L A_p}{\sqrt{t}} \int_0^\alpha \frac{d\alpha}{\sqrt{1-\alpha^e}} \dots\dots\dots(2.1)$$

and following integration of Eq. (2.1) from zero to α , (ratio of the previous fracture area, a , to current fracture area, A) the following can be obtained:

$$q_{LU} = \frac{2C_L A_p}{\sqrt{t}} \left[2\sqrt{t/t_0} (1 - \sqrt{1-\alpha}) \right] \dots\dots\dots(2.2)$$

$$q_{LL} = \frac{2C_L A_p}{\sqrt{t}} \left[\sin^{-1} \alpha \right] \dots\dots\dots(2.3)$$

Where Eq. (2.2) represents the leak-off rate at the upper bound (i.e. power law exponent, $e=1$), and Eq. (2.3) represents the leak-off rate at the lower bound⁶ (i.e. $e = 1/2$).

The fracture's rate of areal growth follows the power law,

$$\tau/t = (\alpha/A)^e = \alpha^e \dots\dots\dots(2.4)$$

and can be bounded by either the assumption of negligible fluid loss into the formation (upper bound), or predominant fluid loss (lower bound), as shown in Fig. 2.3.

Using Eq. (2.2) and assuming that the permeable fracture area, A_p , does not change significantly, from Eqs. (2.3, and 2.4), the rate of fluid loss is expressed as:

$$q_{LU}(t, A) = \frac{4C_L r_p A_f}{\sqrt{t_0}} \left[(1+t_D)^{1/2} - t_D^{1/2} \right] = \frac{4C_L r_p A_f}{\sqrt{t_0}} f_1(t_D) \dots\dots\dots(2.5)$$

$$q_{LL}(t, A) = \frac{2C_L r_p A_f}{\sqrt{t_0}} \left(\sin^{-1}(1+t_D)^{-1/2} \right) = \frac{2C_L r_p A_f}{\sqrt{t_0}} f_2(t_D) \dots\dots\dots(2.6)$$

and by integrating the dimensionless functions, $f_1(t_D)$, $f_2(t_D)$ from $t_D=0$ (shut-in), to t_D , the G-function is obtained:

$$g_u(t_D) = \int_0^{t_D} f_1(t_D) dt_D = 4/3 \left[(1+t_D)^{3/2} - t_D^{3/2} - 1 \right] \dots\dots\dots(2.7)$$

for the upper bound, and

$$g_L(t_D) = \int_0^{t_D} f_2(t_D) dt_D = \left[(1+t_D) \sin^{-1}(1+t_D)^{-1/2} + t_D^{1/2} - \pi/2 \right] \dots\dots\dots(2.8)$$

for the lower bound.

The volume of fluid loss^{10,11} during pumping, which can be obtained by the integration of Eqs. (2.5 and 2.6) from $t = 0$ to t_p (pumping time), considering the permeable fracture area, A_p :

$$V_{LPu} = \int_0^{t_p} q_{Lu} dt = \frac{8}{3} C_L A_p \sqrt{t_p} \dots\dots\dots(2.9)$$

for the upper bound, and

$$V_{LP_L} = \int_0^{t_p} q_{Ll} dt = \pi C_L A_p \sqrt{t_p} \dots\dots\dots(2.10)$$

for the lower bound.

The volume fluid loss after shut-in^{10,11}, is found by the integration of Eqs. (2.5 and 2.6) between the time limits $t_D = 0$ ($\Delta t = 0$) and t_D as follows:

$$V_{LSI} = 2C_L r_p A_f \sqrt{t_0} [g(t_D) - g(t_0)] \dots\dots\dots(2.11)$$

or

$$V_{LSIU} = 2C_L r_p A_f \sqrt{t_0} [g_U(t_D) - g_{LU}(t_0)] \dots\dots\dots(2.12)$$

for the upper bound, and

$$V_{LSIL} = 2C_L r_p A_f \sqrt{t_0} [g_L(t_D) - g_{LU}(t_0)] \dots\dots\dots(2.13)$$

for the lower bound.

Where:

$$g_{LU}(t_o) = 4/3 \text{ for } \alpha = 1 \text{ (upper bound) } \dots\dots\dots(2.14)$$

and

$$g_{LU}(t_o) = \pi/2 \text{ for } \alpha = 1/2 \text{ (lower bound) } \dots\dots\dots(2.15)$$

The fracture width^{10,11}, as a function of the net pressure, $(p_w - p_c)$, and compliance, c_f , is:

$$w_e = c_f(p_w - p_c) \dots\dots\dots(2.16)$$

with the compliance derived as a function of strain modulus, E' , ratio of the average net pressure in the fracture to the wellbore flowing pressure, β_{Ni} (i is substituted by the fracture geometry type as shown bellow), and the fracture geometry as follows:

$$c_{f_{PKN}} = \frac{\pi \beta_{NPKN} h_f}{2E'} \dots\dots\dots(2.17)$$

for the PKN geometry, where h_f is the fracture height.

$$c_{f_{KGD}} = \frac{\pi \beta_{NKGD} x_f}{2E'} \dots\dots\dots(2.18)$$

for the KGD geometry with x_f as the fracture half-length.

$$c_{fRAD} = \frac{\pi \beta_{NRAD} (32/3\pi^2) R_f}{2E'} \dots\dots\dots(2.19)$$

for the radial geometry, where R_f is the fracture half-length.

The ratios of the average net pressure in the fracture to the wellbore flowing pressure, for each fracture geometry, are given as follows:

$$\beta_{NPKN} = (2n' + 2)/(2n' + 3 + \alpha_1) \dots\dots\dots(2.20)$$

for the PKN geometry,

$$\beta_{NKGD} = 0.9 \dots\dots\dots(2.21)$$

for the KGD geometry, and

$$\beta_{NRAD} = 3\pi^2 / 32 \dots\dots\dots(2.22)$$

for the radial geometry, where n is the fluid rheology index, and α_1 an exponent which is a function of the fluid viscosity behavior (i.e. $\alpha_1 = 0$ for the case of uniform viscosity, and $\alpha_1 = 1$ represents linearly decreasing viscosity from the wellbore to the tip of the fracture).

Pressure dependent loss coefficient^{10,11} The above derivations assumed that the fluid loss coefficient was constant, and independent of any variations,

whereas is a function of the difference between the fracturing fluid pressure and reservoir pressure, and therefore:

$$C_c < C_i \left(1 + \frac{p_n}{p_c - p_R} \right)^e \dots\dots\dots(2.23)$$

where:

$$i = 1, \text{ for } e = 1/2 \dots\dots\dots(2.24)$$

$$i = 2, \text{ for } e = 1$$

$$i = 3, \text{ for } e = \begin{cases} 1/2, \text{ incompressible cake} \\ 1/16, \text{ compressible cake} \end{cases}$$

p_n is the net pressure, p_c the closure pressure, and p_r the reservoir pressure.

Fan²⁵ also shown a relationship of the leak-off coefficient as a function of pressure as indicated by the following equation:

$$C_L = \sqrt{\frac{\phi c_f k}{\pi \mu}} (p_w - p_r) \dots\dots\dots(2.25)$$

where:

ϕ is the reservoir porosity, c_f the fluid compressibility, k the reservoir permeability, μ the reservoir fluid viscosity, p_w the pressure at the fracture face, and p_r the initial reservoir pressure.

Height growth Fig. 2.1 shows that two of the models assume constant fracture height, h_f , throughout pumping and shut-in. The KGD model, assumes no width variation in the vertical direction (Fig. 2.1), and therefore the model assumes that the height is approximately the perforated interval with limited penetration²⁶, or it assumes that slip²⁷ occurs between the formations with no transfer of shear stress. As a result height growth for this model will not occur. However vertical height and width changes are possible with the PKN model. Consequently, the appropriate height, h_f , to use is the height of the lower stress formation, generally the gross reservoir section, without including any additional growth of height.

Fluid loss from spurt and opening of natural fractures In essence, two primary effects can cause increased loss during pumping: spurt loss and the opening of natural fractures at a specific value of the fluid pressure²². Spurt loss occurs only during pumping and not after shut-in, when the fracture penetration is assumed to stop. Spurt is defined as volume lost per unit area, and thus has the dimension of width.

Nolte²² distinguishes between fluid loss during pumping, κC_L , and after shut-in, C_L , where:

$$\kappa = \left[1 + b_s / (C_L \sqrt{t_0} g_0) \right] (A_p + A_f) / A_p \dots\dots\dots(2.26)$$

Several critical aspects are to be observed here:

1. The absence, in some of the field cases, of a straight line on the G-function plot, Figs. 1.1 (b) and 1.2, makes the decline analysis unreliable.
2. Negligible spurt loss, especially in the case of high permeability reservoirs, where the fluid loss is attributed almost 80 % to the spurt loss, becomes an unacceptable assumption.
3. The ratio of the average net pressure in the fracture to the wellbore flowing pressure, β_N , as given by Eqs. (2.20-2.22), should be unity if the net pressure in the fracture, were the same at all points. However, β_N can not be one, regardless of the values of α_1 and n' , the exponent for the power-law fluid-flow model described above. Consequently, the fluid rheology, although incorporated into the equation, is not well accounted for, and therefore a different approach should be employed.

Martins et al.²⁶, presented a pressure decline analysis method, for the case of a minifrac, which assumes the fracture to have evolved as a family of confocal ellipses (Fig. 2.6). The concept was employed in conjunction with the principles developed by Nolte^{3,14,22}, and used to estimate the fracture geometry, fracture dimensions, and the loss of fracturing fluid. There are two critical key factors in this model: (1) the technique is presented for the case of a minifrac pressure decline data obtained under the assumption that the length of the fracture is the same order as the perforated interval, when the fracture propagation has been unaffected by the confining strata, and (2) that the evolution of the fracture geometry is indeed in the form of confocal

ellipses. Both aspects are questionable. First, the model is based on laboratory investigation only, conducted by Daneshy²⁸, in the absence of confining strata, and which does not accurately resembles the reservoir conditions. Second, the assumption that the length of the fracture is the same order as the perforated interval, is not a certain phenomena.

Biot et al.¹⁷, presented a new approach to the 2-D problem of fracture propagation based on Lagrangian methods. The Lagrangian formulation is based on the classical form of Lagrange's equations. In essence, he produced a basic equation that expresses the balance between work expanded and work done in propagating a 2-D crack. Existing theories, assume linear elastic behavior of the reservoir and ignores surface energy considerations at the crack tip and plastic deformation effects. Leak-off is treated as an independent process and merged with the fracture propagation problem by iterative methods. The Lagrangian method, is not restricted to elastic behavior, and leak-off can be included as a part of the formulation. Therefore Biot includes leak-off by assuming a piston like displacement of the reservoir fluid by an incompressible fracture fluid filtrate, with a moving boundary between the two.

In essence, the Lagrangian formulation, from classical mechanics, states that:

$$\frac{d}{dt} \left(\frac{\partial L}{\partial \dot{q}_i} \right) - \frac{\partial L}{\partial q_i} = \bar{Q}_i \dots \dots \dots (2.27)$$

where:

$$L = E_K - E_p \dots \dots \dots (2.28)$$

is the Lagrangian function given by the difference between the kinetic, E_K , and potential energy, E_P , of the system. Thus:

$$\bar{Q}_i = -\frac{\partial D}{\partial \dot{q}_i} + Q_i \dots\dots\dots(2.29)$$

with \bar{Q}_i including all forces that are not derived from a potential function, D , the dissipation function, and Q_i representing all remaining forces. Substituting Eqs. (2.28 & 2.29) into Eq. (2.27), and considering the effects given by the kinetic energy negligible, Biot arrived at the desired Lagrangian equation for the purpose of his analysis:

$$\frac{\partial E_P}{\partial q_i} + \frac{\partial D}{\partial \dot{q}_i} = Q_i \dots\dots\dots(2.30)$$

Starting with Eq. (2.30), and introducing the fracture's extension, b_B , from $-L_f$ to $+L_f$ as:

$$b_B = 2b_{fB} f\left(\frac{x}{L_f}\right) = 2b_{fB} f(L_D) \dots\dots\dots(2.31)$$

where the function $f(L_D)$ specifies the shape of the crack, and b_f is the fracture half width as a function of the total crack volume, and assuming Poiseuille flow of a Newtonian fluid in the fracture, as given by the following equation,

$$q_i(x) = -\frac{b_B^3}{12\mu} \frac{\partial p}{\partial x} \dots\dots\dots(2.32)$$

Biot derived a model for the KGD geometry, that can be regarded as a simple energy material balance:

$$E - \frac{V_o}{\beta_B} \int_0^l \frac{\partial p}{\partial x} L_D f(L_D) dL_d = \frac{K\gamma}{2L_f^3} \left(\frac{V_o}{\beta_B} \right)^2 \dots\dots\dots(2.33)$$

The above equation, represents the basic practical result of the Lagrangian analysis, and it can be solved numerically for L_f when the pressure distribution, $\frac{\partial p}{\partial x}$, is known. Furthermore, with L_f known, the fracture width, b_{fB} , and pressure, p_e , can be determined. However, the method has significant limitations, since (1) it considers the flow Newtonian, and consequently can not account for the correct rheology of the fracturing fluid used to create the minifrac, (2) the model can only be applied for the KGD geometry, and the surface energy, E , is neglected.

Lee¹⁹⁻²¹, continued Biot's work, and incorporated Biot's energy balance equation into the pressure decline analysis (minifrac). At that time, minifrac analysis employed by most petroleum industry operators did not consider the rheological properties of the fracturing fluid, nor did Biot's model, as stated earlier in this section. He observed, that the most severe consequence of this omission was that the geometry determined by minifrac analysis differed from that of the fracture design programs based on the same model.

In essence, the method developed and presented by him, considers the following:

1. Rheological properties, and therefore the geometry determined from pressure decline analysis is in agreement with the fracture geometry determined by the fracture design programs.
2. The method does not consider the assumption that the created fracture width is proportional to the pressure difference between the instantaneous shut-in pressure and formation closure pressure. His claim is that when the pressure difference is in the order of 1,000 psi, calculated fracture widths can be several times greater than the width found by the fracture design program that uses the same model.

In addition to the above,

1. His derived model considers the surface energy, E , negligible.
2. The method is only applicable for the KGD geometry.

Meyer and Hagel²⁹ presented asymptotic analytical and numerical solutions for two dimensional and three dimensional type hydraulic fracture geometries, and investigated with them the Geertsma Deklerk (KGD), Perkins-Kern-Nordgren (PKN), and a 3-D type model. In essence, they initially conducted model comparison and parametric studies, and presented simplified design formulae for benchmarking the above types of models. At that stage, they concluded that the KGD model is generally more applicable at low confining stresses (i.e. $L/H \geq 1$). For large fracture length to height ratio, the KGD model predicts wider wellbore widths and shorter lengths than the PKN and 3-D type models.

Later⁵, the same authors published a simulated minifrac analysis. Their work, introduced the momentum conservation equation and new aspects of fluid rheology. A new addition, was another form of G-function:

$$G(\alpha_a, \alpha_{c2}, \theta) \cong \{G(1, \alpha_{c2}, \theta) - G(1/2, \alpha_{c2}, \theta)\}(2\alpha_a - 1) + G(\alpha_{1/2}, \alpha_{c2}, \theta) \dots \dots \dots (2.34)$$

Although, the above function is similar to Nolte's $g(t_D)$ function, it is evaluated at the α_a and α_{c2} , rather than fluid efficiency. On the other hand, from a numerical method point of view, they considered the governing minifrac equations of mass and momentum of conservation, and solved them iteratively to match the measured closure time.

Finally, Hagel and Meyer²⁹ presented an extension of the minifrac procedures existent at that time, to improve the quality of analysis. They introduced a methodology based on history matching the pressure response during pumping and closure for the minifrac treatment. Basically they coupled the traditional minifrac analysis with a three dimensional hydraulic fracturing simulator. The fracture propagation solution, is coupled with the post injection pressure decline analysis. The aim is to reduce the number of parameter uncertainties, to delineate the appropriate fracture geometry model and perform parametric studies. In essence, the fracture-pressure analysis and procedures provided by their work, generally follow the theory of minifrac analysis originally formulated by Nolte^{2,3,14,22,30}

The following aspects can be denoted from their work:

1. Nolte's G-function is a better choice since it accounts for the fracturing fluid efficiency (upper and lower bounds), parameter that plays a significant role in the pressure decline analysis.
2. Their method calls for iterations based on a guessed value for the leak-off coefficient, and is time consuming.

Castillo³¹, introduced a modified fracture pressure decline analysis, including pressure-dependent fluid leak-off. He assumes that the leak-off coefficient is a pressure-dependent variable. However, his assumption is valid for the case in which the leak-off is controlled by a compressible filter cake, with the exception where leak-off is primarily controlled by filtrate viscosity, by an incompressible filter cake, or by reservoir permeability and compressibility.

Also, based on pressure derivative analysis, Castillo introduced new plots (Figs. 2.8 and 2.9), for fracture pressure decline analysis, used for the determination of the fracture parameters ($ISIP$, P_c , P^*), required in the Nolte leak-off calculations. The method is inconclusive, because we can not accurately delineate the fracture parameters from these plots. One main reason is the fact that he derived the pressure with respect to the G-function, thus making practically impossible analysis of the pressure derivative as a function of the shut-in time. And by no means, should use of these plots replace the stress tests (i.e. pump-in flow-back test) used for the determination of closure stress.

Moschovidis³² developed a model for the interpretation of the pressure decline analysis, from minifrac treatments initiated at the interface of two formations. He uses the type curve match method introduced by Nolte³, with a definition of effective or

average leak-off coefficient and an equivalent fracture radius. In his model, the effective leak-off coefficient is the weighted average of the each formation, relative to the minifrac areas in both formations. Also, the equivalent fracture radius, is the radius of a circle of an area equal to the sum of the areas of the minifrac in the two formations.

The critical aspect here is the difficulty of establishing appropriate values for the parameters indicated above, since a value for each formation is practically impossible to define.

Shlyapobersky et al.^{9,21,33} proposes modifications to test procedures used in the industry, at the time they published the paper, and presents techniques for design and analysis of hydraulic fracture tests. The main aspect, sought in this case, was the determination of the overpressure and the total leak-off coefficient which are necessary for the overpressure calibrated design of hydraulic fracture stimulation. The work claims that the test procedures account for the real in-situ conditions of the borehole, formation and the created fracture. The benefit of the test procedure consists of the fact that is performed as an on-site interactive process, meant to quantify as accurately as possible for the in-situ conditions, and such optimize the controlling test parameters , such as the pump rate and pumped volume.

The main assumptions associated with the procedure presented in this work are:

1. The existence of a planar fracture:

- The fracture is propagated far enough from the well, so that the initial fracture orientation, at the wellbore, would not appreciably affect the measurement of the minimum in-situ stress.
 - The injection rate to be appropriately large to ensure that the dominant main fracture is created rather than many small fractures.
 - Non-ideal features of the induced fracture, such as roughness and waviness of the fracture walls, are always present.
2. During injection the fracture area follows the power law, Eq. (2.4)
 3. Shortly after shut-in the fracture propagation ceases and thus becomes negligible.
 4. Uses the theory of elasticity to establish the pressure width relation.
 5. Carter's leak-off model is used with power law pressure dependent fluid loss coefficient^{22,31}
 6. The compressibility of fluid is considered to be constant.

The most critical assumption is the third from the above list, and thus its validity should be always verified during the minifrac test. The reason is simply the fact that there is no direct way to verify this assumption. Therefore, its validity and use are justifiable only if the results of the fracture pressure decline analysis are consistent with and agree with other observations³³.

McLellan³⁴ presented detailed analysis of three minifrac, and small acid fracturing. It is essential to note his findings, after applying the energy based model as presented by Shlyapobersky³³. They are as follows:

1. Storage effects affect, in some cases, the unambiguous determination of the fracture closure pressure from the minifrac.
2. Multiple methods for selecting the fracture closure pressure from shut-in pressure decline data, necessary to avoid interpreting all slope changes as fracture closure phenomena.

Soliman et al.³⁵ developed type curves for the analysis of minifrac in heterogeneous reservoirs. However, the method is limited to only one model, PKN, and in essence follows Nolte's model with one exception, that is the leak-off coefficient is a function of time but not as presented by Carter²⁴ (i.e. square root of time).

Gu³⁶ outlined a 3-D fracturing numerical simulator for hydraulic fracture closure with application to minifrac analysis. He uses the Carter's leak-off model and considers a variable fracture area, and variable in-situ stress, unlike the previous models presented. Gu states that when the fracture grows out of the uniform in-situ stress zone or stress contrasts occur inside the perforated zone, the fracture probably does not hold a constant area and it may shrink back from the high in-situ stress zones during the shut-in period. Therefore, the constant area assumption will not be valid. The study shows that the simulator results in plots with dual slopes (Fig. 2.10), instead of the ideal straight line slope.

However, the problem here is how can one accurately depict the correct slopes, since more than just two slopes can be drawn on a plot with such a curvature (Fig. 2.10) ?

Zhu et al.³⁷ presented a mathematical model incorporating the effects of temperature and fracturing fluid compressibility. From a theoretical point of view, the method has a remarkable level of interest, but in practice, how do we really account for changes in temperature and fracturing fluid compressibility, during the minifrac treatment? They also developed a comprehensive model of minifrac pressure behavior with foam fracturing fluid, based on similar criteria.

Later, McLellan et al.⁷ presented a study regarding the pressure interpretation from minifrac tests in a naturally fractured gas reservoir. In essence, calculated bottomhole pressures are plotted against various time functions (Fig. 2.11), to determine the instantaneous shut-in pressure (*ISIP*) and fracture closure pressure (*FCP*), and the leak-off behavior of various fluid systems. Valuable findings are presented in their work. Leak-off behavior is shown to be dependent on several factors including the choice of fluid additives, the fracture closure pressure or minimum in-situ stress, the presence of natural fractures, and possibly the intermediate and major principal stress. Field case study indicated anomalously high propagation pressures observed during the minifrac test. These high pressures, are believed to have caused either natural fractures, or secondary fractures to open, resulting in nearly one magnitude greater leak-off coefficient than was calculated for lower bottomhole pressures in an earlier test in the same well.

Mayerhofer et al.^{13,38} introduced a new methodology for the estimation of the reservoir permeability from fracture calibration treatments. The methodology derives from the solution of the diffusivity equation for a well with infinite conductivity vertical fracture, as a multi-rate injection, with a superimposed varying filter-cake

skin effect. The transient reservoir response, which is the essential aspect, is then decoupled and used to determine the reservoir permeability. The advantage of having a method for the determination of reservoir permeability from a calibration treatment, is considerable. Often times, the estimation of the reservoir permeability is inaccessible because the candidate wells either do not flow (i.e. tight gas reservoirs) or a pre-treatment pressure transient test would be too long, and of course expensive. The authors have shown that in a large range of reservoir permeabilities (from 0.1 md up to 10 md), and for specific field fracture face resistances, the majority of the pressure gradient is in the reservoir. This is in contrast to the frequently published papers which sustain that the fracture filter-cake is predominant.

The total pressure gradient from the fracture into the reservoir is given by the following components:

$$\Delta p(t_j) = \Delta p_{face}(t_j) + \Delta p_{pinvz}(t_j) + \Delta p_{res}(t_j) \dots \dots \dots (2.35)$$

where:

$\Delta p_{face}(t_j)$ is the pressure drop across the filter cake

$\Delta p_{pinvz}(t_j)$ is the pressure drop across the polymer invaded zone

and

$\Delta p_{res}(t_j)$ is the pressure drop across the reservoir

To assess the influence of the polymer invaded zone, laboratory experiments, using long cores, were performed^{13,15,39}. It was determined that this zone is negligible for common fracturing fluids, and for cores with permeabilities up to 4md. Therefore, the

filter-cake is the dominant component in the pressure drop across the fracture face, and consequently the polymer invaded zone pressure drop component, the second term of the right hand side of Eq.(2.35), is assumed negligible.

For the reservoir component, $\Delta p_{res}(t_j)$, the Gringarten and Ramey⁴⁰ early time infinite conductivity vertical fracture solution is used as the dimensionless pressure:

$$p_D = \sqrt{\pi t_{Dxf}} = \sqrt{\frac{0.000264\pi kt}{\mu \phi c_r x_f^2}} \dots\dots\dots(2.36)$$

Cinco-Ley and Samaniego⁴¹ fracture face skin effect was also modified to account for a varying fracture-face resistance:

$$s = \frac{\pi kR_s}{2x_f} = [\pi kR_0 R_D(t)]/2x_f \dots\dots\dots(2.37)$$

where

$$R_D(t) = \frac{R_s}{R_0} \dots\dots\dots(2.38)$$

is a normalized resistance accounting for the approximate increase of the fracture-face resistance,

$$R_D(t) = \sqrt{\frac{t_n}{t_m}} \dots\dots\dots(2.39)$$

At the end of pumping, $R_D = 1$.

Combining Eqs. (2.36-2.39), with varying fracture area and varying leak-off rate, is the pressure change during pumping is obtained:

$$\Delta p(t_m) = p_i - p(t_m) = 4\alpha_p \sqrt{\frac{\alpha_t \mu \pi}{k \phi c_t} \left[\sum_{j=1}^m \left(\frac{q_{l,j}}{A_{p,j}} - \frac{q_{l,j-1}}{A_{p,j-1}} \right) \sqrt{t_n - t_{j-1}} \right]} + (2\alpha_p \mu_f \pi R_o / A_{p,m}) R_{D,m} q_{lm} \dots \dots \dots (2.40)$$

Eq. (2.40) represents the superposition of the pressure drops in the formation resulting from each incremental change of the leak-off velocity, $q_{l,j} / A_{p,j}$ during injection¹³.

Dividing Eq. (2.40), after some algebraic arrangements, by $(q_{Fn} R_{D,n} - q_{lm} R_{D,n})$ leads to a straight line (Fig. 2.12), when plotting the term on the left hand side vs. the summation term divided by $(q_{Fn} R_{D,n} - q_{lm} R_{D,n})$ on the right hand side. The reservoir permeability can be determined from the slope, m , of this plot as follows:

$$k = 84.22 (\pi \mu / \phi c, m^2) \dots \dots \dots (2.41)$$

and the filter cake resistance, R_o , from the intercept, b :

$$R_o = b / 282.4 \pi \mu_f \dots \dots \dots (2.42)$$

A few aspects are to be noted here:

1. The methodology, requires a significant level of simulations, computations and plotting, based on estimated values for the fracture area, A_f , at any time during the injection period as a function of the volume injected, of the pressure drop and its derivative. Not only is the method difficult to apply, since often times none of the expected behavior matches the field data, but how can one determine the fracture area and the leak-off rate as the fracture grows? Also, there is no specific model used for the estimation of the fracture geometry.
2. The permeability and the filter-cake resistance, can only be determined if the plots of the field data match the simulated ones (see Figs. 1-8) of Mayerhofer et al.¹³
3. Nolte's plot of the net pressure versus the G-function, (Fig. 8) of Mayerhofer et al.¹³, shows once again a curve instead of a straight line, as expected from simulation. Therefore, a correct slope can not be delineated from it.

Thompson and Church¹ discussed the design, execution, and evaluation of minifrac in the field, presenting a practical approach and case study. The intend of there paper was to discuss the basic concept of the minifrac treatment. They suggested guidelines, on how to design a minifrac, record the bottomhole pressure (BHP), obtain closure and interpret the data.

Dusterhoft et al.⁴² proposed improved minifrac analysis technique in high permeability formations. He observed that traditional minifrac analysis techniques fail to account for the correct fluid loss behavior of the gels used to frac reservoirs with high permeability. Borate cross-linked fluids and linear HEC gels are by far the most commonly used fluids for such formations. They showed that extensive laboratory testing indicated that the fluid loss behavior of these gels differ significantly from that

described by conventional fluid loss models. Also noted was the fact that traditional minifrac analysis techniques fail to account for the correct fluid loss behavior of these gels, and consequently this can lead to severe errors in the estimation of leak-off parameters, resulting in over or under designed jobs. In the case of high permeability formations, the spurt loss (Fig. 2.13), can be a major part of the total fluid loss. For very high permeability (i.e. 300 md), the spurt loss may be as much as 90% of the total fluid loss. As far as the filter-cake coefficient, C_w , is concerned, it was suggested that the properties of the polymer filter-cake are fairly independent of the formation permeability. Also, the authors stated that the fluid leak-off volume should not be considered proportional with the square root of time in the case of high permeability formations.

However, the minifrac mass balance equation allows for the calculation of only one unknown (i.e. either spurt loss, or leak-off coefficient). Therefore, they proposed that the leak-off coefficient be determined from the laboratory data, and the minifrac analysis to be used for the determination of the spurt loss. Finally, laboratory analysis indicated that the potential of minifrac using the conventional technique is not as severe for liner gels, as it is for the crosslinked gels.

Economides et al.⁴³ extended Mayerhofer's technique from homogeneous to heterogeneous reservoirs, and presented a model for the interpretation of fracture calibration tests in naturally fractured reservoirs. The sequence of log-log diagnosis, followed by parameter computation from specialized plots, was the primary objective of the study. However, the work is only presenting theoretical modeling and no practical field case for the validation of the method.

Gu et al.⁴⁴, modeled the determination of reservoir permeability from impulse fracture injection. However, it is essential to carefully analyze this aspect. In other words, a suggestion that impulse test analysis can be applied to injection tests in the same manner as in the case of much shorter injection times, requires consideration of the length of time needed to establish pseudo-radial flow. When the fracture created by the injection test is equal or exceeds 50 ft, it may take several hours, or even days, to observe the onset of a pseudo-radial flow. Yet, the radial flow response may occur within minutes of closure, and in that case, analysis after closure may offer independent confirmation of the $(k\alpha_f^2)$ ¹³.

Abousleiman et al.⁴⁵ presented a theory and its application for the post-fracture pressure transient analysis, seeking the determination of the formation permeability by micro or mini-hydraulic fracturing. The proposed procedure, known as “impulse fracture test,” was employed. The benefit of the method, relies on the fact that the hydraulically induced fracture transverses the near wellbore damaged zone, and exposes a larger formation area to flow. Therefore, the formation permeability and the pressure of the reservoir, are expected to be more representative. The theory is based on the distribution of sources with variable intensity along the fracture trajectory. The methodology presented is valuable, however it can not benefit the requirements of a fracture job design, since this is a post-fracture pressure transient analysis.

Vithal et al.⁴⁶, continued Dusterhoft et al.⁴² work for the application of an improved minifrac analysis technique in high permeability reservoirs. The main

stated objective of the methodology is the consideration of spurt loss and pressure decline analysis that is not limited to a function of square root only. However, no specific solution is presented for the determination of spurt loss.

Leshchyshyn et al.⁴⁷ looked at minifrac analysis of shear parting in Alberta reservoirs and its impact towards the on-site fracture design. Their objective was to address the early sand-off problem, that can be generated by exceeding leak-off (i.e. higher than $0.005 \text{ ft} \sqrt{\text{time}}$). The high leak-off can be attributed to two factors:

1. High permeability
2. Induced shear fracturing near the wellbore

Two types of sand-off have been identified:

1. A sand-off generated by underestimation of the reservoir permeability followed by a leak-off that exceeds the fracture growth. Such wells tend to sand-off from the fracture tip backwards, to the wellbore, known as the “tip screen-out.” Although this type of sand-off is usually undesirable, the propped fracture width is maximized, and results in maximum fracture conductivity.
2. The type of sand-off is the one that takes place near the wellbore. Such wells usually become poor producers.

From a minifrac design and analysis point of view, their work presents valuable information. Also one additional observation, made by the authors, deserves consideration for future modeling, that is the product fluid compressibility porosity used in composite analysis is an essential parameter for determining the boundary distance. No specific algorithm, or modeling is presented in their work.

Poulsen⁴⁸ presented a methodology of in-situ test for determining growth parameters for a hydraulic fracture. The applicability of this model is questionable for the following reasons:

1. It does not consider any form of relationship between the leak-off and pressure.
2. It assumes independence of the fracture growth behavior, when in fact it is well known that not to be the case.
3. It does not account for the fracture height, which is an indispensable parameter for the PKN geometry.

Sunil et al.⁴⁹ on the subject of frac pack treatments, as one of the most effective completion methods for the combined benefits of sand control and stimulation in the case of high permeability formations, a calibration treatment evaluation methodology was presented. The main suggested steps are highlighted bellow:

1. Laboratory data and log estimates of stress.
2. Identification of near wellbore pressure losses.
3. Closure pressure determination: the preferred method suggested is a step/flow back rate test.
4. Pressure decline analysis: the traditional analytical decline analysis following a pump-in/shut-in calibration treatment is applied to obtain estimates of the fluid leak-off coefficient. The $\frac{3}{4}$ rule, developed by Nolte et al.⁴, is employed.
5. Reservoir flow diagnostic: if pseudo-radial flow is reached during the calibration treatment, the specialized plots presented in this work can be used to determine reservoir pressure and the formation transmissibility.

6. Pressure history matching: the fracture parameter estimates, are to be refined by making use of pressure history inversion.
7. Verification and evaluation of results.

Fan²⁵ showed an interpretation model for fracture calibration treatments for both low and high permeability reservoirs. The model describes fluid flow into the porous medium with consideration of a variable filter cake, non-Newtonian invasion effects, and superposition of fracture pressure. He does not make use of the leak-off model, instead chooses a pressure profile. The parameters determined by the application of this model are the reservoir permeability, filter cake resistance, and the leak-off coefficient as a function of the pressure drop across the filter cake. In essence, the reservoir permeability and filter cake resistance are determined in a similar manner as presented earlier by Mayerhofer^{15,16}. Note that the plots used for the determination of the above parameters (Figs. 2.14 and 2.15), indicate the possibility of a negative intercept which generates the same consequences observed earlier with regard to the Mayerhofer's technique^{15,16}.

Tinker et al.⁵⁰ conducted minifrac tests and bottomhole treating pressure analysis for the improvement of the fracture stimulation design and execution. They made observations following the fracture stimulation of twenty five in-fill wells. The step-rate test was used for the identification of fracture extension rate and closure pressure. Minifrac tests were performed on every completion, and significant variation of the leak-off coefficient was observed. No modeling is presented in their work.

Valko and Economides³⁸ modeled the fluid leak-off delineation in high permeability fracturing. Starting with the original concept proposed by Carter, Howard and Fast²⁴, their work reviewed the description of fracturing fluid leak-off in view of modeling flow in porous media. It is shown how various linear leak-off models have been developed and why a new radial leak-off concept is necessary for high permeability formations. Using Laplace space methods the radial leak-off is analyzed and compared with the linear leak-off. The following main observations have been made:

1. A large discrepancy in calculated leak-off volumes (in the case of radial versus linear leak-off) is not an indication that the bulk leak-off coefficient approach gives unreasonable results.
2. The Mayerhofe et al. technique partly solves the decomposition problem (i.e. filter-cake resistance and reservoir pressure drop component, from which permeability is determined), for the reasons mentioned earlier in this section. Also, the second order derivative, generates a remarkable degree of sensitivity resulting in plots that can not be of any use.
3. The radial model presented, is physically more sound than previous approaches. It predicts more leak-off than the linear model, and it shows an almost linear variation of the leak-off volume with time, unlike the square-root type, or the G-function.
4. However in this work a rigorous procedure for the interpretation of the minifrac, in terms of radial leak-off, was not presented.

5. Mayerhofer et al. technique, as presented in this work, overestimates a few fold the reservoir permeability, and thus it requires further improvement.

Ispas et al.¹² continued the work developed by Valko et al.³⁸, and presented a methodology of fluid leak-off analysis in high permeability fracturing. The methodology is based on two previous published methods used for the determination of the leak-off parameters from the pressure fall-off stage of calibration treatment. The first method is the well known technology, Nolte-Shlyapobersky, used to determine an overall leak-off coefficient. The second method is a modified – improved form of the Mayerhofer et al. technique^{16,39}, and additional details will be later discussed in this work.

Nolte et al.⁵¹ extended the work and provided a study of after closure analysis of fracture calibration tests. The paper provides a framework for adding the after closure fracturing pressure analysis to the pre-treatment calibration testing sequence that defines fracture geometry and fluid loss parameters. The after closure period contains the pseudo-linear flow period that is the focus of this work, and the pseudo-radial flow period that has been previously addressed in a comprehensive manner. The primary role for the linear flow is to define spurt loss and validate information available from other parts of the calibration treatment. Reservoir linear flow also provides the remaining and missing link for the fracturing chain of events.

In summary, the following have been concluded based on the methodology and analysis presented in this paper:

1. After closure analysis has applications for low to high permeability reservoirs.

2. The most significant contributions provided by after closure linear flow, are the only prospect for quantifying spurt-loss, a distinct information of closure time and pressure for a shut-in decline, and the validation of the fluid loss analysis by reservoir analysis.
3. An outline was provided for the proposed method of application and field cases examples were used to demonstrate the information provided and the synergy between various periods of the calibration testing.
4. In addition to quantitative information, the after closure period provides a significant insight into the characteristics of the fluid loss behavior. Thus, five distinct types of behavior were identified and discussed.

Nolte's work adds significant improvement, mainly when considering the methodology of analysis for the after closure period. However, there is a very sensitive aspect to be considered, that is the non-uniqueness which can generate inconclusive results, including the determination of spurt loss. The non-uniqueness, referred to in this work, consists of the fact that different results can be obtain for a variety of parameters used for the simulation, as shown in their paper.

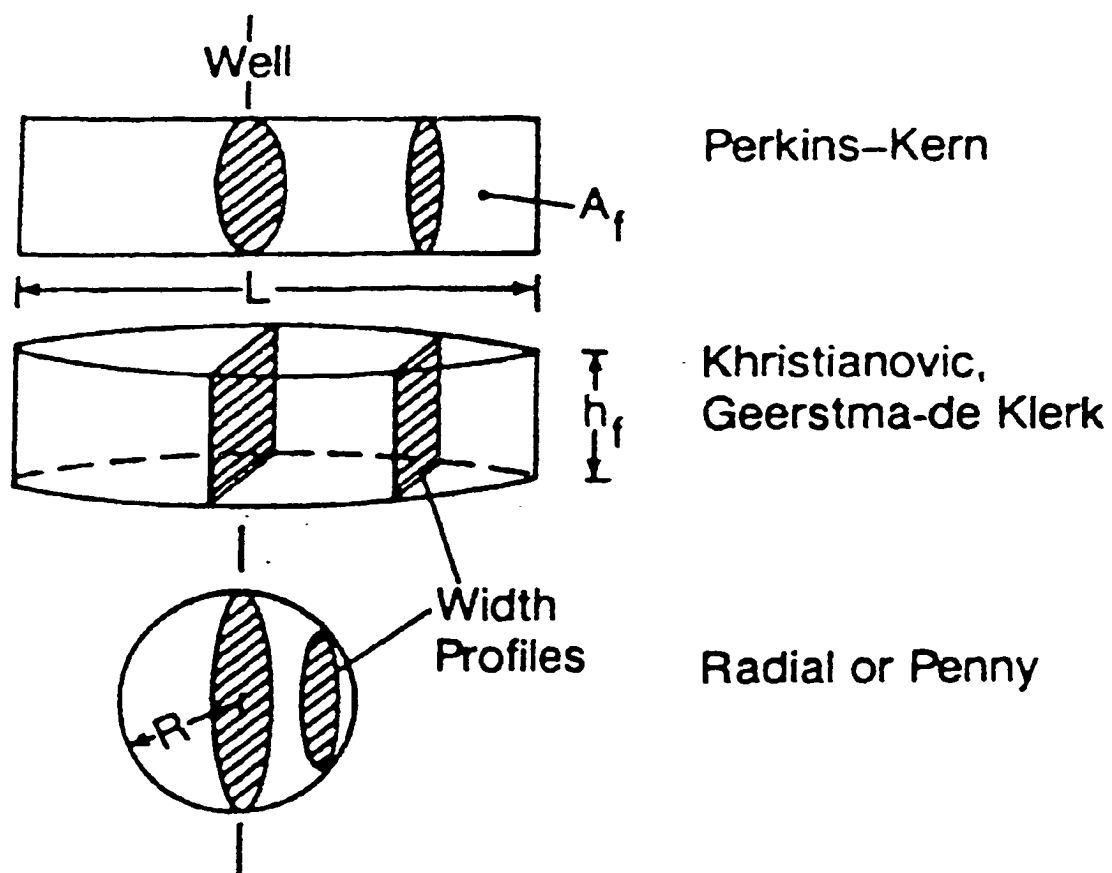


Fig. 2.1 – Schematic of fracture models, adapted from Nolte²²

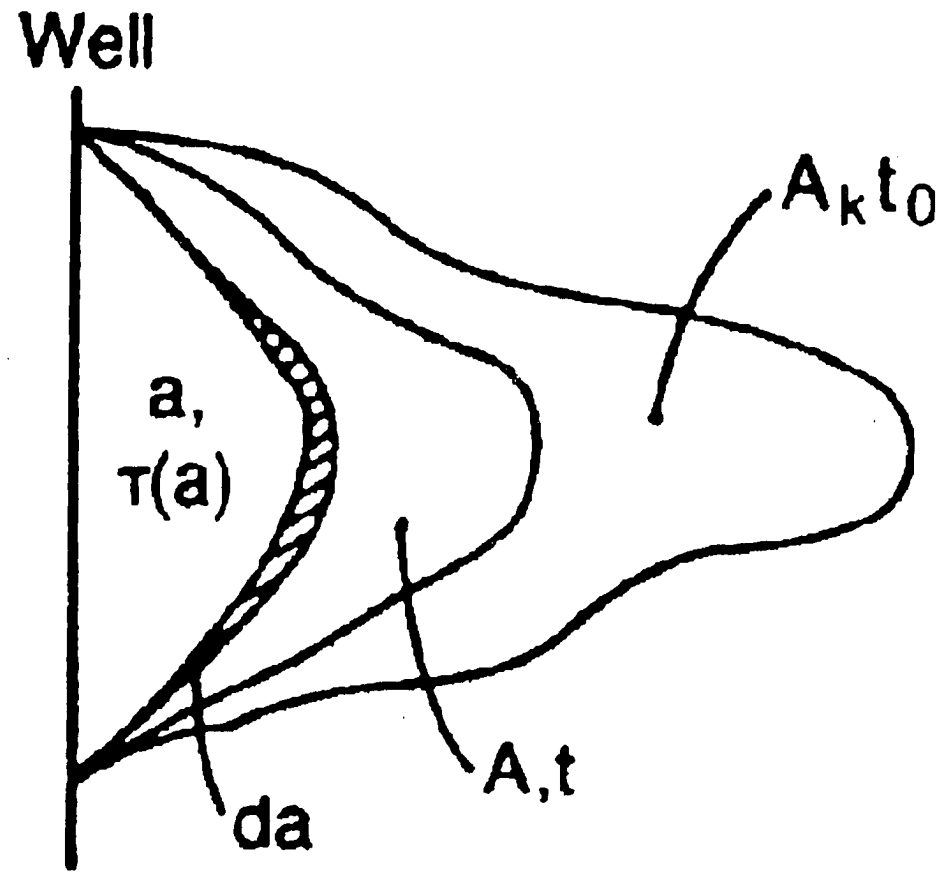


Fig. 2.2 – Schematics for areas and times in derivations, adapted from Nolte¹³

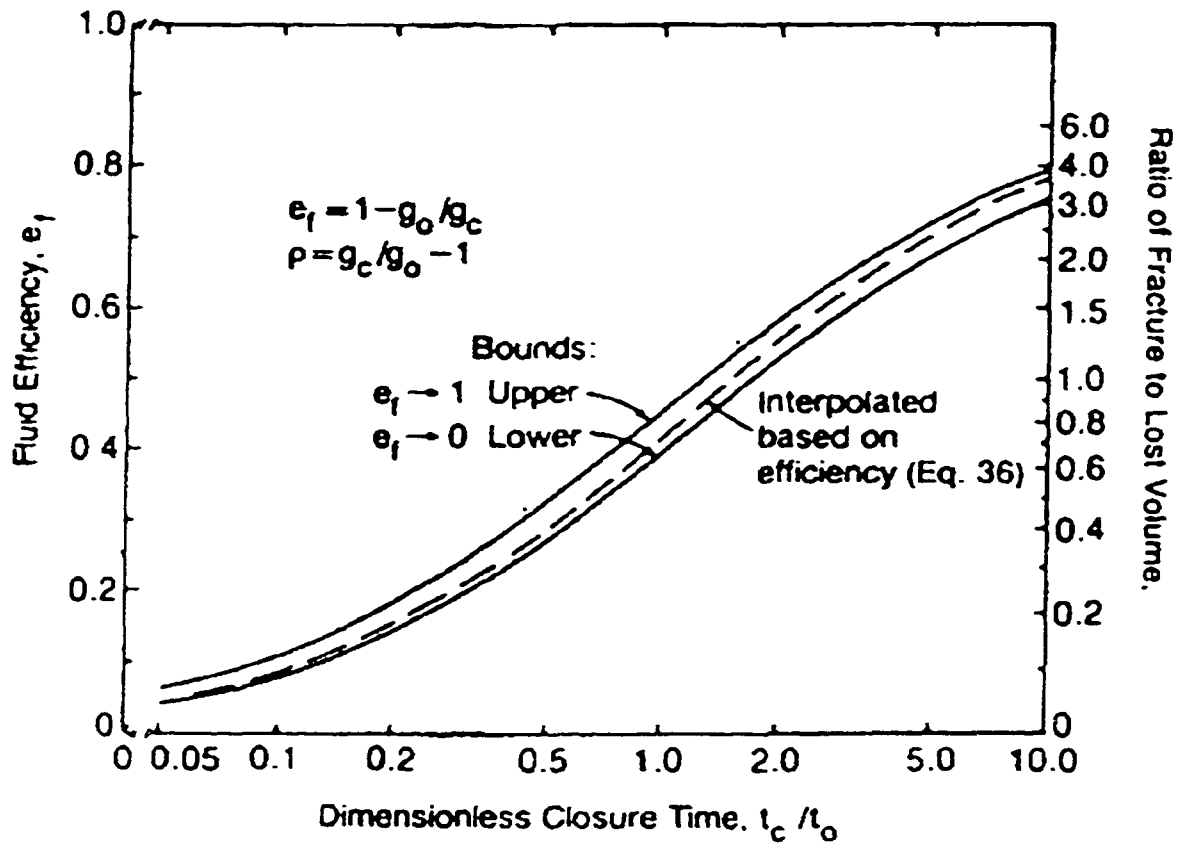


Fig. 2.3 – Fluid efficiency from closure time, adapted from Nolte²²

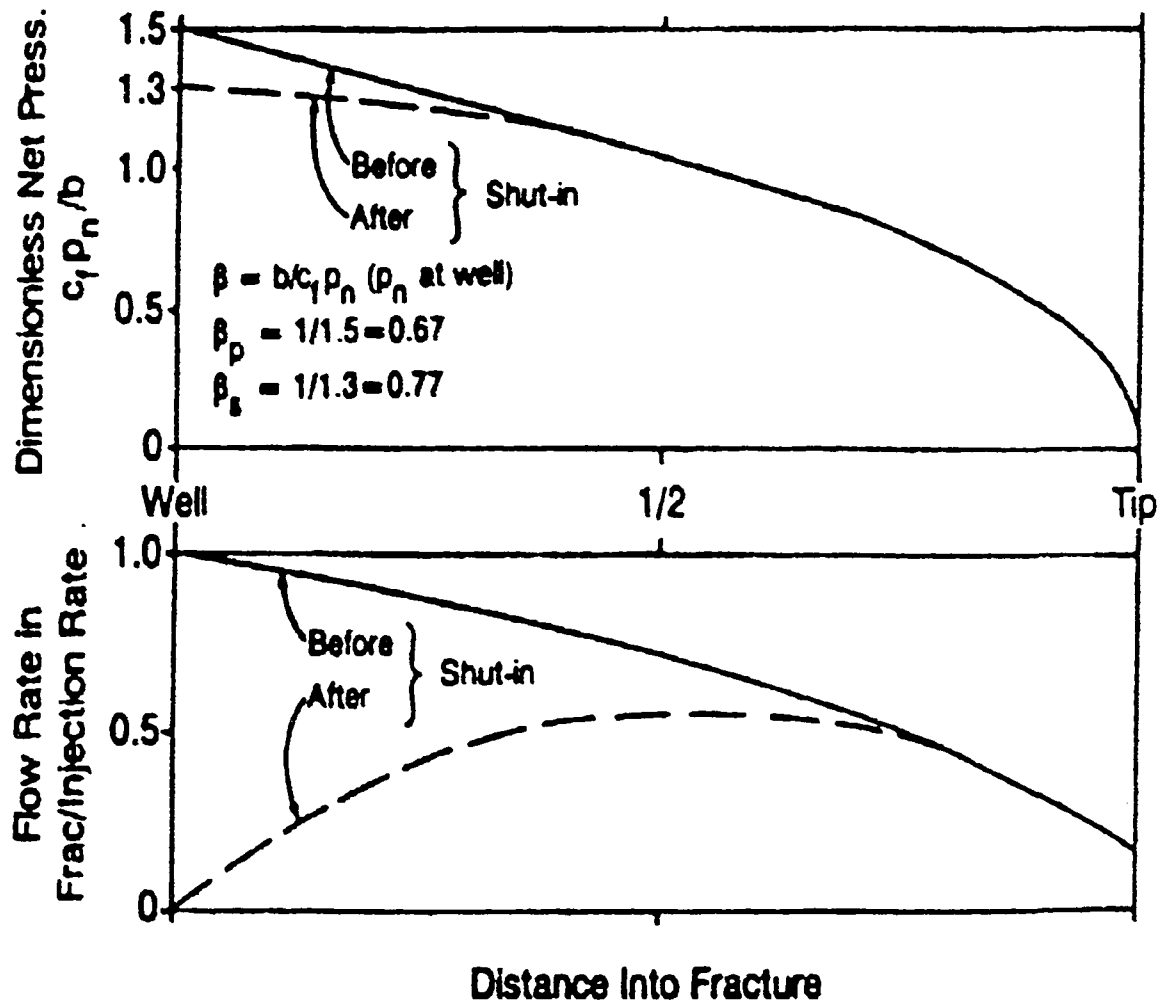


Fig. 2.4 – Pressure and flow in fracture for shut-in, adapted from Nolte²²

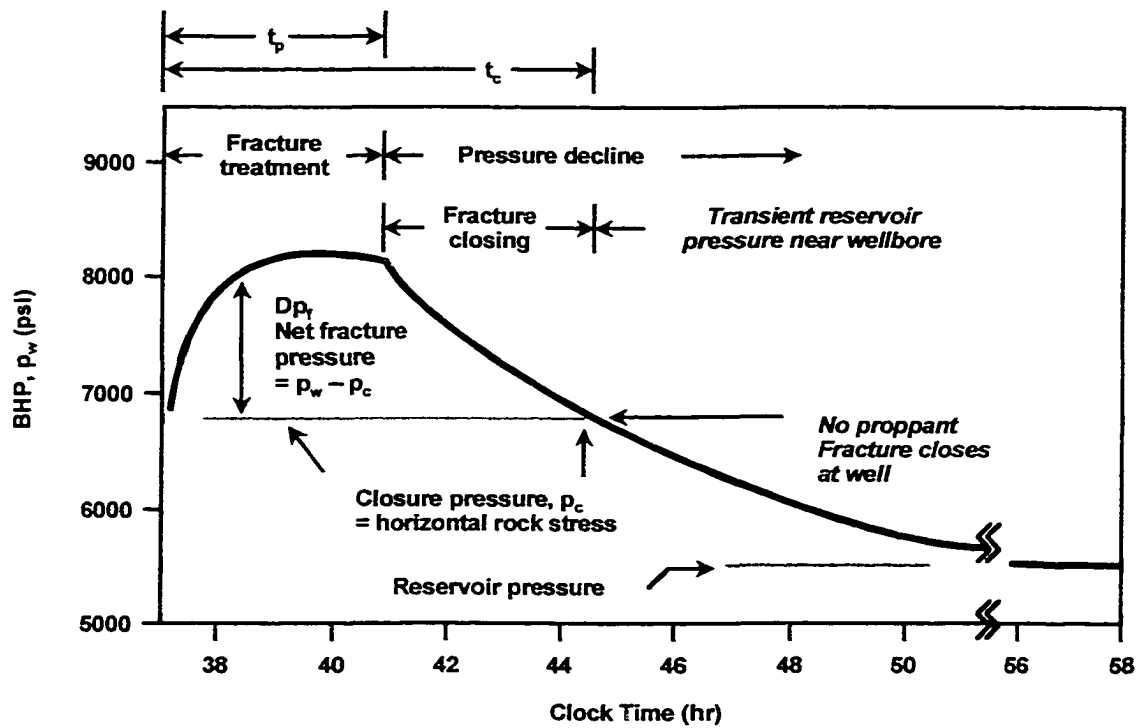


Fig. 2.5 – Bottomhole pressure versus time, adapted from Nolte⁸

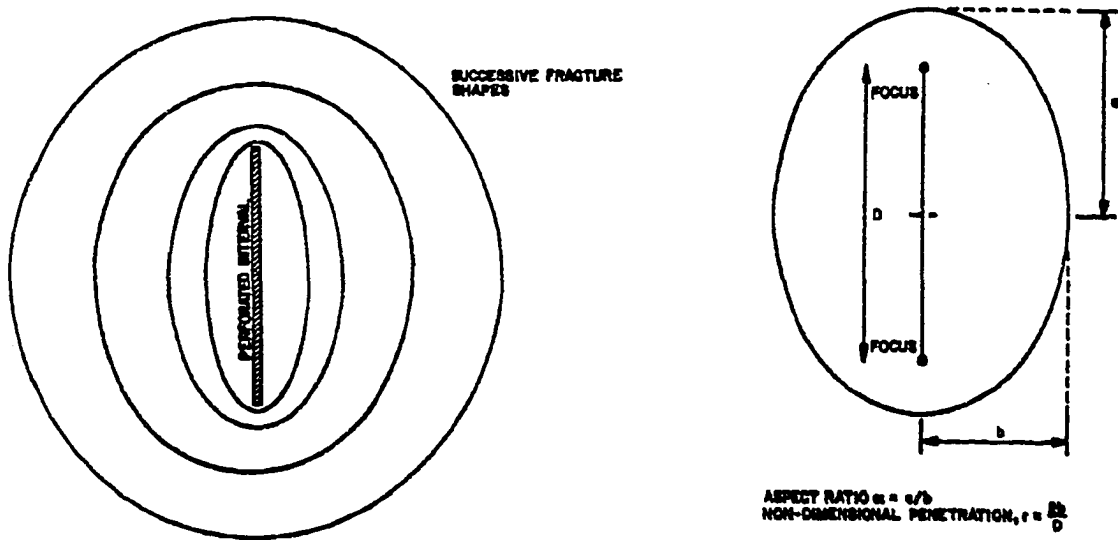


Fig. 2.6 – Illustration of fracture evolution as a family of confocal ellipses, adapted from Martins et al³⁵

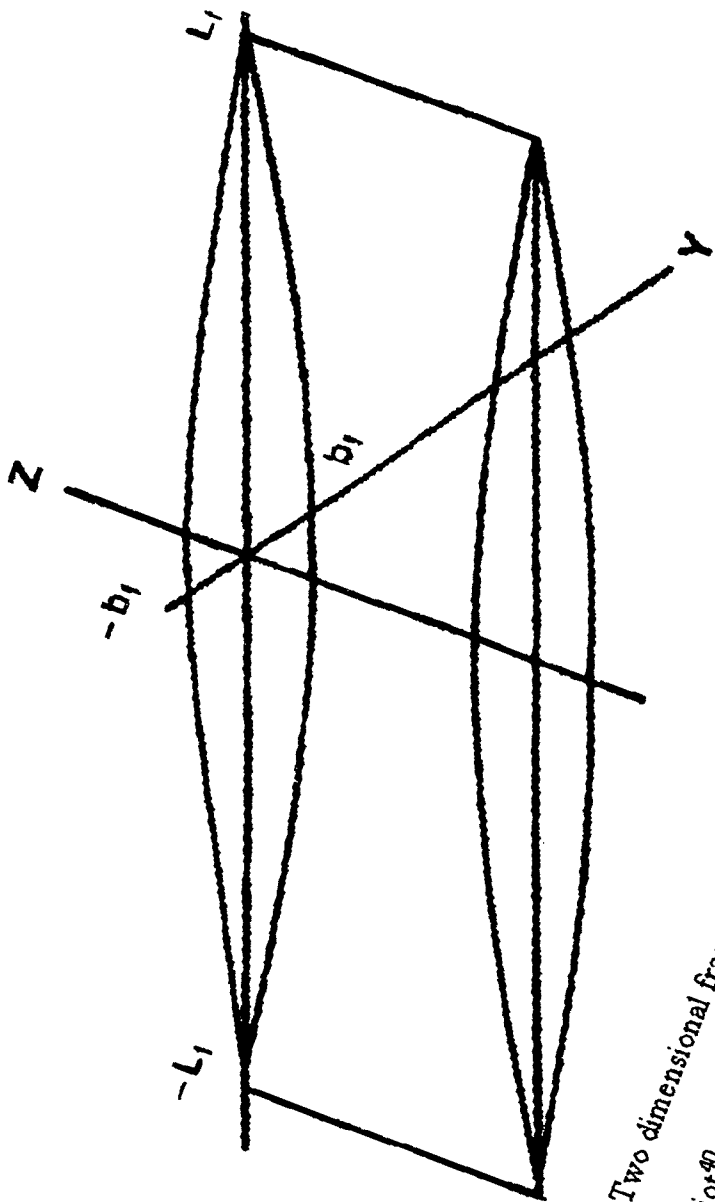


Fig. 2.7 - Two dimensional fracture of unit height (RGD geometry), adapted from
Biot, 40

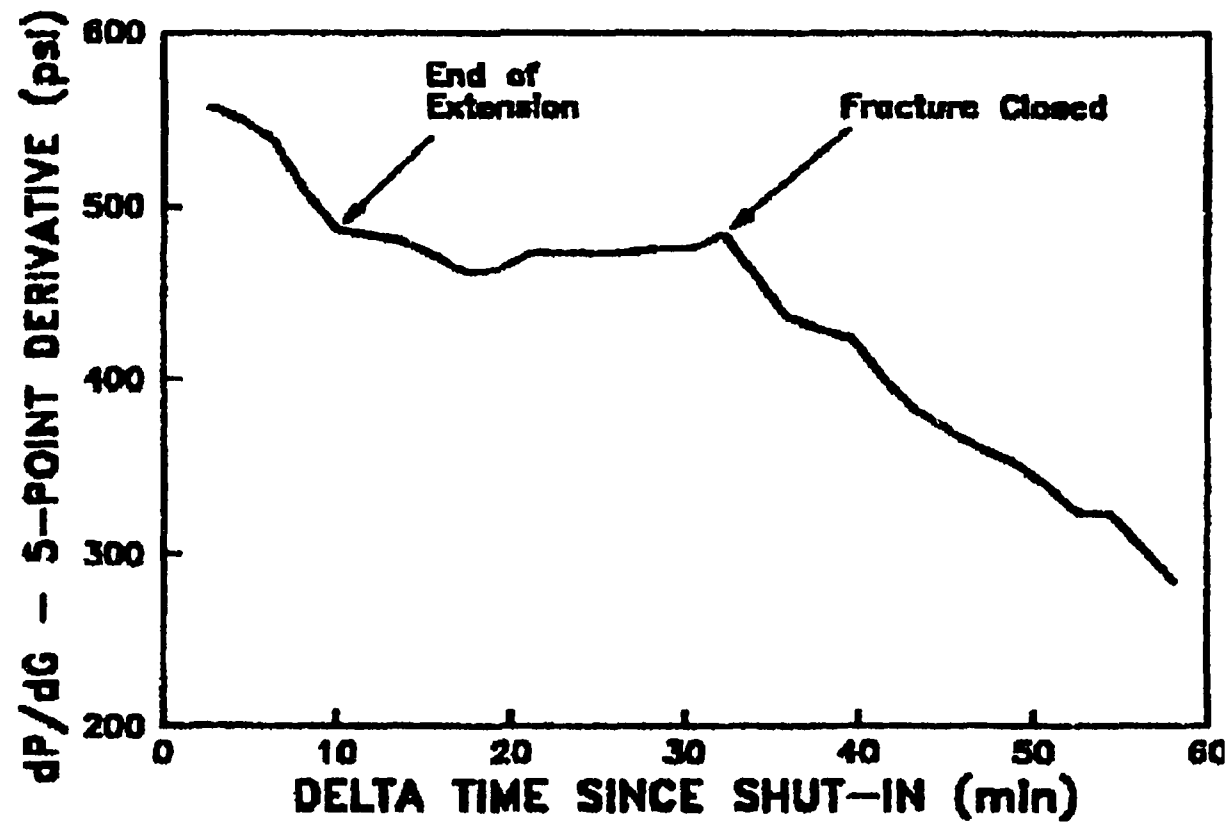


Fig. 2.8 - G-function derivative plot, adapted from Castillo¹⁰

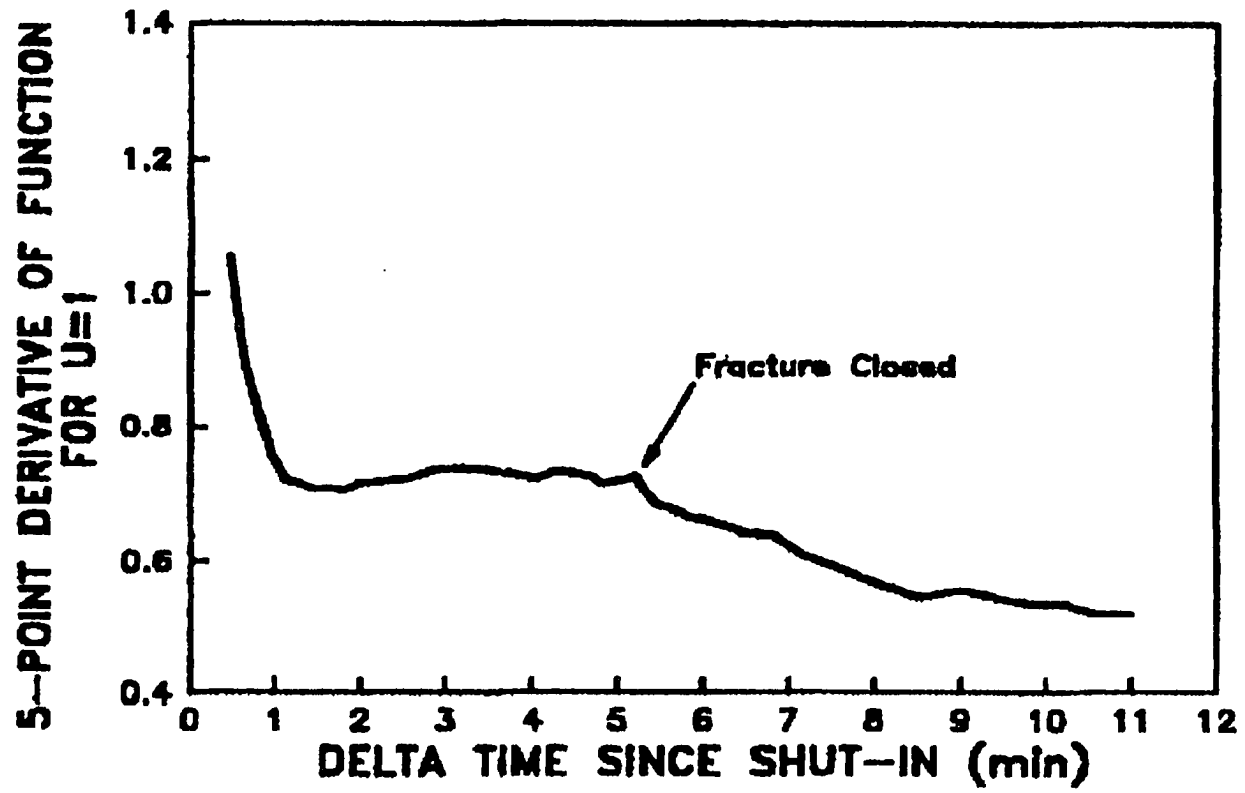


Fig. 2.9 - Pressure function derivative plot, adapted from Castillo¹⁰

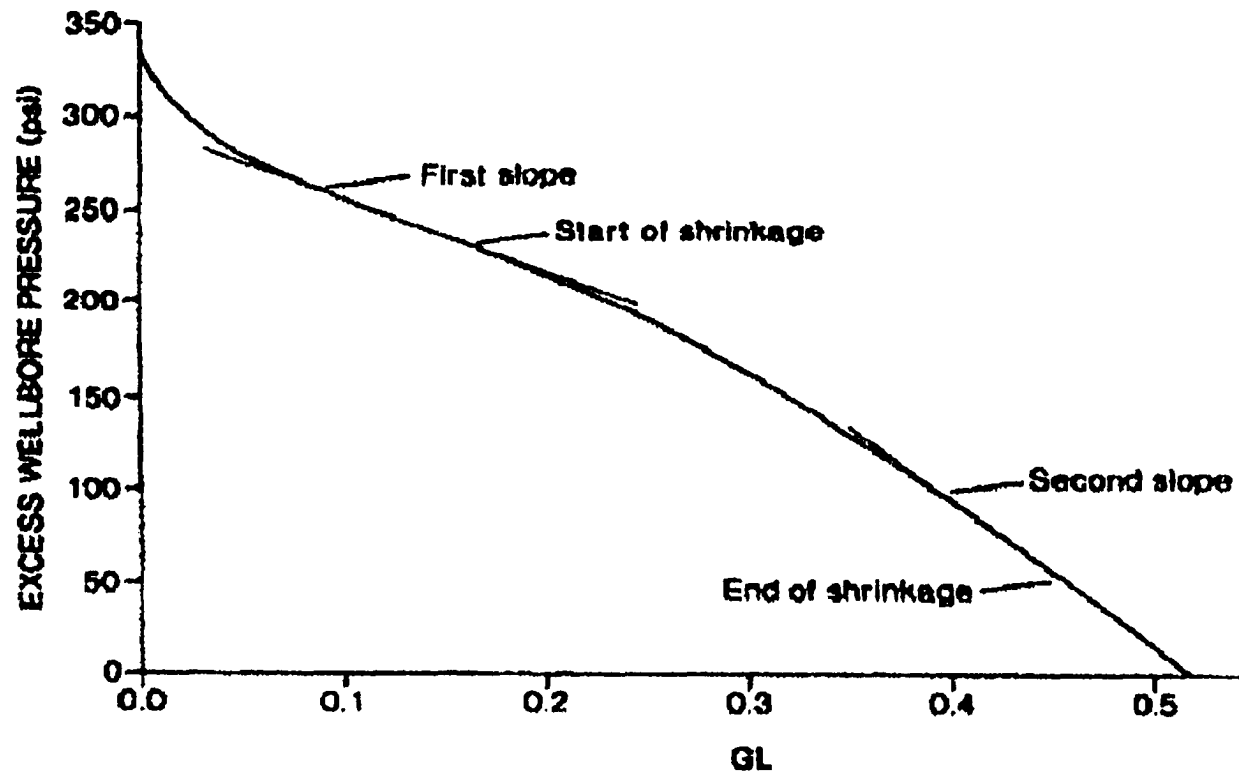


Fig. 2.10 – Excess wellbore pressure vs. GL function for stress contrast case, adapted after Gu. H⁴⁵

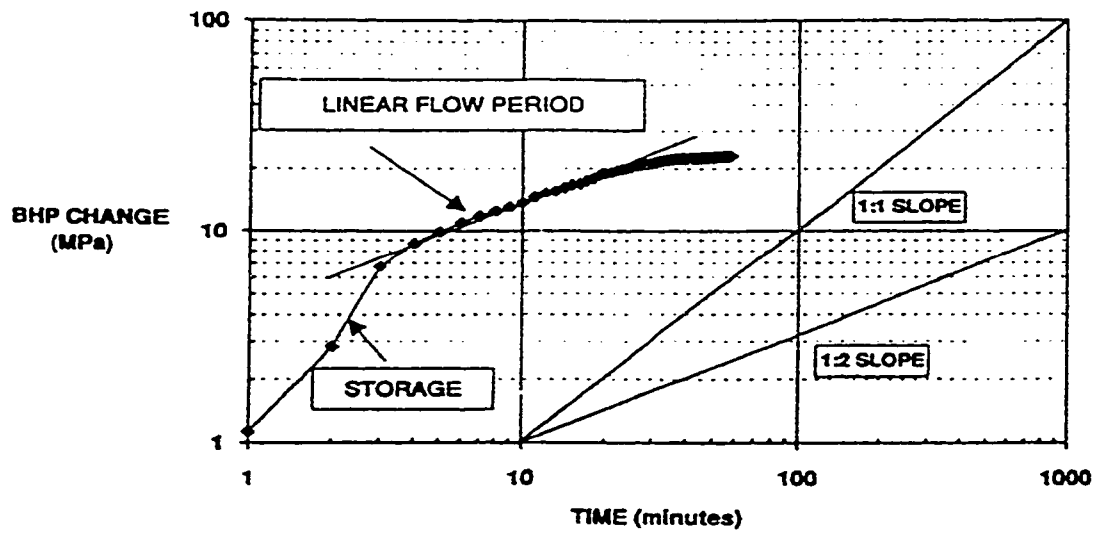
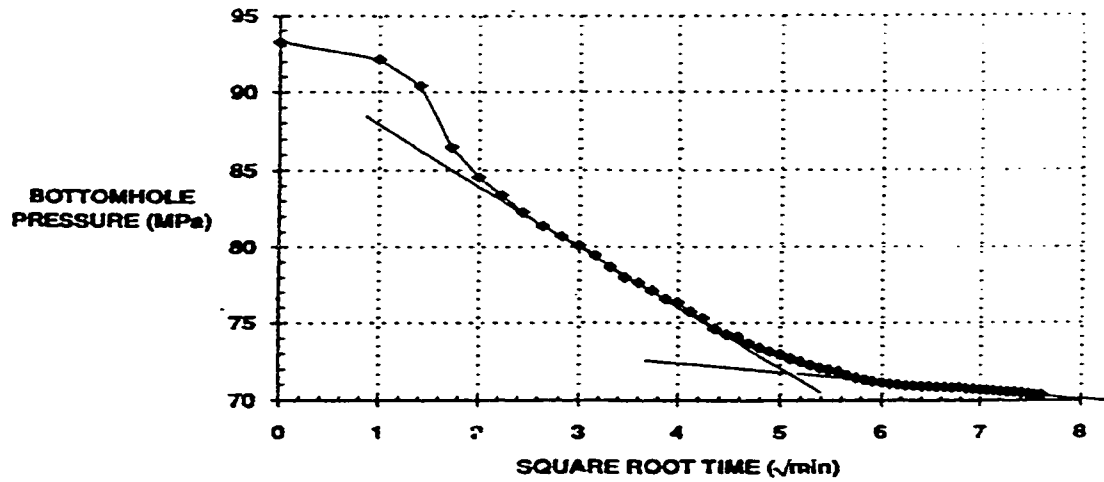


Fig. 2.11 – Bottomhole pressure vs. square root of time, and time, adapted after McLellan et al.⁷

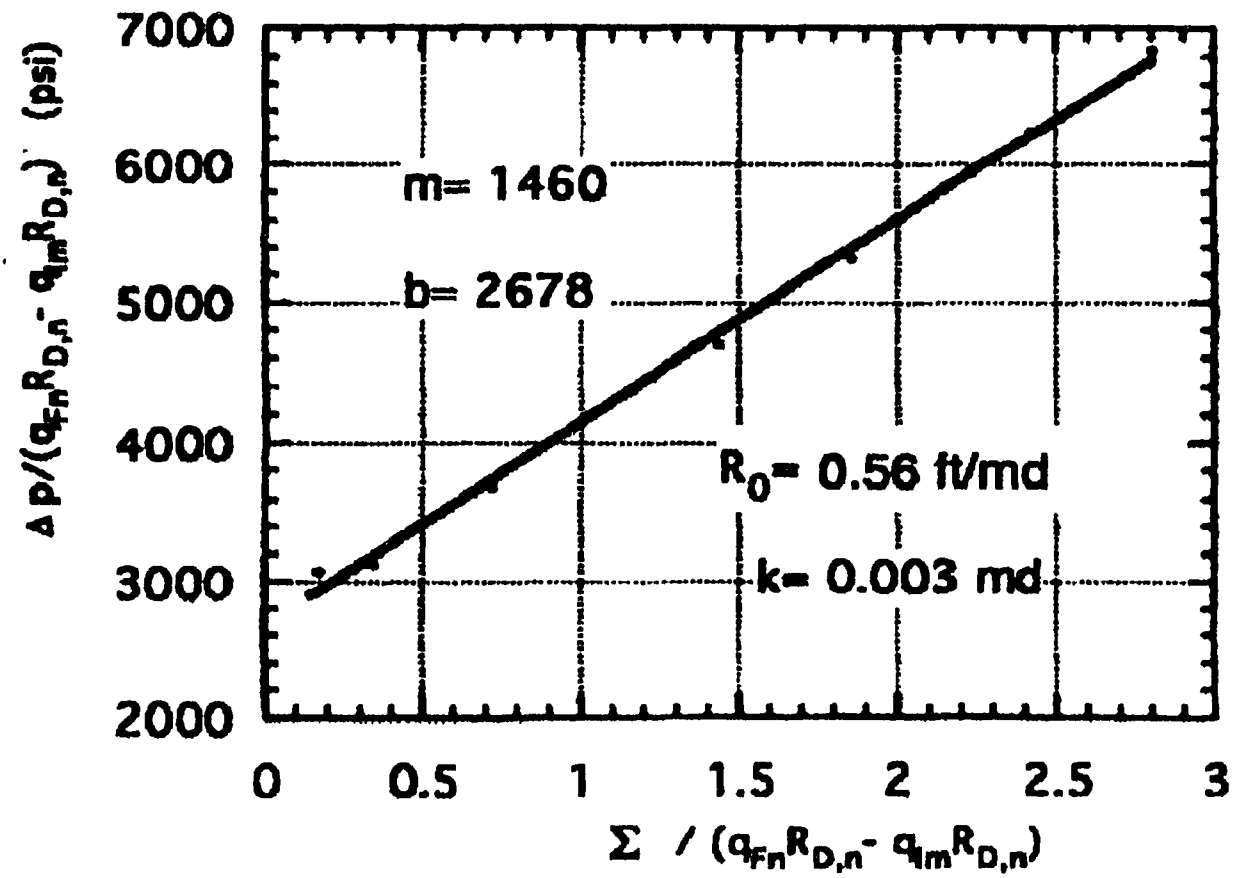


Fig. 2.12 – Specialized plot, adapted from Mayerhofer et al.⁵

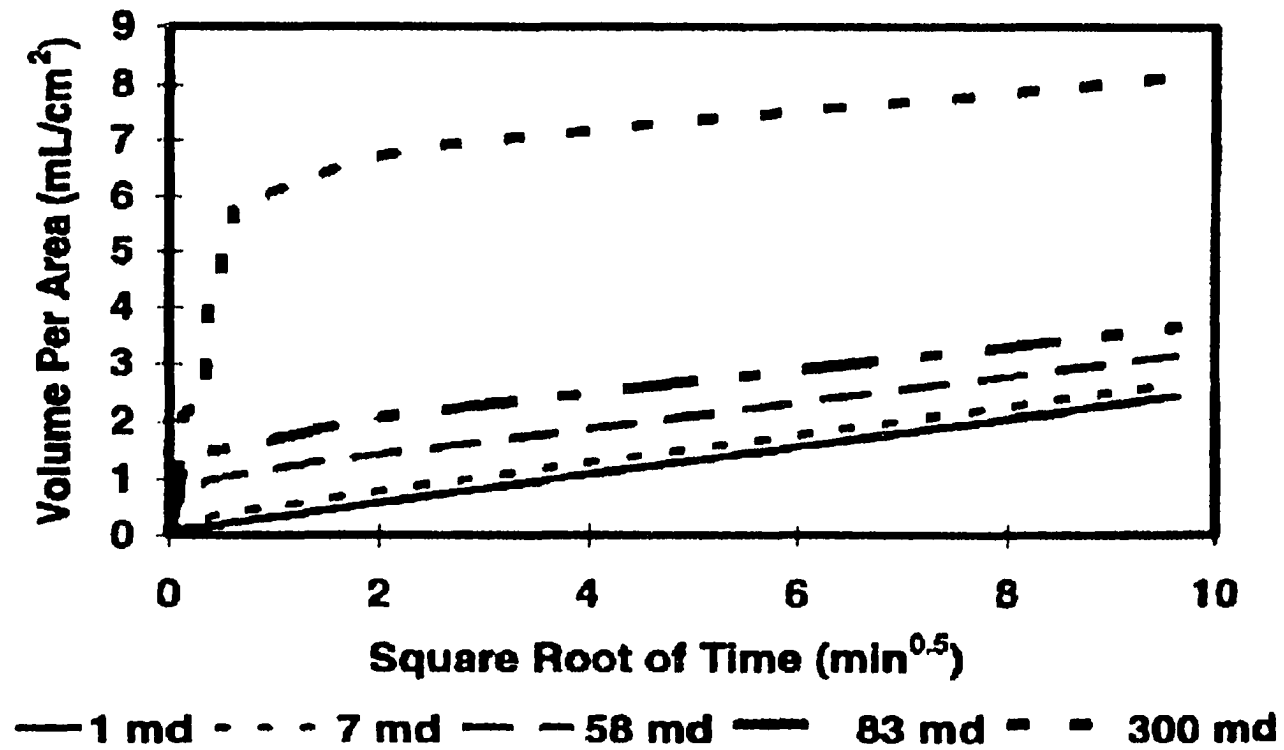


Fig. 2.13 – Effect of permeability on fluid leak-off, adapted from Dusterhoft et al.⁵²

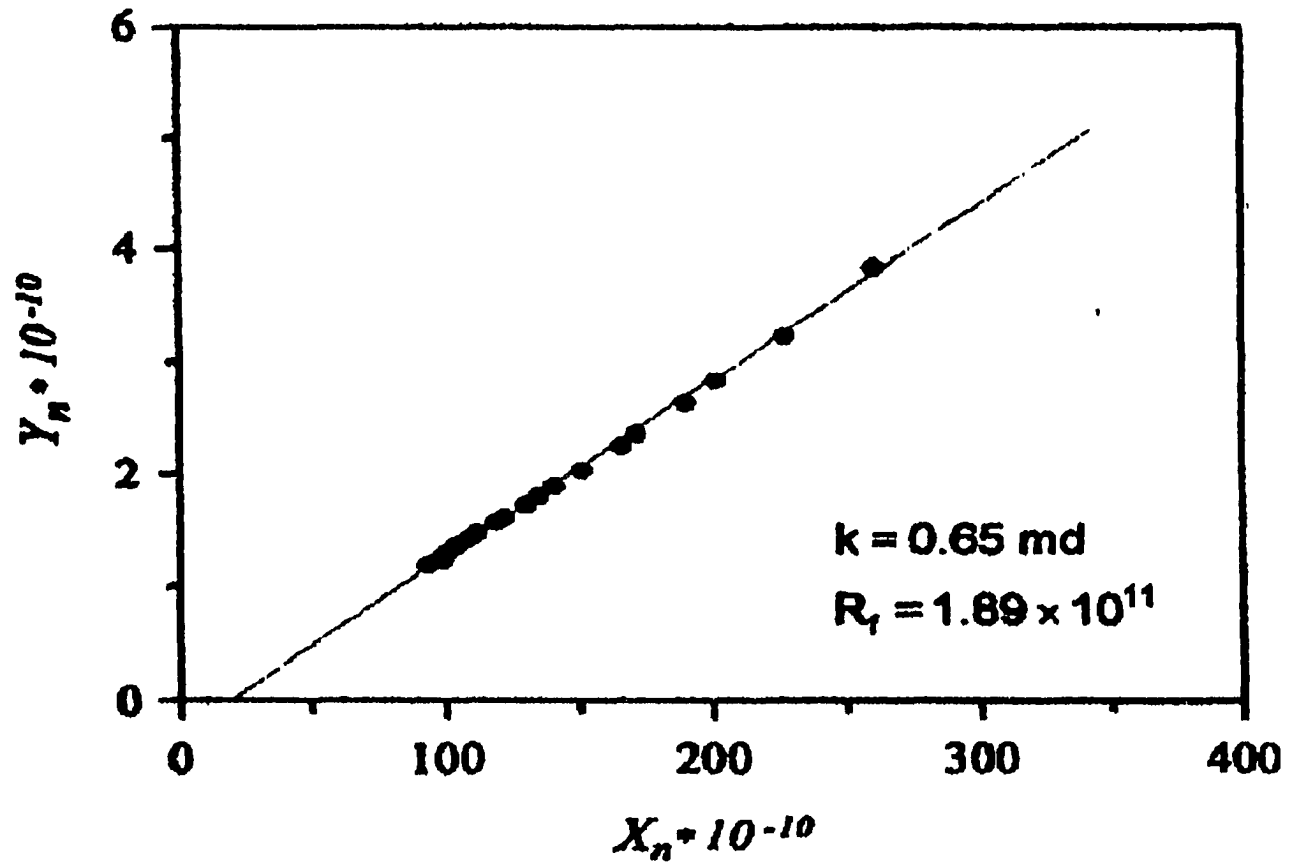


Fig. 2.14 – Plot for the determination of the reservoir permeability, k , and filter cake resistance, R_f , - case 1, adapted from Fan Young⁵⁸

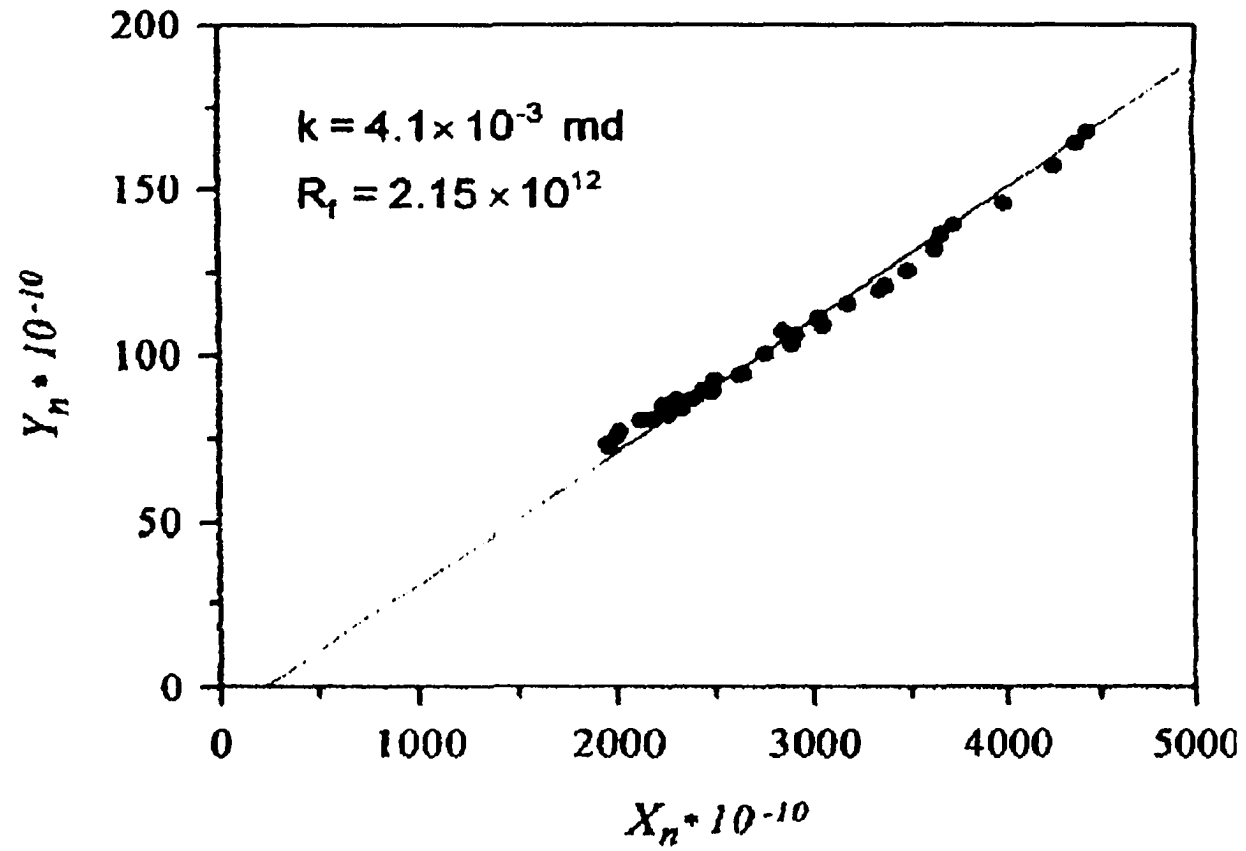


Fig. 2.15 – Plot for the determination of the reservoir permeability, k , and filter cake resistance, R_f , - case 2, adapted from Fan Young⁵⁸

CHAPTER 3

HYDRAULIC FRACTURING – THEORETICAL ASPECTS

3.1 Mechanics of Fracturing

The stress distribution, in an elastic medium, is based on the theory of linear poro-elasticity as developed by Geertsma, Timoshenko, Sneddon, Griffith and others^{53,54,55,56,57,58}. Let us consider an uncased vertical wellbore, under the action of horizontal in-situ stresses, σ_{\min} and σ_{\max} , as shown in Fig. 3.1. The breakdown pressure, P_b , will be given by the theory of elasticity as following^{57,58}:

$$P_b = 3\sigma_{\min} - \sigma_{\max} + \sigma_T \dots\dots\dots(3.1)$$

where:

σ_{\min} = minimum in-situ stress

σ_{\max} = maximum in-situ stress

σ_T = tensile failure stress of the rock

The theory of liner fractures in non-porous media, or the equilibrium of fractures in non-porous perfectly brittle materials, can help us (1) describe the stress distribution and deformation, under various loading conditions and (2) determine the stability of the fracture⁵⁹. Thus, approximating a linear fracture with a thin elliptic cut, and using the theory of elasticity, strains and stresses can be calculated.

Sneddon^{53,54} presented a solution of the two dimensional stress problem for a linear fracture in a non-porous medium, loaded with fluid under pressure and

subjected to compression at every location. For the case of uniform fluid pressure inside the fracture, and under plane strain conditions, he derived the following relation for the displacement in the direction perpendicular to the fracture:

$$w(x) = \frac{2(1 - \nu^2)}{E} \left(\sqrt{1 - \left(\frac{x}{L_f} \right)^2} \right) (P_f - S_h) \dots \dots \dots (3.2)$$

$w(x)$ = displacement in the direction perpendicular to the fracture

x = distance along the fracture from the fracture center

L_f = fracture half-length

P_f = fluid pressure in fracture

S_h = compressive stress applied at infinity

= Poisson's ratio

E = Young's modulus

Eq. (3.2) represents an ellipse with maximum width at the center of the wellbore.

Griffith, Irwin, and Barenblatt^{54,55,57}, presented the following methods for the elastic stress solution for the above presented system:

a) Griffith method

Using the energy balance, he determined the stability of the fractures.

Three forms of energy work are the main components of the balance equation (1) the

work energy, from outside the system, (2) the surface energy and (3) the elastic strain energy of the system. If no work is performed on the system, the increase in surface energy associated with fracture extension, is to be provided by the strain energy, which will decrease. In the case work is done on the system, it will be absorbed by the strain energy and the surface energy, and thus both will increase. However, in both situations, the energy balance can be written as following⁵⁷:

$$\frac{\partial U_f}{\partial L_f} - \frac{\partial W_f}{\partial L_f} = 0 \dots\dots\dots(3.3)$$

$$U_f = 4\gamma L_f h_m \dots\dots\dots(3.4)$$

$$W_f = \frac{\pi(1-\nu^2)L_f^2 h}{E} (P_f - S_h)^2 \dots\dots\dots(3.5)$$

where:

U_f = surface energy of the fracture

W_f = strain energy of the fracture

h_m = thickness of the elastic material

γ = specific surface energy of the elastic material

and substituting Eqs. (3.1) and (3.5) into Eq. (3.3) gives the minimum pressure above which fractures extend, or the maximum pressure below which fractures are stable:

$$P_{fp} = S_h + \sqrt{\frac{2E\gamma}{\pi L_f (1-\nu^2)}} \dots\dots\dots(3.6)$$

b) Irwin Method

Irwin further showed that fracture propagation conditions, as presented by Griffith, can be related to the stress distribution in the vicinity of the fracture tip⁵⁶ (Fig. 3.2), as follows:

$$\tau_{yy} = \frac{K}{\sqrt{2\pi \Delta x}} \dots\dots\dots(3.7)$$

where:

τ_{yy} = normal vertical stress

K = stress intensity factor, which is a function of fracture dimensions and loading,

and for a linear fracture is given by:

$$K = (P_{fp} - S_h) \sqrt{\pi L_f} \dots\dots\dots(3.8)$$

Also, the critical fracture toughness, K_{Icr} is considered, above which the fracture is bound to occur. Therefore, from Eq. (3.8), the fracture propagation pressure will be:

$$P_{fp} = S_h + \frac{K_{Icr}}{\sqrt{\pi L_f}} \dots\dots\dots(3.9)$$

c) Barenblatt method

Barenblatt⁵⁵ presents the most desirable solution to the problem of fracture stability, because he took into account the cohesion forces at the fracture tip, and showed that the fracture must close perfectly at the tip and that the stress at that

location remains finite.

For our case, a linear fracture loaded with fluid at a uniform pressure distribution inside of it, and subjected to the compressional stress, S_h , he derived the following equation that represents the fracture stability:

$$\frac{C}{\sqrt{2L_f}} = \int_0^{L_f} \frac{P_{fp} - S_h}{\sqrt{L_f^2 - x^2}} dx \dots\dots\dots(3.10)$$

where C is the cohesion modulus, also known as a material constant.

Following the integration of Eq. (3.10), the propagation pressure becomes:

$$P_{fp} = S_h + \frac{C}{\pi} \sqrt{\frac{2}{L_f}} \dots\dots\dots(3.11)$$

A comparison of Eqs. (3.6), (3.9) and (3.11) can lead to a relationship between the specific surface energy, γ , critical toughness, K_{Icr} , and cohesion modulus, C :

$$\frac{\pi E \gamma}{(1 - \nu^2)} = \frac{\pi}{2} K_{Icr}^2 = C^2 \dots\dots\dots(3.12)$$

3.2 Fluid Pressure Profile

On the other hand, referring at Fig. 3.4, the maximum pressure is the initial breakdown pressure, P_b , which is the pressure at which the fracture is being induced at the wellbore. Following this, the pressure drops to a propagating pressure and continues until the pumps shut-in. This is the time when the pressure suddenly

drops to a lower value but it continues to falloff, due to fluid leak-off from the fracture into the reservoir, until it finally reaches the reservoir pressure. The pressure value, at which the fluid flow into the fracture has ceased, it's called the instantaneous shut-in pressure (*ISIP*), which somewhat higher than the closure pressure, P_c .

Yew⁵⁸ indicated that Eq. (3.1) is valid for a perfectly elastic (brittle) medium, but in reality we have a porous medium through which fluid can flow. Using the poroelasticity theory Schmidt and Zoback⁶¹ modified Eq. (3.1) as follows:

a) for formations that are impermeable to the fracturing fluid,

$$P_b = \frac{3\sigma_{\min} - \sigma_{\max} + \sigma_T}{1 + \phi} \dots\dots\dots(3.13)$$

b) and for the case of permeable formations,

$$P_b = \frac{3\sigma_{\min} - \sigma_{\max} + \sigma_T - P_p \alpha_B \frac{1-2\nu}{1-\nu}}{1 + \phi + \alpha_B \frac{1-2\nu}{1-\nu}} \dots\dots\dots(3.14)$$

where:

P_p = pore pressure

ϕ = porosity

= Poisson's ratio for dry rock

$$\alpha = 1 - \frac{B_{dr}}{B_{sm}} = \text{Biot's constant, } 1 \geq \alpha \geq 0 .$$

3.3 Constant Height Fracture Models

If the wellbore is fractured at depths bellow 4,000-5,000 ft, then the fracture is expected to have an horizontal profile, but since the depth at which fractures are performed is higher than 5,000 ft, the fracture will be vertical and perpendicular to the minimum in-situ stress (Fig. 3.1). Also, Warpinski et al.^{64,65} studied the main two factors that control the vertical growth of the fracture, (1) the contrast in material properties and (2) the contrast in vertical distribution of in-situ stress, and found the latest to be predominant. Laboratory investigation led the authors to conclude that an in-situ stress contrast, which exceeds 400 psi, is sufficient to contain the vertical growth of the hydraulic fracture.

Three fracture models will be considered in this work: (1) the Khristianovic-Geertsma-de Klerk⁶⁴ -KGD model (Fig. 3.5), Perkins-Kern-Nordgren^{27,65} -PKN model (Fig. 3.6), and the Radial model (Figs. 3.7 and 3.8). The first two models are the basic constant height models. The radial geometry occurs when the vertical minimum in-situ stress has a uniform distribution, and is expected to take the shape of a circle. Mathematically is a two dimensional fracture similar to the constant height fracture models⁵⁸. Valko¹¹ presented a mathematical relationship of the ratio of permeable to total fracture surface area, for a case in which the total fracture height is higher than the permeable fracture height (Fig. 3.8).

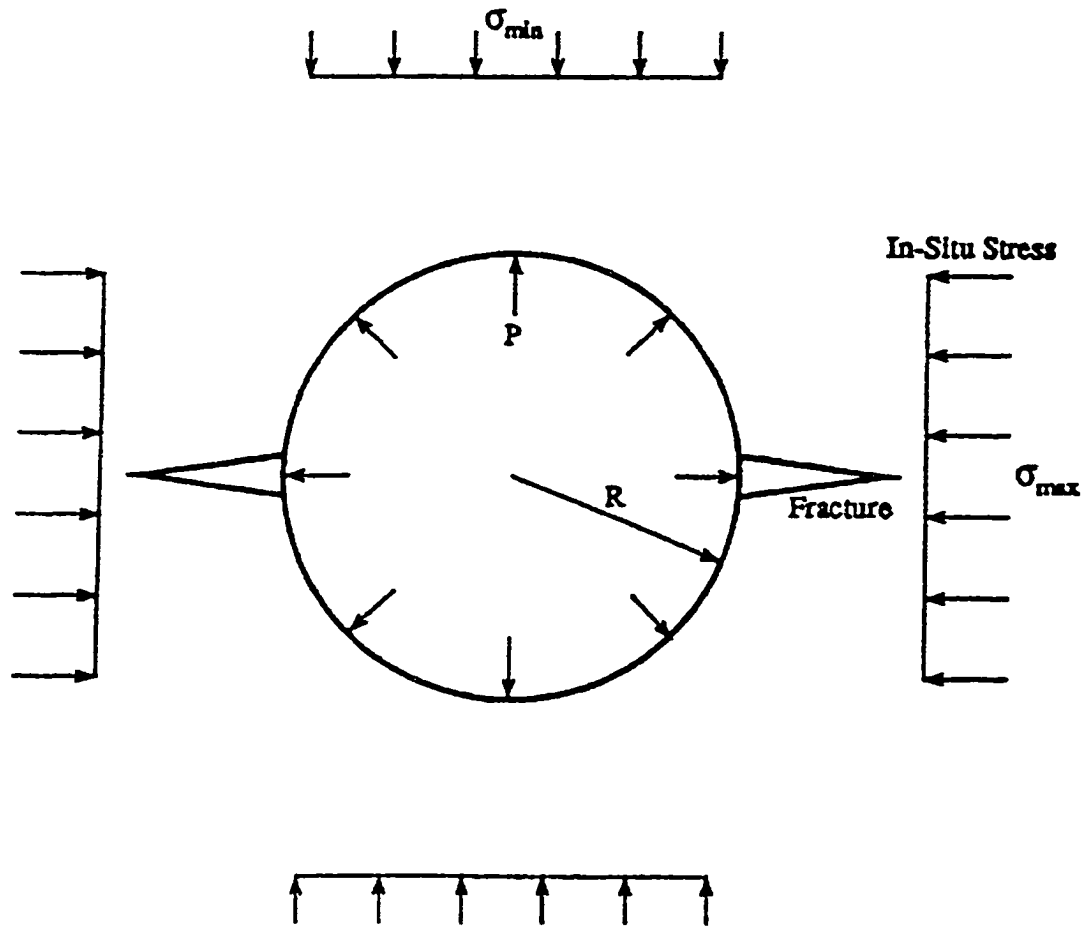


Fig. 3.1 – Horizontal section of a vertical wellbore under the action of in-situ stresses and hole pressure, adapted from Yew, C.H.⁵⁸

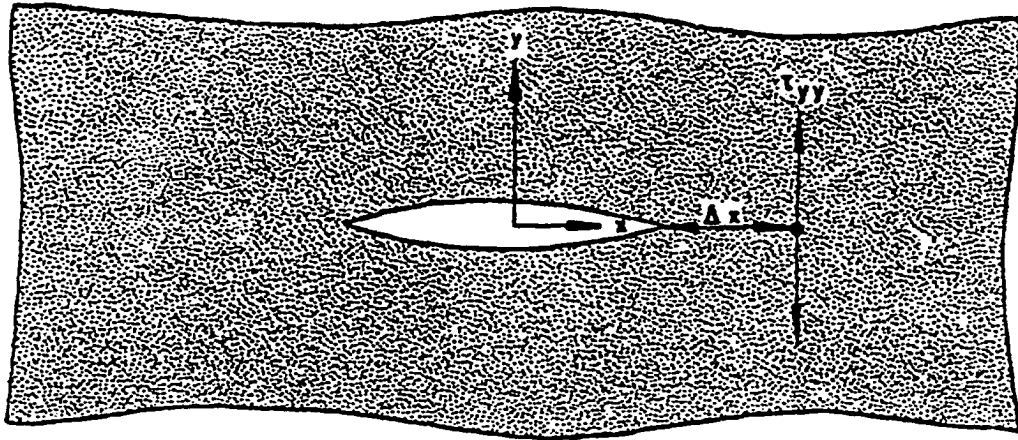


Fig. 3.2 – Normal stress at fracture tip, adapted from Hagoort⁶⁰

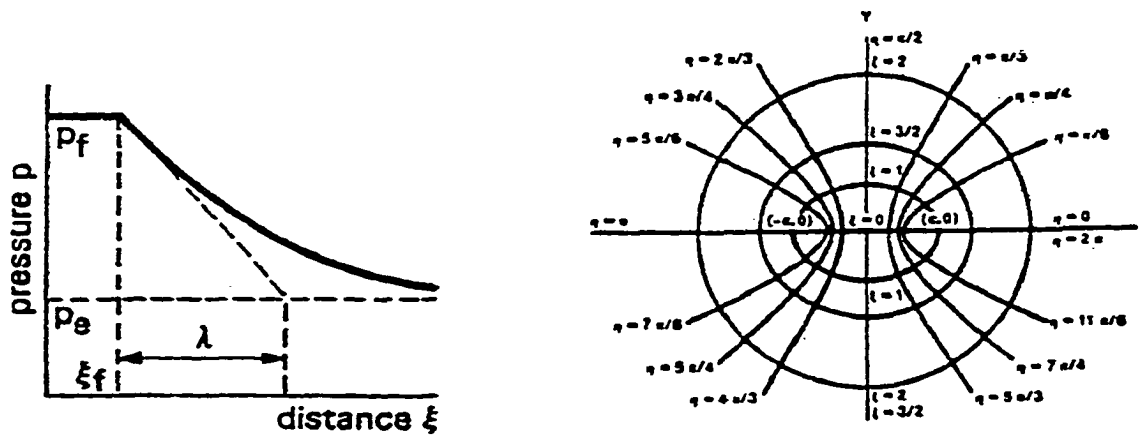


Fig. 3.3 – Pore pressure profile (left) and elliptic coordinates (right), adapted from Hagoort⁶⁰

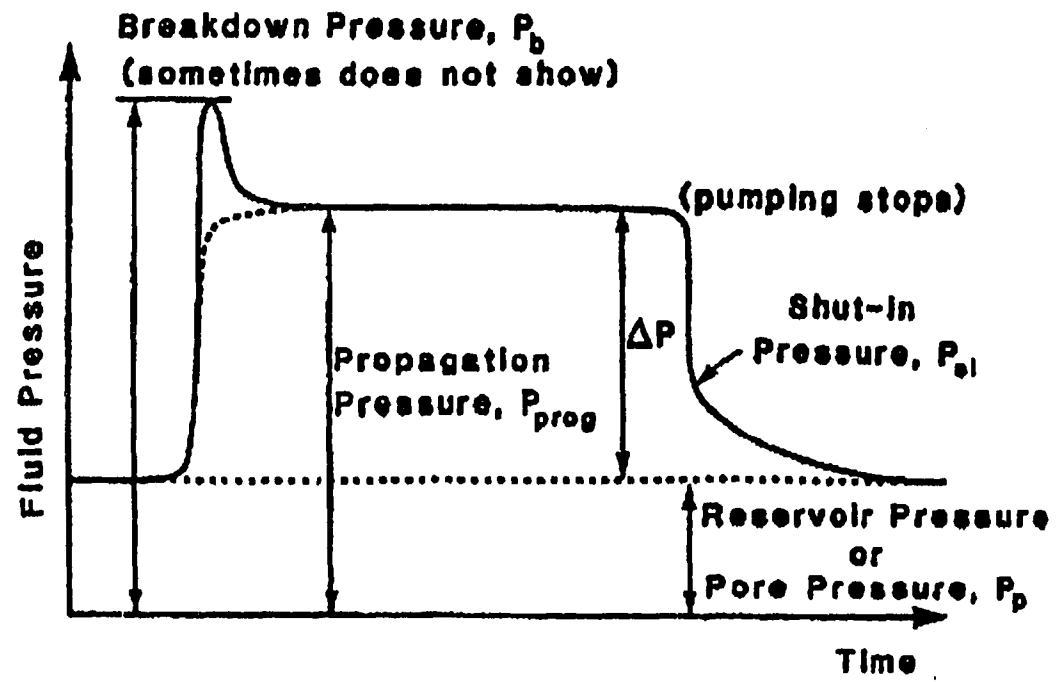


Fig. 3.4 – Downhole pressure profile, adapted from Yee, C.H.⁶⁴

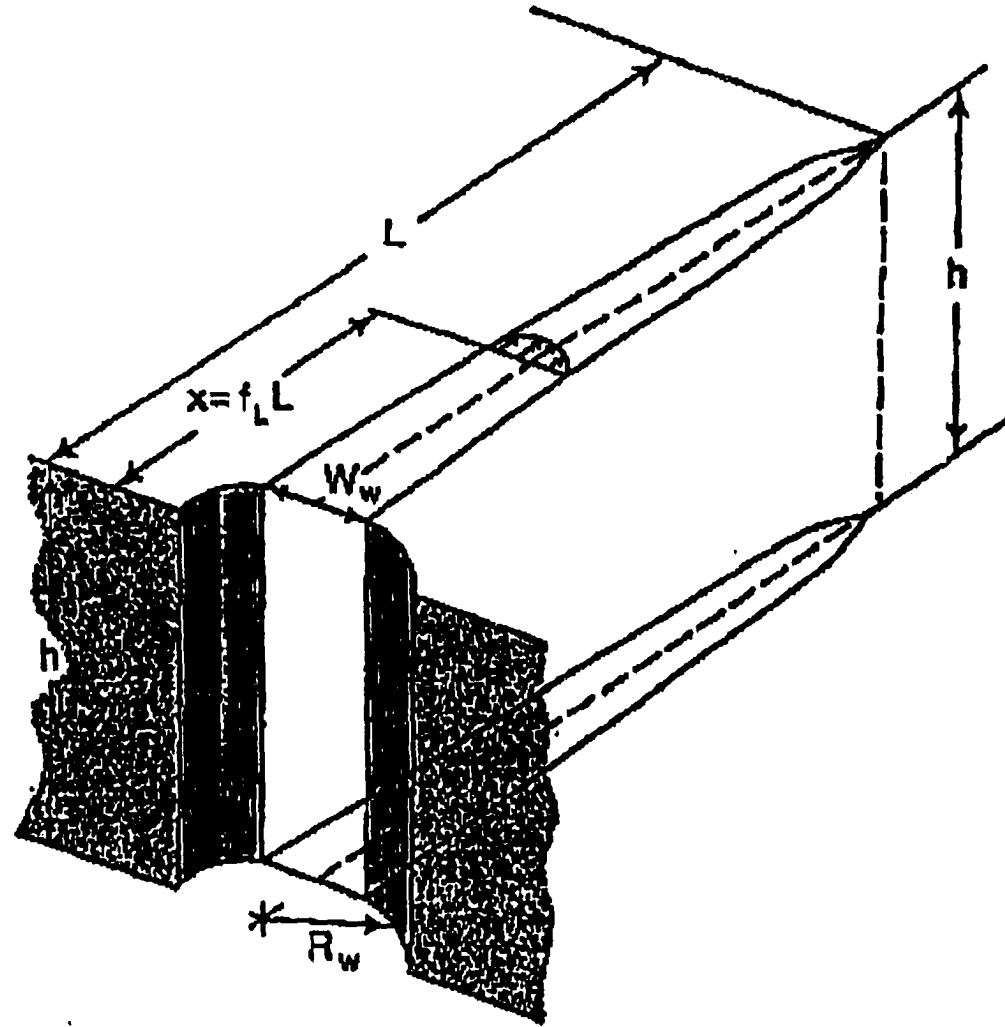


Fig. 3.5 – KGD constant height fracture model, adapted from Yew⁶⁴

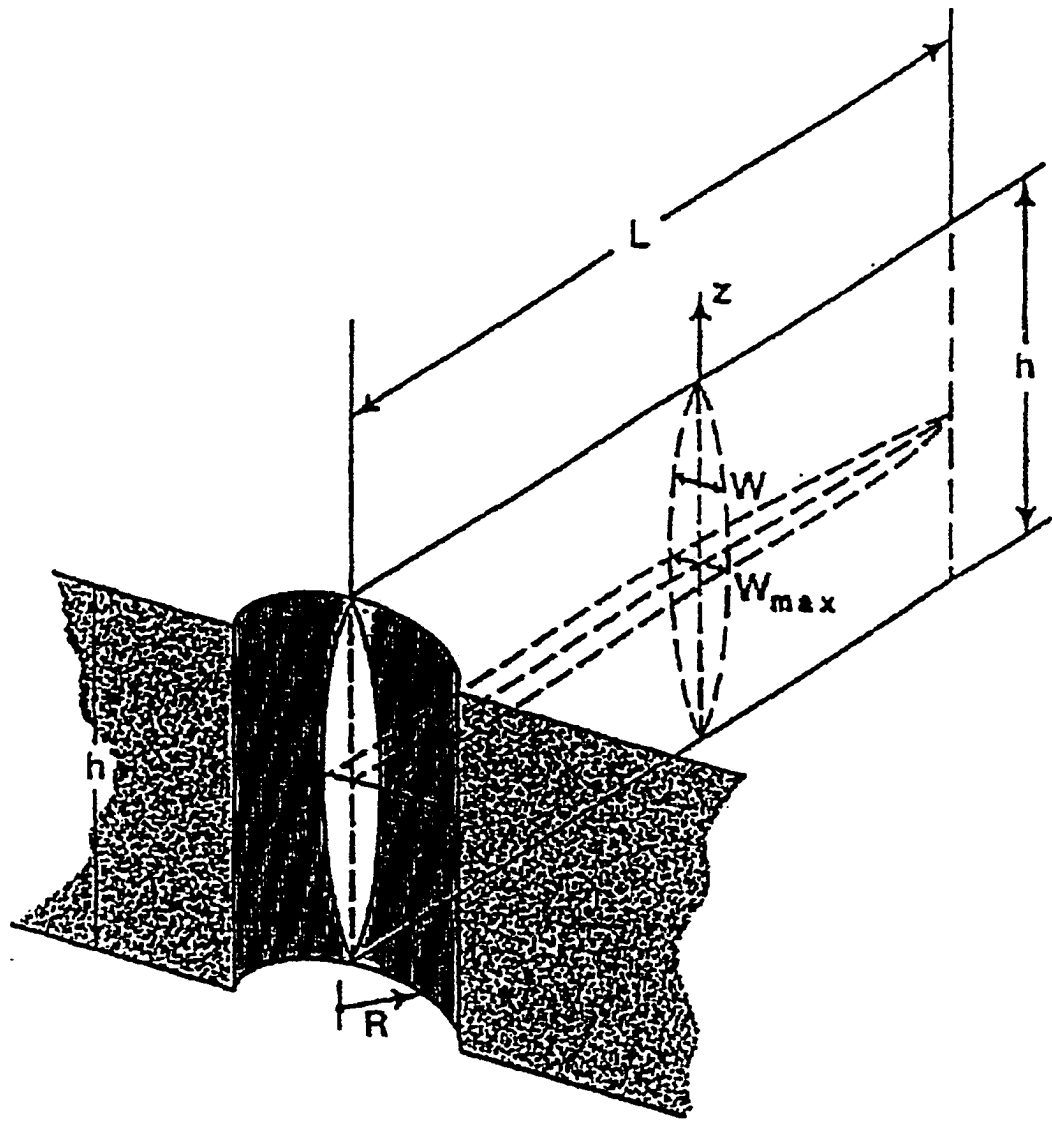


Fig. 3.6 – The PKN constant height fracture model, adapted from Yew⁵⁸

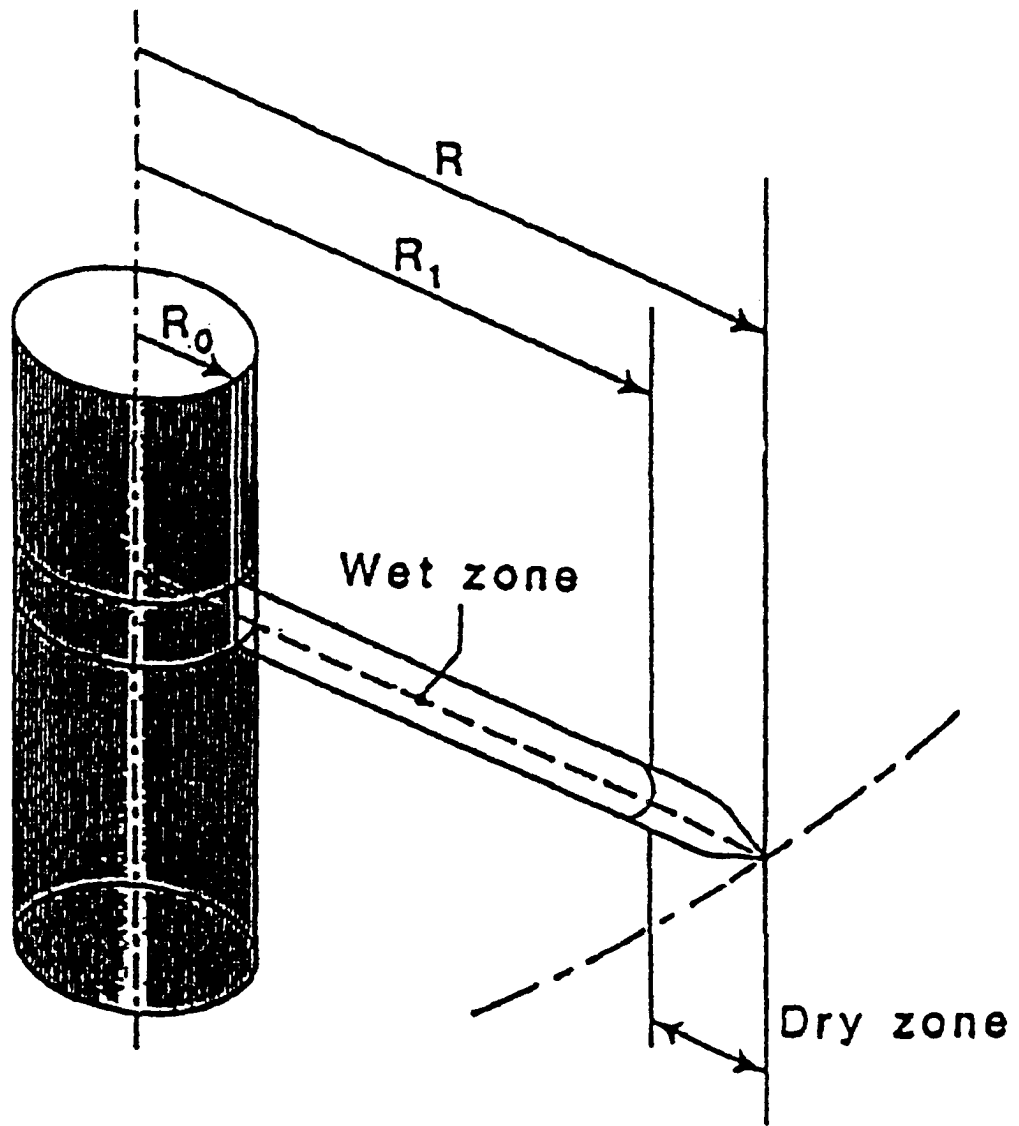
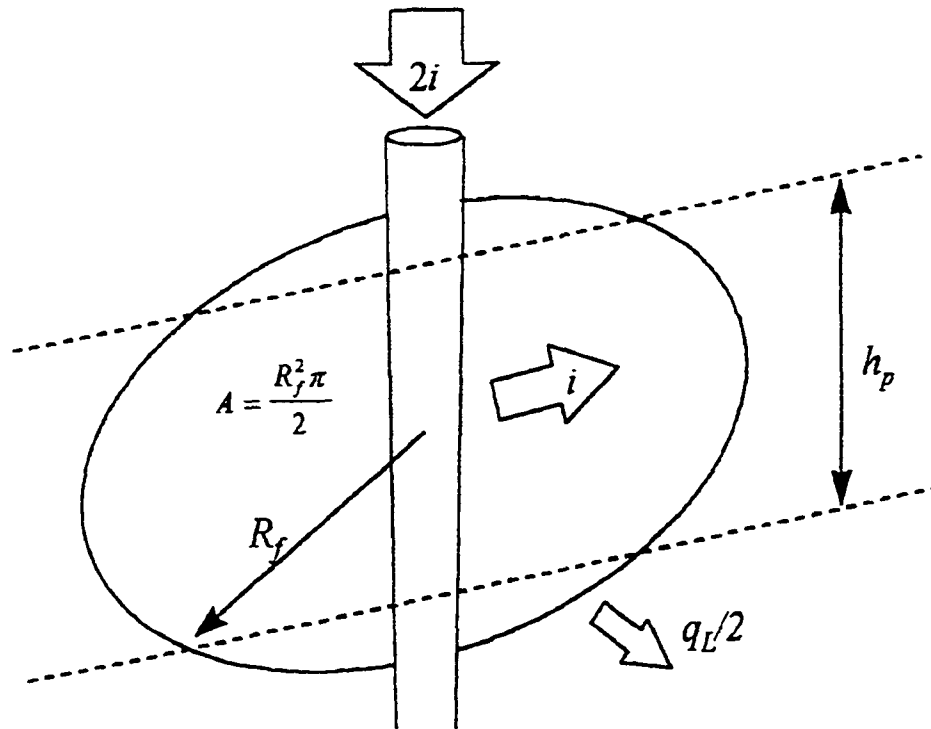


Fig. 3.7 – Circular fracture with dry zone, adapted from Yew⁵⁸



$$r_p = \frac{2}{\pi} \left\{ \frac{h_p}{2R_f} \left[\frac{h_p}{2R_f} \left(1 - \frac{h_p}{2R_f} \right) \right]^{0.5} + \arcsin \frac{h_p}{2R_f} \right\}$$

Fig. 3.8 – Radial geometry- ratio of permeable to total surface area, adapted from Valko and Economides¹¹

CHAPTER 4

A COUPLED MODEL FOR THE PREDICTION OF FLUID AND RESERVOIR PROPERTIES FROM MINIFRAC TESTS

4.1 Introduction

Ispas et al.¹² presented an improved model of an earlier version of minifrac analysis. This paper is based on two methods, used for the determination of the leak-off parameters from the pressure fall-off stage of a calibration treatment. The first method is the well known technology, which we have called the Nolte-Shlyapobersky^{3,14,33} method to determine an overall leak-off coefficient. The second method is an improved form of the Mayerhofer et al.^{13,15} technique, which attempts to de-couple the two main elements of the leak-off process: the filter-cake resistance and the transient flow in the formation.

4.2 Fracturing Fluid Coefficient

Carter's Leakoff Model

Carter (see the Appendix to the work of Howard and Fast⁶⁶), assumed that the leak-off velocity, u_L , is given by:

$$u_L = \frac{C_L}{\sqrt{t}} \dots\dots\dots (4.1)$$

where C_L is the leak-off coefficient, and t is the elapsed time since the start of the leak-off process. The integration of Eqs. (4.1 and 2.1) yields:

$$\frac{V_L}{A_L} = 2C_L\sqrt{t_p} + S_p \dots\dots\dots (4.2)$$

Where V_L is the volume of fluid loss through the fracture's surface, A_L , and the integration constant, S_p , is the spurt loss coefficient.

Nolte and Economides^{6,10} showed that application of Eq. (4.2) requires the tracking of the opening time of the different fracture elements during pumping. Therefore, if only the overall material balance is considered:

$$V_i = V + V_L \dots\dots\dots (4.3)$$

we can re-write Eq. (4.2) to reflect the opening time distribution factor, κ as follows:

$$V_i = V + \kappa(2A_p C_L \sqrt{t_p}) + 2A_p S_p \dots\dots\dots (4.4)$$

where V_i is the injected volume of fluid in one wing of the fracture, and V is the volume of one fracture wing at the end of pumping. Note that the group $2AS_p$ is the equivalent of the amount of loss volume due to spurt during treatment. This can also be expressed as $2A_p w_s$, since the spurt loss is the loss volume per fracture face area, and represents the fracture width loss due to spurt for both fracture faces.

The distribution factor, κ , is a dimensionless coefficient and multiplied with the fracture fluid leak-off coefficient, C_L , gives an equivalent fluid loss coefficient which will produce a total fluid loss during the pumping period.

On the other hand, the volume of fracturing fluid lost during pumping can be written as⁶:

$$V_L = \kappa (2A_p C_L \sqrt{t_p}) g(0) \dots\dots\dots(4.5)$$

Further, a relationship was derived for the determination of the opening time distribution factor, κ , as a function of the fluid efficiency as follows:

$$\kappa = \frac{(1 - \eta)\bar{w} - 2\eta S_p}{2\eta C_L \sqrt{t_p}} \dots\dots\dots(4.6)$$

or,

$$\eta = \frac{\bar{w}}{2\kappa C_L \sqrt{t_p} + \bar{w} + 2S_p} \dots\dots\dots(4.7)$$

The above shows that the term $2\kappa C_L \sqrt{t}$ can be considered the leak-off width, while $2S_p$, the spurt width, w_s . Note that the spurt loss has the units of length since it represents the ratio of the lost volume to the unit fracture face area. In essence, spurt loss can be represented as point sources moving with the tips of the fracture during its propagation. The spurt loss will cease as soon as the fracture propagation stops. This differentiates the spurt loss from the fracture leak-off coefficient, since the latest is distributed over the complete fracture surface, and stops

when the fracture closes. Noticeable is also the fact that the opening time distribution factor is only considered during the fluid pumping period, and it has a value of 1 after shut-in.

There are two primary effects that can cause increased loss during pumping, and that is the spurt loss and the opening of natural fractures, at some values of fluid injection pressure. Nolte⁶ addressed this in the following terms:

If the decline analysis is performed below the opening/closing value of pressure, the inferred conditions for fluid loss would not reflect the increase of fluid loss area, when the fissures were open. The actual loss for this case should be based on the area given by the sum of the permeable or loss area, and the open fissure area. Fluid loss to spurt occurs, as mentioned above, when a portion of the formation is first fractured and is generally assumed to essentially occur instantaneously. Therefore spurt loss will occur only during pumping and not after shut-in, when the fracture penetration is assumed to stop. Nolte¹¹ derived an equation for the determination of the loss volume during pumping, V_L , as follows:

$$V_L = 2\kappa C_L r_p A_f \sqrt{t_p} g_0 \dots\dots\dots(4.8)$$

where C_L is the fluid loss coefficient without open fissures or spurt (generally determined in the lab or from decline analysis), r_p is the ratio of permeable to fractured area, t_p is the injection or pumping time, and g_0 is the *G-function*, at a

shut-in dimensionless time $t_D=0$, with its corresponding values for the upper and lower boundaries⁶:

$$g_0 = \begin{cases} 4/3 \\ \pi/2 \end{cases} \dots\dots\dots(4.9)$$

From inspection of Eq. (4.8) for the loss volume resulting from time dependent fluid loss, with the effect of natural fractures opening during pumping included, it follows that:

$$\kappa = [1 + S_p / (C_L \sqrt{t_p} g_0)] (A_p + A_{of}) / A_p \dots\dots\dots(4.10)$$

where:

A_{of} is the open fissure area, and

$$\kappa_s = [1 + S_p / (C_L \sqrt{t_p} g_0)] \dots\dots\dots(4.11)$$

In the case where spurt loss, S_p , is expected to be significant, the spurt components, κ and κ_s , can be estimated from laboratory data for corresponding values of leak-off and spurt, as a function of the fracturing fluid and formation. A value of $\kappa_s=1$ indicates the absence of spurt loss, and $\kappa_s=5$ a significant spurt loss (up to 80-90 % in high permeable reservoirs)¹⁸.

When the model is applied to the pressure fall-off stage of a calibration treatment, some assumptions have to be postulated concerning the evolution of the

fracture face. The widely accepted assumption due to Nolte is that the evolution in time is according to a power law with a constant exponent, α , Eq. (2.4).

For such a case, Valko¹¹ developed the observed pressure equation in the wellbore during the fall-off period. This equation is based on Nolte-Shlyapobersky's^{9,10} theory:

$$p_w = \left(p_c + \frac{s_f V_i}{A_f} - 2s_f S_p \right) - (2s_f C_L \sqrt{t_p}) \times g(\Delta t_D, \alpha) = b_N + m_N \times g(\Delta t_D, \alpha) \dots \dots \dots (4.12)$$

where p_w and p_c are the sand face (wellbore) pressure and the fracture closure pressure respectively; V_i is the volume of fluid injected into one wing of the fracture; A_f is the fracture face area corresponding to one wing and one face, s_f is the fracture stiffness coefficient, (inverse of the compliance), t_p is the pumping time prior to the fall-off and Δt_D is the dimensionless ratio of the shut-in time to the pumping time. The $g(\Delta t_D, \alpha)$ function is a well-defined mathematical function related to the so-called Hyper-geometric function (later shown in this section). Note that the above equation, as given in earlier publications¹¹ lacks two important parameters: (1) the ratio of the permeable to fractured areas, r_p , and the ratio of the spatial pressure to wellbore average pressure, β_N . They assumed a confined fracture (not always true), and therefore $r_p = 1$. Another assumption was that the average spatial pressure to wellbore average pressure become equal as soon as the fracture

ceases to propagate (i.e. immediately after shut-in). This assumption is also questionable since the leak-off continues to take place after shut-in and until the fracture closes, and this sustains the fact that the ratio can not be considered equal to one.

Formulas for the computation of the fracture compliance, c_f , the fracture half length (i.e. x_f , corresponding to the PKN and KGD models, and R_f , for the Radial model) as well as the lost width, w_L , the leak-off coefficient, C_L , and the fluid efficiency, η , are presented in Appendix A.

The ratio of the leak-off volume to the product $2C_L A_f \sqrt{t_p}$ is denoted by $g_0(\alpha)$. Assuming that the fracture surface remains constant, after the fluid injection period, Nolte^{6,14} extended the definition as follows:

$$g(\Delta t_D, \alpha) = \frac{V_{L(t_p+\Delta t)}}{2C_L A_f \sqrt{t_p}} \dots\dots\dots(4.13)$$

where t_p is the injection time (end of pumping), Δt is the shut-in time, and $V_{L(t_p+\Delta t)}$ is the sum of the volume loss during the injection and shut-in times. However if the spurt loss would be considered, the total loss could be larger. The dimensionless shut-in time is given by:

$$\Delta t_D = \frac{t - t_p}{t_p} \dots\dots\dots(4.14)$$

Since the fluid leaks off and does not return into the fracture, $g(\Delta t_D, \alpha)$ should be a monotonically increasing function. Therefore, if we consider an elementary surface, dA (Fig. 2.2) which opens at time τ , and the differential of the leak-off flow rate as:

$$\frac{\partial V_L}{\partial t} = \frac{C_L}{\sqrt{t - \tau(A)}} dA \dots\dots\dots(4.15)$$

assuming that the history of the fracture surface growth (i.e. $A(\tau)$ and or its inverse function $\tau(A)$), is known¹¹). Next, the leak-off flow rate through both fracture faces will be given by the summation of each flow rate corresponding to surface elements at each other opening time, τ , as follows:

$$q_L = 2 \int_0^{A(t)} \frac{C_L}{\sqrt{t - \tau(A)}} dA \dots\dots\dots(4.16)$$

or,

$$q_L = 2 \int_0^t \frac{C_L}{\sqrt{t - \tau}} \frac{dA}{dt} d\tau \dots\dots\dots(4.17)$$

Note, that not all the fluid pumped into the fracture leaks-off, and therefore the fracture grows at the following grow rate:

$$q_{FGR}(w, A) = A \frac{dw}{dt} + w \frac{dA}{dt} \dots\dots\dots(4.18)$$

and the additional loss due to spurt corresponding to each new fracture surface, during the injection period and until the fracture propagation will cease, will be given by:

$$2S_p \frac{dA}{dt} \dots\dots\dots(4.19)$$

Carter²⁴ derived a material balance in terms of flow rates, showing that the injection rate, q_i , entering one wing of the fracture at time t is given by the sum of all the leak-off rates and the growth rate of the fracture volume as follows:

$$q_i = 2 \int_0^t \frac{C_L}{\sqrt{t-\tau}} \frac{dA}{dt} d\tau + A \frac{dw}{dt} + w \frac{dA}{dt} + 2S_p \frac{dA}{dt} \dots\dots\dots(4.20)$$

He found an analytical solution for Eq. (4.20), making the assumption that the fracture width is not variable (i.e. does not increase) while the fracture propagates. Thus the fracture face area at time t , $A(t)$, will be given by the following equation:

$$A(t) = \frac{(2S_p + w)q_i}{4C_L^2 \pi} \left[\exp(\beta_c^2) \operatorname{erf}(\beta_c) + \frac{2\beta_c}{\sqrt{\pi}} - 1 \right] \dots\dots\dots(4.21)$$

where:

$$\beta_C = \frac{2C_L \sqrt{\pi t}}{2S_p + w} \dots\dots\dots 4.22)$$

The value of the fluid loss volume through the elementary surface, dA , is obtained by the integration of Eq. (4.16), which between the opening time, τ , and the end of pumping, t_p , becomes:

$$dV_L = dA \int_{\tau}^{t_p} \frac{C_L}{\sqrt{t - \tau}} dt \dots\dots\dots (4.23)$$

where t is the actual time. Integration of Eq. (4.23) over the fractured face area, from zero to A_p (Fig. 2.2), gives the volume of fluid leak-off with respect to the surface as follows:

$$V_L = 2 \int_0^{A_p} \int_{\tau}^{t_p} \frac{C_L}{\sqrt{t - \tau}} d\tau dA \dots\dots\dots (4.24)$$

and substituting Eq. (4.24) into Eq. (4.13), the $g_0(\alpha)$ function can now be derived as follows:

$$g_0(\alpha) = \frac{1}{A_k} \int_0^{A_k} \frac{1}{\sqrt{t_p}} \left(\frac{dt}{\sqrt{t - \tau}} \right) dA \dots\dots\dots (4.25)$$

where the opening time is given by Nolte⁶ as:

$$\tau = t_p \left(\frac{A}{A_p} \right)^{1/\alpha} \dots\dots\dots(4.26)$$

or, in dimensionless variables:

$$t_D = \frac{t}{t_p} \dots\dots\dots(4.27)$$

$$A_D = \frac{A}{A_p} \dots\dots\dots(4.28)$$

$$\tau_D = \frac{\tau}{t_p} \dots\dots\dots(4.29)$$

A combination of Eqs. (4.25-4.29) yields:

$$g_0(\alpha) = \int_0^1 \left(\int_{\alpha \sqrt{A_D}}^1 \frac{dt_D}{\sqrt{t_D - \alpha \sqrt{A_D}}} \right) dA_D \dots\dots\dots(4.30)$$

or,

$$g_0(\alpha) = \frac{\alpha \sqrt{\pi} \Gamma(\alpha)}{\Gamma(1.5 + \alpha)} \dots\dots\dots(4.31)$$

Using the definition of the Euler Gamma function, and the Mathematica package, the following approximation was developed and incorporated into the program of the coupled model:

$$g_0(\alpha) = \frac{g_N(\alpha)}{g_M(\alpha)} \dots\dots\dots(4.32)$$

Both functions, $g_N(\alpha)$ and $g_M(\alpha)$, are shown in Appendix A.

In the case where $\Delta t_D \neq 0$, Eq. (4.30) becomes:

$$g(\Delta t_D, \alpha) = \int_0^1 \left(\int_{\alpha\sqrt{A_D}}^{1+\Delta t} \frac{dt_D}{\sqrt{t_D - \alpha\sqrt{A_D}}} \right) dA_D \dots\dots\dots(4.33)$$

Nolte⁶ gave a solution of the above equation for the upper and lower bound (i.e. $\alpha = 1$ and $1/2$ respectively, Eqs. 2.7 and 2.8). Valko and Economides¹¹ gave a closed solution of Eq. (4.33) for any value of α as follows:

$$g(\Delta t_D, \alpha) = \frac{4\alpha\sqrt{\Delta t_D} + 2\sqrt{1 + \Delta t_D} xF\left[1/2; \alpha; 1 + \alpha; (1 + \Delta t_D)^{-1}\right]}{1 + 2\alpha} \dots\dots\dots(4.34)$$

where:

$F\left[1/2; \alpha; 1 + \alpha; (1 + \Delta t_D)^{-1}\right]$ is the hyper-geometric function.

The program used to solve Eq. (4.33) is shown in Appendix A. Using the definition and properties of the hyper-geometric function, presented by Abramovitz and Stegun⁶⁷ :

$${}_2F_1[a, b; c; z] = \frac{\Gamma(c)}{\Gamma(b)\Gamma(c-b)} x \int_0^1 t^{b-1} (1-t)^{c-b-1} (1-tz)^{-a} dt \dots\dots\dots(4.35)$$

and using the Mathematica package, the hyper-geometric, HF , and $g(\Delta t_D, \alpha)$ functions can be computed as follows:

$$HF = F\left[1/2; \alpha; 1 + \alpha; (1 + \Delta t_D)^{-1}\right] = \frac{\Gamma[1 + \alpha]}{\Gamma[\alpha]\Gamma[1]} \left[\int_0^1 t^{\alpha-1} dt - (1 + \Delta t_D)^{-1} \int_0^1 t^{\frac{2\alpha-3}{2}} dt \right].$$

.....(4.36)

$$g(\Delta t_D, \alpha) = \frac{4\alpha\sqrt{\Delta t_D} + 2\sqrt{1 + \Delta t_D} x \frac{\Gamma[1 + \alpha]}{\Gamma[\alpha]\Gamma[1]} \left[\int_0^1 t^{\alpha-1} dt - (1 + \Delta t_D)^{-1} \int_0^1 t^{\frac{2\alpha-3}{2}} dt \right]}{1 + 2\alpha}$$

.....(4.37)

Approximate values of the G-function, $g(\Delta t_D, \alpha)$, where computed for all three geometries (PKN, KGD, and Radial), and are presented in Appendix A. Note that the fracture growth power law exponent, α , for the computation of the G-function of Eq. (4.34), has the following values: 4/3 for the PKN geometry, 2/3 for the KGD geometry, and 8/9 for the radial geometry. That corresponds to the case of a Newtonian fluid (i.e. the fluid rheology index, $n = 1$). However, in practice, the calibration treatment is performed with the same type of fluid that will later on be used for the actual fracture job, and thus the rheology must be considered. Nolte⁴ has shown that for injection of a power law fluid at a constant rate, the fracture growth power law exponent, α , can be found analytically for all three basic geometry models. He shown that by taking a derivative with respect to time of Eq. (4.26) in the

limit of high and low fluid efficiency, η , will lead to the following values for α :

$\alpha = \frac{1}{2}$ for the PKN and KGD models

$\alpha = \frac{1}{4}$ for the radial model

for the lower bound (i.e. $\eta = 0$), and

$$\alpha = \frac{2n + 2}{2n + 3} \text{ for the PKN model} \dots\dots\dots(4.38)$$

$$\alpha = \frac{n + 1}{n + 2} \text{ for the KGD model} \dots\dots\dots(4.39)$$

and

$$\alpha = \frac{2n + 2}{3n + 6} \text{ for the radial model} \dots\dots\dots(4.40)$$

Eqs. (4.38-4.40) were derived for the upper bound (i.e. fluid efficiency $\eta = 1$)

In essence, the importance of Eq. (4.12) is valid if it leads to a straight-line plot when pressure is plotted against the G-function. However, as mentioned earlier in this work, that is not always the case (see Figs. 1.1 b and 1.2).

In the case when a plot of the net pressure versus the G-function is a straight line, the slope m_N contains relevant information regarding the leak-off coefficient, C_L . Except for the PKN model, however, this information is not readily available, because the fracture stiffness contains the yet unknown fracture half-length or radius (see Appendix Eqs. A18 and A19). Therefore an additional assumption is necessary

to obtain the fracture extent. This assumption, postulated by Shlyapobersky, states that the spurt loss can be neglected and hence, the intercept b_N can be used to obtain the fracture extent. Since the no-spurt-loss assumption is an integral part of the methodology, the Nolte-Shlyapobersky method yields an essentially one-parameter description of the leak-off process.

4.3 Improved pressure decline model (P_w-II)

If Nolte's assumption (i.e. that the fracture area will evolve based on the power law model, Eq. (4.36), at a constant value of α following the shut-in time) is considered, then the fracture volume at the end of pumping is given by the total volume of fluid injected minus the sum of the volume due to spurt loss and leak-off, as follows:

$$V = V_i - (V_{sp} + V_L) \dots\dots\dots(4.41)$$

or,

$$V = V_i - 2r_p A_f S_p - 2r_p A_f C_L \sqrt{t_p} g(\Delta t_D, \alpha) \dots\dots\dots(4.42)$$

where the dimensionless time, Δt_D , is given by Eq. (4.14), as shown earlier in this chapter.

The actual fracture volume is given by the product of the permeable fracture face area, A_p , considered constant during the fall off period, and the average width of the fracture, \bar{w} . Note that the maximum fracture width corresponds to the end of the pumping time:

$$w = w(t_p) \dots \dots \dots (4.43)$$

and:

$$A_p = r_p A_f \dots \dots \dots (4.44)$$

where A_f is the fracture area, and the ratio between the permeable fracture area and the fracture area can be then written as follows:

$$r_p = \frac{A_p}{A_f} = \frac{x_f h_p}{x_f h_f} = \frac{h_p}{h_f} \dots \dots \dots (4.45)$$

Therefore substituting Eqs. (4.43) and (4.4) into Eq. (4.42), the actual fracture volume will be given by:

$$A_f \bar{w} = V_i - 2S_p r_p A_f - 2r_p A_f C_L \sqrt{t} g(\Delta t_D, \alpha) \dots \dots \dots (4.46)$$

And a combination of Eqs. (4.13) and (4.46) yields:

$$\bar{w} = \frac{V_i}{A_f} - 2r_p S_p - 2r_p C_L \sqrt{t} g(\Delta t_D, \alpha) \dots \dots \dots (4.47)$$

Note that what determines the fracture width variation is the G-function, $g(\Delta t_D, \alpha)$, the pumping time, t , the leak-off coefficient, C_L , and the spurt loss, S_p . We want to find a way by which to estimate the average fracture width decrease (i.e. the fracture closure process, or pressure decline). This can be done considering the fact that the

average fracture width, \bar{w} , is directly proportional to the net pressure, p_n (i.e. this is founded on the basic theory that describes the formation as a linear elastic medium⁷). Therefore, a relationship between the average fracture width, net pressure and fracture compliance, c_f , can be written as follows:

$$\bar{w} = p_n c_f \dots\dots\dots (4.48)$$

with::

$$p_n = p_w - p_c$$

where p_c is the closure pressure, or minimum in-situ stress, Eqs. (3.13) and (3.14), and the fracture compliance is given by Eqs. (2.17-2.19) for each fracture geometry.

The fracture compliance coefficient is the inverse of the fracture stiffness (i.e. stiffness can has the same role as Hook's constant). Consequently, the linear relationship given by Eq. (4.48), leads to a new form of Eq. (4.47), as a function of the net pressure, or:

$$P_w II = \left(p_c + \frac{V_i}{A_f c_f} - \frac{2r_p S_p}{c_f} \right) - \left(\frac{2C_L r_p \sqrt{t_p}}{c_f} \right) \times g(\Delta t_D, \alpha) = b_N + m_N \times g(\Delta t_D, \alpha) \dots\dots\dots (4.49)$$

A plot of the wellbore pressure, $P_w II$ versus the G-function, Eq. (4.49), should result in a straight line of slope, m_N , and intercept, b_N , if the fracture face area, fracture compliance and leak-off coefficient do not vary with time. From the slope

one can then determine the leak-off coefficient, C_L , and from the intercept the fracture average width, \bar{w} , the fracture half-length, x_f (for the PKN and KGD geometries), or R_f for the radial case, and the fracturing fluid efficiency, η . However, there are cases when a straight line can not be attained, Figs. (1.1b, 1.2, and 1.3), for reasons shown above and earlier in this work. Thus, if the plot is a curve, other means (See section 4.6) of analysis and interpretation should be employed to substitute for the above model (i.e. Eq. 4.49).

The above equation, although similar in format with the one derived earlier¹², Eq. (4.12), has the following new components in its structure, as a part of this work:

- a) The ratio of the fracture permeable to fracture height, r_p , as shown by Eq. (4.45)
- b) The ratio of the spatial average to the wellbore net pressure, β_N to account for the non-Newtonian fluid behavior. A derivative with respect to $g(\Delta t_D, \alpha)$ of Eq. (4.49) will lead to :

$$\frac{dP_w II}{d[g(\Delta t_D, \alpha)]} = \frac{2C_L \sqrt{t_p}}{c_f} \dots\dots\dots(4.50)$$

Where $c_f = c_f(\beta_N)$. This indicates that for a constant fracture face area, the only variable that can alter the linear behavior of the pressure versus the G-function, is β_N . Consequently a deviation from the ideal expected behavior as shown in Nolte's analysis⁴, Figs. (1.1a and 1.2) can be explained by the occurrence of fracture geometry changes, unlike the opinion of other

authors¹¹ who consider the ratio of spatial average to the wellbore net pressure, $\beta_N = 1$ after shut in. If the net pressure in the fracture were the same at all points, then a value of $\beta_N = 1$ would be valid. However, Nolte^{3,4} showed that during and after pumping there is fluid flow from the wellbore region to the extremities of the fracture, and this generates a pressure gradient until the fluid is completely lost into formation. Fig. 2.4 shows the simulated pressure and flow rate in a fracture both before and after shut-in³. In his study and analysis Nolte³ also shows that β_N prior and after pumping has different values due to flow rate and pressure gradient reduction in the entrance area of the fracture. Some authors erroneously consider the pressure reduction at shut-in a part of the pressure drop through the perforations. In this sense note that the fracture average width is constant immediately before and after shut-in. Consequently $\frac{\beta_p}{\beta_s}$ is equal to the ratio of the net pressure immediately before and after shut-in. In this work, the ratio of spatial average to the wellbore net pressure after shut-in, $\beta_s = \beta_{Ni}$, Eqs. (2.20-2.22) is considered, since we analyze the decline period of the test.

- c) Fluid rheology consideration for the computation of the maximum fracture width, w_{\max}^i as a function of the fracture average width, \bar{w} . The index i is used for the fracture geometry type. Pertinent equations are shown in section 4.4 of this chapter, and Appendix A.

d) Spurt loss, S_p , which can be implemented for all three geometries as shown in section 4.5 and Appendix A.

4.4 Non-Newtonian behavior of the fracturing fluid

A minifrac test implies the injection into the reservoir of a fluid with same or similar properties as the one later used for the completion of the actual frac job. Since viscosity of such fluids is one of the most important qualities associated with the fracturing fluid, Non - Newtonian behavior must be considered. Therefore the pressure decline model, Eq. (4.49), can be improved by incorporating the above mentioned fluid behavior. To do so, we need to add one additional equation which relates the equivalent Newtonian viscosity, μ_e with the flow rate, assuming power law behavior.

4.4.1 Fracture width equations for the basic 2D fracture geometries

To best describe the propagation of hydraulically induced fracture, we need to combine elasticity, fluid flow, and the material balance. Given the fluid injection history of the minifrac test, we can predict the evolution with time of the wellbore pressure and fracture dimensions. Since the height of a the fracture will be considered fixed in this work, the models presented will predict the other two dimensions, fracture half-length, x_f (i.e. PKN and KGD geometries) or R_f (i.e. radial geometry), and fracture average width, \bar{w} . From the elastic energy theory, the strain energy is the energy excess stored in the medium if a fracture is present. Sneddon⁵⁵

formulated a mathematical expression for a pressurized line crack which has an elliptical distribution, to evaluate the width of the crack as:

$$w(x) = \frac{4p_0^2}{E'} \sqrt{c^2 - x^2} \dots\dots\dots(4.51)$$

where p_0 is the constant pressure applied on the surface of both fracture faces from the inside, (Fig. 3.2), c is the fracture half-length (distance from the center of the fracture to its tip, and x is the variable distance from the center of the fracture.

The volume of one wing of the fracture, V , can be found by integrating Eq. (4.51) multiplied with the height of the fracture:

$$V = h_f \int_0^c \frac{4p_0^2}{E'} \sqrt{c^2 - x^2} dx = \frac{\pi p_{n0} h_f c^2}{E'} \dots\dots\dots(4.52)$$

The fracture average width can be found by dividing the fracture volume to its area:

$$\bar{w} = \frac{\frac{\pi p_{n0} h_f c^2}{E'}}{h_f c} = \frac{\pi p_{n0} c}{E'} \dots\dots\dots(4.53)$$

The volume for one wing of a radial crack¹¹ is given by:

$$V = \frac{1}{2} \int_0^{R_f} 2r\pi \left(\frac{8p_n}{E'} \sqrt{R_f^2 - r^2} \right) dr = \frac{8R_f^3 p_n}{3E'} \dots\dots\dots(4.54)$$

and the volume divided by area will yield the average fracture width:

$$\bar{w} = \frac{8R_f^3 p_n}{\left(\frac{\pi R^2}{2}\right) 3E'} = \frac{16 p_n R_f}{3\pi E'} \dots\dots\dots(4.55)$$

Daneshy²⁸, Valko and Economides¹¹, and other authors, showed that a shape factor, γ , is necessary to correct the average fracture width as a function of it's maximum value:

$$\gamma = \pi/5 \text{ for an elliptical cross sectional area (PKN geometry) } \dots\dots\dots(4.56)$$

$$\gamma = \pi/4 \text{ for a slot cross sectional area (KGD geometry) } \dots\dots\dots(4.57)$$

and

$$\gamma = \pi/4 \text{ for a radial cross sectional area (Radial geometry) } \dots\dots\dots(4.58)$$

4.4.1.1 PKN width equation

Perkins and Kern⁶⁵ considered zero net pressure at the tip of the fracture and the average fluid linear velocity at any location was approximated by the ratio of the injection rate, in one wing, and the cross sectional area. Also the pressure drop of a Newtonian fluid in an elliptical cross sectional area is given by:

$$\frac{\Delta p}{L} = \frac{64 \mu q}{\pi w_w^3 h_f} \dots\dots\dots(4.59)$$

where, w_w , is the maximum fracture width and is obtained from Eq. (4.51) at the

wellbore (i.e. $x = 0$). Assuming $c = h_f/2$, this becomes:

$$w_w = \frac{2h_f p_n}{E'} \dots\dots\dots(4.60)$$

Substituting Eq. (4.60) into Eq. (4.59) the following differential equation is obtained:

$$\frac{dp}{dx} = -\frac{8\mu qE'^3}{\pi h_f^4 p_n^3} \dots\dots\dots(4.61)$$

A solution of Eq. (4.61) is obtained by its integration between the wellbore and tip of the fracture, based on Perkins and Kern postulate that the net pressure at the tip of the fracture is zero:

$$p_n = \frac{1}{h_f} \sqrt[4]{\frac{32\mu E'^3 q x_f}{\pi}} \dots\dots\dots(4.62)$$

And combination of Eqs. (4.60) and (4.62) gives:

$$w_w = \sqrt[4]{\frac{512}{\pi} \frac{\mu q x_f}{E'^3}} = 3.57 \sqrt[4]{\frac{\mu q x_f}{E'^3}} \dots\dots\dots(4.63)$$

An estimated average fracture width, \bar{w} , is given by the wellbore maximum width multiplied with a shape factor¹¹, $\gamma = \pi/5$:

$$\bar{w} = \gamma w_w = 2.24 \sqrt[4]{\frac{\mu q x_f}{E'^3}} \dots\dots\dots(4.64)$$

4.4.1.2 KGD width equation

In a similar manner, as in the case of the PKN geometry, the maximum fracture width at the wellbore is estimated to be:

$$w_w = \sqrt[4]{\frac{336 \mu q x_f^2}{\pi E^3 h_f}} = 3.22 \sqrt[4]{\frac{\mu q x_f^2}{E^3 h_f}} \dots\dots\dots(4.65)$$

In this case the shape factor is considered as $\gamma = \pi/4$, and the average fracture width:

$$\bar{w} = \gamma w_w = 2.53 \sqrt[4]{\frac{\mu q x_f^2}{E^3 h_f}} \dots\dots\dots(4.66)$$

4.4.1.3 Radial width equation

In this case, the fracture width equation is¹¹:

$$\bar{w} = 2.66 \sqrt[4]{\frac{\mu q x_f^2}{E^3 h_f}} \dots\dots\dots(4.67)$$

and if we consider:

$x_f = h_f / 2 = R_f$, Eq. (4.67) becomes:

$$\bar{w} = 2.24 \sqrt[4]{\frac{\mu q R_f}{E}} \dots\dots\dots(4.68)$$

4.4.2 Equivalent Newtonian viscosity

Also known as the effective or apparent viscosity, the equivalent Newtonian viscosity is defined by Hagen-Poiseuille law (i.e. Eq. (4.59) for an elliptical cross sectional area). Based on this law and assuming power law fluid behavior, the following equations of the equivalent Newtonian viscosity for each geometry have been derived¹¹:

$$\mu_{ePKN} = K \left[\frac{1 + (\pi - 1)n}{n} \right]^n \left(\frac{2\pi \bar{v}}{w_w} \right)^{n-1} \dots\dots\dots(4.69)$$

$$\mu_{eKGD} = K \frac{2^{n-1}}{3} \left[\frac{1 + 2n}{n} \right]^n \left(\frac{\bar{v}}{w_w} \right)^{n-1} \dots\dots\dots(4.70)$$

$$\mu_{eRAD} = K 2^{n-1} \left[\frac{1 + 3n}{n} \right]^n (w_w)^{1-n} (\bar{v})^{n-1} \dots\dots\dots(4.71)$$

4.4.2.1 Modified maximum fracture width – PKN geometry

The average velocity, \bar{v} , of the fluid through an elliptical cross sectional area open to flow, is given by the ratio of the injection rate, q and the average cross sectional area, $\bar{w}h_f$:

$$\bar{v} = \frac{q}{\bar{w}h_f} \dots\dots\dots(4.72)$$

The fracture average width, considering the shape factor, Eq. (4.56), is:

$$\bar{w} = \gamma w_w = (\pi/5)w_w \dots\dots\dots(4.73)$$

and substituting Eqs. (4.69), (4.72), and (4.73) into Eq. (4.63), the maximum fracture width as a function of the equivalent Newtonian viscosity is obtained:

$$w_{wPKN}^{EN} = 3.57^{\frac{2}{n+1}} E'^{\frac{-1}{2n+2}} \left\{ 12.5^{n-1} Kx_f \left[\frac{1+n(\pi-1)}{n} \right]^n \left(\frac{1}{\pi} \right)^n q \left(\frac{q}{h_f} \right)^{n-1} \right\}^{\frac{1}{2n+2}} \dots\dots\dots(4.74)$$

4.4.2.2 Modified maximum fracture width – KGD geometry

The average velocity, \bar{v} , of the fluid through a slot cross sectional area open to flow, is given by the ratio of the injection rate, q , and the average cross sectional area, $\bar{w}h_f$:

$$\bar{v} = \frac{q}{\bar{w}h_f} \dots\dots\dots(4.75)$$

The fracture average width, considering the shape factor, Eq. (4.57), is:

$$\bar{w} = \gamma w_w = (\pi/4)w_w \dots\dots\dots(4.76)$$

and substituting Eqs. (4.70), (4.75), and (4.76) into Eq. (4.65), the maximum fracture width as a function of the equivalent Newtonian viscosity is obtained:

$$w_{wKGD}^{EN} = 3.22^{\frac{2}{n+1}} \left[\frac{2^{n-1}}{3} K x_f^2 \left(\frac{1+2n}{n} \right)^n \frac{q}{E' h_f} \left(\frac{16 q}{\pi^2 h_f} \right)^{n-1} \right]^{\frac{1}{2n+2}}$$

.....(4.77)

4.4.2.3 Modified maximum fracture width – Radial geometry

In a similar manner, as shown above for the other two geometries, the average velocity, \bar{v} , of the fluid through a radial cross sectional area open to flow, is given by

the ratio of the injection rate, q , and the average cross sectional area, $\pi \left(\frac{\bar{w}}{2} \right)^2$:

$$\bar{v} = \frac{4q}{\pi \bar{w}^2} \dots\dots\dots(4.78)$$

The fracture average width, considering the shape factor, Eq. (4.58), is:

$$\bar{w} = \gamma w_w = (\pi/4) w_w \dots\dots\dots(4.79)$$

and substituting Eqs. (4.71), (4.78), and (4.79) into Eq. (4.68), the maximum fracture width as a function of the equivalent Newtonian viscosity is obtained:

$$w_{wRAD}^{EN} = 3.57^{\frac{2}{n+1}} (4E')^{\frac{-1}{2n+2}} \left[3.225^{n-1} K \left(\frac{1+3n}{n} \right)^n q^n R_f^{2-n} \right]^{\frac{1}{2n+2}}$$

.....(4.80)

The above width equations, based on equivalent Newtonian viscosity, are incorporated into the main model.

4.5 Spurt loss estimation

Inspection of Eqs. (4.49 and 4.53:4.55), shows that it is possible to evaluate the spurt loss as follows:

PKN geometry:

$$S_{pPKN} = \frac{1}{2r_p} \left[\frac{V_i}{x_f h_f} - \frac{\pi \beta_{NPKN} h_f}{2E'} (b_N - p_C) \right] \dots\dots\dots(4.81)$$

KGD geometry:

$$S_{pKGD} = \frac{1}{2r_p} \left[\frac{V_i}{x_f h_f} - \frac{\pi \beta_{KGD} x_f}{2E'} (b_N - p_C) \right] \dots\dots\dots(4.82)$$

RADIAL geometry:

$$S_{pRAD} = \frac{1}{2r_p} \left[\frac{V_i}{\pi R_f^2} - \frac{16R_f \beta_{RAD}}{3\pi E'} (b_N - p_C) \right] \dots\dots\dots(4.83)$$

Note that Eqs. (4.81:4.83) have two unknowns, the spurt loss and the half fracture length. Several alternatives for the incorporation of spurt loss into the model, Eq. (4.49), will be presented next.

4.5.1 Material balance approach

The spurt loss can be estimated if additional information could be obtained by

coupling the end of the injection period with the instantaneous shut-in of a minifrac test¹¹. If the assumption that the fracture propagation will cease at the end of the pumping period is valid, then the average width should not change. Therefore the best straight line fit of the pressure versus the G-function, Eq. (4.49) can be used as following:

$$ISIP = b_N + m_N g_0(\alpha_i) \dots \dots \dots (4.84)$$

where:

ISIP is the instantaneous shut-in pressure and *i* is the index corresponding to the fracture geometry type.

4.5.1.1 Spurt loss approximation – PKN geometry

From Eq. (4.48) the average fracture width after injection can be estimated as:

$$\bar{w}_{ISIP}^{PKN} = (ISIP - Pc) c_f \dots \dots \dots (4.85)$$

Combining Eqs. (A-2, 4.63 , 4.84, and 4.85) and solving for the fracture half length, x_f yields:

$$x_f = 0.242 \left[\frac{(b_N + 1.41495 m_N - Pc) \beta h_f}{E'} \right]^4 \frac{E' t_p}{\mu V_i} \dots \dots \dots (4.86)$$

where: $1.41495 = g_0\left(\frac{4}{5}\right)$ corresponding to a shut-in time, $\Delta t = 0$.

Substituting Eq. (4.86) into Eq. (4.81), leads to an estimate of the spurt loss as follows:

$$Sp_{PKN}^{MB} = \frac{1}{2r_p} \left[\frac{4.13223E'^3V_i^2\mu}{h_f^5\beta_{PKN}^4t_p(b_N + 1.41495m_N - Pc)^4} - \frac{h_f(b_N - Pc)\pi\beta_{PKN}}{2E'} \right] \dots\dots\dots(4.87)$$

4.5.1.2 Spurt loss approximation – KGD geometry

From Eq. (4.48) the average fracture width after injection can be estimated as:

$$\bar{w}_{ISIP}^{KGD} = (ISIP - Pc)c_f \dots\dots\dots(4.88)$$

Combining Eqs. (A-3, 4.65 , 4.84, and 4.88) and solving for the fracture half length, x_f yields:

$$x_f = 2.594 \left[\frac{E'}{\beta_{KGD}(b_N + 1.47837m_N - Pc)} \right]^2 \left(\frac{\mu V_i}{E'h_ft_p} \right)^{1/2} \dots\dots\dots(4.89)$$

where: $1.47837 = g_0 \left(\frac{2}{3} \right)$ corresponding to a shut-in time, $\Delta t = 0$.

Substituting Eq. (4.89) into Eq. (4.82), leads to an estimate of the spurt loss as follows:

$$Sp_{KGD}^{MB} = \frac{1}{2r_p} \left[\frac{0.3855(b_N + 1.47837m_N - Pc)^2 V_i \beta_{KGD}^2}{E'^2 h_f (V_i \mu / h_f E' t_p)^{1/2}} - \frac{4.0746 E' (b_N - Pc) (V_i \mu / h_f E' t_p)^{1/2}}{(b_N + 1.47837m_N - Pc)^2 \beta_{KGD}} \right] \dots\dots\dots(4.90)$$

4.5.1.3 Spurt loss approximation – Radial geometry

From Eq. (4.48) the average fracture width after injection can be estimated as:

$$\bar{w}_{ISIP}^{RAD} = (ISIP - Pc) c_f \dots\dots\dots(4.91)$$

Combining Eqs. (A-4, 4.63 , 4.84, and 4.91) and solving for the fracture half length, R_f yields:

$$R_f = 1.447 \left[\frac{E'}{\beta_{KGD} (b_N + 1.37689m_N - Pc)} \right]^{4/3} \left(\frac{\mu V_i}{E' t_p} \right)^{1/3} \dots\dots\dots(4.92)$$

where: $1.37689 = g_0 \left(\frac{8}{9} \right)$ corresponding to a shut-in time, $\Delta t = 0$.

Note that the derivations above contain a G-function corresponding to a shut-in time, $\Delta t = 0$, since the *ISIP* value is read at that specific time.

Substituting Eq. (4.92) into Eq. (4.83), leads to an estimate of the spurt loss as follows:

$$Sp_{RAD}^{MB} = \frac{1}{2r_p} \left[\frac{0.152V_i}{\left(\frac{E'}{(b_N + 1.37689m_N - Pc)\beta} \right)^{8/3} \left(\frac{V_i\mu}{E't_p} \right)^{2/3}} - \frac{2.4565(b_N - Pc) \left(\frac{E'}{(b_N + 1.37689m_N - Pc)\beta} \right)^{4/3} \beta \left(\frac{V_i\mu}{E't_p} \right)^{1/3}}{E'} \right] \dots\dots\dots(4.93)$$

4.5.2 Laboratory measurements

Perhaps the most relevant information one can obtain about spurt loss, is from a lab test performed on a core sample taken from the reservoir selected for hydraulic fracturing. Carter²⁴ has shown, Eqs. (4.2 and 4.94), that the filtrate volume, V_{fc} , through a core sample during a period of time, t , will lead to the determination of spurt loss, V_{sp} . This can be obtained as the intercept of a plot of the filtrate volume versus the square root of time, as shown in Fig. 5.1.

$$V_{fc} = m\sqrt{t} + V_{sp} \dots\dots\dots(4.94)$$

If the spurt loss can be evaluated, via one of the above indicated procedures or other

methods (i.e. Fig. C-43), then the fracture half length can be evaluated for each fracture geometry, as a function of the spurt loss. This can be obtained from Eqs. (4.49 and 4.81:4.83) as follows:

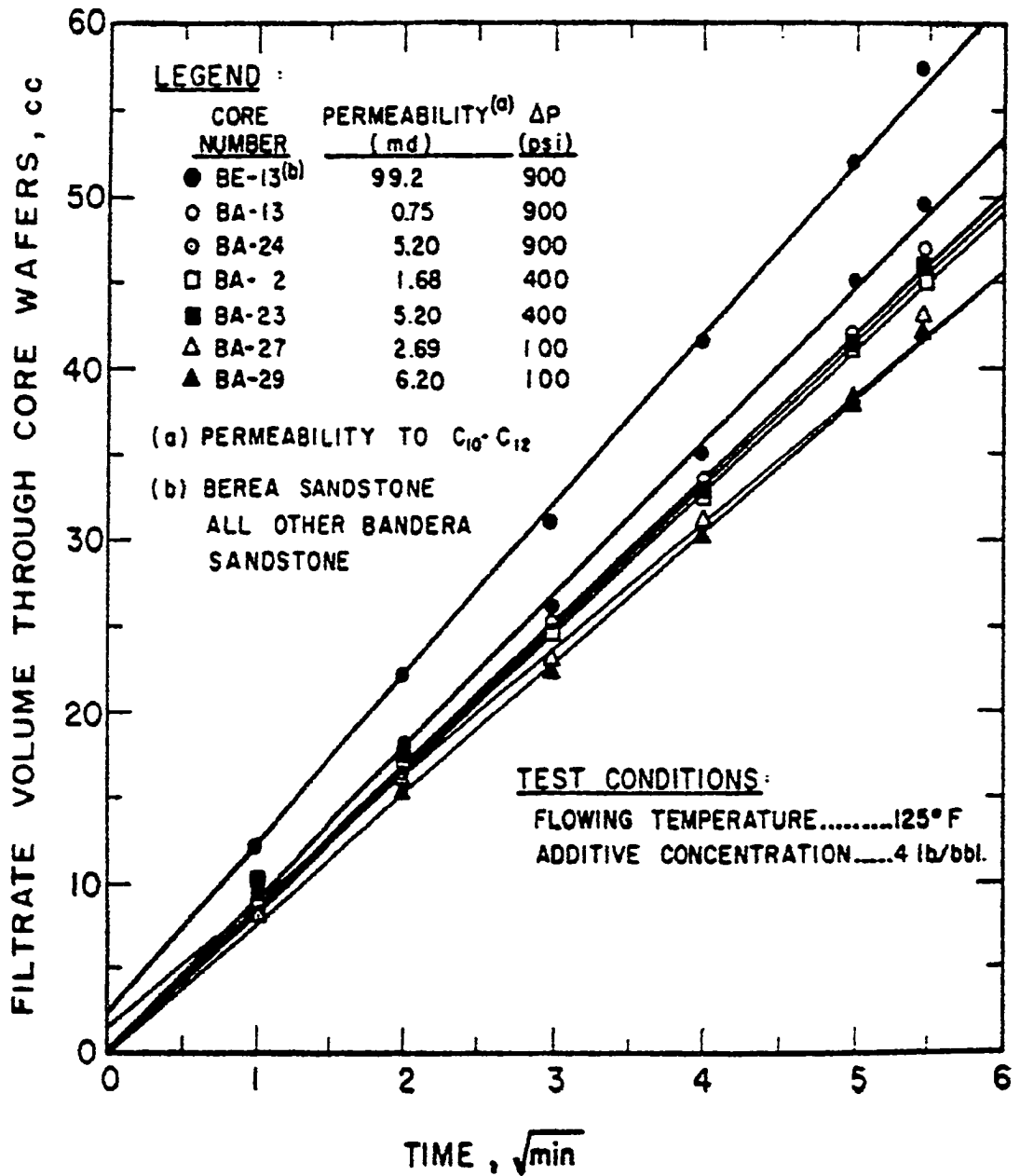


Fig. 4.1 – Fluid loss characteristics, adapted from Carter²⁴

4.5.3 Spurt loss from synergy analysis

Nolte^{8,51} provides a technical framework for adding after-closure fracturing-pressure analysis to the pre-treatment calibration-testing sequence that defines fracture geometry and fluid-loss characteristics. A companion paper⁸ provides the general framework for applying this analysis and for its integration with the other parts of the testing sequence.

In his work, he shows that the after-closure period contains the reservoir pseudo-linear flow period that is the focus, and the pseudo-radial flow period that has been previously addressed in a comprehensive manner. Radial flow defines the reservoir parameters. The primary roles for linear-flow are to define spurt loss, after a calibration treatment, and to use the reservoir's perspective of the fracture length to validate information available from other parts of the calibration sequence. The focus of this paper is on after-closure pseudo-linear flow. As discussed in the more general presentation, reservoir linear-flow provides the last link for the fracturing-pressure chain-of-events. This chain gives a continuum of increasing information about the fracture geometry, fracturing fluid, and reservoir with feedback to validate or question prior information. The proposed timeline of events (and information) begins with a small-volume injection (for closure pressure) and shut-in (for reservoir transmissibility and initial pressure); pumping the fracture calibration treatment (for fracture geometry characteristics); the shut-in closure-decline (for total fluid-loss coefficient and fracture length to validate geometry); the period immediately after closure (for separating the various fluid-loss mechanisms and validating closure pressure); after-closure linear-flow (for spurt-loss and to validate fracture length); and

in the case of high-permeability, transitional flow (for validating various parameter combinations) and radial-flow (for validating reservoir transmissibility and initial pressure).

An effective and compact way of including spurt loss is to define a dimensionless spurt coefficient that depends on the spurt value (S_p , having the dimension of length) and the total fluid-loss coefficient, as shown below and earlier in this work:

$$\kappa \equiv 1 + \left[S_p / (g_0 C_T \sqrt{t_p}) \right]; \quad \eta = \frac{V_{fp}}{V_i}; \dots\dots\dots(4.94a)$$

$$V_{LP} = 2g_0 \kappa C_T A \sqrt{t_p} = (1 - \eta)V_i; \quad g_0 \rightarrow \frac{\pi}{2}, \eta \rightarrow 0 \dots\dots\dots(4.94b)$$

These equations also show that the selected definition for the spurt coefficient produces a simple multiplication with the loss coefficient. The definition also implies that for no spurt loss, $\kappa = 1$, Eq. (4.94c) gives the interpretation for values greater than unity; e.g., $\kappa = 5$ reflects 80% of the fluid loss, during pumping, coming from spurt-loss.

$$V_{L\kappa} / V_{LP} = \{\kappa - 1\} / \kappa; \quad V_{L\kappa} / V_{LT} = (\kappa - 1)(1 - \eta) / \kappa \dots\dots\dots(4.94c)$$

The difficulty here consists of the fact that the spurt loss coefficient, κ , was determined empirically (i.e. simulations^{8,51}) and of non-uniqueness when trying to delineate the correct slope corresponding to a pseudo-linear flow regime. However,

the study presented by Nolte is very well documented and deserves further consideration.

4.5.4 Fracture half-length determination as a function of spurt loss – PKN

Substituting the spurt loss in Eq. (4.81) and solving for the fracture half-length leads to:

$$x_f = \frac{2E'V_i}{\pi h_f^2 \beta (b_N - P_c) + 4h_f E' r_p S_p} \dots\dots\dots(4.95)$$

4.5.5 Fracture half-length determination as a function of spurt loss – KGD

A similar substitution of the spurt loss in Eq. (4.82), and solving for the fracture half-length, will result in:

$$x_f = \frac{2E' \left[\sqrt{(h_f r_p S_p)^2 - \frac{\pi h_f \beta}{2E'} (b_N - P_c) V_i} - h_f r_p S_p \right]}{\pi h_f \beta (b_N - P_c)} \dots\dots\dots(4.96)$$

4.5.6 Fracture half-length determination as a function of spurt loss – Radial

If we substitute the spurt loss in Eq. (4.83), the following polynomial equation will result:

$$AR_f^3 + BR_f^2 + C = 0 \dots\dots\dots(4.97)$$

One real and two complex solutions where found solving Eq. (4.97):

$$R_1 = \frac{\left(3A\sqrt{4B^3 + 27A^2C}\sqrt{3C} - 2B^3 - 27A^2C\right)^{1/3}}{3A\sqrt[3]{2}} + \frac{\sqrt[3]{2}B^2}{3A\left(3A\sqrt{4B^3 + 27A^2C}\sqrt{3C} - 2B^3 - 27A^2C\right)^{1/3}} - \frac{B}{3A} \dots\dots\dots(4.98)$$

$$R_2 = \frac{(1 - I\sqrt{3})\left(3A\sqrt{4B^3 + 27A^2C}\sqrt{3C} - 2B^3 - 27A^2C\right)^{1/3}}{6A\sqrt[3]{2}} - \frac{(1 + I\sqrt{3})B^2}{3A\sqrt[3]{4}\left(3A\sqrt{4B^3 + 27A^2C}\sqrt{3C} - 2B^3 - 27A^2C\right)^{1/3}} - \frac{B}{3A} \dots\dots\dots(4.99)$$

$$R_2 = \frac{(1 + I\sqrt{3})\left(3A\sqrt{4B^3 + 27A^2C}\sqrt{3C} - 2B^3 - 27A^2C\right)^{1/3}}{6A\sqrt[3]{2}} - \frac{(1 - I\sqrt{3})B^2}{3A\sqrt[3]{4}\left(3A\sqrt{4B^3 + 27A^2C}\sqrt{3C} - 2B^3 - 27A^2C\right)^{1/3}} - \frac{B}{3A} \dots\dots\dots(4.100)$$

The real solution, Eq. (4.98), will be retained for the computation of the fracture half length, R_f , where:

$$A = 16\pi\beta(b_N - P_c) \dots\dots\dots(4.101)$$

$$B = 6\pi^2 S_p r_p E' \dots\dots\dots(4.102)$$

$$C = -3V_i \pi E' \dots\dots\dots(4.103)$$

4.5.7 Spurt loss estimation by use of a high pressure simulator

Lord et al.⁷³ describes the results of fluid-loss tests conducted with various hydraulic fracturing fluids through the use of a large-scale, high-temperature, high-pressure simulator that has several unique capabilities. Among these capabilities is the ability perform dynamic fluid loss experiments over a large surface area under 1,000 psi differential pressure. Fig. C-43 shows that significant spurt loss can be identified (i.e. 69 gal/100 ft²) in a porous medium that has only a permeability of 6.9 md.

4.5.8 Spurt loss from empirical correlations

Ridha⁷⁴ shows in his work empirical equations for the estimation of spurt loss:

$$S_p = 0.2510^{-3} k_r (P_{inj} - P_i) \text{ without Matriseal}$$

$$S_p = 0.5010^{-4} k_r (P_{inj} - P_i) \text{ with Matriseal}$$

Inspection of the above equations clearly indicate that spurt loss is not a negligible fluid loss component, and that is direct proportional with the reservoir permeability.

4.6 Pressure derivative model ($P_w'II$)

Castillo³¹, introduced a modified fracture pressure decline analysis model, including pressure-dependent fluid leak-off. This is an improvement indeed, since Nolte's initial derivations assumed the leak-off coefficient as a pressure-independent constant. However, his assumption is valid for the case in which the leak-off is controlled by a compressible filter cake, with the exception where leak-off is primarily controlled by filtrate viscosity, by an incompressible filter cake, or by reservoir permeability and compressibility.

Castillo introduced new pressure derivative plots (Figs. 2.8 and 2.9), for fracture pressure decline analysis, that determines the fracture parameters ($ISIP, P_C, P^*$), required in the Nolte leak-off calculations. In essence he took a derivative of the wellbore pressure with respect to the G-function and plotted this versus the shut-in time. His claim is that one can determine the fracture end of extension and the closure pressure with its corresponding time. However, a closer look at these plots, (Figs. 2.8 and 2.9), show no uniqueness based on which one could infer the above parameters, and thus the method is inconclusive, because we can not accurately delineate the fracture parameters from these plots. And by no means, should use of these plots

replace the stress tests (i.e. pump-in flow-back test) used for the determination of closure stress.

Instead, if we take a derivative with respect to time, *and not the G-function*, of Eqs. (2.7 and 2.8), corresponding to the upper and lower limits, then the following can be obtained:

$$P_w' H = m_N' F(t) \dots \dots \dots (4.104)$$

Eq. (4.104) should be a straight line of slope, m_N' given by the following relationship:

$$m_N' = - \frac{4r_p C_L \sqrt{t_p}}{c_f t_p} \dots \dots \dots (4.105)$$

and

$$F(t)_u = \left(1 + \frac{t}{t_p}\right)^{1/2} - \left(\frac{t}{t_p}\right)^{1/2} \dots \dots \dots (4.106)$$

for the upper bound, and

$$F(t)_L = \frac{1}{t_p} \left\{ \frac{1}{2} \left(\frac{t_p}{t}\right)^2 - \left[\frac{1+t}{2t_p \sqrt{1 - \left(1 + \frac{t}{t_p}\right)^2}} \operatorname{Arcsin} \left(1 + \frac{t}{t_p}\right)^{3/2} \right] \right\} +$$

$$\frac{1}{\text{Arcsin}\left(1 + \frac{t}{t_p}\right)^{3/2}} \quad \dots\dots\dots(4.107)$$

for the lower bound.

In the case where a plot of the pressure versus the G-function of Eq. (4.49) leads to a curve instead of a straight line, any analysis would be inconclusive since no correct slope, m_N , or intercept, b_N , can be delineated, Figs. (1.1b, 1.2, and 1.3). Consequently, a plot of the pressure derivative, $P_w'II$, versus $F(t)_j$ will enable us to more accurately delineate the correct slope of a line that best fits the curve or a section of it. This is possible since Eq. (4.51) must have a zero intercept.

Note that only the pressure derivative for the upper bound can be used, since the lower bound $F(t)_L$, Eq. (4.54), is a function of $\text{ArcSin}(1 + t/t_p)$, and can not be computed for values of $t/t_p > 0$. However Nolte^{3,14} showed, Fig. 2.3, that the difference between the two bounds is within acceptable limits (i.e. error less than 10 %).

4.7 Filtercake–Reservoir Flow Leakoff Model

Mayerhofer^{13,15,16} published a filter-cake reservoir flow leak-off model. In his model he considers the total pressure drop between the fracture and the reservoir as follows:

$$\Delta p(t_n) = \Delta p_{face}(t_n) + \Delta p_{res}(t_n) + \Delta p_{pimvz}(t_n) \dots\dots\dots(4.108)$$

where $\Delta p_{face}(t_n)$ is the pressure drop across the fracture face dominated by the filter-cake. It is considered steady-state in the sense, that it depends on the flow through the filter-cake, but not on its history. On the other hand, $\Delta p_{res}(t_n)$ is the pressure drop in the reservoir, having a truly transient nature (i.e. depending on not only the actual flow but also on the history of the leak-off process). The third component of Eq. (4.108) is the pressure drop across the polymer invaded zone, $\Delta p_{pimvz}(t_n)$. Its influence was studied^{11,13,16} and found to be negligible.

In this approach the first term has one determinable parameter: the filter-cake resistance, Eq. (4.24), and the second term contains the other determinable parameter, the formation permeability, Eq. (4.27). While the first parameter is mostly the property of the fracturing fluid and can be affected by the composition, the second parameter is the property of the formation and is a given for the fracturing engineer.

From the Mayerhofer et al.^{13,15} technique two parameters are sought: the filter-cake resistance, R_o , and the reservoir permeability. A short review of the main components of his model for pressure transient behavior is presented in chapter 2 of this work, Eqs. (2.35-2.42). However, the following observations are delineated in regard to the method:

1. The methodology, requires a significant level of simulations, computations and plotting, based on estimated values for the fracture area, A_f , at any time during the injection period as a function of the volume injected, of the pressure drop and its derivative. Not only is the method difficult to apply, since often times none of

the expected behavior matches the field data, but how can one determine the fracture area and the leak-off rate as the fracture grows? In essence, during the fracture propagation the leak-off rates, q_{Lj} , are not exactly known. We do not even have the correct times, t_j , corresponding to the $n_s + 1$ leak-off rates. Also, there is no specific model used for the estimation of the fracture geometry.

2. The permeability and the filter-cake resistance, can only be determined if the plots of the field data match the simulated ones (see Figs. 1-8) of Mayerhofer et al.¹³
3. Another useful observation is in regard to the non-linearity of Nolte's plot of the net pressure versus the G-function, (Fig. 8) of Mayerhofer et al.¹³, which shows once again a curve instead of a straight line. Therefore, a correct slope can not be delineated from it.

However the concepts and basics of Mayerhofer's model are very valuable and used as a main platform for the derivation of the following improved filter-cake reservoir fluid flow model.

The pressure drop in the reservoir can be found from a pressure transient model for fluid injection into a porous medium for the case of infinite conductivity fracture. A general solution for the case of fluid injection through a fractured reservoir was developed and presented by Cinco-Ley and Meng⁶⁸. The equation was taken into Laplace domain, assuming equal length intervals, x_{Dj} as follows:

$$\bar{P}_{res,D}(s) - \frac{1}{2} \sum_{i=1}^n \bar{q}_{fDi}(s) \int_{x_{Di}}^{x_{Di+1}} \left[K_0(x_{Di} - x') \sqrt{sf(s)} + K_0(x_{Di} + x') \sqrt{sf(s)} \right] dx' +$$

$$\frac{\pi}{(k_f b_f)_D} \sum_{i=1}^j \left[\frac{(\Delta x)^2}{2} + \Delta x(x_{Dj} - i\Delta x) \right] \bar{q}_{fDi}(s) + \frac{(\Delta x)^2}{8} \bar{q}_{fDi}(s) = \frac{\pi x_{Dj}}{(k_f b_f)_D s} \dots\dots\dots(4.109)$$

Writing this equation for every equal length interval of the fracture, a system of n equations is obtained. The system contains $n + 1$ unknowns. The first n unknowns consist of dimensionless flow rates per unit of fracture length, $\bar{q}_{fDi}(s)$, for $i = 1, 2, 3, \dots, n$ and the $n + 1$ -th unknown is $\bar{P}_{res,D}(s)$. In addition, we need to consider the fact that the flow of a fracturing fluid passes through the filter-cake, built-up on the fracture face, before it reaches the reservoir. Therefore, an additional equation will describe the leak-off rate at a given time as follows:

$$\sum_{i=1}^n \bar{q}_{fDi}(s) = \frac{\Delta x}{s} \dots\dots\dots(4.110)$$

An inverted form of Eq. (4.109) is well known and has the following form:

$$P_{res,D} = \sqrt{\pi t_{Dxf}} \dots\dots\dots(4.111)$$

In essence the above solution can be obtained by solving the system of Eqs. (4.109 and 4.110), or making use of a type curve⁶⁸.

Duhamel's theorem enables us to treat the linearity of the diffusivity equation by the principle of superposition, as a sequence of constant rates. The rate history is

known while the actual leak-off rate, q_n , is not. The above mentioned principle leads to the pressure drop across the reservoir, $\Delta p_{res}(t)$, given by the following equation:

$$\Delta p_{res}(t_n) = \frac{\mu_r}{\pi k_r h_p} \sum_{j=1}^n (q_j - q_{j-1}) p_D [(t_n - t_{j-1})_D] \dots \dots \dots (4.112)$$

Gingarten and Ramey's⁶⁹ solution for an infinite conductivity fracture can be also written as follows:

$$p_D [(t_n - t_{j-1})_D] = \sqrt{\frac{\pi k_r}{\phi c_i \mu_r x_n^2} (t_n - t_{j-1})} \dots \dots \dots (4.113)$$

The dimensionless pressure, Eq. (4.113), is determined with respect to a dimensionless time which corresponds to an actual fracture half-length, x_n at a time t_n and not t_j which is unknown. For the interpretation of the fall-off test, we have (t_n, p_n) data points after shut-in time (i.e. $n > n_s$), where n_s is the index which corresponds to the first pair of data immediately after shut-in, and n is the corresponding index for any other pair of data following shut-in. The data are considered until the fracture closes (i.e. closure time t_c).

The main focus will be on Eq. (4.108), with its main components defined as follows:

The filter-cake pressure drop term, as given by Mayerhofer¹³, is:

$$\Delta p_{face}(t_n) = q_n \frac{R_o}{2r_p A_f} \sqrt{\frac{t_n}{t_p}} \dots\dots\dots(4.114)$$

where q_n is the leak-off rate corresponding to a time t_n , and R_o is the filter-cake resistance, which was derived by Mayerhofer¹³ based on analogy with the fracture face skin factor⁶⁸. And the second term is the pressure drop across the reservoir, as described by Eq. (4.112).

Substituting Eqs. (4.112) and (4.114) in Eq. (4.108) leads to:

$$\Delta p(t_n) = \frac{R_o}{2r_p A_n} \sqrt{\frac{t_n}{t_e}} q_n + \frac{\mu_r}{\pi k_r h_p} \sum_{j=1}^n (q_j - q_{j-1}) P_D \left[(t_n - t_{j-1})_D \right] \dots\dots\dots(4.115)$$

If Eq. (4.115) is re-arranged as:

$$\Delta p(t_n) = \frac{R_o}{2r_p A_n} \sqrt{\frac{t_n}{t_e}} q_n + \Delta p_{res}(t) = \frac{R_o}{2r_p A_n} \sqrt{\frac{t_n}{t_e}} q_n + \frac{\mu_r}{\pi k_r h_p} S \dots\dots\dots(4.116)$$

where:

$$S = (q_1 - q_0) P_D(t_n - t_0) + (q_2 - q_1) P_D(t_n - t_1) + \dots + (q_{n-1} - q_{n-2}) P_D(t_n - t_{n-2}) + (q_n - q_{n-1}) P_D(t_n - t_{n-1})$$

then the actual leak-off rate for one wing can be determined:

$$q_n = \frac{\Delta p(t_n) - \frac{\mu_r}{\pi k_r h_p} \left[-q_{n-1} P_D(t_{Dn} - t_{Dn-1}) + \sum_{j=1}^{n-1} (q_j - q_{j-1}) P_D \left[(t_n - t_{j-1})_D \right] \right]}{\frac{R_0}{2r_p A_n} \sqrt{\frac{t_n}{t_e}} + \frac{\mu_r P_D \left[(t_n - t_{n-1})_D \right]}{\pi k_r h_p}}$$

.....(4.117)

Substituting Eq. (4.113) in Eq. (4.117) and re-arranging yields:

$$q_n = \frac{\Delta p(t_n) - \frac{\mu_r}{\pi k_r h_p} \left[-q_{n-1} P_D(t_{Dn} - t_{Dn-1}) + \sum_{j=1}^{n-1} (q_j - q_{j-1}) \sqrt{\frac{\pi k_r}{\phi c_i \mu_r x_n^2} (t_n - t_{j-1})} \right]}{\frac{1}{A_p} \left[\frac{R_0}{2} \sqrt{\frac{t_n}{t_e}} + \sqrt{\frac{\mu}{\pi \phi c_i k_r} (t_n - t_{j-1})} \right]}$$

.....(4.118)

The above equation can be used for the determination of the actual leak-off rate during both the propagation of the hydraulic fracture and closure. Mayerhofer¹³ showed that the leak-off rates are a function of the observed decline pressure.

From the net pressure definition, Eq. (4.48) the fracture width is given by:

$$w_j = c_f P_n = c_f (P_{j-1} - P_j) \dots \dots \dots (4.119)$$

$$w_{j-1} = c_f P_n = c_f (P_{j-2} - P_{j-1}) \dots \dots \dots (4.120)$$

And also by the ratio between the leak-off volume and fracture face area as:

$$w_j = \frac{V_j}{Af} \text{ and } w_{j-1} = \frac{V_{j-1}}{Af} \dots\dots\dots(4.121)$$

The leak-off rate is given by the leak-off volume divided by time:

$$q_j = \frac{V_j}{\Delta t_j} \text{ and } q_{j-1} = \frac{V_{j-1}}{\Delta t_{j-1}} \dots\dots\dots(4.122)$$

Combining Eqs. (4.119-4.122) it follows that:

$$q_j = c_f \frac{A_f (p_{j-1} - p_j)}{\Delta t_j} \dots\dots\dots(4.123)$$

$$q_{j-1} = c_f \frac{A_f (p_{j-2} - p_{j-1})}{\Delta t_{j-1}} \dots\dots\dots(4.124)$$

If we substitute Eq. (4.113) in Eq. (4.112), the pressure drop across the reservoir becomes:

$$\Delta p_{res}(t_n) = \frac{\mu_r}{\pi k_r A_p} \sum_{j=1}^n (q_j - q_{j-1}) \sqrt{\frac{\pi k_r}{\phi c_i \mu_r} (t_n - t_{j-1})} \dots\dots\dots(4.125)$$

and with further substitution of the ratio of the permeable to total fracture areas, given by Eq. (4.45), Eq. (4.125) will be:

$$\Delta p_{res}(t_n) = \frac{\mu_r}{\pi k_r r_p A_f} \sum_{j=1}^n (q_j - q_{j-1}) \sqrt{\frac{\pi k_r}{\phi c_t \mu_r} (t_n - t_{j-1})} \dots \dots \dots (4.126)$$

To further proceed, we need to consider the fact that the leak-off rates during the fracture propagation are not known from $j = 1$ to $n_s + 1$. Consequently one key reasonable assumption must be made, and that is that the first $n_s + 1$ leak-off rates are equal to an apparent leak-off rate which can be computed via the previous model, Eq. (4.49), as a function of the average leak-off width and fracture area:

$$q_a = \frac{w_L A_f}{t_p} \dots \dots \dots (4.127)$$

From $j = 1$ to $n_s + 2$, the reservoir pressure drop can be written as:

$$\frac{1}{k_r^{1/2} A_f r_p} \left(\frac{\mu}{\pi \phi c_t} \right)^{1/2} \left[(q_1 - q_0)(t_1 - t_0)^{1/2} + (q_2 - q_1)(t_2 - t_1)^{1/2} + \dots \right. \\ \left. (q_{n_s+2} - q_{n_s+1})(t_n - t_{n_s+1})^{1/2} \dots \dots \dots (4.128) \right]$$

and from $j = n_s + 3$ to n , substituting Eqs. (4.123 and 4.124) in Eq. (4.125) gives:

$$\frac{1}{k_r^{1/2} A_f r_p} \left(\frac{\mu}{\pi \phi c_t} \right)^{1/2} \left[\sum_{j=n_s+3}^n c_f \frac{A_f (p_{j-1} - p_j)}{\Delta t_j} - c_f \frac{A_f (p_{j-2} - p_{j-1})}{\Delta t_{j-1}} \right] \dots (4.129)$$

Combining and re-arranging Eqs. (4.128) and (4.129) leads to:

$$\begin{aligned} \Delta p(t_n) = & c_f \frac{R_0}{2r_p} \sqrt{\frac{t_n}{t_p}} \frac{p_{n-1} - p_n}{\Delta t_n} + \\ & \frac{1}{k_r^{1/2} A_f r_p} \left(\frac{\mu}{\pi \phi c_t} \right)^{1/2} \left[(q_1) t_n^{1/2} + \sum_{j=2}^{n_s+2} (q_j - q_{j-1}) (t_n - t_{j-1})^{1/2} \right] + \\ & \frac{c_f}{k_r^{1/2} r_p} \left(\frac{\mu}{\pi \phi c_t} \right)^{1/2} \left[\sum_{j=n_s+3}^n \frac{(p_{j-1} - p_j)}{\Delta t_j} - \frac{(p_{j-2} - p_{j-1})}{\Delta t_{j-1}} (t_n - t_{j-1})^{1/2} \right] \end{aligned} \dots (4.130)$$

Where the total reservoir pressure can be written as the difference between the fracture pressure, p_n , at time, t_n , and the initial reservoir pressure, p_i :

$$\Delta p(t_n) = p_n - p_i \dots (4.131)$$

The term in the first square bracket of Eq. (4.130) can be written as follows:

$$\left[(q_1)t_n^{1/2} + \sum_{j=2}^{n_s+2} (q_j - q_{j-1})(t_n - t_{j-1})^{1/2} \right] =$$

$$(q_1)t_n^{1/2} + c_f A_f \left(\frac{p_{n_s+1} - p_{n_s+2}}{t_n - t_{n_s+1}} \right) (t_n - t_{n_s+1})^{1/2} - q_{n_s+1} (t_n - t_{n_s+1})^{1/2} \dots \dots \dots (4.132)$$

Earlier, we made the assumption that the first $n_s + 1$ leak-off rates are equal to an apparent leak-off rate, and thus:

$$q_1 = q_{n_s+1} = q_a \dots \dots \dots (4.133)$$

Substituting Eqs. (4.127, 4.131, 4.132, and 4.133) in Eq. (4.130), and rearranging, results in the following filter-cake reservoir pressure equation:

$$p_n - p_i = c_f \frac{R_0}{2r_p} \sqrt{\frac{t_n}{t_p} \frac{p_{n-1} - p_n}{\Delta t_n}} + \frac{c_f}{k_r^{1/2} r_p} \left(\frac{\mu}{\pi \phi c_t} \right)^{1/2} \left[\left(\frac{p_{n_s+1} - p_{n_s+2}}{t_n - t_{n_s+1}} \right) (t_n - t_{n_s+1})^{1/2} + \sum_{j=n_s+3}^n \left(\frac{p_{j-1} - p_j}{\Delta t_j} - \frac{p_{j-2} - p_{j-1}}{\Delta t_{j-1}} \right) (t_n - t_{j-1})^{1/2} \right] + \frac{1}{k_r^{1/2} A_f r_p} \left(\frac{\mu}{\pi \phi c_t} \right)^{1/2} \left[w_L \frac{A_f}{t_p} t_n^{1/2} - w_L \frac{A_f}{t_p} (t_n - t_{n_s+1})^{1/2} \right]$$

or,

$$\frac{p_n - p_i}{p_{n-1} - p_n} \frac{\Delta t_n}{\sqrt{t_p t_n}} = \frac{c_f R_0}{2r_p t_p} + \frac{c_f}{(k_r r_p)^{1/2}} \left(\frac{\mu}{\pi \phi c_t r_p} \right)^{1/2} \frac{\Delta t_n}{(p_{n-1} - p_n) \sqrt{t_p t_n}} \cdot$$

$$\left[\left(\frac{p_{n_s+1} - p_{n_s+2}}{t_n - t_{n_s+1}} \right) (t_n - t_{n_s+1})^{1/2} + \sum_{j=n_s+3}^n \frac{(p_{j-1} - p_j)}{\Delta t_j} - \frac{(p_{j-2} - p_{j-1})}{\Delta t_{j-1}} (t_n - t_{j-1})^{1/2} \right]$$

$$+ \frac{w_L}{(k_r r_p)^{1/2}} \left(\frac{\mu}{\pi \phi c_t r_p} \right)^{1/2} \left[\frac{t_n^{1/2} - (t_n - t_{n_s+1})^{1/2}}{(p_{n-1} - p_n) t_p^{3/2}} \Delta t_n \right] \dots \dots \dots (4.134)$$

Following simple algebraic re-arrangements, Eq. (4.134) becomes:

$$Y(n) = b_M + m_M X(n) \dots \dots \dots (4.135)$$

where the dependent variable is given by:

$$Y(n) = \frac{p_n - p_i}{d_n \sqrt{t_p t_n}} \dots \dots \dots (4.136)$$

the intercept is:

$$b_M = \frac{c_f R_0}{2r_p t_p} \dots \dots \dots (4.137)$$

the slope:

$$m_M = \frac{c_f}{(k_r r_p)^{1/2}} \dots \dots \dots (4.138)$$

and the independent variable:

$$X(n) = \left(\frac{\mu}{\pi \phi c_t r_p} \right)^{1/2} \left\{ \left[\left(\frac{p_{n_s+1} - p_{n_s+2}}{t_n - t_{n_s+1}} \right) (t_n - t_{n_s+1})^{1/2} \right. \right. \\ \left. \left. + \sum_{j=n_s+3}^n \frac{(p_{j-1} - p_j)}{\Delta t_j} - \frac{(p_{j-2} - p_{j-1})}{\Delta t_{j-1}} (t_n - t_{j-1})^{1/2} \right] + \frac{\bar{w}}{c_f} \left[\frac{t_n^{1/2} - (t_n - t_{n_s+1})^{1/2}}{(p_{n-1} - p_n) k_r t_n^{3/2}} \Delta t_n \right] \right\} \dots \dots \dots (4.139)$$

Equation (4.135) describes a straight line of intercept b_M and slope m_M (see Figs. C-5, C-10, C-15, C-17, and C-21).

The main output parameters of the above equation are the filter-cake resistance, R_o , determined from the intercept, b_M , and the reservoir permeability, k_r , extracted from the slope, m_M , of Eq. (4.140).

The necessary modeling equations are presented in Appendix B. They incorporate both cases, (1) no spurt loss assumption and (2) spurt loss identified, showed earlier in this work (i.e. section 4.5 of chapter 4). A complete set of equations is presented for each fracture geometry.

CHAPTER 5
METHODOLOGY AND COMPUTER PROGRAM

5.1 Methodology

Based on the algorithm presented in chapter 4 and Appendixes A and B of this work, the following step by step procedure is recommended:

- I. Following a minifrac test, acquire, compute and prepare the following required input parameters:
 - a) Pressure and time data pertinent to both the injection and the fall-off periods of the minifrac, (P, t) .
 - b) Injection flow rate, q_i , and the total volume of fluid injected into the fracture, V_i .
 - c) Type of fracturing fluid and its key rheological parameters (i.e. n' and K').
 - d) Formation porosity, ϕ .
 - e) Reservoir total compressibility, c_t .
 - f) Reservoir fluid viscosity, μ_r .
 - g) Fracturing fluid viscosity, μ_f .
 - h) Poisson's ratio, ν .
 - i) Young's Modulus, E .
 - j) Fracture permeable height, h_p .
 - k) Fracture height, h_f .

- l) Pumping time, t_p .
 - m) Initial reservoir pressure, P_i .
- II. Convert the time data into shut-in time intervals (i.e. Δt)
 - III. Plot, on a cartesian graph, the pressure data versus time (i.e. Figs. C-1, C-6, C-11, and C-18).
 - IV. Filter the pressure-time data if necessary (i.e. if significant noise is shown – Fig. C-16).
 - V. Select the corresponding fall-off period from the plot (i.e. Figs. C-1, C-6, C-11, and C-18).
 - VI. Determine the initial shut-in pressure from the pressure versus time plots (i.e. Figs. C-1, C-6, C-11, and C-18).
 - VII. Compute \sqrt{dt} and plot, on a cartesian graph, the pressure versus \sqrt{dt} , of the fall-off period (i.e. Figs. C-2, C-7, C-12, C-19).
 - VIII. From Figs. C-2, C-7, C-12, C-19, identify the correct slope of the straight line corresponding to the final closure period, and estimate the closure pressure and closure time.
 - IX. Plot on a log-log graph the net-pressure versus time (i.e. also known as the Nolte-Smith plot - Figs. C-3, C-8, C-13).
 - X. From Figs. C-3, C-8, C-13), identify the fracture geometry which will be later used for modeling purposes.

5.1.1 PKN geometry

1. Compute the $g(\Delta t_D, \alpha)$ function corresponding to the fall-off period using Eq. (A-47).
2. Compute $g_0(\alpha)$ for $\alpha = 4/5$, from Eq. (A-42).
3. Compute the pressure derivative, $P_w'II$, and $F(t)$ functions using Eqs. (4.104 and 4.106).
4. Plot the pressure derivative function, as $P_w'II \cdot F(t)$ versus $F(t)^2$, on a cartesian graph, Fig. C-22.
5. For pressure-time data corresponding to the decline period, plot the bottomhole pressure, versus the $g(\Delta t_D, \alpha)$ function (i.e. Figs. C-4, C-9, C-14, C-20, C-26).
6. If the plot from the previous step is a straight line, then delineate the slope, m_N , and the intercept, b_N from it.
7. If the plot from step 5 is a curve, instead of a straight line, a correct slope can not be identified. Therefore use $P_w'II \cdot F(t)$ versus $F(t)^2$, Fig. C-22, to determine the pressure derivative slope, m_N' .
8. Compute the leak-off coefficient, C_L , from the slope of the pressure derivative plot, using Eq. (4.105). Otherwise, calculate the leak-off coefficient from step 6 using Eq. (A-17).

9. Next, calculate the expected slopes and intercepts of Figs. C-4, C-9, C-14, C-20, and C-26, using Eq. (4.49). To complete this step, the leak-off coefficient determined on step 8 is required.
10. Identify, as shown in the steps bellow, if the spurt loss is present (i.e. expected on reservoirs with medium to high permeabilities).
11. Estimate the spurt loss, S_p , as a function of the fracture half-length calculated at the previous step using Eq. (4.87).
12. If the spurt loss value is greater then zero , then calculate the fracture compliance, c_f from eq. A-2.
13. Calculate the fracture half-length, x_f , using Eq. (A-11).
14. Calculate the average fracture width, \bar{w}_L , from Eq. (A-30)
15. Estimate the fluid efficiency, η , from Eq. (A-35).
16. From the second part of the coupled model (i.e. filter-cake reservoir transient analysis), Compute $Y(n(i))$ and $X(n(i))$ from the fall-off period, using Eqs. (B-17 and B-20). Note that variables determined from the first part of the model, are used here (i.e. the average fracture width, and the fracture half length).
17. Plot $Y(n(i))$ versus $X(n(i))$ on a cartesian graph (i.e. Figs. C-5, C-10, C-15, C-17, C-21, and C-27), and from the best straight line fit determine the slope, m_M , and the intercept, b_M .
18. Next, calculate the filter-cake resistance, R_o , from Eq. (B-18), and the reservoir permeability, k_r , from Eq. (B-19).

19. If the spurt loss is known, from a lab test, or another method of evaluation, compute the fracture half-length from Eq. (A-11) as a function of the spurt loss. Next, follow steps 14 through 18 as shown above.
20. If the spurt loss calculated from Eq. (4.87) has a negative value, or is unavailable from any other source, the entire algorithm will be based on a no-spurt loss assumption, as shown in the following steps.
21. Calculate the fracture half-length, x_f , using Eq. (A-8).
22. Determine the leak-off coefficient, C_L , from Eq. (A-17).
23. Calculate the fluid efficiency from Eq. A-27.
24. From the second part of the coupled model (i.e. filter-cake reservoir transient analysis), Compute $Y(n(i))$ and $X(n(i))$ from the fall-off period, using Eqs. (B-2 and B-5). Note that the variables determined from the first part of the model, are used here (i.e. the average fracture width, and the fracture half length).
25. Plot $Y(n(i))$ versus $X(n(i))$ on a cartesian graph (i.e. Figs. C-5, C-15, C-17, C-21, and C-27), and from the best straight line fit, determine the slope, m_M , and the intercept, b_M .
26. Next, calculate the filter-cake resistance, R_o , from Eq. (B-3), and the reservoir permeability, k_r , from Eq. (B-4).

5.1.2 KGD geometry

1. Compute the $g(\Delta t_D, \alpha)$ function corresponding to the fall-off period using Eq. (A-51).
2. Compute $g_0(\alpha)$ for $\alpha = 4/5$, from Eq. (A-42).
3. Compute the pressure derivative, $P_w'II$, and $F(t)$ functions using Eqs. (4.104 and 4.106).
4. Plot the pressure derivative function, as $P_w'II \cdot F(t)$ versus $F(t)^2$, on a cartesian graph, Fig. C-22.
5. For pressure-time data corresponding to the decline period, plot the bottomhole pressure, versus the $g(\Delta t_D, \alpha)$ function (i.e. Figs. C-4, C-9, C-14, C-20).
6. If the plot from the previous step is a straight line, then delineate the slope, m_N , and the intercept, b_N from it.
7. If the plot from step 5 is a curve, instead of a straight line, a correct slope can not be identified. Therefore use a plot of $P_w'II \cdot F(t)$ versus $F(t)^2$, Fig. C-22, to determine the pressure derivative slope, m_N' .
8. Compute the leak-off coefficient, C_L , from the slope of the pressure derivative plot, using Eq. (4.105). Otherwise, calculate the leak-off coefficient from step 6 using Eq. (A-18).

9. Next, calculate the expected slopes and intercepts, of Figs. C-4, C-9, C-14, C-20, and C-26 using Eq. (4.49). To complete this step, the leak-off coefficient determined on step 8 is required.
10. Identify, as shown in the steps bellow, if the spurt loss is present (i.e. expected on reservoirs with medium to high permeabilities).
11. Estimate the spurt loss, S_p , as a function of the fracture half-length calculated at the previous step using Eq. (4.87).
12. If the spurt loss value is greater then zero , then calculate the fracture compliance, c_f from Eq. (A-3).
13. Calculate the fracture half-length, x_f , using Eq. (A-12).
14. Calculate the average fracture width, \bar{w}_L , from Eq. (A-31)
15. Estimate the fluid efficiency, η , from Eq. (A-35).
16. From the second part of the coupled model (i.e. filter-cake reservoir transient analysis), Compute $Y(n(i))$ and $X(n(i))$ from the fall-off period, using Eqs. (B-22 and B-25). Note that variables determined from the first part of the model, are used here (i.e. the average fracture width, and the fracture half length).
17. Plot $Y(n(i))$ versus $X(n(i))$ on a cartesian graph (i.e. Figs. C-5, C-10, C-15, C-17, C-21, and C-27), and from the best straight line fit determine the slope, m_M , and the intercept, b_M .
18. Next, calculate the filter-cake resistance, R_o , from Eq. (B-23), and the reservoir permeability, k_r , from Eq. (B-24).

19. If the spurt loss is known, from a lab test, or another method of evaluation, compute the fracture half-length from Eq. (A-12) as a function of the spurt loss. Next, follow steps 14 through 18 as shown above.
20. If the spurt loss calculated from Eq. (4.87) has a negative value, or is unavailable from any other source, the entire algorithm will be based on a no-spurt loss assumption, as shown in the following steps.
21. Calculate the fracture half-length, x_f , using Eq. (A-9).
22. Determine the leak-off coefficient, C_L , from Eq. (A-18).
23. Calculate the fluid efficiency from Eq. A-28.
24. From the second part of the coupled model (i.e. filter-cake reservoir transient analysis), Compute $Y(n(i))$ and $X(n(i))$ from the fall-off period, using Eqs. (B-2 and B-5). Note that the variables determined from the first part of the model, are used here (i.e. the average fracture width, and the fracture half length).
25. Plot $Y(n(i))$ versus $X(n(i))$ on a cartesian graph (i.e. Figs. C-5, C-15, C-17, C-21, and C-27), and from the best straight line fit, determine the slope, m_M , and the intercept, b_M .
26. Next, calculate the filter-cake resistance, R_o , from Eq. (B-3), and the reservoir permeability, k_r , from Eq. (B-4).

5.1.3 Radial geometry

1. Compute the $g(\Delta t_D, \alpha)$ function corresponding to the fall-off period using Eq. (A-53).
2. Compute $g_0(\alpha)$ for $\alpha = 4/5$, from Eq. (A-42).
3. Compute the pressure derivative, $P_w'II$, and $F(t)$ functions using Eqs. (4.104 and 4.106).
4. Plot the pressure derivative function, as $P_w'II \cdot F(t)$ versus $F(t)^2$, on a cartesian graph, Fig. C-22.
5. For pressure-time data corresponding to the decline period, plot the bottomhole pressure, versus the $g(\Delta t_D, \alpha)$ function (i.e. Figs. C-4, C-9, C-14, C-20, and C-26).
6. If the plot from the previous step is a straight line, then delineate the slope, m_N , and the intercept, b_N from it.
7. If the plot from step 5 is a curve, instead of a straight line, a correct slope can not be identified. Therefore use a plot of $P_w'II \cdot F(t)$ versus $F(t)^2$, Figs. C-22, to determine the pressure derivative slope, m_N' .
8. Compute the leak-off coefficient, C_L , from the slope of the pressure derivative plot, using Eq. (4.105). Otherwise, calculate the leak-off coefficient from step 6 using Eq. (A-19).

9. Next, calculate the expected slopes and intercepts, of Figs. C-4, C-9, C-14, C-20, and C-26 using Eq. (4.49). To complete this step, the leak-off coefficient determined on step 8 is required.
10. Identify, as shown in the steps bellow, if the spurt loss is present (i.e. expected on reservoirs with medium to high permeabilities).
11. Estimate the spurt loss, S_p , as a function of the fracture half-length calculated at the previous step using Eq. (4.87).
12. If the spurt loss value is greater then zero , then calculate the fracture compliance, c_f from eq. A-3.
13. Calculate the fracture half-length, R_f , using Eq. (A-13).
14. Calculate the average fracture width, \bar{w}_L , from Eq. (A-22)
15. Estimate the fluid efficiency, η , from Eq. (A-29).
16. From the second part of the coupled model (i.e. filter-cake reservoir transient analysis), Compute $Y(n(i))$ and $X(n(i))$ from the fall-off period, using Eqs. (B-27 and B-30). Note that the variables determined from the first part of the model, are used here (i.e. the average fracture width, and the fracture half length).
17. Plot $Y(n(i))$ versus $X(n(i))$ on a cartesian graph (i.e. Figs. C-5, C-10, C-15, C-17, C-21, and C-27), and from the best straight line fit determine the slope, m_M , and the intercept, b_M .
18. Next, calculate the filter-cake resistance, R_o , from Eq. (B-28), and the reservoir permeability, k_r , from Eq. (B-29).

19. If the spurt loss is known, from a lab test, or another method of evaluation, compute the fracture half-length from Eq. (A-13) as a function of the spurt loss. Next, follow steps 14 through 18 as shown above.
20. If the spurt loss calculated from Eq. (4.87) has a negative value, or is unavailable from any other source, the entire algorithm will be based on a no-spurt loss assumption, as shown in the following steps.
21. Calculate the fracture half-length, x_f , using Eq. (A-10).
22. Determine the leak-off coefficient, C_L , from Eq. (A-19).
23. Calculate the fluid efficiency from Eq. A-37.
24. From the second part of the coupled model (i.e. filter-cake reservoir transient analysis), Compute $Y(n(i))$ and $X(n(i))$ from the fall-off period, using Eqs. (B-12 and B-15). Note that the variables determined from the first part of the model, are used here (i.e. the average fracture width, and the fracture half length).
25. Plot $Y(n(i))$ versus $X(n(i))$ on a cartesian graph (i.e. Figs. C-5, C-15, C-17, C-21, and C-27), and from the best straight line fit, determine the slope, m_M , and the intercept, b_M .
26. Next, calculate the filter-cake resistance, R_o , from Eq. (B-13), and the reservoir permeability, k_r , from Eq. (B-14).

5.2 Computer Program for the coupled model

Based on the above methodology, a computer program, that incorporates both

modeling techniques and is applicable for all three-fracture geometries, was developed. The main components of the program are shown in a flow chart, Appendix E, for each fracture geometry (i.e. PKN, KGD, and radial). The program is written in Fortran language and reads all the input parameters from one data file. In spite of a significant number of computations performed, a complete run takes no longer than one minute. All the required computations are performed by this program, including automatic curve fitting for both models (i.e. pressure decline analysis and filter-cake reservoir flow leak-off). Based on the best straight line fit of both plots, the pressure versus G-function plot and $Y(n(i))$ versus $X(n(i))$ plot, the program automatically computes the values of the slope and intercept. The only parts of the algorithm that are not incorporated in this program are the data filtering procedure, and the pressure derivative for the following reasons:

1. Data filtering require complex mathematical algorithms capable of processing any type of curve obtained from a pressure time data set.
2. The same is true for the computation of the pressure derivative, since simple methods (i.e. two-point derivative or Bourdet et. Al) are not satisfactory (i.e. significant noise makes it difficult to interpret the characteristics of the curve).

To complete the data filtering and pressure derivative computations, a commercial software (Jandel Scientific) was used.

A list of the input data, for the main program, is given in the previous section, step I (a:m). The main output parameters are:

1. pressure time data points, $p(i)$, $t(i)$, and $\sqrt{t(i)}$
2. g-function, $g(i)$, and its corresponding shut-in time pairs, $t(i)$
3. spurt-loss, S_p , fracture half-length, x_f (for PKN and KGD geometry)
and R_f for the radial geometry
4. average fracture width, \bar{w}_L
5. fluid leak-off coefficient, C_L
6. fluid efficiency, η
7. pairs of $Y(n(i))$ and $X(n(i))$ values corresponding to shut-in times,
from the filter-cake reservoir flow model
8. filter-cake resistance, R_o
9. and reservoir permeability, k_r

All variables (i.e. input and output parameters) are in oil field units.

CHAPTER 6

APPLICATIONS AND SENSITIVITY ANALYSIS

6.1 Applications

In this section the methodology shown in chapter 5 will be applied to fracture calibration treatments from five field cases. Additional information and final results, from the analysis of each treatment, is shown in Appendix C.

6.1.1 Case M1

This is a calibration treatment applied to an oil well. The purpose of this job is, as stated earlier in this work, to collect information about the leak-off characteristics of the fracturing fluid (i.e. leak-off coefficient, C_L , and fluid efficiency, η). Determination of the fracture dimensions (i.e. fracture half-length, x_f , and average fracture width, \bar{w}_L) and estimation of the fracture geometry model is also accomplished by means of interpretation and analysis from a minifrac test. The same test can enable us to compute the reservoir permeability, k_r , and the filter-cake resistance, R_o . As a result, it is critical that the subsequent fracturing job be conducted with the same fracturing fluid and used during the treatment.

The test was performed by injecting 3150 gallons (75 bbl) of borate water base fracturing fluid (no proppant), at an approximate rate of 16 bpm (pumping time was 4.7 minutes). This is a formation described by a porosity $\phi = 20\%$, reservoir

fluid viscosity, $\mu = 1.4$ cp, initial reservoir pressure, $p_i = 2146$ psi, and the fracture permeable height, $h_p = 40$ ft, and the fracture height, $h_f = 45$ feet. The elastic properties of the porous medium are known as Young's Modulus, $E = 1.00 \times 10^6$ psi, and Poisson's ratio, $\nu = 0.25$. Other required parameters are shown in Table C-1A, Appendix C.

Following step one, collection of reservoir and fluid properties required as input data, a cartesian plot of pressure versus time, Fig. C-1, was produced (see data in Table C-1B), and from it the pumping time, $t_p = 4.76$ min, and initial shut-in pressure, $ISIP = 3293$ psi, were determined. It was found that a filtering of the pressure time data, as required by step 4 of the methodology (section 1, chapter 5) was not necessary. From the same plot, the corresponding fall-off period for analysis was selected between the initial shut-in pressure and the end of the pressure decline curve. A cartesian plot, Fig. (C-2), of the fall-off pressure versus square root of time (data shown in Table C-1B, Appendix C), indicates that the approximate closure pressure (i.e. the corresponding value to the in-situ minimum stress) is $P_c = 2503$ psi at a closure time, $t_c = 11.3$ minutes. The selection of the closure pressure was done based on the profile of the curve (i.e. second change of slope) and confirmed by a step rate test (data not provided in this work).

A log-log plot, Fig. C-3, of the injection net pressure versus square root of time (data shown in Table C-1D, Appendix C), enables us to determine that a radial geometry most likely occurred during the treatment (i.e. a slight deviation towards a negative slope detected at the end of the curve).

Using Eqs. (A-42) and (A-53), the G-functions, $g(\Delta t_D, \alpha)$, at a shut-in time $\Delta t_D \neq 0$, and $g_0(\alpha)$ corresponding to a shut-in time, $\Delta t_D = 0$ are computed (data are shown in Table C-1C). Following the above computations, an automated curve-fit of the fall-off pressure versus the G-function is performed by the computer program (see flow chart – Appendix E). The program completes the entire series of calculations, regardless of a best or worse fit obtained at this step. Next, an inspection of the cartesian plot, Fig. C-4, of the fall-off pressure versus the G-function, enables us to assess if the plot is a straight line or not. In this case, with the exception of the first 4 points, the plot indicates a straight line, and thus the application of the pressure derivative (steps 3, 4, and 7, 8) is not necessary since the slope and the intercept can be clearly delineated from the graph. This is also automatically performed by the computer program, using Eq. (4.49). For our case an intercept, $b_N = 3131.24$ psi and a slope, $m_N = -175$ psi were determined.

A next step is to determine if there is spurt loss using the equation derived in this work, Eq. (4.93) as follows:

$$S_p = \frac{1}{2(0.352)} \left\{ \left[\frac{0.152(2.832E - 2)}{\left(\frac{1.07E6}{0.925(3131.24 + 1.37689 \cdot (-175)) - 2503.1} \right)^{8/3}} \right] \right\}$$

$$\frac{1}{\left[(2.252E - 10) \frac{(211)(421.06)}{(1.07E6)(4.76)} \right]^{1/3}} - 2.4565(3131.24 - 2503.1)$$

$$\frac{\left(\frac{1.07E6}{0.925(3131.24 + 1.37689 \cdot (-175) - 2503.1)} \right)^{4/3}}{1.07E6}$$

$$0.925 \left[(2.252E - 10) \frac{(211)(421.06)}{(1.07E6)(4.76)} \right]^{1/3} \left. \vphantom{0.925} \right\} = -6.8E-03 \text{ ft} = -5.8 \text{ gal/100 ft}^2$$

A negative value of the above, is an indication that the spurt loss could not be identified, and thus all computations will be performed based on a no spurt loss assumption as follows:

The fracture half-length using Eq. (A-10):

$$R_{fNS}^{RAD} = \sqrt[3]{\frac{3(1.07E6)(421.06)}{8(0.925)(3131.24 - 2503.1)}} = 66.2 \text{ ft}$$

The fracture compliance using Eq. (A-3):

$$c_f = \frac{16(0.925)(66.2)}{3\pi(1.07E6)} = 9.72E-5 \text{ ft/psi}$$

The fluid leak-off coefficient from Eq. (A-19):

$$C_L = \frac{8(66.2)(-(-175))}{3(\pi(0.356)(\sqrt{4.76})(1.07E6))} = 1.18 \text{ E-02 } ft/\sqrt{\text{min}}$$

The fracture average width from Eq. A-22:

$$\bar{w}_{NS}^{RAD} = 12(5.33) \frac{(66.2)(0.925)(-(-175))(1.377)}{\pi(1.07E6)} = 2.81E-01 \text{ in}$$

The fracture fluid efficiency from Eq. (A-29):

$$\eta_{NS}^{RAD} = 1 - \frac{175(1.377)}{(3131.24 - 2503.1)} = 61.63 \%$$

The second part of the model consists of solving the main components of Eq. (4.140), $Y(n)$ and $X(n)$ for the fall-off period between the initial shut-in pressure and closure pressure. This again is automatically performed by the computer program (Table C-1C), as in the case of the G-function, followed by an automatic curve-fit. Then a cartesian plot of $Y(n)$ versus $X(n)$ is produced, Fig. C-5. From the best straight line fit, the intercept, $b_M=0.2$, and the slope, $m_M=2.439E+08$. Next, the filter-cake resistance and the reservoir permeability are computed as follows:

The filter cake-resistance using Eq. (B-13):

$$R_{NS}^{RAD} = \frac{4(0.356)(1.07E6)(4.76)(0.2)}{\pi(66.2)} = 6.97E+03 \text{ psi} - \text{min} / \text{ft}$$

And the reservoir permeability from Eq. (B-14):

$$K_{NS}^{RAD} = 9.431E13 \left(\frac{66.2}{2.439E8} \right)^2 \frac{1}{0.352} = 19.5 \text{ md}$$

6.1.2 Case M2

This is a calibration treatment applied to the same oil well, only to an upper producing interval.

The test was performed by injecting 3150 gallons (75 bbl) of borate water base fracturing fluid (no proppant), at an approximate rate of 23 bpm (pumping time was 3.3 minutes). This is a formation described by a porosity $\phi = 20\%$, reservoir fluid viscosity, $\mu = 1.4$ cp, initial reservoir pressure, $p_i = 1768$ psi, and the fracture permeable height, $h_p = 32$ ft, and fracture total height, $h_f = 46$ feet. The elastic properties of the porous medium are known as Young's Modulus, $E = 1.00 \times 10^6$ psi, and Poisson's ratio, $\nu = 0.25$. Other required parameters are shown in Table C-2A, Appendix C.

Following step one, collection of reservoir and fluid properties required as input data, a cartesian plot of pressure versus time, Fig. C-6, was produced (see data

in Table C-2B), and from it the pumping time, $t_p = 3.3$ min, and initial shut-in pressure, $ISIP = 3298$ psi were determined. It was found that a filtering of the pressure time data, as required by step 4 of the methodology (section 1, chapter 5) was not necessary. From the same plot, the corresponding fall-off period for analysis was selected between the initial shut-in pressure and the end of the pressure decline curve. A cartesian plot, Fig. (C-7), of the fall-off pressure versus square root of time (data shown in Table C-2B, Appendix C), indicates that the approximate closure pressure (i.e. the corresponding value to the in-situ minimum stress) is $P_c = 2923$ psi at a closure time, $t_c = 2.7$ minutes. The selection of the closure pressure was done based on the profile of the curve (change of slope) and confirmed by a step rate test (data not provided in this work).

A log-log plot, Fig. C-8, of the injection net pressure versus square root of time (data shown in Table C-2B, Appendix C), enables us to determine that a radial geometry most likely occurred during the treatment (i.e. a slight deviation towards a negative slope detected at the end of the curve).

Using Eqs. (A-42) and (A-53), the G-functions, $g(\Delta t_D, \alpha)$, at a shut-in time $\Delta t_D \neq 0$, and $g_0(\alpha)$ corresponding to a shut-in time, $\Delta t_D = 0$ are computed (data are shown in Table C-2C). Following the above computations, an automated curve-fit of the fall-off pressure versus the G-function is performed by the computer program (see flow chart – Appendix E). The program completes the entire series of calculations, regardless of a best or worse fit obtained at this step. Next, an inspection of the cartesian plot, Fig. C-9, of the fall-off pressure versus the G-function, enables

us to assess if the plot is a straight line or not. In this case the plot also indicates a straight line, and thus an application of the pressure derivative (steps 3, 4, and 7, 8) is not necessary since the slope and the intercept can be clearly delineated from the graph. This is also automatically performed by the computer program, using Eq. (4.49). For our case an intercept, $b_N = 3545.5$ psi and a slope, $m_N = -342.83$ psi were determined.

A next step is to determine if there is spurt loss using Eq. (4.93) as follows:

$$S_p = \frac{1}{2(0.288)} \left\{ \left[\frac{0.152(2.832E-2)}{\left(\frac{1.07E6}{0.925(3545.5 + 1.37689 \cdot (-342.83)) - 2928.7} \right)^{8/3}} \right] \right\}$$

$$\frac{1}{\left[(2.252E-10) \frac{(211)(421.06)}{(1.07E6)(3.3)} \right]^{1/3}} - 2.4565(3545.5 - 2928.7)$$

$$\frac{\left(\frac{1.07E6}{0.925(3545.5 + 1.37689 \cdot (-342.83)) - 2928.7} \right)^{4/3}}{1.07E6}$$

$$0.925 \left[(2.252E - 10) \frac{(211)(421.06)}{(1.07E6)(3.3)} \right]^{1/3} \left. \vphantom{0.925} \right\} = -3.31E-02 \text{ ft} = -26 \text{ gal}/100 \text{ ft}^2$$

Again, a negative value of the above, is an indication that the spurt loss could not be identified, and thus all computations will be performed based on a no spurt loss assumption as follows:

The fracture half-length using Eq. (A-10):

$$R_{fNS}^{RAD} = \sqrt[3]{\frac{3(1.07E6)(421.06)}{8(0.925)(3545.5 - 2928.7)}} = 66.6 \text{ ft}$$

The fracture compliance using Eq. (A-3):

$$c_f = \frac{16(0.925)(66.6)}{3\pi(1.07E6)} = 9.78E-5 \text{ ft}/\text{psi}$$

The fluid leak-off coefficient from Eq. (A-19):

$$C_L = \frac{8(66.6)(-(-175))}{3(\pi(0.288)(\sqrt{3.3})(1.07E6))} = 3.46 \text{ E-02 } \text{ ft}/\sqrt{\text{min}}$$

The fracture average width from Eq. A-22:

$$\bar{w}_{NS}^{RAD} = 12(5.33) \frac{(66.6)(0.925)(-(-342))(1.377)}{\pi(1.07E6)} = 5.53 \text{ E-01 in}$$

The fracture fluid efficiency from Eq. (A-29):

$$\eta_{NS}^{RAD} = 1 - \frac{175(1.377)}{(3545.5 - 2928.7)} = 23.65 \%$$

The second part of the model consists of solving the main components of Eq. (4.140), $Y(n)$ and $X(n)$, for the fall-off period between the initial shut-in pressure and the closure pressure. This again is automatically performed by the computer program (Table C-2C), as in the case of the G-function, followed by an automatic curve-fit, and a cartesian plot of $Y(n)$ versus $X(n)$ is produced, Fig. C-10. From the best straight line fit, the intercept, $b_M = 0.576$, and the slope, $m_M = 2.77E+08$. Next, the filter-cake resistance and reservoir permeability are computed as follows:

The filter cake-resistance using Eq. (B-13):

$$R_{NS}^{RAD} = \frac{4(0.288)(1.07E6)(3.3)(0.2)}{\pi(66.6)} = 3.88E+03 \text{ psi - min / ft}$$

And the reservoir permeability from Eq. (B-14):

$$K_{NS}^{RAD} = 9.431E13 \left(\frac{66.6}{2.77E8} \right)^2 \frac{1}{0.288} = 18.9 \text{ md}$$

6.1.3 Case M3

This is a calibration treatment applied to a gas well at another location and a different formation type.

The test was performed by injecting 28350 gallons (675 bbl) of borate water base fracturing fluid (no proppant), at an approximate rate of 30 bpm (pumping time was 22.5 minutes). This is a formation described by a porosity $\phi = 43\%$, reservoir fluid viscosity, $\mu = 1.4$ cp, initial reservoir pressure, $p_i = 5500$ psi, and the fracture permeable height, $h_p = 95$, and the fracture total height, $h_f = 280$ feet. The elastic properties of the porous medium are known as Young's Modulus, $E = 1.1 \times 10^6$ psi, and Poisson's ratio, $\nu = 0.27$. Other required parameters are shown in Table C-3A, Appendix C.

Following step one, collection of reservoir and fluid properties required as input data, a cartesian plot of pressure versus time, Fig. C-11, was produced (see data in Table C-3B), and from it a pumping time, $t_p = 22.5$ min, and initial shut-in pressure, $ISIP = 6694$ psi were determined. It was found that a filtering of the pressure time data, as required by step 4 of the methodology (section 1, chapter 5) was necessary. The reason was a data noise that produced an unreliable plot of $Y(n)$ versus $X(n)$, Fig. C-15. From Fig. C-11, the corresponding fall-off period for

analysis was selected between the initial shut-in pressure and the end of the pressure decline curve. A cartesian plot, Fig. (C-12), of the fall-off pressure versus square root of time (data shown in Table C-3B, Appendix C), indicates that the approximate closure pressure (i.e. the corresponding value to the in-situ minimum stress) is $P_c = 6388$ psi at a closure time, $t_c = 20.94$ minutes. The selection of the closure pressure was done based on the profile of the curve (i.e. second change of slope) and confirmed by a step rate test (data not provided in this work).

A log-log plot, Fig. C-13, of the injection net pressure versus square root of time (data shown in Table C-3B, Appendix C), enables us to determine that a radial geometry most likely occurred during the treatment (i.e. a negative slope of the curve).

Using Eq. (A-42) and (A-53), the G-functions, $g(\Delta t_D, \alpha)$, at a shut-in time $\Delta t_D \neq 0$, and $g_0(\alpha)$ corresponding to a shut-in time, $\Delta t_D = 0$ are computed (data are shown in Table C-3C). Following the above computations, an automated curve-fit of the fall-off pressure versus the G-function is performed by the computer program (see flow chart – Appendix E). The program completes the entire series of calculations, regardless of a best or worse fit obtained at this step. Next, an inspection of the cartesian plot, Fig. C-14, of the fall-off pressure versus the G-function, enables us to assess if the plot is a straight line or not. In this case, with the exception of the first 3 points, the plot indicates a straight line, and thus an application of the pressure derivative (steps 3, 4, and 7, 8) is not necessary since the slope and the intercept can be clearly delineated from the graph. This is also automatically performed by the

computer program, using Eq. (4.49). For our case an intercept, $b_N = 6964.64$ psi and a slope, $m_N = -227.36$ psi were determined.

A next step is to determine if there is spurt loss using Eq. (4.93) as follows:

$$S_p = \frac{1}{2(.388)} \left\{ \left[\frac{0.152(2.832E - 2)}{\left(\frac{1.1E6}{0.925(6964.64 + 1.37689 \cdot (-227.36) - 6388)} \right)^{8/3}} \right] \right\}$$

$$\frac{1}{\left[(2.252E - 10) \frac{(224)(3789.8)}{(1.1E6)(22.5)} \right]^{1/3}} - 2.4565(6964.64 - 6388)$$

$$\frac{\left(\frac{1.07E6}{0.925(6964.64 + 1.37689 \cdot (-227.36) - 6388)} \right)^{4/3}}{1.1E6}$$

$$0.925 \left[(2.252E - 10) \frac{(224)(3789.8)}{(1.1E6)(22.5)} \right]^{1/3} \left\} = -7.6E-02 \text{ ft} = -59 \text{ gal}/100 \text{ ft}^2$$

A negative value of the above, is an indication that the spurt loss could not be identified, and thus all computations will be performed based on a no spurt loss assumption as follows:

The fracture half-length using Eq. (A-10):

$$R_{fNS}^{RAD} = \sqrt[3]{\frac{3(1.1E6)(3789.8)}{8(0.925)(6964.64 - 6388)}} = 143 \text{ ft}$$

The fracture compliance using Eq. (A-3):

$$c_f = \frac{16(0.925)(143)}{3\pi(1.1E6)} = 2.04E-04 \text{ ft/psi}$$

The fluid leak-off coefficient from Eq. (A-19):

$$C_L = \frac{8(143)(-(-227.36))}{3(\pi(0.388)(\sqrt{22.5})(1.1E6))} = 1.36 \text{ E-02 } ft/\sqrt{\text{min}}$$

The fracture average width from Eq. A-22:

$$\bar{w} = 12(5.33) \frac{(143)(0.925)(1.377)}{\pi(1.1E6)} = 7.6E-01 \text{ in}$$

The fracture fluid efficiency from Eq. (A-29):

$$\eta_{NS}^{RAD} = 1 - \frac{227.36(1.377)}{(6964.64 - 6388)} = 45.7\%$$

The second part of the model consists of solving the main components of Eq. (4.140), $Y(n)$ and $X(n)$ for the fall-off period between the initial shut-in pressure and closure pressure. This again is automatically performed by the computer program (Table C-3C), as in the case of the G-function, followed by an automatic curve-fit. Then a cartesian plot of $Y(n)$ versus $X(n)$ is produced, Fig. C-15. Notice in this case the data noise, Fig. C-16, and its direct consequence reflected in Fig. C-15. Thus, data filtering becomes necessary. This was performed with a special two dimensional curve fitting software (Jandel Scientific). Next, the data were again input into the main computer program developed for the computation and analysis of minifrac tests presented in this work. A new plot, Fig. C-17, was obtained which displays a very smooth straight line. From the best straight line fit, the intercept, $b_M=0.267$, and the slope, $m_M=6.66E+08$. Next, the filter-cake resistance and reservoir permeability were computed as follows:

The filter cake-resistance using Eq. (B-13):

$$R_{NS}^{RAD} = \frac{4(0.388)(1.1E6)(22.5)(0.2)}{\pi(143)} = 1.71E+04 \text{ psi} - \text{min} / \text{ft}$$

And the reservoir permeability from Eq. (B-14):

$$K_{NS}^{RAD} = 9.431E13 \left(\frac{143}{6.66E8} \right)^2 \frac{1}{0.388} = 11.2 \text{ md}$$

6.1.4 Case M4

This is a calibration treatment applied to an oil well. The test was performed by injecting 21315 gallons (507.5 bbl) of borate water base fracturing fluid (no proppant), at an approximate rate of 15 bpm (pumping time was 35 minutes). This is a formation described by a porosity $\phi = 23\%$, reservoir fluid viscosity, $\mu = 1.6$ cp, initial reservoir pressure, $p_i = 3685$ psi, and the fracture permeable height, $h_p = 120$ ft, and the fracture total height, $h_f = 120$ feet. The elastic properties of the porous medium are known as Young's Modulus, $E = 5.5 \times 10^6$ psi, and Poisson's ratio, $\nu = 0.27$. Other required parameters are shown in Table C-4A, Appendix C.

Following step one (i.e. collection of reservoir and fluid properties required as input data), a cartesian plot of pressure versus time, Fig. C-18, was produced (see data in Table C-4B). Unfortunately the injection part is not available for this case. However, the pumping time was reported as $t_p = 35$ min, and the initial shut-in pressure, $ISIP = 5995$ psi. It was found that a filtering of the pressure time data, as required by step 4 of the methodology (section 1, chapter 5) was not necessary since a plot of pressure versus the G-function, Fig. C-20, shows a perfect straight line. From the same plot, the corresponding fall-off period for analysis was selected between the

initial shut-in pressure and the end of the pressure decline curve. A cartesian plot, Fig. (C-19), of the fall-off pressure versus square root of time (data shown in Table C-4B, Appendix C), indicates that the approximate closure pressure (i.e. the corresponding value to the in-situ minimum stress) is $P_c = 5225$ psi at a closure time, $t_c = 42$ minutes. The selection of the closure pressure was done based on the profile of the curve (i.e. second change of slope).

A log-log plot of the injection net pressure versus square root of time is not available due to lack of pressure time data from the injection part of the test.

Using Eqs. (A-42) and (A-53), the G-functions, $g(\Delta t_D, \alpha)$, at a shut-in time $\Delta t_D \neq 0$, and $g_0(\alpha)$ corresponding to a shut-in time, $\Delta t_D = 0$ are computed (data are shown in Table C-4C). Following the above computations, an automated curve-fit of the fall-off pressure versus the G-function is performed by the computer program (see flow chart – Appendix E). The program completes the entire series of calculations, regardless of a best or worse fit obtained at this step. Next, an inspection of the cartesian plot, Fig. C-20, of the fall-off pressure versus the G-function, enables us to assess if the plot is a straight line or not. In this case the plot indicates a straight line, and thus an application of the pressure derivative (steps 3, 4, and 7, 8) is not necessary since the slope and the intercept can be clearly delineated from the graph. This is also automatically performed by the computer program, using Eq. (4.49). For our case an intercept, $b_N = 6505.83$ psi and a slope, $m_N = -479.36$ psi were determined.

A next step is to determine if there is spurt loss, Eq. (4.93) as follows:

$$S_p = \frac{1}{2(1.0)} \left\{ \left[\frac{0.152(2.832E - 2)}{\left(\frac{6.0E6}{0.925(6505.83 + 1.37689 \cdot (-479.36) - 5225)} \right)^{8/3}} \right] \cdot \frac{1}{\left[(2.252E - 10) \frac{(202)(2849.4)}{(6.0E6)(35)} \right]^{1/3}} - 2.4565(6505.83 - 5225)}{\left(\frac{3.0E6}{0.925(6505.83 + 1.37689 \cdot (-479.36) - 5225)} \right)^{4/3} \cdot 3.0E6} \right\} = -1.01E-02 \text{ ft} = -78 \text{ gal/100 ft}^2$$

A negative value of the spurt loss is an indication that the spurt loss could not be identified, and thus all computations will be performed based on a no spurt loss assumption as follows:

The fracture half-length using Eq. (A-10):

$$R_{fNS}^{RAD} = \sqrt[3]{\frac{3(6.0E6)(2849.4)}{8(0.925)(6505.4 - 5225)}} = 175 \text{ ft}$$

The fracture compliance using Eq. (A-4):

$$c_f = \frac{16(0.925)(175)}{3\pi(6.0E6)} = 4.24 \text{ E-5 ft/psi}$$

The fluid leak-off coefficient from Eq. (A-19):

$$C_L = \frac{8(175)(-(-479.36))}{3(\pi(1)(\sqrt{35})(6.0E6))} = 2.01 \text{ E-03 ft}/\sqrt{\text{min}}$$

The fracture average width from Eq. A-22:

$$\bar{w}_{NS}^{RAD} = 12(5.33) \frac{(175)(0.925)(1.377)}{\pi(6.0E6)} = 3.64 \text{ E-01 in}$$

The fracture fluid efficiency from Eq. (A-29):

$$\eta_{NS}^{RAD} = 1 - \frac{(479.36)(1.377)}{(6505.4 - 5225)} = 48.48\%$$

Note that the ratio of the permeable to fractured height, r_p , used in this case, is one, since the fracture is contained in the permeable area.

The second part of the model consists of solving the main components of Eq. (4.140), $Y(n)$ and $X(n)$, for the fall-off period between the initial shut-in pressure and closure pressure. Again, as mentioned earlier, this step is automatically performed by the computer program and the output data are shown in Table C-4C. At this stage an automatic curve-fit follows. Next, a cartesian plot of $Y(n)$ versus $X(n)$ is produced, Fig. C-21. From the best straight line fit, the intercept, $b_M=1.89$, and the slope, $m_M=4.05E+08$. Next, the filter-cake resistance and reservoir permeability were computed as follows:

The filter cake-resistance using Eq. (B-13):

$$R_{NS}^{RAD} = \frac{4(1)(6.0E6)(35)(0.2)}{\pi(175)} = 3.05 E+05 \text{ psi} - \text{min} / \text{ft}$$

And the reservoir permeability from Eq. (B-14):

$$K_{NS}^{RAD} = 9.431E13 \left(\frac{175}{4.05E8} \right)^2 \frac{1}{1} = 17.7 \text{ md}$$

Pressure derivative

To test the reliability of the pressure derivative model, developed as part of this work, we need to select a case where a plot of the fall-off pressure versus the G-function is a straight line. Another aspect to be considered, for validation purposes, is the selection of a data set where pressure time data from a minifrac test were analyzed previously. The data set selected and presented here as case M4, is from an oil well. In that study, using Nolte's technique, a leak-off coefficient, $C_L = 1.91 \text{ E-03 } ft/\sqrt{\text{min}}$ was found. The results obtained with model presented in this research, indicate a leak-off coefficient, $C_L = 2.01 \text{ E-03 } ft/\sqrt{\text{min}}$, as expected. A next step is to make use of the pressure derivative model, Eqs. (4.104 – 4.107), and analyze the data assuming the pressure versus G-function plot was not a straight line, as shown in Fig. C-20, but rather a curve (i.e. Figs. 1.1 b, and 1.2). In such a case, a correct delineation of a slope and intercept is impossible, and a simple straight line fit through the curve is unacceptable.

Using Eqs. (4.104 – 4.106), the derivative of the pressure data with respect to time was computed (see data in Table C-4D) and a cartesian plot of $P'(t) \cdot F(t)$ versus $F(t)^2$ produced, as shown in Fig. C-22.

Next, a straight line was fit through zero intercept (note that this is a known point) and the leak-off coefficient, C_L , was calculated using Eq. (4.105) as follows:

$$C_L = -\frac{c_f t_p m_N}{4(r_p)(\sqrt{t_p})} = -\frac{(4.24E-05)35(-33)}{4(1)\sqrt{35}} = 2.06 E-03 \text{ ft}/\sqrt{\text{min}}$$

Noticeable is a good agreement between the value of the leak-off coefficient obtained by the use of the pressure derivative and the one obtained from the pressure versus G-function shown in this work earlier.

Also, as a result of post-fracture analysis, the following could be concluded regarding the results obtained from the minifrac tests and their interpretation with the coupled model presented here:

6.1.5 Case M5

This is a calibration treatment applied to an oil well at another location and a different formation type.

The test was performed by injecting 23000 gallons (547.6 bbl) of borate water base fracturing fluid (no proppant), at an approximate rate of 30.4 bpm (pumping time was 18 minutes). This is a formation described by a porosity $\phi = 41 \%$, reservoir fluid viscosity, $\mu = 1.6$ cp, initial reservoir pressure, $p_i = 4930$ psi, and the fracture permeable height, $h_p = 130$, and the fracture total height, $h_f = 130$ feet. The elastic properties of the porous medium are known as Young's Modulus, $E = 6.5 \times 10^5$ psi, and Poisson's ratio, $\nu = 0.27$. Other required parameters are shown in Table C-5A, Appendix C.

Following step one, collection of reservoir and fluid properties required as input data, a cartesian plot of pressure versus time, Fig. C-23, was produced (see data in Table C-5B), and from it a pumping time, $t_p = 18$ min, and initial shut-in pressure, $ISIP = 6040$ psi were determined. A cartesian plot, Fig. (C-24), of the fall-off pressure versus square root of time (data shown in Table C-5B, Appendix C), indicates that the approximate closure pressure (i.e. the corresponding value to the in-situ minimum stress) is $P_c = 5816$ psi at a closure time, $t_c = 19.26$ minutes. The selection of the closure pressure was done based on the profile of the curve (i.e. second change of slope) and confirmed by a step rate test (data not provided in this work).

A log-log plot, Fig. C-25, of the injection net pressure versus square root of time (data shown in Table C-3B, Appendix C), enables us to determine that a KGD geometry most likely occurred during the treatment (i.e. almost a flat slope of the curve).

Using Eq. (A-42) and (A-47), the G-functions, $g(\Delta t_D, \alpha)$, at a shut-in time $\Delta t_D \neq 0$, and $g_0(\alpha)$ corresponding to a shut-in time, $\Delta t_D = 0$ are computed (data are shown in Table C-5C). Following the above computations, an automated curve-fit of the fall-off pressure versus the G-function is performed by the computer program (see flow chart – Appendix E). The program completes the entire series of calculations, regardless of a best or worse fit obtained at this step. Next, an inspection of the cartesian plot, Fig. C-26, of the fall-off pressure versus the G-function, enables us to assess if the plot is a straight line or not. In this case the application of the

pressure derivative (steps 3, 4, and 7, 8) is not necessary since the slope and the intercept can be clearly delineated from the graph. This is also automatically performed by the computer program, using Eq. (4.49). For our case an intercept, $b_N = 6338.2$ psi and a slope, $m_N = -207$ psi were determined.

A next step is to determine if there is spurt loss using Eq. (4.90) as follows:

$$S_p = \frac{1}{2(1.0)} \left\{ \frac{0.3855 [(4.37 + 1.47837(-0.143) - 4)E7]^2 87.06(0.9)^2}{(4.48E9)^2 (28.5) \left[\frac{(87.06)(0.256)}{(39.6)(4.48E9)(1080)} \right]^{1/2}} \right\} -$$

$$\frac{(4.076)(4.48E9) [(4.37 - 4)E7] \left[\frac{(87.06)(0.256)}{(39.6)(4.48E9)(1080)} \right]^{1/2}}{[(4.37 + 1.47837(-0.143) - 4)E7]^2 (0.9)} \left. \right\} 39.37 =$$

$$= .0059 \frac{ft^3}{ft^2} = 4.4 \frac{gal}{100 ft^2}$$

This time, a positive value of the above is an indication that there is spurt loss and thus all computations will be performed based on spurt loss analysis. Using the new equations derived in this work, the following can be calculated:

The fracture half-length, as a function of spurt loss, using Eq. (A-12):

$$x_{fSL}^{KGD} = \frac{2(7E5) \left[\sqrt{[(130)(1)(0.0059)]^2 + \frac{\pi(130)0.9(6338.2 - 5816)(3074.7)}{2(6.5E5)}} - (130)(1)(0.0059) \right]}{\pi(130)(0.9)(6338.2 - 5816)}$$

$$= 139 \text{ ft}$$

The fracture compliance using Eq. (A-3):

$$c_f = \frac{\pi(0.9)(139)}{2(6.5E5)} = 3.02 \text{ E-04 ft/psi}$$

The fluid leak-off coefficient from Eq. (A-18):

$$C_L = \frac{\pi(139)}{4(1)\sqrt{18}(6.5E5)} (-1(-207)) = 8.21 \text{ E-03 ft}/\sqrt{\text{min}}$$

The fracture average width, as a function of spurt loss, from Eq. A-31:

$$\bar{w}_{SL}^{KGD} = \left\{ \frac{3074.7}{(139)(130)} - 2 \left[(1)(0.0059) + (1)(8.21E-03)\sqrt{18}(1.478) \right] \right\} 12 =$$

$$= 6.62E-01 \text{ in}$$

The fracture fluid efficiency from Eq. (A-36):

$$\eta_{SL}^{KGD} = 1 - \frac{207(1.478) - 2(1)(0.0059)}{3074.7} = 45.7\%$$

$$\frac{(139)(130)(3.02E-04)}{}$$

The second part of the model consists of solving the main components of Eq. (4.140), $Y(n)$ and $X(n)$ for the fall-off period between the initial shut-in pressure and closure pressure. This again is automatically performed by the computer program (Table C-5C), as in the case of the G-function, followed by an automatic curve-fit. Then a cartesian plot of $Y(n)$ versus $X(n)$ is produced, Fig. C-27. From the best straight line fit, the intercept, $b_M = 0.871$, and the slope, $m_M = 1.33E+09$. Next, the filter-cake resistance and reservoir permeability were computed as follows:

The filter cake-resistance, as a function of spurt loss, using Eq. (B-23):

$$R_{SL}^{KGD} = \frac{4.44(1)(6.5E5)(18)(0.871)}{\pi}$$

$$\frac{[\pi(130)(0.9)(6338.2 - 5816)]}{2(6.5E5) \left[\sqrt{[(130)(1)(0.0059)]^2 + \frac{\pi(130)0.9(6338.2 - 5816)(3074.7)}{2(6.5E5)}} - (130)(1)(0.0059) \right]}$$

$$= 1.03 E+05 \text{ psi} - \text{min} / \text{ft}$$

Finally, the reservoir permeability, as a function of spurt loss, is given by Eq. (B-24):

$$K_{SL}^{KGD} = (9.431E13) \left(\frac{1}{1} \right) (0.871).$$

$$\left\{ \frac{2(6.5E5) \left[\sqrt{[(130)(1)(0.0059)]^2 + \frac{\pi(130)0.9(6338.2 - 5816)(3074.7)}{2(6.5E5)} - (130)(1)(0.0059)} \right]}{\pi(130)(0.9)(6338.2 - 5816)} \right\}^2$$

$$= 1.03 \text{ md}$$

Let us now see the results had no spurt loss been identified. To evaluate this, the computation of the above parameters (i.e. fluid and reservoir properties) will be repeated for the case of no spurt loss as follows:

The fracture half-length using Eq. (A-9):

$$x_{fNS}^{KGD} = \sqrt{\frac{2(6.5E5)(3074.7)}{\pi(130)(0.9)(6338.2 - 5816)}} = 144.0 \text{ ft}$$

The fracture compliance using Eq. (A-3):

$$c_f = \frac{\pi(0.9)(144)}{2(6.5E5)} = 3.13 \text{ E-04 ft/psi}$$

The fluid leak-off coefficient from Eq. (A-18):

$$C_L = \frac{\pi(144)}{4(1)\sqrt{18}(6.5E5)}(-1(-207)) = 8.51 E-03 \text{ ft}/\sqrt{\text{min}}$$

The fracture average width from Eq. (A-21):

$$\bar{w}_{NS}^{KGD} = \left\{ \frac{3074.7}{(144)(130)} - 2[(1)(8.51E-03)\sqrt{18}(1.478)] \right\} 12 = 6.86 E-01 \text{ in}$$

The fracture fluid efficiency from Eq. (A-28):

$$\eta_{NS}^{KGD} = 1 - \frac{207(1.478)}{\frac{3074.7}{(144)(130)(3.13E-04)}} = 47.2 \%$$

And from the second part of the coupled model, the filter cake-resistance is obtained from Eq. (B-8):

$$R_{NS}^{KGD} = \frac{4.44(1)(6.5E5)(18)(0.871)}{\pi} \left[\frac{2(6.5E5)}{\pi(130)0.9(6338.2 - 5816)(3074.7)} \right]^{1/2}$$

$$= 9.98 E+04 \text{ psi} - \text{min} / \text{ft}$$

The reservoir permeability is given by Eq. (B-9):

$$K_{NS}^{KGD} = (9.431E13) \left(\frac{1}{1} \right) (0.871) \cdot \left[\sqrt{\frac{2(6.5E5)(3074.7)}{\pi(130)(0.9)(6338.2 - 5816)}} \right]^2 = 1.11 \text{ md}$$

In this case, the identification of spurt loss provides the opportunity for a complete evaluation of the final results, when compared with those obtained assuming no spurt loss. If the calculations were made based on no spurt loss assumption, the following observations could be made for this specific case:

- a) The reservoir permeability is overestimated with 7.2 %
- b) The fracture half-length is 5 ft longer
- c) And the fracture width and fluid efficiency are 3.5 % wider, and 10.5 % greater than in the case when spurt loss is present

These results are as expected since the spurt loss in this case is not significant (i.e. only $4.4 \frac{gal}{100 ft^2}$). Therefore, if the fluid and reservoir properties were evaluated as if no spurt loss was present, the errors would not be significant. Another observation consists of the fact that the spurt loss found in this case is low. This is in agreement with the reservoir type (i.e. low permeability).

Following the analysis and interpretation of all five field cases presented above, the following can be concluded:

1. The reservoir permeabilities obtained from cases M1 and M2, are in good agreement with each other (i.e. 19.5 md for case M1 and 18.9 md for case M2). Note that both cases represent two productive intervals of the same well. They were also confirmed by results obtained from subsequent build-up tests performed at a later time following the actual fracturing job and a significant production time.

2. As far as the third case is concerned (i.e. M3), well tests analysis and history matching of several wells, from that reservoir, indicated permeability values between 8 and 12 md. The permeability obtained from the minifrac test with the model presented in this study is 11.2 md, and is in good agreement with the above.
3. For the fourth application, case M4, the permeability could not be confirmed from independent tests. However, excellent agreement is shown between the results (i.e. leak-off coefficient) obtained from both the pressure and pressure derivative models.
4. The analysis of the last data set, case M5, led to permeability values of 1.03 and 1.11 md respectively, (i.e. based on spurt and no spurt loss analysis). This was confirmed by results obtained from build up tests and history matching analysis which indicated permeabilities from 1 to 4 md for that specific reservoir.
5. As stated earlier, parameters obtained from the first part of the model (i.e fracture width and fracture half-length, which in turn are functions of the leak-off coefficient), are used in the second part (filter-cake reservoir flow). Their validity was indirectly confirmed by a good agreement of the reservoir permeability values obtained from both the coupled model presented here and from post-fracture tests.
6. A significant advantage of the improved Mayerhofer technique is that it differentiates between the filter cake and the reservoir permeability. Note that not one case, out of five presented in this work, developed a negative

intercept of the diagnostic cartesian plot of $Y(n)$ versus $X(n)$. A negative intercept, produced by the application of the original technique introduced by Mayerhofer, would imply a negative energy which is unrealistic. Comparative diagnostic plots are shown in Appendix C (see Figs. 33-42).

7. Negative values of the spurt loss, lead us to perform analysis based on no spurt loss assumption. If the spurt loss can be estimated, as shown in case M5, or from a lab test, then the new equations presented here can be successfully used for the estimation of more accurate fracture dimensions (i.e. fracture width and fracture half-length), and fluid and reservoir properties (i.e. leak-off coefficient, fluid efficiency, filter-cake resistance and reservoir permeability).
8. Although this coupled model has significant improvements, as opposed to its earlier versions^{13,15,16}, there are situations in which the pressure-time data set shows relatively considerable noise (i.e. Fig. C-16). If that is the case, a filtering operation of the original pressure-time data is recommended to aid the applicability of the second part of the model. This can be done by various methods. In this work, the data were filtered making use of a 2-D commercial filtering and curve-fitting software (Jandel Scientific). The results presented in Fig. C-17, clearly show the benefits of these data processing, which are reflected by the reservoir permeability value obtained in this specific case.
9. The new pressure derivative equation, proved to be a reasonable alternate of the current pressure decline analysis, where a plot of the pressure versus the

G-function is a curve instead of a straight line. For a better evaluation of the applicability of the pressure derivative equation, analysis were performed for all five filed cases. Cartesian plots of the pressure derivative equation (i.e. $P'(t) \cdot F(t)$ versus $F(t)^2$) are shown in Appendix C (see Figs. C-28 through C-32) as well as the computations of the leak-off coefficient, C_L . Additionally, the final results obtained from both pressure and pressure derivative analysis is shown in Table-5G. Inspection of these results indicate that they are in good agreement, with the exception of the first two field applications (i.e. cases M1 and M2). This due to non-linearity generated by the first few points of the fall off pressure data, following the initial shut-in pressure.

10. Consideration of the ratio of the permeable fracture area to the total fracture area is also essential. Nolte included this in his original derivations, but the later developed model, based on Nolte-Shlyapobersky's technique, did not. This parameter can affect results considerably (i.e. more than 50%) if the permeable fracture height and the fracture height are not the same (i.e. unconfined fracture).
11. The same is true regarding the ratio of the spatial to wellbore average pressure ratio. This was also part of the original Nolte's derivations with consideration for the elastic properties of the formation (i.e. fracture compliance). However, for reasons presented earlier in this research, some authors believe it has a value of one as soon as the fracture ceases to

propagate. This assumption is not realistic since the leak-off continues to take place after shut-in and until the fracture closes. Consequently, this was incorporated into the equations derived for the coupled model presented in this work, to ensure a more realistic and accurate interpretation of the pressure decline analysis obtained from a minifrac test. Non-Newtonian aspects is also incorporated via this ratio (see Eqs. (A-5, A-6, and A-7)). Also modified relationships, for the estimation of the average fracture width during the propagation, were derived in this work (Eqs. (4.73, 4.74, and 4.77)) as a function of the equivalent Newtonian fracturing fluid viscosity. They are valid only for the fracture propagation (i.e. during injection).

12. Finally, the improved model derived for the filter-cake reservoir flow part, proves to be more accurate than its earlier versions. One of the most significant achievements of this improvement, consists of a correct separation between the effects of the pressure drop across the filter-cake (i.e. the filter cake resistance) and the pressure drop across the reservoir, thus enabling us to obtain reasonable values of the reservoir permeability.

6.2 Sensitivity Analysis

In addition to the decline data smoothing procedure described above, sensitivity analysis was applied to investigate the impact of the uncertainty of the input reservoir and treatment parameters. Accurate formation parameters are critical whether designing a stimulation or analyzing a calibration treatment. Shown in this research, are a few representative plots, Figs. D-1 – D-8, for Case M1. The Poisson's ratio, ν

and Young's Modulus, E , affect the estimation of the fracture extension, x_f as shown in Figs. D-1, and D2. For example, if Young's Modulus is chosen to be $E = 1.0E+6$ psi, the fracture extension is approximately 66 ft, while for $E = 5E+06$ psi, the fracture half length increases to about 100 ft. It was found that Young's Modulus is critical for the estimation of the leak-off coefficient, C_L , not only because it affects directly the interpretation of the slope, but also because it has a secondary effect via the fracture extent. (Fig. D-3) and even a tertiary effect via the r_p ratio. Similarly, the estimate of the reservoir permeability, k , is also very sensitive to the elasticity modulus (Fig. D-4.)

Figures D5-6 show sensitivities of the estimated parameters with respect to other input variables. It was also observed, that the reservoir initial pressure, Fig. D-7, formation fluid viscosity, Fig. D-8, porosity, and closure pressure are as critical as any other parameter in the model. While the sensitivity analysis results shown here is valid for one particular field case, similar trends were found in the other cases.

CHAPTER 7

CONCLUSIONS AND RECOMMENDATIONS

7.1 Conclusions

This research was undertaken to address the study of minifrac tests for the determination of fluid and reservoir properties. The main objective of the minifrac is to determine the above mentioned hydraulic fracturing parameters necessary for the design of an effective fracture stimulation. Therefore a fracture calibration, also known as a minifrac test, is used to help optimize the hydraulic fracture treatment design, since it provides critical information pertaining to the well to be treated.

The potential niche for the application and interpretation of such test consists in the determination of fluid leak-off characteristics, (i.e. leak-off coefficient, spurt loss, fracturing fluid efficiency, and filter cake-resistance) , fracture dimensions (i.e. average fracture width and fracture half-length), and also a very valuable parameter, the reservoir permeability.

To overcome significant operational and economic constraints, generated by conventional well testing, the fracture calibration is used to achieve robust application with a minimal amount of incremental cost or operational delay time. In essence, it is remarkable the fact that such a test does not require special equipment beyond that generally available on a drilling rig, or pumping operation and testing requirements of less than three to five hours. Not only that the conventional tests require considerable length of time, but short time tests such as a drill-steam or impulse test, often provide only small range (local estimates) of the formation properties, which in addition may

very well be contaminated by local formation damage effects. One key parameter, the reservoir permeability, is expected to be more reliable when determined from a the fall-off analysis of a minifrac test, since the fracture breaks the barriers formed by the near wellbore damage, and the area of investigation is obviously greater than just the borehole area itself.

Based on the results of this research, the following conclusions are offered:

1. An improved coupled model for the determination of fluid and reservoir properties from minifrac tests was developed. The model has two main components in its structure: (1) the pressure decline analysis based on Nolte-Shlyapobersky technique^{3,11,14,33}, and (2) the filter-cake reservoir flow (transient flow analysis) based on Mayerhofer's technique^{15,16,39}. The improved model correctly delineates the separation of the filter-cake component from the reservoir transient flow, and consequently reliable values of the filter-cake resistance and reservoir permeability are obtained. Not a single case, out of the five field minifrac tests presented in this work and analyzed by the improved model, show a negative intercept which would lead to erroneous values of the above two parameters (i.e. as is the case when using earlier versions for such analysis).
2. Spurt loss analysis is introduced in this research. New equations were developed for the determination of the fluid and reservoir properties from minifrac tests, when the spurt loss can be identified.
3. A new pressure derivative equation was developed. This can be used to correctly delineate the slope of a straight line from a plot of the pressure derivative versus a function of the shut-in time. From this slope, the leak-off coefficient can be

determined and once this is known the rest of the fluid and reservoir properties can be calculated from the pressure equation.

4. Sensitivity analysis was performed to assess the most sensitive parameters and how they can affect the final interpretation of the minifrac test when using this coupled model.
5. Five field cases were used to demonstrate that the coupled model presented in this research is a versatile and simple tool, which can be used for the determination of fluid and reservoir properties from minifrac tests.

7.2 Recommendations

Following a review of the published technical papers and also work in the area of fracture calibration treatments, the following recommendations for future research are made:

- A. Research and extend the interpretation of fall-off analysis based on Biot's approach to the 2-D problem of fracture propagation based on Lagrangian methods. The Lagrangian formulation is based on the classical form of Lagrange's equations, Eqs. (2.27-2.30). In essence, he produced a basic equation that expresses the balance between work expended and work done in propagating a 2-D crack. Existing theories, assume linear elastic behavior of the reservoir and ignores surface energy considerations at the crack tip and plastic deformation effects. Leak-off is treated as an independent process and merged with the fracture propagation problem by iterative methods. The Lagrangian method, is not restricted to elastic behavior, and leak-off can be included as a part of the

formulation. Therefore Biot includes leak-off by assuming a piston like displacement of the reservoir fluid by an incompressible fracture fluid filtrate, with a moving boundary between the two. Lee^{19,20,21}, continued Biot's work, and incorporated Biot's energy balance equation into the pressure decline analysis, Eq. (2.33).

He solved Eq. (2.23) numerically for a KGD geometry and incorporated the correct rheology of the fracturing fluid used to create the minifrac. However his solution as well as Biot's, assumes that the surface energy, E , can be neglected. On the other hand, the method should be extended for the other two geometries as well (i.e. PKN and Radial). Consequently two essential steps need to be taken for the continuation of their work:

1. consideration of the crack shape function, $f(L_D)$ of Eq. (2.23) and also of a corresponding definition of the fracture width. As far as the crack shape is concerned, the preceding analysis assumed that this was given. However this is not a prerequisite of the Lagrangian formulation¹⁷. The crack shape can be determined by methods based on various assumptions, and for strict analysis Barrenblatt⁵⁵ conditions at the tip must be considered. He showed that to avoid infinite stress at the tip of the fracture, the fluid flow can not extent all the way to the tip. The exact shape of the crack at the tip and over the rest of its length is determined by the fluid pressure distribution¹⁷.
2. Regarding the PKN model, the fracture width has an elliptical shape on a vertical direction, Fig. 3.6, and can be written as²⁹:

$$w(x, \xi, t) = w(x, 0, t)(1 - \xi)^{1/2} \dots\dots\dots(7.1)$$

where:

$w(x, \xi, t)$ is the fracture width at any position, ξ , $\xi = z/h_f$ and $w(x, 0, t)$ is the maximum fracture width at the centerline at any x position. Further, this width can be expressed as a function of the fracture opening pressure as follows:

$$w(x, 0, t) = \frac{\Gamma_w(1 - \nu)}{G} h_f P_n \dots\dots\dots(7.2)$$

where Γ_w is a width opening pressure coefficient, ν is Poisson's ratio, G the stress modulus, and P_n the net pressure²⁹.

3. For the radial geometry, this can be approximated with a parabolic shape, in which case the fracture width is given as follows:

$$w(r, t) = w(0, t)(1 - r/R)^{\Gamma_w} \dots\dots\dots(7.3)$$

where the gamma coefficient varies from 1/2 (i.e. low fluid efficiency) to 1 (for high fluid efficiency)²⁹.

4. Regarding the neglected surface energy term, E , of Eq. (7.1), Griffith⁵⁷ showed an equation for the stability of the fracture using the energy balance, Eq. (3.3). From this equation, the surface energy is:

$$U_f = 4\gamma L_f h_f \dots\dots\dots(7.4)$$

where:

U_f = surface energy of the fracture (noted E in Eq. (2.23))

hf = thickness of the elastic material (fracture half-length in our case)

γ = specific surface energy of the elastic material

The only unknown in Eq. (7.4) is the surface energy of the elastic material. This can be estimated approximately from the elastic constants or from the specific energy of evaporation. Experimental determinations of γ have been made by measuring the force needed for propagating a crack of known dimensions and then applying Griffith energy argument. For cases not complicated by local plastic deformations (which of interest to us since we consider the reservoir an elastic medium), or by multiple fracturing at the crack tip (therefore not applicable in the case of naturally fractured reservoirs), the experimentally derived values of γ agree reasonably well with theoretical predicted values, thus lending support to Griffith's theory. Typical values for γ of the order of 10 Jm^{-2} have been reported for ceramics and rocks.

Therefore, knowing γ and following substitution of Eq. (7.4) in Eq. (2.23), Biot's energy equation for the KGD geometry becomes:

$$4\gamma L_f h_f - \frac{V_o}{\beta_B} \int_0^1 \frac{\partial p}{\partial x} L_D f(L_D) dL_d = \frac{K\gamma}{2L_f^3} \left(\frac{V_o}{\beta_B} \right)^2 \dots\dots\dots(7.5)$$

And from a numerical solution of the above equation, a more accurate fracture half-length can be determined. A similar procedure needs to be employed for the other geometry types (i.e. PKN and Radial).

B. Extend the pressure decline analysis between the shut-in and closure pressure, to the after-closure period. The latest published works known are by Valko¹¹ and Nolte^{8,51}. Nolte provides a technical framework for adding after-closure fracturing-pressure analysis to the pre-treatment calibration-testing sequence that defines fracture geometry and fluid-loss characteristics. A companion paper⁸ provides the general framework for applying this analysis and for its integration with the other parts of the testing sequence. In his work, he shows that the after-closure period contains the reservoir pseudo-linear flow period that is the focus, and the pseudo-radial flow period that has been previously addressed in a comprehensive manner. Radial flow defines the reservoir parameters. The primary roles for linear-flow are to define spurt loss, after a calibration (“minifrac”) treatment, and to use the reservoir’s perspective of the fracture length to validate information available from other parts of the calibration sequence. His work shows a valuable approach based on Carslaw and Jaeger⁷¹ formulation of heat conduction through a solid medium. The critical aspects with the methodology presented in Nolte’s work⁸ is non-uniqueness when trying to identify the correct slope for both the linear and the radial flow regime, and an empirically determined spurt loss coefficient. Valko¹¹, claims that once the leak-off from the fracture into the reservoir stops, the fracture “remembers” the actual geometric distribution of the leak-off history less and less. Therefore the wellbore pressure can be calculated assuming an equivalent radius and applying the radial leak-off law. He solves this in a Laplace space with the convolution

method. However, the work does not present a rigorous procedure to the problem of interpreting a calibration treatment in terms of radial leak-off.

- C. Introduce the effects of the reservoir temperature on the analysis and interpretation of a minifrac test where incompressible fracturing fluids are used for injection. Zhu Ding⁷² presented a comprehensive model to simulate pressure and temperature behavior and their interference in a minifrac test for the case when foams or other compressible fluids are injected during the test.

Nomenclature

α	=	exponent of fracture area growth, dimensionless
q_{app}	=	apparent leak-off rate, ft^3 / min
$\Delta p(t)$	=	total pressure drop in the reservoir, psi
$G(\alpha_a, \alpha_{c2}, \theta)$	=	a function similar to Nolte's G-function, developed by
$g(t_o)$	=	$g(t_D = 0)$
α_B	=	Biot's constant, $1 \geq \alpha \geq 0$
β_B	=	Biot's shape constant
β_B	=	Nolte's ratio of average spatial pressure to wellbore average net pressure, psi
P_b	=	breakdown pressure, psi
C	=	cohesion modulus (material constant)
c_f	=	compliance, psi / ft
S_h	=	compressive stress applied at infinity, psi
α_p	=	constant, 141.2, (oil field units)
α_r	=	constant, 264×10^{-6} (oil field units)
C_c	=	corrected value of the leak-off coefficient, ft / \sqrt{min}
κ	=	correction factor for C while pumping, dimensionless
K_{Icr}	=	critical toughness, psi
L_D	=	dimensionless distance along the fracture
$f(t_D)$	=	dimensionless loss rate ratio
$g(t_D)$	=	dimensionless loss volume function
t_D	=	dimensionless shut-in time
$w(x)$	=	displacement in the direction perpendicular to the fracture, in
D	=	dissipation function
R	=	filter-cake resistance, $psi - min / ft$
P_f	=	fluid pressure in the fracture, psi
Q_i	=	forces not derived from a dissipation function
\overline{Q}_i	=	forces not derived from a potential function, lbf
q_l	=	fraction of $q_t = q_n$, contributing to leak-off only
A_f	=	fracture area, ft^2
s	=	fracture face skin
b_{fB}	=	fracture half width, at the end of fracture entrance, in
P_{fp}	=	fracture propagation pressure, psi

b_B	=	fracture width as a function of x and t , used by Biot, <i>in</i>
\bar{q}_i	=	general coordinates for the system
a, A	=	general variable for the area
$F\left[1/2; 1 + \alpha; (1 + \Delta t_D)^{-1}\right]$	=	hypergeometric function
t_o	=	injection time, min
b_N	=	intercept, Nolte-Shlyapobersky model
E_k	=	kinetic energy of the system, $ft \cdot lbf$
L	=	Lagrange's function given by difference between kinetic and potential
q_{Fn}	=	leak-off rate during closing, ft^3 / min
u_L	=	leak-off velocity, Carter's model, ft / min
σ_{\max}	=	maximum in-situ stress, <i>psi</i>
σ_{\min}	=	minimum in-situ stress, <i>psi</i>
τ_{yy}	=	normal vertical stress, <i>psi</i>
$R_D(t)$	=	normalized filter-cake resistance, dimensionless
A_{of}, A_L	=	open fissure area, ft^2
A_p, A_k	=	permeable or loss area, ft^2
A_p	=	permeable or loss rate, ft^2
ν	=	Poisson's ratio
E_p	=	Potential energy of the system, $ft \cdot lbf$
$\Delta p_{face}(t)$	=	pressure drop across the filter-cake, <i>psi</i>
$\Delta p_{pinvz}(t)$	=	pressure drop across the polymer invaded zone, <i>psi</i>
$\Delta p_{res}(t)$	=	pressure drop in the reservoir, <i>psi</i>
β	=	ratio of average to wellbore net pressure, dimensionless
f_p	=	ratio of permeable area to the fracture area, dimensionless
E	=	separation energy of the system, $ft \cdot lbf$
m_N	=	slope, Nolte-Shlyapobersky model
γ	=	specific surface energy of the elastic medium, lbf / ft^2
S_l	=	spurt loss coefficient
W_f	=	strain energy of the fracture, $ft \cdot lbf$
K	=	stress intensity factor
U_f	=	surface energy at the fracture face, $ft \cdot lbf$
σ_T	=	tensile failure stress of the rock, <i>psi</i>
h_m	=	thickness of the elastic material, <i>in</i>
τ	=	time to create the fracture area, min

α_1	=	viscosity degradation coefficient ($\alpha_1=1$, linear viscosity; $\alpha_1=0$,
V_o, V	=	volume of fracture from entrance to L_f (i.e. x_f)
P_w	=	wellbore pressure at shut-in, <i>psi</i>
η	=	fluid efficiency, dimensionless
ν	=	Poisson ratio, dimensionless
ϕ	=	porosity, dimensionless
μ_r	=	viscosity of reservoir fluid, <i>cp</i>
L_f, x_f	=	fracture half length, <i>ft</i>
$f(L_D)$	=	fracture shape function
q_{l_j}, q_n	=	leak of rate during pumping, ft^3 / min
b_M	=	intercept, Improved Mayerhofer's technique
b_N	=	intercept, Nolte-Shlyapobersky method
C_L	=	Carter leakoff coefficient, $ft / \sqrt{\text{min}}$
c_i	=	total reservoir compressibility, $1 / \text{psi}$
		dimensionless
E	=	Young's Modulus, <i>psi</i>
E'	=	plane strain modulus, <i>psi</i> , $E'=E/(1-\nu^2)$
		energy of the system
h_f	=	fracture height, <i>ft</i>
h_p	=	permeable height, <i>ft</i>
i	=	injection rate per one wing, <i>gal / min</i>
k_r	=	reservoir permeability, <i>md</i>
		Meyer ³⁸
m_M	=	slope, Mayerhofer et al. method
m_N	=	slope, Nolte method
n	=	index of time step
n'	=	generalized flow behavior index,
n_e	=	number of time steps during pumping
p_c	=	closure pressure, <i>psi</i>
p_r	=	reservoir pressure, <i>psi</i>
q_n	=	leakoff rate from one wing through two faces, ft^3 / min
R_f	=	radius of a radial fracture, <i>ft</i>
R_o	=	reference filter-cake resistance at the end of pumping, $\text{psi} - \text{min} / \text{ft}$
r_p	=	ratio of permeable to fracture area
s_f	=	fracture stiffness (proportionality constant in the pressure vs. width relationship psi / ft)
S_p	=	spurt loss coefficient, ft^3 / ft^2
t	=	time, <i>min</i>

t_p, t_m	=	time at end of pumping, <i>min</i>
t_n	=	time at (end of) step n, <i>min</i> uniform viscosity)
V	=	volume of one fracture wing, <i>gal</i>
V_i	=	volume of injected fluid into 1 wing, <i>gal</i>
W_p, \bar{w}	=	average fracture width at end of pumping, <i>in</i>
w_L	=	leak-off width, <i>in</i>
w_n	=	average fracture width at time step n, <i>in</i>
x_p	=	fracture half length at end of pumping, <i>ft</i>
x_f	=	fracture half length, <i>ft</i>

References

1. Thompson J.W., and Church D.C.: "Design, Execution, and Evaluation of Minifrac in the Field: A Practical Approach and Case Study," SPE 26034, 83-93, May 1993
2. Nolte, K.G. and Smith, M.B.: "Interpretation of Fracturing Pressures," *JPT* 1767, Sep. 1981.
3. Nolte, K.G.: "Determination of Proppant and Fluid Schedules from Fracturing Pressure Decline," *SPEPE*, pp. 255-265, (July) 1986. (originally SPE 8341, 1979)
4. Nolte, K.G., Mack, M.G., and Lie, W.L.: "A Systematic Method for Applying Fracturing Pressure Decline," SPE 25845, Rocky Mountains Regional Low Permeability Symposium., Denver, April 12-14, 1993.
5. Hagel M.W., and Meyer B.R.: "Utilizing Minifrac-Data to Improve Design and Production," Petroleum Society of CIM, 1992
6. Gidley, L.J. et al.: *Recent Advances in Hydraulic Fracturing*, SPE Monograph, Vol.12, 309
7. McLellan, P.J., and Janz H.J.: "New Insights into Fracturing Pressure Interpretation: Case Study of minifrac tests in a naturally fractured gas reservoir," *JCPT*, Vol. 30, No.6, Dec. 1991
8. Nolte, K.G.: "Background for After-Closure Analysis of Calibration Tests," unsolicited SPE 39407 July, 1997.
9. Shlyapobersky J., Wong G.K., and Walhaug W.W.: "Overpressure Calibrated Design of Hydraulic Fracture Stimulations," SPE 18194, 133-148, Oct. 1988
10. Economides, M.J. and Nolte, K.G. "*Reservoir Stimulation* (2nd ed.)," Prentice Hall, Englewood Cliffs, NJ. 1989.
11. Valkó P. and Economides, M.J. *Hydraulic Fracture mechanics*, Wiley, Chichester, England. 1995.
12. Ispas, I.N., Tiab, D., Britt, L.K., Valko, P., Economides, M.J. "Methodology of Fluid Leakoff Analysis in High-Permeability Fracturing," SPE 39476, Feb. 1998
13. Mayerhofer, M.J., Economides, M.J. and Ehlig-Economides, C.A.: "Pressure Transient Analysis of Fracture Calibration Tests," SPE 26527 presented at 68th Annual Technical Conference and Exhibition, Houston, Texas, 3-6 Oct, 1993.

14. Nolte, K.G.: "Determination of Fracture Parameters from Fracture Pressure Decline," SPE 8341 presented at the 54th Annual Technical Conference, Las Vegas, Sept. 1979
15. Mayerhofer, M.J., and Economides, M.J.: "Permeability Estimation From Fracture Calibration Treatments," SPE 26039, 117-128, 26-28 May 1993
16. Mayerhofer, M.J., and Economides, M.J.: "Field Cases for Permeability Determination from Minifrac," SPE 26999, 111-117, 27-29 April 1994
17. Biot M.A., Masse L., and Medlin W.L.: "A Two Dimensional Theory of Fracture Propagation," SPEPE, 17-30, January 1986
18. Lee W.S.: "Study of the Effects of Fluid Rheology on Minifrac Analysis," SPE 16916, 377-386, Sept. 27-30, 1987
19. Lee W.S.: "New Method of Mini-Frac Analysis Offers Greater Accuracy and Enhanced Applicability," SPE 15941, 231-238, Nov. 1986
20. Lee W.S.: "Mini-Frac Analysis Based on Ellipsoidal Geometry," SPE 15369, Oct. 1986
21. Lee W.S.: "Pressure Decline Analysis With the Christianovich and Zheltov and Penny-Shaped Geometry Model Fracturing," SPE/DOE 13872, 227-237, May 1985
22. Nolte, K.G.: "A General Analysis of Fracturing Pressure Decline with Applications to Three Models," *SPEFE* 571-583, Dec. 1986, and also Chapter 14 and Appendix J of the SPE Monograph: Recent Advances in Hydraulic Fracturing Vol. 12, 1989.
23. Nolte, K.G.: "Fracturing Design Considerations Based on Pressure Analysis," paper SPE 10911, 1982 [and published as two papers in *SPEPE* 22, Feb. 1988].
24. Carter, R.D.: Appendix. of: "Optimum Fluid Characteristics for Fracture Extension," *Drilling and Prod. Prac.* API 1957.
25. Fan, Y.: "A new Interpretation for Fracture Calibration Treatments," SPE 37401, 107-115, March 1997
26. Martins J.P., and Harper T.R.: "Mini-Frac Pressure Decline Analysis for Fractures Evolving From Long Perforated Intervals and Unaffected by Confining Strata," SPE/DOE 13869, 203-210, 1985
27. Nordgren, R.P.: "Propagation of a Vertical Hydraulic Fracture," SPEJ, 306-314, June 1970
28. Daneshy, A.A.: "On the Design of Vertical Hydraulic Fractures," JPT, 83-97, 1973

29. Meyer B.R.: "Design Formulae for 2-D and 3-D Vertical Fractures: Model Comparison and Parametric Studies," SPE 15240 1986
30. Nolte, K.G.: "Fracturing Pressure Analysis for Non-Ideal Behavior," *JPT* 210, Feb. 1991.
31. Castillo, J.L.: "Modified Pressure Decline Analysis Including pressure -Dependent Leak-off," SPE 16417 presented at the SPE Rocky Mountain Regional Low Permeability Reservoirs Symposium, Denver, CO, May 18-19, 1987.
32. Moschovidis Z.A.: "Interpretation of Pressure Decline for Minifrac Treatments Initiated at the Interface of Two Formations," SPE 16188, 15-27, 1987
33. Shlyapobersky J., Walhaug, W.W., Sheffield. R.E., Huckabee, P.T.: "Field Determination of Fracturing Parameters for Overpressure Calibrated Design of Hydraulic Fracturing," SPE 18195, 63rd Annual Technical Conference and Ex. Houston, TX, Oct 2-5, 1988.
34. McLellan, P.J., and Janz, H.J.: "Analysis of Minifrac Shut-In Pressures, Limestone/Burnt Timber Area, Alberta," CIM/SPE 90-44, June 1990
35. Soliman M.Y., Kuhlman R.D., and Poulsen D.K.: "Minifrac Analysis for Heterogeneous Reservoirs," CIM/SPE 90-5, June 1990
36. Gu H., and Leung K.H.: "Three-Dimensional Numerical Simulation of Hydraulic Fracture Closure With Application to Minifrac Analysis," SPE 20657, 403-415, 1990
37. Zhu, D., and Hill A.D.: "The Effect of Temperature on Minifrac Pressure Decline," SPE 22874, 569-581, Oct. 1991
38. Valko, P. and Economides, M.J.: "Fluid Leakoff Delineation in High Permeability Fracturing," SPE 37403, Production Operations Symposium., Oklahoma City, OK, March 9-12, 1997.
39. Mayerhofer, M.J., and Economides, M.J.: "Interpretation of Early and Late-Time Transient Filtration Phenomena of Cross-linked Polymer Gels in Front of Long Cores," SPE 25489, 1933
40. Gringarten, A.C., Ramey, H.J., Jr, and Raghavan, R.: "Unsteady-State Pressure Distributions Created by a Well With a Single Infinite-Conductivity Vertical Fracture," *SPEJ* 347, March 1974.
41. Samaniego, F.V. and Cinco-Lay H.: "Transient Pressure Analysis for Variable Rate Testing of Gas Wells", SPE 21831, 249-258 , April 1991.

42. Dusterhoft R., Vithal S., and McMechan D.: "Improved Mini-Frac Analysis Technique in High-Permeability Formations," SPE 30103, 265-274, May 1995
43. Eligh-Economides, C.A., Fan Y., and Economides, M.J.: "Interpretation of Fracture Calibration Tests in Naturally Fractured Reservoirs," SPE 28690, 217-227, Oct. 1994
44. Gu, H. et al.: "Formation Permeability Determination Using Impulse-Fracture Injection," SPE 25425, March 21-23, 1993
45. Abousleiman, Y., Cheng, A.H-D. and Gu, H.: "Formation Permeability Determination by Micro or Mini-Hydraulic Fracturing," *J. Ener. Res. Tech.* 104, Jun. 1994.
46. Vithal S., McMechan D., Walters, H., and Dusterhoft R.: "Application of Improved Minifrac Analysis Technique in High-Permeability Formations," Proceedings Indonesian Petroleum Association, 24th Annual Convention, Oct. 1995
47. Leshchyshyn, T.H., Seffari, A., and Ali, F.: "Minifrac Analysis of Shear Parting in Alberta Reservoirs and its Impact Towards On-Site Fracture Design," CPS, Paper 96-79, June 10-12, 1996.
48. Poulsen, D.K.: "Equilibrium Minifrac Test and Analysis," SPE 36438, 225-233, 6-9 Oct. 1996.
49. Sunil, N.G., Tibbles, R., and Nolte, K.G.: "Evaluation of Calibration Treatments, for Frac Pack Completions, in Offshore West Africa," SPE 38192, 459-474, June 2-3, 1997
50. Tinker, S.J., Baycroft, P.D., Ellis, R.C., and Fitzhugh, E.: "Minifrac Tests and Bottomhole Treating Pressure Analysis Improve Design and Execution of Fracture Stimulations," SPE 37431, 369-380, March 9-11, 1997
51. Nolte, K.G., Maniere, J.L. and Owens K.A.: "After-Closure Analysis of Fracture Calibration Tests" SPE 38676 presented at ATCE, San Antonio, TX, Oct 5-8, 1997.
52. Geertsma, J., Klerk, F.: "A Rapid Method of Predicting Width and Extent of Hydraulically Induced Fractures," JPT, 1571-1581, Dec. 1969
53. Sneddon, I.N.: "The Distribution of Stress in the Neighbourhood of a Crack in an Elastic Solid," Proceedings of the Royal Society A, Vol. 187, 23-54, Dec. 1946
54. Sneddon, I.N., and Lowengrub, M.: "Crack Problems in the Classical Theory of Elasticity," 1996

55. Barenblatt, G.I.: "The Mathematical Theory of Equilibrium Cracks in Brittle Fracture," *Advances in Applied Mechanics*, Vol. 7, 285-359, 1962
56. Irwin, G.R.: "Analysis of Stress and Strains Near the End of Crack Traversing a Plate," *Journal of Applied Mechanics*, Vol.24, 361-364, Sept 1957
57. Griffith, A.A.: "The Phenomena of Rupture and Flow in Solids," *Philosophical Transactions of the Royal Society of London*, Vol. A221, 60-95, 1921
58. Yew, C.H.: "Mechanics of Hydraulic Fracturing," Gulf Publishing Co., 1997
59. Timoshenko, S., and Goodier, N.J. *Theory of elasticity*, 2nd ed. McGraw Hill, 1951
60. Hagoort, J.: "Waterflood-Induced Hydraulic Fracturing," Thesis at University of Delft, PB81-248262, 1980.
61. Schmidt, D.R., and Zoback, M.D.: "Poroelectricity Effects in the Determination of Minimum Horizontal Principal Stress in Hydraulic Fracturing Tests – A proposed Breakdown Equation Employing a Modified Effective Stress Relation for Tensile Failure," *IJRM, MSGA*, vol. 26, no. 6, 499-506, 1989.
62. Warpinski, N.R., Schmidt, R.A., and Northrop, D.A.: "In-situ Stresses: The Predominant Influence of Hydraulic Fracture Containment," *SPE/DOE 8932*, May 1980.
63. Warpinski, N.R., Clark, J.A., Schmidt, R.A., and Huddle, C.W.: "Laboratory Investigation on the Effect of In-situ Stress on Hydraulic Fracture Containment," *SPEJ*, 333-340, June 1980.
64. Khristianovic, S.A., and Zheltov, Y.P.: "Formation of Vertical Fractures," *Proceedings Fourth World Petroleum Congress Section II/T.O.P.*, 578-586
65. Perkins, T.K., and Kern, L.R.: "Widths of Hydraulic Fractures," *AIME*, 937-949, Sept. 1961
66. Howard G.C. and Fast, C.R.: "Optimum Fluid Characteristics for Fracture Extension," *Drilling and Production Prac.*, API pp 261-270, 1957. (Appendix by E.D. Carter)
67. Abramovitz, M., and Stengun, I.A.: "Handbook of Mathematical Functions," Dover, NY, 1972.
68. Cinco-Ley, H., and Meng, H.Z.: "Pressure Transient Analysis of Wells with Finite Conductivity Vertical Fracture in Double Porosity Reservoirs," *SPE 18172* presented at the 63rd Annual Technical Conference and Exhibition, Houston, Oct. 2-5, 1988.

69. Gringarten, A.C. and Ramey, A.J., Jr.: "Unsteady State Pressure Distributions Created by a Well with a Single-Infinite Conductivity Vertical Fracture," *SPEJ*, 347-360, Aug. 1974.
70. Cinco-Ley, H., and Samaniego-V.F.: "Transient Pressure Analysis: Finite Conductivity-Fracture Case vs Damaged-Fracture Case," SPE 10179 presented at the 1981 SPE Annual Technical Conference and Exhibition, San Antonio, Oct. 4-7
71. Carslaw, H.S. and Jaeger, J.C.: "Conduction of Heat in Solids," 2nd Ed. 1959, Oxford University Press, Great Britain.
72. Zhu, D.: "Modeling of Minifracture Pressure Behavior for a Compressible Fluid," PhD Dissertation University of Texas at Austin, 1992
73. Lord, D.L., Vinod, P.S., Shah, S.N., and Bishop, M.L.: "An Investigation of Fluid Leak-off Phenomena by use of a High Pressure Simulator," SPE 52394 presented at the 1995 SPE Annual Technical Conference, Dallas 22-25 October.
74. Ridha, M.O.: "Modeling of Fracture Closure During Calibration Treatment," MS Thesis, University of Oklahoma 1999.
75. Gu, H., Elbel, J.L., Nolte, K.G., Cheng, A.H-D. and Abousleiman, Y.: "Formation Permeability Determination Using Impulse Fracture Injection," SPE 25425, Production Operations Symposium., Oklahoma City, OK, March 21-23, 1993
76. Ayoub, J.A., Bourdet, F.P. and Chauvel, Y.L.: "Impulse Testing," *SPEFE* 534, Sept. 1988.
77. Earlougher, R.C.: "Advances in Well Test Analysis," SPE Monograph, Vol. 5, 1977
78. Raghavan, R., Reynolds, A.C., and Meng, H.Z.: "Analysis of Pressure Buildup Data Following a Short Flow Period," *JPT*, 904, April 1982.
79. Van Everdingen A.F, and Hurst W.: "The Application of Laplace Transformations to Flow Problems in Reservoirs," *Transactions*, p. 305, Dec . 1949
80. Ehlig-Economides C.A., and Ramey H.J. : "Pressure Buildup for Wells Produced at Constant Pressure," *SPEJ*, p. 105, Feb. 1981
81. Bennett C.O.: " Analysis of Fractured Wells," PhD Dissertation University of Tulsa, 1981.
82. Tinker, S.J.: "Mini-Frac Tests and Bottomhole Treating Pressure Analysis Improve Design Execution of Fracture Simulations," SPE 37431, 369-380, 1997

83. Poulsen, D.K.: "A general Theory of Minifracturing," SPE 37407, 177-187, 1997
84. Gulrajani, N.S., Mack G.M., and Elbel J.: "Pressure History Inversion for Implementation of Fracture Treatments," SPE 63439, 1996
85. Meyer B.R., and Hagel M.W.: "Simulated Mini-Frac Analysis," Petroleum Society of CIM, June 12-16, 1988
86. Zhu, D., and Hill A.D.: "A Comprehensive Model of Mini-Frac Pressure Behavior With Foam Fracturing Fluids," SPE 25846, April 1993
87. Warembourg P.A.: "New Analysis Technology for Determining Fracture Parameters from Calibration Treatments: Case Histories, Rocky Mountain Area," SPE 17502, 273-287, May 1988
88. Gulrajani S.N., Tibbles, R.J., and Nolte, K.G.: "Evaluation of Calibration Treatments, for Frac Pack Completions, in Offshore West," SPE 38192, 459-474, June 1997
89. Abe, H., Mura, T., and Keer, M.: "Growth Rate of a Penny-Shaped Crack in Hydraulic Fracturing of Rocks," Journal of Geophysical Research, 5335-5340, Oct. 1976
90. Gringarten, A.C., Ramey, H.J., Jr.: "Unsteady-State Pressure Distributions Created by a Well With a Single Horizontal Fracture, Partial Penetration, or Restricted Entry," Transactions Vol. 257, 1974
91. Hubert, K. and Willis, D.G.: "Mechanics of Hydraulic Fracturing," AIME, Vol. 210, 153-163, 1957
92. Perkins, T.K., and Gonzales, J.A.: "Changes in Earth Stress Around a Wellbore Caused by Radially Symmetrical Pressure and Temperature Gradients," AIME, 129-137, Apr. 1984
93. Alekseenko, O.P., Vaisman, A.M., and Zazovsky, A.F.: "A New Approach to Fracturing Test Interpretation Using The PKN Model," Int. J. Rock Mech. & Min. Sci. 34:3-4, No. 356, 1997
94. Haimson, B., and Fairhurst C.: "Initiation and Extension of Hydraulic Fractures in Rocks," SPEJ, 310-318, 1967
95. Shah, S.N., Lord, D.L., and Tan, H.C.: "Recent Advances in the Fluid Mechanics and Rheology of Fracturing Fluids," SPE 22391, 621-636, March 1992
96. Dobkins, T.: "Procedures, Results, and Benefits of Detailed Fracture Treatment Analysis," SPE 10130, Oct. 1981

97. McGowen, J.M., Vithal, L., Parker, M.A., Rahimi, A., and Martch Jr., W.E.: "Fluid Selection for Fracturing High Permeability Formations," SPE 26559, Oct. 1993
98. Hedayati, S., Abass, H.H., Soliman, M.Y., Boyd, D.: "Review of Prefracturing Testing and Effect of Measured Parameters on Fracture Design," Southwestern Petroleum Short Course – 92, 116-150
99. Ahmen, U., Kelkar, S., and Schatz, J.: "Minifrac: An Aid to Formation In-Situ Stress and Permeability Measurements," 24th U.S. Symposium of Rock Mechanics 319-326, June 1983
100. Hopkins, C.W.: "The Importance of In-Situ Stress Profiles in Hydraulic-Fracturing Applications," JPT, 944-948, Sept. 1997
101. Wright, C.A., Minner, W.A., and Snow, D.M.: "Robust Technique for Real-Time Closure Stress Determination," SPE 30503, 543-553, Oct. 1995
102. Pater, C.A.: "Physical and Numerical Modeling of Hydraulic Fracture Closure," SPEPF, 122-128, May 1996
103. Bowie, O.L.: "Analysis of an Infinite Plate Containing Radial Cracks Originating at the Boundary of an Internal Circular Hole," Journal of Mathematics and Physics, Vol. 35, 61-72, 1956
104. Middlebrook, M.L., Aud, W.W., Harkrider, J.D., and Hansen, J.T.: "An Evolving Approach in the Analysis of Stress Test Pressure Decline Data," SPE 29599, 549-566, March 1995
105. Woodland, D.C., and Bell, J.S.: "In-Situ Stress Magnitudes From Minifrac Records in Western Canada," CIM/SPE No. 88-36-67, June 1988
106. Rosepiler, M.J.: "Determination of Principal Stresses and Confinement of Hydraulic Fractures in Cotton Valey," SPE 8405, Sept. 1979
107. Detournay, E., and Cheng, H.D.: "Poroelastic Response of a Borehole in a Non-Hydrostatic Stress Field," Int. J. Rock Mech. Min. Sci. & Geomech. Abstr., Vol. 25, 171-182, 1988
108. Detournay, E., and Carbonell, R.: "Fracture Mechanics Analysis of the Breakdown Process in Minifrac or Leak-off Tests," Eurok'94, 399-407, 1994
109. Hayashi, K., and Ito, T.: "Determination of the Minimum Horizontal principal Stress from Pressure Decay After Breakdown in Hydraulic Fracturing," Geothermal Resources Council Transactions, Vol.15, 483-486, Oct. 1991
110. Koning, E.J.L., and Niko, H.: "Fractured Water Injection Wells: A Pressure Falloff

Test for Determining Fracture Dimensions,” SPE 14458, Sept. 1985

111. Mukherjee, H., Larkin, S., and Kordziel, W.: “Extension of Fracture Pressure Decline Curve Analysis to Fissured Formations,” SPE 21872, April 1991

Appendix A

Modeling Equations (Pressure Decline Analysis)

Pressure variation during the shut-in period:

$$P_{wII} = \left(p_c + \frac{V_i}{A_f c_f} - \frac{2r_p S_p}{c_f} \right) - \left(\frac{2C_L r_p \sqrt{t_p}}{c_f} \right) \times g(\Delta t_D, \alpha) = b_N + m_N \times g(\Delta t_D, \alpha) \dots \dots \dots (A-1)$$

Fracture compliance, c_f corresponding to each fracture geometry¹⁰:

$$c_{fPKN} = \frac{\pi \beta_{PKN} h_f}{2E'} \dots \dots \dots (A-2)$$

for the PKN geometry, where h_f is the fracture height.

$$c_{fKGD} = \frac{\pi \beta_{KGD} x_f}{2E'} \dots \dots \dots (A-3)$$

for the KGD geometry with x_f as the fracture half-length.

$$c_{fRAD} = \frac{\pi \beta_{RAD} (32/3\pi^2) R_f}{2E'} \dots \dots \dots (A-4)$$

for the radial geometry, where R_f is the fracture half-length.

The ratios of the average net pressure in the fracture to the wellbore flowing pressure, for each fracture geometry, are given as follows:

$$\beta_{NPKN} = (2n' + 2)/(2n' + 3 + \alpha_1) \dots\dots\dots(A-5)$$

for the PKN geometry,

$$\beta_{NKGD} = 0.9 \dots\dots\dots(A-6)$$

for the KGD geometry, and

$$\beta_{NRAD} = 3\pi^2 / 32 \dots\dots\dots(A-7)$$

for the radial geometry, where n is the fluid rheology index, and α_1 an exponent which is a function of the fluid viscosity behavior (i.e. $\alpha_1 = 0$ for the case of uniform viscosity, and $\alpha_1 = 1$ represents linearly decreasing viscosity from the wellbore to the tip of the fracture).

Fracture half-length from the intercept, b_N , of Eq. (A-1):

L-1 No spurt loss case^{11, 12}

PKN geometry

$$x_{fNS}^{PKN} = \frac{2E'V_i}{\pi h_f^2 \beta_{PKN} (b_{NS}^{PKN} - p_C)} \dots\dots\dots(A-8)$$

KGD geometry

$$x_{fNS}^{KGD} = \sqrt{\frac{2E'V_i}{\pi h_f \beta_{KGD} (b_{NS}^{KGD} - p_C)}} \dots\dots\dots(A-9)$$

RADIAL geometry

$$R_{NS}^{RAD} = \sqrt[3]{\frac{3E'V_i}{8\beta_{RAD}(b_{NS}^{RAD} - P_c)}} \dots\dots\dots(A-10)$$

L-1 Spurt loss case

PKN geometry

$$x_{JSL}^{PKN} = \frac{2E'V_i}{\pi h_f^2 \beta_{PKN} (b_{SL}^{PKN} - P_c) + 4h_f E' r_p S_p} \dots\dots\dots(A-11)$$

KGD Geometry

$$x_{JSL}^{KGD} = \frac{2E' \left[\sqrt{(h_f r_p S_p)^2 + \frac{\pi h_f \beta_{KGD}}{2E'} (b_{SL}^{KGD} - P_c) V_i} - h_f r_p S_p \right]}{\pi h_f \beta_{KGD} (b_{SL}^{KGD} - P_c)} \dots\dots\dots(A-12)$$

Radial geometry

$$R_{JSL}^{RAD} = \frac{\left(3A\sqrt{4B^3 + 27A^2C\sqrt{3C}} - 2B^3 - 27A^2C\right)^{1/3}}{3A\sqrt{2}} + \frac{\sqrt[3]{2B^2}}{3A\left(3A\sqrt{4B^3 + 27A^2C\sqrt{3C}} - 2B^3 - 27A^2C\right)^{1/3}} - \frac{B}{3A} \dots\dots\dots(A-13)$$

where:

$$A = 16\pi\beta_{RAD} (b_{SL}^{RAD} - P_c) \dots\dots\dots(A-14)$$

$$B = 6\pi^2 S_p r_p E' \dots\dots\dots(A-15)$$

$$C = -3V_i \pi E' \dots\dots\dots(A-16)$$

Leak-off coefficient from the slope, m_N , of Eq. (A-1):

The leak-off coefficient, C_L can be computed from Eq. (A-1) as follows:

PKN geometry

$$C_L = \frac{\pi h_f}{4r_p \sqrt{t_p} E'} (-m_N) \dots\dots\dots(A-17)$$

KGD geometry

$$C_L = \frac{\pi x_f}{4r_p \sqrt{t_p} E'} (-m_N) \dots\dots\dots(A-18)$$

RADIAL geometry

$$C_L = \frac{8R_f}{3\pi r_p \sqrt{t_p} E'} (-m_N) \dots\dots\dots(A-19)$$

Fracture average width, \bar{w} , and fluid efficiency, η , as a function of both the slope, m_N , and the intercept, b_N , of Eq. (A-1):

E-1 No spurt case

From Eqs. (4.46, and 4.47) the average fracture width is given by the difference between the maximum fracture width and the leak-off width, as follows:

PKN geometry:

$$\bar{w}_{NS}^{PKN} = \frac{V_i}{x_{fNS}^{PKN} h_f} - 2r_p C_L \sqrt{t_p} g_0 (4/5) \dots \dots \dots (A-20)$$

KGD geometry:

$$\bar{w}_{NS}^{KGD} = \frac{V_i}{x_{fNS}^{KGD} h_f} - 2r_p C_L \sqrt{t_p} g_0 (2/3) \dots \dots \dots (A-21)$$

Radial geometry:

$$\bar{w}_{NS}^{RAD} = \frac{V_i}{\pi (R_{fNS}^{RAD})^2} - 2r_p C_L \sqrt{t_p} g_0 (8/9) \dots \dots \dots (A-22)$$

where the leak-off width is:

$$w_L^{PKN} = 2r_p C_L \sqrt{t_p} g_0 (4/5) \dots \dots \dots (A-23)$$

$$w_L^{KGD} = 2r_p C_L \sqrt{t_p} g_0(2/3) \dots \dots \dots (A-24)$$

$$w_L^{RAD} = 2r_p C_L \sqrt{t_p} g_0(8/9) \dots \dots \dots (A-25)$$

The fluid efficiency is given by the ration between the volume of the fracture created and the volume of fluid injected:

$$\eta = \frac{V_f}{V_i} \dots \dots \dots (A-26)$$

Dividing Eqs. (A-20: A-22) by the fracture compliance, c_f , and combining with Eqs. (A-1) and (A-26), it follows that for the:

PKN geometry

$$\eta_{NS}^{PKN} = \frac{\frac{V_i}{x_{fNS}^{PKN} h_f c_f} - \frac{2r_p C_L \sqrt{t_p} g_0(4/5)}{c_f}}{\frac{V_i}{x_{fNS}^{PKN} h_f c_f}} = 1 + \frac{m_{NS}^{PKN} g_0(4/5)}{\frac{V_i}{x_{fNS}^{PKN} h_f c_f}} \dots \dots \dots (A-27)$$

KGD geometry

$$\eta_{NS}^{KGD} = \frac{\frac{V_i}{x_{fNS}^{KGD} h_f c_f} - \frac{2r_p C_L \sqrt{t_p} g_0(2/3)}{c_f}}{\frac{V_i}{x_{fNS}^{KGD} h_f c_f}} = 1 + \frac{m_{NS}^{KGD} g_0(2/3)}{\frac{V_i}{x_{fNS}^{KGD} h_f c_f}} \dots \dots \dots (A-28)$$

Radial geometry

$$m_{NS}^{RAD} = \frac{\frac{V_i}{\pi (R_{fNS}^{RAD})^2 c_f} - \frac{2r_p C_L \sqrt{t_p} g_0 (8/9)}{c_f}}{\frac{V_i}{\pi (R_{fNS}^{RAD})^2 c_f}} = 1 + \frac{m_{NS}^{RAD} g_0 (8/9)}{\frac{V_i}{\pi (R_{fNS}^{RAD})^2 c_f}} \dots\dots\dots (A-29)$$

where from Eq. (A-1):

$$\frac{V_i}{x_{fNS}^{PKN} h_f c_f} = b_{NS}^{PKN} - p_c \text{ from Eq. (A-1) and}$$

$$\frac{V_i}{x_{fNS}^{KGD} h_f c_f} = b_{NS}^{KGD} - p_c, \text{ and}$$

$$\frac{V_i}{\pi (R_{fNS}^{RAD})^2 c_f} = b_{NS}^{RAD} - p_c$$

E-2 Spurt loss case

From Eqs. (4.46, and 4.47) the average fracture width is given by the difference between the maximum fracture width and the sum of spurt width and leak-off width, as follows:

PKN geometry:

$$\overline{w}_{SL}^{PKN} = \frac{V_i}{x_{SL}^{PKN} h_f} - 2 \left[r_p S_p + r_p C_L \sqrt{t_p} g_0(\alpha) \right] \dots\dots\dots (A-30)$$

KGD geometry:

$$\overline{w}_{SL}^{KGD} = \frac{V_i}{x_{SL}^{KGD} h_f} - 2 \left[r_p S_p + r_p C_L \sqrt{t_p} g_0(\alpha) \right] \dots\dots\dots (A-31)$$

Radial geometry:

$$\overline{w}_{SL}^{RAD} = \frac{V_i}{\pi (R_{fNS}^{RAD})^2} - 2 \left[r_p S_p + r_p C_L \sqrt{t_p} g_0(\alpha) \right] \dots\dots\dots (A-32)$$

where the spurt width is:

$$S_w = 2r_p S_p \dots\dots\dots (A-33)$$

and the leak-off width is given by Eqs. (A-23:A-25).

The fluid efficiency is given by the ration between the volume of the fracture created and the volume of fluid injected:

$$\eta = \frac{V_f}{V_i} \dots\dots\dots (A-34)$$

Dividing Eqs. (A-30: A-32) by the fracture compliance, c_f , and combining with Eqs.

(A-1) and (A-34), it follows that for the:

PKN geometry

$$\eta_{SL}^{PKN} = \frac{\frac{V_i}{x_{SL}^{PKN} h_f c_f} - \frac{2r_p C_L \sqrt{t_p} g_0(4/5)}{c_f} - \frac{2r_p S_p}{c_f}}{\frac{V_i}{x_{SL}^{PKN} h_f c_f}} = 1 + \left[\frac{m_{SL}^{PKN} g_0(4/5) - \frac{2r_p S_p}{c_f}}{\frac{V_i}{x_{SL}^{PKN} h_f c_f}} \right]$$

.....(A-35)

KGD Geometry

$$\eta_{SL}^{KGD} = \frac{\frac{V_i}{x_{SL}^{KGD} h_f c_f} - \frac{2r_p C_L \sqrt{t_p} g_0(4/5)}{c_f} - \frac{2r_p S_p}{c_f}}{\frac{V_i}{x_{SL}^{KGD} h_f c_f}} = 1 + \left[\frac{m_{SL}^{KGD} g_0(2/3) - \frac{2r_p S_p}{c_f}}{\frac{V_i}{x_{SL}^{KGD} h_f c_f}} \right]$$

.....(A-36)

Radial geometry

$$\eta_{SL}^{RAD} = \frac{\frac{V_i}{\pi (R_{fNS}^{RAD})^2 c_f} - \frac{2r_p C_L \sqrt{t_p} g_0(8/9)}{c_f} - \frac{2r_p S_p}{c_f}}{\frac{V_i}{\pi (R_{fNS}^{RAD})^2 c_f}} =$$

$$1 + \left[\frac{m_{SL}^{RAD} g_0 (8/9) - \frac{2r_p S_p}{c_f}}{\frac{V_i}{\pi (R_{SL}^{RAD})^2 c_f}} \right] \dots \dots \dots (A-37)$$

Where for the PKN and KGD geometries: $r_p = h_p / h_f$ (or $r_p = 1$ if the fracture is contained in the permeable layer) and for the RADIAL geometry^{11,12}:

$$r_p = \frac{2}{\pi} \left\{ \left[\left(\frac{h_p}{2R_f} \right)^2 \left(1 - \frac{h_p}{2R_f} \right) \right]^{0.5} + \text{Arcsin} \frac{h_p}{2R_f} \right\} \dots \dots \dots (A-38)$$

(or $r_p = 1$ if the fracture is contained in the permeable layer.)

G-function solution and approximations:

A) The following program, written in Mathematica language, was used to solve the

G-function¹¹, Eq. (4.33):

```
(*Program GFUNCTION *)
H1=Simplify[-Integrate[1/Sqrt[tD-tauD],{tD,1+dtD,tauD}]]/.tauD
->AD^(1/alpha)
H2=Integrate[H1,{AD,0,1}]
G[x_,y_]:=H2/.{dtD->x,alpha->y}
G0[y_]:=g[0,y]
```

Where:

$$g(\Delta t_D, \alpha) = \int_0^1 \left(\int_{\alpha \sqrt{A_D}}^{1+\Delta t} \frac{dt_D}{\sqrt{t_D - \alpha \sqrt{A_D}}} \right) dA_D \dots \dots \dots (A-39)$$

$$H_1 = \int_0^1 (H_2) dA_D \dots\dots\dots(A-40)$$

$$H_2 = \int_{\alpha\sqrt{A_D}}^{1+\Delta t} \frac{dt_D}{\sqrt{t_D - \alpha\sqrt{A_D}}} \dots\dots\dots(A-41)$$

and the following solutions were found:

$$g_0(\alpha) = \frac{2^{2\alpha} \alpha [\Gamma[\alpha]]^2}{(1 + 2\alpha) \Gamma[2\alpha]} \dots\dots\dots(A-42)$$

for a dimensionless time (i.e. ratio of shut-in to injection time) $\Delta t_D = 0$, and

$$g(\Delta t_D, \alpha) = \frac{4\alpha\sqrt{\Delta t_D} + 2\sqrt{1 + \Delta t_D} x \frac{\Gamma[1 + \alpha]}{\Gamma[\alpha]\Gamma[1]} \left[\int_0^1 t^{\alpha-1} dt - (1 + \Delta t_D) \int_0^1 t^{\frac{2\alpha-3}{2}} dt \right]}{1 + 2\alpha} \dots\dots\dots(A-43)$$

for a dimensionless time (i.e. ratio of shut-in to injection time) $\Delta t_D \neq 0$.

Note that Eq. (A-48), given by Valko and Economides¹¹ is identical with Eq. (4.31) based on the special properties of the Gamma function.

The G-function values at a zero dimensionless shut-in time (i.e. $\Delta t_D = 0$), used in the above equations are computed with Gamma function for each geometry as follows:

PKN geometry

$$g_0\left(\frac{4}{5}\right) = \frac{2^{2\left(\frac{4}{5}\right)} \frac{4}{5} \left[\Gamma\left[\frac{4}{5}\right] \right]^2}{\left(1 + 2\left(\frac{4}{5}\right)\right) \Gamma\left[2\left(\frac{4}{5}\right)\right]} = 1.41495$$

KGD geometry

$$g_0\left(\frac{2}{3}\right) = \frac{2^{2\left(\frac{2}{3}\right)} \frac{2}{3} \left[\Gamma\left[\frac{2}{3}\right] \right]^2}{\left(1 + 2\left(\frac{2}{3}\right)\right) \Gamma\left[2\left(\frac{2}{3}\right)\right]} = 1.47837$$

RADIAL geometry

$$g_0\left(\frac{8}{9}\right) = \frac{2^{2\left(\frac{8}{9}\right)} \frac{8}{9} \left[\Gamma\left[\frac{8}{9}\right] \right]^2}{\left(1 + 2\left(\frac{8}{9}\right)\right) \Gamma\left[2\left(\frac{8}{9}\right)\right]} = 1.37689$$

B) For a dimensionless time (i.e. ratio of shut-in to injection time) $\Delta t_D = 0$, using the definition of the Euler Gamma function⁶⁷, and the Mathematica package, approximate computational values for the G-function are given as follows:

For a dimensionless time (i.e. ratio of shut-in to injection time) $\Delta t_D = 0$

$$g_N(\alpha) = 1.9 + 1.96458\alpha + 0.5141989\alpha^2 + 0.0286518\alpha^3 \dots\dots\dots(A-44)$$

and

$$g_M(\alpha) = 0.95 + 1.565315\alpha + 0.7015294\alpha^2 + 0.087314215\alpha^3 + 1.42022 \times 10^{-3}\alpha^4 \dots\dots\dots(A-45)$$

where:

$$g_0(\alpha) = \frac{g_N(\alpha)}{g_M(\alpha)} \dots\dots\dots(A-46)$$

and for a dimensionless time (i.e. ratio of shut-in to injection time) $\Delta t_D \neq 0$:

$$g\left(\Delta t_D, \frac{4}{5}\right) = \frac{g_N\left(\Delta t_D, \frac{4}{5}\right)}{g_M\left(\Delta t_D, \frac{4}{5}\right)} \dots\dots\dots(A-47)$$

for the PKN geometry, where:

$$g_N\left(\Delta t_D, \frac{4}{5}\right) = 1.3442025 + 75.441875d + 600.83415d^2 + 1228.4165d^3 + 725.0305d^4 + 89.360515d^5 \dots\dots\dots(A-48)$$

$$g_M\left(\Delta t_D, \frac{4}{5}\right) = 0.9 + 52.11073d^2 + 363.9545d^3 + 513.3249d^4 + 159.35395d^5 + 6.1667255d^6 \dots\dots\dots(A-49)$$

$$g\left(\Delta t_D, \frac{2}{3}\right) = \frac{g_N\left(\Delta t_D, \frac{2}{3}\right)}{g_M\left(\Delta t_D, \frac{2}{3}\right)} \dots\dots\dots (A-50)$$

for the KGD geometry, where:

$$g_N\left(\Delta t_D, \frac{2}{3}\right) = 1.4044325 + 77.8472775d + 603.5863d^2 + 1188.9535d^3 + \\ 681.8245d^4 + 82.50085d^5 \dots\dots\dots (A-51)$$

$$g_M\left(\Delta t_D, \frac{2}{3}\right) = 0.95 + 51.572175d + 353.78d^2 + 486.7553d^3 + 148.22945d^4 + \\ 5.6615725d^5 - 0.066205975d^6 \dots\dots\dots (A-52)$$

and

$$g\left(\Delta t_D, \frac{8}{9}\right) = \frac{g_N\left(\Delta t_D, \frac{8}{9}\right)}{g_M\left(\Delta t_D, \frac{8}{9}\right)} \dots\dots\dots (A-53)$$

for the RADIAL geometry, where:

$$g_N\left(\Delta t_D, \frac{8}{9}\right) = 1.3080455 + 73.96738d + 598.728d^2 + 1251.492d^3 + \\ 751.165d^4 + 93.527215d^5 \dots\dots\dots (A-54)$$

$$g_M\left(\Delta t_D, \frac{8}{9}\right) = 0.95 + 52.432875d + 370.06015d^2 + 529.359d^3 + 166.1455d^4 + \\ 6.47786d^5 - 0.076790115d^6 \dots\dots\dots (A-55)$$

Appendix B

Modeling Equations (Filter-cake – Reservoir Flow Leak-Off Transient Analysis)

The following main formulas are incorporated into a computer program (see chapter 5 of this work).

In essence here we have both cases (1) no spurt loss and (2) spurt loss.

B-I No spurt loss

If no spurt loss is identified (see section 4.5), then the following equations are used:

PKN geometry

Eq. (4.134) can be written as follows:

$$Y(n)_{NS}^{PKN} = b_{MNS}^{PKN} + m_{MNS}^{PKN} X(n)_{NS}^{PKN} \dots\dots\dots(B-1)$$

where the independent variable is:

$$Y(n)_{NS}^{PKN} = \frac{p_n - p_i}{p_{n-1} - p_n} \frac{\Delta t_n}{\sqrt{t_p t_n}} \dots\dots\dots(B-2)$$

A combination of Eqs. (2.17), (2.20), and (4.137), yields the filter-cake resistance:

$$R_{NS}^{PKN} = \frac{4E' r_p t_p}{\pi h_f} \left[\frac{2n' + 3 + \alpha_1}{2n' + 2} \right] b_{MNS}^{PKN} \dots\dots\dots(B-3)$$

Combining Eqs. (4.138), (4.139) and (A-2) gives the reservoir permeability:

$$k_{NS}^{PKN} = \frac{1}{r_p} \left[\frac{h_f}{m_{MNS}^{PKN}} \right]^2 \dots\dots\dots(B-4)$$

and the independent variable:

$$X(n)_{NS}^{PKN} = \left[\frac{2n' + 2}{2E'(2n' + 3 + a_1)} \right] \sqrt{\pi} \left(\frac{\mu_r}{\phi c_t} \right)^{1/2} \left\{ \left[\left(\frac{p_{n_s+1} - p_{n_s+2}}{t_n - t_{n_s+1}} \right) (t_n - t_{n_s+1})^{1/2} + \right. \right. \\ \left. \left. \sum_{j=n_s+3}^n \frac{(p_{j-1} - p_j)}{\Delta t_j} - \frac{(p_{j-2} - p_{j-1})}{\Delta t_{j-1}} (t_n - t_{j-1})^{1/2} \right] + \right. \\ \left. \frac{\bar{w}_{NS}^{PKN}}{h_f \sqrt{\pi}} \left[\frac{t_n^{1/2} - (t_n - t_{n_s+1})^{1/2}}{(p_{n-1} - p_n) t_p t_n^{3/2}} \Delta t_n \right] \right\} \dots\dots\dots(B-5)$$

B-I KGD geometry

Eq. (4.134) can be written as follows:

$$Y(n)_{NS}^{KGD} = b_{MNS}^{KGD} + m_{MNS}^{KGD} X(n)_{NS}^{KGD} \dots\dots\dots(B-6)$$

where the dependent variable is:

$$Y(n)_{NS}^{KGD} = \frac{p_n - p_i}{p_{n-1} - p_n} \frac{\Delta t_n}{\sqrt{t_p t_n}} \dots\dots\dots(B-7)$$

A combination of Eqs. (2.18), (2.21), (4.137) and (A-9), yields the filter-cake resistance:

$$R_{NS}^{KGD} = \frac{4.44 E' r_p t_p}{\pi} \left(\frac{\pi h_f \beta_{KGD} (b_{NS}^{KGD} - p_c)}{2 E' V_i} \right)^{1/2} b_{MNS}^{KGD} \dots\dots\dots (B-8)$$

Combining Eqs. (4.138), (4.139), (A-3), and (A-9), yields the reservoir permeability:

$$k_{NS}^{KGD} = \frac{1}{r_p (m_{MNS}^{KGD})^2} \left(\frac{2 E' V_i}{\pi h_f \beta_{KGD} (b_{NS}^{KGD} - p_c)} \right) \dots\dots\dots (B-9)$$

and the independent variable:

$$X(n)_{NS}^{KGD} = \frac{0.45}{E'} \sqrt{\pi} \left(\frac{\mu_r}{\phi c_t} \right)^{1/2} \left\{ \left[\left(\frac{p_{n_s+1} - p_{n_s+2}}{t_n - t_{n_s+1}} \right) (t_n - t_{n_s+1})^{1/2} + \sum_{j=n_s+3}^n \frac{(p_{j-1} - p_j)}{\Delta t_j} - \frac{(p_{j-2} - p_{j-1})}{\Delta t_{j-1}} (t_n - t_{j-1})^{1/2} \right] + \frac{\bar{W}_{NS}^{KGD}}{x_{jNS}^{KGD} \sqrt{\pi}} \left[\frac{t_n^{1/2} - (t_n - t_{n_s+1})^{1/2}}{(p_{n-1} - p_n) r_p t_n^{3/2}} \Delta t_n \right] \right\} \dots\dots\dots (B-10)$$

B-1 Radial geometry

Eq. (4.134) can be written as follows:

$$Y(n)_{NS}^{RAD} = b_{MNS}^{RAD} + m_{MNS}^{RAD} X(n)_{NS}^{RAD} \dots\dots\dots (B-11)$$

where the dependent variable is:

$$Y(n)_{NS}^{RAD} = \frac{p_n - p_i}{p_{n-1} - p_n} \frac{\Delta t_n}{\sqrt{t_p t_n}} \dots\dots\dots(B-12)$$

A combination of Eqs. (2.19), (2.22), (4.137), and (A-10) yields the filter-cake resistance:

$$R_{NS}^{RAD} = \frac{4E' r_p t_p}{\pi} \left(\frac{8\beta_{RAD} (b_{NS}^{RAD} - p_C)}{3E' V_i} \right)^{1/3} b_{MNS}^{RAD} \dots\dots\dots(B-13)$$

Combining Eqs. (4.138), (4.139), (A-4), and (A-10), yields the reservoir permeability:

$$k_{NS}^{RAD} = \frac{1}{r_p (m_{MNS}^{RAD})^2} \left(\frac{3E' V_i}{8\beta_{RAD} (b_{NS}^{RAD} - p_C)} \right)^{2/3} \dots\dots\dots(B-14)$$

and the independent variable:

$$X(n)_{NS}^{RAD} = \frac{\sqrt{\pi}}{2E'} \left(\frac{\mu_r}{\phi c_i} \right)^{1/2} \left\{ \left[\left(\frac{p_{n_s+1} - p_{n_s+2}}{t_n - t_{n_s+1}} \right) (t_n - t_{n_s+1})^{1/2} + \sum_{j=n_s+3}^n \frac{(p_{j-1} - p_j)}{\Delta t_j} - \frac{(p_{j-2} - p_{j-1})}{\Delta t_{j-1}} (t_n - t_{j-1})^{1/2} \right] + \frac{\bar{W}_{NS}^{RAD}}{R_{fNS}^{RAD}} \left[\frac{t_n^{1/2} - (t_n - t_{n_s+1})^{1/2}}{(p_{n-1} - p_n) t_p t_n^{3/2}} \Delta t_n \right] \right\} \dots\dots\dots(B-15)$$

B-II Spurt loss

If spurt loss is identified (see section 4.5), then the following equations are used:

PKN geometry

$$Y(n)_{SL}^{PKN} = b_{MSL}^{PKN} + m_{MSL}^{PKN} X(n)_{SL}^{PKN} \dots\dots\dots(B-16)$$

where the dependent variable is:

$$Y(n)_{SL}^{PKN} = \frac{p_n - p_i}{p_{n-1} - p_n} \frac{\Delta t_n}{\sqrt{t_p t_n}} \dots\dots\dots(B-17)$$

A combination of Eqs. (2.17), (2.20), and (4.137), yields the filter-cake resistance:

$$R_{SL}^{PKN} = \frac{4E' r_p t_p}{\pi h_f} \left[\frac{2n' + 3 + a_1}{2n' + 2} \right] b_{MSL}^{PKN} \dots\dots\dots(B-18)$$

Combining Eqs. (4.138), (4.139) and (A-2) gives the reservoir permeability:

$$k_{SL}^{PKN} = \frac{1}{r_p} \left[\frac{h_f}{m_{MSL}^{PKN}} \right]^2 \dots\dots\dots(B-19)$$

From Eq. (4.134):

$$X(n)_{SL}^{PKN} = \left[\frac{2n' + 2}{2E'(2n' + 3 + a_1)} \right] \sqrt{\pi} \left(\frac{\mu_r}{\phi c_i} \right)^{1/2} \left\{ \left[\left(\frac{p_{n_s+i} - p_{n_s+2}}{t_n - t_{n_s+1}} \right) (t_n - t_{n_s+1}) \right]^{1/2} + \right.$$

$$\sum_{j=n_s+3}^n \left[\frac{(p_{j-1} - p_j)}{\Delta t_j} - \frac{(p_{j-2} - p_{j-1})}{\Delta t_{j-1}} (t_n - t_{j-1})^{1/2} \right] +$$

$$\left. \frac{\overline{W}_{SL}^{PKN}}{h_f \sqrt{\pi}} \left[\frac{t_n^{1/2} - (t_n - t_{n_s+1})^{1/2}}{(p_{n-1} - p_n) t_p t_n^{3/2}} \Delta t_n \right] \right\}$$

.....(B-20)

B-I KGD geometry

$$Y(n)_{SL}^{KGD} = b_{MSL}^{PKN} + m_{MSL}^{KGD} X(n)_{SL}^{KGD} \dots\dots\dots(B-21)$$

where the dependent variable is:

$$Y(n)_{SL}^{KGD} = \frac{p_n - p_i}{p_{n-1} - p_n} \frac{\Delta t_n}{\sqrt{t_p t_n}} \dots\dots\dots(B-22)$$

A combination of Eqs. (2.18), (2.21), (4.137) and (A-12), yields the filter-cake resistance:

$$R_{SL}^{KGD} = \frac{4.44 E' r_p t_p}{\pi} \frac{\pi h_f \beta_{KGD} (b_{SL}^{KGD} - P_c)}{2E' \left[\sqrt{(h_f r_p S_p)^2 + \frac{\pi h_f \beta_{KGD} (b_{SL}^{KGD} - P_c)}{2E'} V_i} - h_f r_p S_p \right]} b_{MSL}^{KGD}$$

.....(B-23)

Combining Eqs. (4.138), (4.139), (A-3), and (A-12), yields the reservoir permeability:

Gives the reservoir permeability:

$$k_{SL}^{KGD} = \frac{1}{r_p} \left(\frac{2E' \left[\sqrt{(h_f r_p S_p)^2 + \frac{\pi h_f \beta_{KGD}}{2E'} (b_{SL}^{KGD} - P_c) V_i} - h_f r_p S_p \right]}{m_{MSL}^{KGD} \pi h_f \beta_{KGD} (b_{SL}^{KGD} - P_c)} \right)^2 \dots\dots\dots(B-24)$$

and the independent variable:

$$X(n)_{SL}^{KGD} = \frac{0.45}{E'} \sqrt{\pi} \left(\frac{\mu_r}{\phi c_t} \right)^{1/2} \left\{ \left[\left(\frac{p_{n_s+1} - p_{n_s+2}}{t_n - t_{n_s+1}} \right) (t_n - t_{n_s+1})^{1/2} + \sum_{j=n_s+3}^n \frac{(p_{j-1} - p_j)}{\Delta t_j} - \frac{(p_{j-2} - p_{j-1})}{\Delta t_{j-1}} (t_n - t_{j-1})^{1/2} \right] + \frac{\bar{W}_{SL}^{KGD}}{x_{fSL}^{KGD} \sqrt{\pi}} \left[\frac{t_n^{1/2} - (t_n - t_{n_s+1})^{1/2}}{(p_{n-1} - p_n) t_p t_n^{3/2}} \Delta t_n \right] \right\} \dots\dots\dots(B-25)$$

B-I Radial geometry

$$Y(n)_{SL}^{RAD} = b_{MSL}^{RAD} + m_{MSL}^{RAD} X(n)_{SL}^{RAD} \dots\dots\dots(B-26)$$

where the dependent variable is:

$$Y(n)_{SL}^{RAD} = \frac{p_n - p_i}{p_{n-1} - p_n} \frac{\Delta t_n}{\sqrt{t_p t_n}} \dots\dots\dots (B-27)$$

A combination of Eqs. (2.19), (2.22), (4.137), and (A-13), yields the filter-cake resistance:

$$R_{SL}^{RAD} = \frac{4E' r_p t_p}{\pi} \left(\frac{D_1 D_2 + D_3}{D_1} \right) b_{MSL}^{RAD} \dots\dots\dots (B-28)$$

Combining Eqs. (4.138), (4.139) and (A-4) gives the reservoir permeability:

$$k_{SL}^{RAD} = \frac{1}{r_p} \left[\frac{D_1 D_2 + D_3}{D_1 m_{MSL}^{RAD}} \right]^2 \dots\dots\dots (B-29)$$

and the independent variable:

$$X(n)_{SL}^{RAD} = \frac{\sqrt{\pi}}{2E'} \left(\frac{\mu_r}{\phi c_t} \right)^{1/2} \left\{ \left[\left(\frac{p_{n_s+1} - p_{n_s+2}}{t_n - t_{n_s+1}} \right) (t_n - t_{n_s+1})^{1/2} + \sum_{j=n_s+3}^n \frac{(p_{j-1} - p_j)}{\Delta t_j} - \frac{(p_{j-2} - p_{j-1})}{\Delta t_{j-1}} (t_n - t_{j-1})^{1/2} \right] + \frac{\bar{W}_{NS}^{RAD}}{R_{fSL}^{RAD}} \left[\frac{t_n^{1/2} - (t_n - t_{n_s+1})^{1/2}}{(p_{n-1} - p_n) t_p t_n^{3/2}} \Delta t_n \right] \right\} \dots\dots\dots (B-30)$$

where:

$$D_1 = 6A \left\{ 3A \sqrt{(4B^3 + 27A^2C)BC} - 2B^3 - 27A^2C \right\}^{1/3} \dots\dots\dots(B-31)$$

$$D_2 = 2\sqrt[3]{2} B^2 - 2B \left\{ 3A \sqrt{(4B^3 + 27A^2C)BC} - 2B^3 - 27A^2C \right\}^{1/3} \dots\dots\dots(B-32)$$

and

$$D_3 = \sqrt[3]{2^2} \left\{ 3A \sqrt{(4B^3 + 27A^2C)BC} - 2B^3 - 27A^2C \right\}^{2/3} \dots\dots\dots(B-33)$$

Parameters A , B , and C are shown in Appendix A, Eqs. (A-14), (A-15), and (A-16).

Appendix C

Applications-Input and Output Data

Table C-1A - Input parameters - case M1

Parameter	Description	Units	Value
ϕ	Reservoir porosity	fraction	0.2
c_t	reservoir total compressibility	1/psi	7.69E-05
μ_r	reservoir fluid viscosity	cp	1.4
μ_f	fracture fluid viscosity	cp	211
V_i	vol. of injected fluid	gal	3150
h_p	permeable height	ft	40
h_f	fracture height	ft	45
t_p	pumping time	min	4.76
t_c	fracture closure time	min	11.3
P_c	closure pressure	psi	2503.1
P_i	Initial reservoir pressure	psi	2146
$ISIP$	Initial shut-in pressure	psi	3293
E	Young's Modulus	psi	1.0E+06
ν	Poisson's ratio	fraction	0.25
E'	Plain-strain modulus	psi	1.07+06
	Fracture area - power law exponent		
α	RAD Model		8/9
n'	flow behavior index	fraction	0.5
K'	Ratio of shear stress to shear rate	lbf s ^{0.5} /ft ²	0.071
β_{RAD}	Average pressure ratio (wellbore-tip)		0.925

Table C-1B Fall off time - pressure data - case M1

t	$\Delta t_{fall-off}$	\sqrt{dt}	P_w	t	$\Delta t_{fall-off}$	\sqrt{dt}	P_w
min	min	$\sqrt{\text{min}}$	Psi	min	min	$\sqrt{\text{min}}$	Psi
33.717	0.717	0.846	2911.201	53.333	20.333	4.509	2378.481
34.116	1.116	1.057	2788.290	53.733	20.733	4.553	2373.190
34.516	1.516	1.231	2744.804	54.133	21.133	4.597	2367.972
34.917	1.917	1.390	2705.542	54.533	21.533	4.640	2362.791
35.333	2.333	1.527	2670.278	54.933	21.933	4.683	2357.653
35.733	2.733	1.653	2655.856	55.333	22.333	4.726	2352.521
36.133	3.133	1.770	2652.025	55.733	22.733	4.768	2347.483
36.533	3.533	1.880	2647.234	56.133	23.133	4.810	2342.428
36.933	3.933	1.983	2641.118	56.533	23.533	4.851	2337.344
37.333	4.333	2.082	2635.042	56.933	23.933	4.892	2332.298
37.733	4.733	2.176	2628.585	57.333	24.333	4.933	2327.344
38.133	5.133	2.266	2615.313	57.733	24.733	4.973	2325.375
38.533	5.533	2.352	2608.689	58.133	25.133	5.013	2317.784
38.933	5.933	2.436	2600.928	58.533	25.533	5.053	2313.133
39.333	6.333	2.517	2593.764	58.933	25.933	5.092	2308.260
39.733	6.733	2.595	2585.988	59.333	26.333	5.132	2303.702
40.133	7.133	2.671	2578.937	59.733	26.733	5.170	2298.905
40.533	7.533	2.745	2571.202	60.133	27.133	5.209	2294.410
40.933	7.933	2.817	2564.018	60.533	27.533	5.247	2289.749
41.333	8.333	2.887	2557.210	60.933	27.933	5.285	2285.273
41.733	8.733	2.955	2551.132	61.333	28.333	5.323	2280.679
42.133	9.133	3.022	2544.665	61.733	28.733	5.360	2276.193
42.533	9.533	3.088	2538.022	62.133	29.133	5.398	2271.653
42.933	9.933	3.152	2532.241	62.533	29.533	5.434	2267.185
43.333	10.333	3.215	2526.230	62.933	29.933	5.471	2262.701
43.733	10.733	3.276	2519.609	63.333	30.333	5.508	2258.285
44.133	11.133	3.337	2513.068	63.733	30.733	5.544	2253.879
44.533	11.533	3.396	2507.066	64.133	31.133	5.580	2249.461
44.933	11.933	3.454	2500.952	64.533	31.533	5.615	2245.029
45.333	12.333	3.512	2494.939	64.933	31.933	5.651	2240.709
45.733	12.733	3.568	2488.931	65.333	32.333	5.686	2236.420
46.133	13.133	3.624	2482.848	65.733	32.733	5.721	2232.170

46.533	13.533	3.679	2476.817	66.133	33.133	5.756	2227.978
46.933	13.933	3.733	2470.710	66.533	33.533	5.791	2223.775
47.333	14.333	3.786	2464.465	66.933	33.933	5.825	2219.627
47.733	14.733	3.838	2458.385	67.333	34.333	5.859	2215.507
48.133	15.133	3.890	2452.496	67.733	34.733	5.895	2211.407
48.533	15.533	3.941	2446.505	68.150	35.150	5.929	2207.166
48.933	15.933	3.992	2440.555	68.550	35.550	5.962	2203.120
49.333	16.333	4.041	2434.719	68.950	35.950	5.996	2199.088
49.733	16.733	4.091	2428.868	69.350	36.350	6.029	2195.058
50.133	17.133	4.139	2423.058	69.750	36.750	6.062	2191.078
50.533	17.533	4.187	2417.303	70.150	37.150	6.095	2187.163
50.933	17.933	4.235	2411.645	70.550	37.550	6.128	2183.250
51.333	18.333	4.282	2405.962	70.950	37.950	6.160	2179.401
51.733	18.733	4.328	2400.282	71.350	38.350	6.193	2175.554
52.133	19.133	4.374	2394.712	71.750	38.750	6.225	2171.716
52.533	19.533	4.420	2389.255	72.150	39.150	6.257	2167.917
52.933	19.933	4.465	2383.805	72.550	39.550	6.289	2164.138
72.950	39.950	6.321	2160.358	92.550	59.550	7.717	2002.980
73.350	40.350	6.352	2156.558	92.950	59.950	7.743	2000.167
73.750	40.750	6.384	2152.797	93.350	60.350	7.769	1997.432
74.150	41.150	6.415	2149.060	93.750	60.750	7.794	1994.719
74.550	41.550	6.446	2145.374	94.150	61.150	7.820	1991.976
74.950	41.950	6.477	2141.744	94.550	61.550	7.845	1989.260
75.350	42.350	6.506	2138.156	94.950	61.950	7.871	1986.541
75.733	42.733	6.537	2134.729	95.350	62.350	7.896	1983.827
76.133	43.133	6.568	2131.141	95.750	62.750	7.921	1981.136
76.533	43.533	6.598	2127.636	96.150	63.150	7.947	1978.470
76.933	43.933	6.628	2124.101	96.550	63.550	7.972	1975.807
77.333	44.333	6.658	2120.643	96.950	63.950	7.997	1973.167
77.733	44.733	6.688	2117.178	97.350	64.350	8.022	1970.554
78.133	45.133	6.718	2113.751	97.750	64.750	8.047	1967.943
78.533	45.533	6.748	2110.327	98.150	65.150	8.075	1965.333
78.933	45.933	6.781	2106.928	98.600	65.600	8.099	1962.408
79.383	46.383	6.811	2103.129	99.000	66.000	8.124	1959.838
79.783	46.783	6.840	2099.769	99.400	66.400	8.149	1957.261
80.183	47.183	6.869	2096.357	99.800	66.800	8.173	1954.700
80.583	47.583	6.898	2093.008	100.200	67.200	8.199	1952.149
80.983	47.983	6.927	2089.708	100.616	67.616	8.221	1949.543
81.383	48.383	6.956	2086.413	100.983	67.983	8.245	1947.234

81.783	48.783	6.985	2083.072	101.383	68.383	8.269	1944.748
82.183	49.183	7.013	2079.791	101.783	68.783	8.294	1942.264
82.583	49.583	7.042	2076.552	102.183	69.183	8.318	1939.772
82.983	49.983	7.070	2073.356	102.583	69.583	8.342	1937.283
83.383	50.383	7.098	2070.207	102.983	69.983	8.366	1934.830
83.783	50.783	7.126	2067.074	103.383	70.383	8.389	1932.388
84.183	51.183	7.154	2063.954	103.783	70.783	8.413	1929.947
84.583	51.583	7.182	2060.871	104.183	71.183	8.437	1927.482
84.983	51.983	7.210	2057.765	104.583	71.583	8.461	1925.017
85.383	52.383	7.238	2054.680	104.983	71.983	8.484	1922.607
85.783	52.783	7.263	2051.650	105.383	72.383	8.508	1920.222
86.150	53.150	7.290	2048.905	105.783	72.783	8.531	1917.847
86.550	53.550	7.318	2045.923	106.183	73.183	8.555	1915.480
86.950	53.950	7.345	2042.980	106.583	73.583	8.578	1913.137
87.350	54.350	7.372	2040.057	106.983	73.983	8.601	1910.787
87.750	54.750	7.399	2037.156	107.383	74.383	8.625	1908.472
88.150	55.150	7.426	2034.236	107.783	74.783	8.648	1906.161
88.550	55.550	7.453	2031.317	108.183	75.183	8.671	1903.844
88.950	55.950	7.480	2028.434	108.583	75.583	8.694	1901.554
89.350	56.350	7.507	2025.550	108.983	75.983	8.717	1899.295
89.750	56.750	7.533	2022.652	109.383	76.383	8.740	1897.052
90.150	57.150	7.560	2019.772	109.783	76.783	8.763	1894.815
90.550	57.550	7.586	2016.947	110.183	77.183	8.785	1892.570
90.950	57.950	7.612	2014.171	110.583	77.583	8.808	1890.351
91.350	58.350	7.639	2011.414	110.983	77.983	8.831	1888.121
91.750	58.750	7.665	2008.611	111.383	78.383	8.853	1885.925
92.150	59.150	7.691	2005.790	111.783	78.783	8.876	1883.728
112.183	79.183	8.898	1881.560	118.183	85.183	9.229	1850.147
112.583	79.583	8.921	1879.375	118.583	85.583	9.251	1848.118
112.983	79.983	8.943	1877.215	118.983	85.983	9.273	1846.088
113.383	80.383	8.966	1875.055	119.383	86.383	9.294	1844.072
113.783	80.783	8.988	1872.904	119.783	86.783	9.316	1842.047
114.183	81.183	9.010	1870.777	120.183	87.183	9.337	1840.061
114.583	81.583	9.032	1868.664	120.583	87.583	9.359	1838.082
114.983	81.983	9.054	1866.538	120.983	87.983	9.380	1836.108
115.383	82.383	9.077	1864.472	121.383	88.383	9.401	1834.139
115.783	82.783	9.099	1862.405	121.783	88.783	9.422	1832.192
116.183	83.183	9.120	1860.358	122.183	89.183	9.444	1830.261
116.583	83.583	9.142	1858.318	122.583	89.583	9.465	1828.345

116.983	83.983	9.164	1856.288	122.983	89.983	9.486	1826.442
117.383	84.383	9.186	1854.255	123.383	90.383	9.507	1824.655
117.783	84.783	9.208	1852.188	123.783	90.783	9.528	1822.702

Table C-1C G-function and diagnostic functions - case M1

$G(\Delta t_D, \alpha)$	P_w	$P_w FIT$	$X(n)$	$Y(n)$	$Y(n)$
	Psi	Psi			
0	3131.24	3131.24	0	0.176310	0.17631
2.07794	2911.2	2766.44	6.5E-10	0.453	0.33474
2.15877	2788.29	2752.25	3.1E-09	1.0064	0.9438
2.23646	2744.8	2738.61	4.5E-09	1.31031	1.28103
2.31143	2705.54	2725.45	5.7E-09	1.56065	1.55585
2.3869	2670.28	2712.21	6.7E-09	1.78952	1.80227
2.45699	2655.86	2699.9	7.6E-09	1.99189	2.01987
2.52511	2652.03	2687.94	8.4E-09	2.18054	2.22009
2.5914	2647.23	2676.3	9.2E-09	2.35871	2.40656
2.65596	2641.12	2664.97	9.9E-09	2.52844	2.58167
2.71891	2635.04	2653.92	1.1E-08	2.69136	2.74735
2.78038	2628.58	2643.13	1.1E-08	2.84874	2.90509
2.84053	2615.31	2632.57	1.2E-08	3.00168	3.05614
2.89944	2608.69	2622.23	1.2E-08	3.15071	3.20123
2.95712	2600.93	2612.1	1.3E-08	3.29647	3.34113
3.01365	2593.76	2602.18	1.4E-08	3.43961	3.47661
3.06911	2585.99	2592.44	1.4E-08	3.58044	3.6081
3.1236	2578.94	2582.87	1.5E-08	3.71937	3.73607
3.17718	2571.2	2573.47	1.5E-08	3.85653	3.86078
3.22982	2564.02	2564.23	1.6E-08	3.9924	3.98273
3.28159	2557.21	2555.14	1.6E-08	4.12719	4.1022
3.33254	2551.13	2546.19	1.7E-08	4.2611	4.21944
3.38273	2544.67	2537.38	1.7E-08	4.39405	4.33445
3.43222	2538.02	2528.69	1.8E-08	4.52656	4.44774
3.48096	2532.24	2520.14	1.8E-08	4.65888	4.55961
3.52901	2526.23	2511.7			
3.5764	2519.61	2503.38			
3.62319	2513.07	2495.17			
3.6694	2507.07	2487.06			

Table C-1D Net pressure during injection - case M1

Δt_{inj}	P_n
min	psi
0.0565	2089.03
0.35655	3699.41
0.75646	3765.53
1.15636	3772.03
1.5565	3770.97
1.95653	3778.57
2.35655	3877.42
2.75645	3761.2
3.15636	3755.04
3.5565	3735.86

Table C-1E Synthesis of computed fluid and reservoir properties - case M1

S_p	c_f	R_f	\bar{w}	C_L	η	R_o	k_r
ft	ft / psi	ft	in	ft / $\sqrt{\text{min}}$	%	(psi - min) / ft	md
-6.8E-03	9.72E-05	66.2	2.81E-01	1.18E-02	61.63	6.95E+03	19.5

Table C-2A - Input parameters - case M2

Parameter	Description	Units	Value
ϕ	Reservoir porosity	fraction	0.2
c_t	reserve total compressibility	1/psi	7.69E-05
μ_r	reservoir fluid viscosity	cp	1.4
μ_f	fracture fluid viscosity	cp	211
V_i	vol. of injected fluid	gal	3150
h_p	permeable height	ft	32
h_f	fracture height	ft	32
t_p	pumping time	min	3.3
t_c	fracture closure time	min	2.7
P_c	closure pressure	psi	2928.7
P_i	Initial reservoir pressure	psi	1768
$ISIP$	Initial shut-in pressure	psi	3298
E	Young's Modulus	psi	1.00E+06
ν	Poisson's ratio	fraction	0.25
E'	Plain-strain modulus	psi	1.07E+06
	Fracture area - power law exponent		
α	RAD Model		4/5
n'	flow behavior index	fraction	0.5
K'	Ratio of shear stress to shear rate	Lbf s ^{0.5} /ft ²	0.071
β_{RAD}	Average pressure ratio (wellbore-tip)		0.925

Table C-2B Fall off time - pressure data - case M2

t	$\Delta t_{fall-off}$	\sqrt{dt}	P_w	t	$\Delta t_{fall-off}$	\sqrt{dt}	P_w
min	min	$\sqrt{\text{min}}$	Psi	min	min	$\sqrt{\text{min}}$	Psi
2147.66	0.65771	0.811	3189.73	2150.62	3.62451	1.90382	2904.57
2147.69	0.69092	0.83121	3173.5	2150.66	3.65771	1.91252	2903.83
2147.72	0.72437	0.8511	3031.94	2150.69	3.69092	1.92118	2903.09
2147.76	0.75781	0.87052	3028.56	2150.72	3.72437	1.92986	2902.31
2147.79	0.79102	0.88939	3025.57	2150.76	3.75781	1.93851	2901.62
2147.82	0.82446	0.908	3022.79	2150.79	3.79102	1.94705	2900.88
2147.86	0.85767	0.9261	3020.06	2150.82	3.82446	1.95562	2900.15
2147.89	0.89111	0.94399	3017.72	2150.86	3.85767	1.96409	2899.49
2147.92	0.92432	0.96141	3015.42	2150.89	3.89111	1.97259	2898.78
2147.96	0.95776	0.97865	3013.21	2150.92	3.92432	1.98099	2898.08
2147.99	0.99121	0.9956	3011.2	2150.96	3.95776	1.98941	2897.4
2148.02	1.02441	1.01213	3009.11	2150.99	3.99121	1.9978	2896.67
2148.06	1.05762	1.02841	3007.16	2151.02	4.02441	2.00609	2896.02
2148.09	1.09106	1.04454	3005.22	2151.06	4.05762	2.01435	2895.34
2148.12	1.12451	1.06043	3003.16	2151.09	4.09106	2.02264	2894.71
2148.16	1.15771	1.07597	3001.3	2151.12	4.12451	2.03089	2894.11
2148.19	1.19092	1.09129	2999.34	2151.16	4.15771	2.03905	2893.47
2148.22	1.22437	1.10651	2997.33	2151.19	4.19092	2.04717	2892.84
2148.26	1.25781	1.12152	2995.47	2151.22	4.22437	2.05533	2892.19
2148.29	1.29102	1.13623	2993.42	2151.26	4.25781	2.06345	2891.52
2148.32	1.32446	1.15085	2991.47	2151.29	4.29102	2.07148	2890.97
2148.36	1.35767	1.16519	2989.52	2151.32	4.32446	2.07953	2890.36
2148.39	1.39111	1.17945	2987.4	2151.36	4.35767	2.0875	2889.75
2148.42	1.42432	1.19345	2985.51	2151.39	4.39111	2.0955	2889.24
2148.46	1.45776	1.20738	2983.58	2151.42	4.42432	2.10341	2888.68
2148.49	1.49121	1.22115	2981.58	2151.46	4.45776	2.11134	2888.02
2148.52	1.52441	1.23467	2979.74	2151.49	4.49121	2.11925	2887.36
2148.56	1.55762	1.24805	2977.79	2151.52	4.52441	2.12707	2886.71
2148.59	1.59106	1.26137	2975.95	2151.56	4.55762	2.13486	2886.15
2148.62	1.62451	1.27456	2974.2	2151.59	4.59106	2.14268	2885.55
2148.66	1.65771	1.28752	2972.32	2151.62	4.62451	2.15047	2884.95
2148.69	1.69092	1.30035	2970.62	2151.66	4.65771	2.15817	2884.4
2148.72	1.72437	1.31315	2968.93	2151.69	4.69092	2.16585	2883.78
2148.76	1.75781	1.32583	2967.17	2151.72	4.72437	2.17356	2883.23

2148.79	1.79102	1.33829	2965.56	2151.76	4.75781	2.18124	2882.76
2148.82	1.82446	1.35073	2963.86	2151.79	4.79102	2.18884	2882.23
2148.86	1.85767	1.36296	2962.25	2151.82	4.82446	2.19647	2881.77
2148.89	1.89111	1.37518	2960.72	2151.86	4.85767	2.20401	2881.28
2148.92	1.92432	1.3872	2959.09	2151.89	4.89111	2.21159	2880.69
2148.96	1.95776	1.3992	2957.64	2151.92	4.92432	2.21908	2880.22
2148.99	1.99121	1.4111	2956.16	2151.96	4.95776	2.2266	2879.73
2149.02	2.02441	1.42282	2954.6	2151.99	4.99121	2.2341	2879.23
2149.06	2.05762	1.43444	2953.2	2152.02	5.02441	2.24152	2878.76
2149.09	2.09106	1.44605	2951.68	2152.06	5.05762	2.24891	2878.23
2149.12	2.12451	1.45757	2950.18	2152.09	5.09106	2.25634	2877.75
2149.16	2.15771	1.46892	2948.79	2152.12	5.12451	2.26374	2877.22
2149.19	2.19092	1.48017	2947.3	2152.16	5.15771	2.27106	2876.68
2149.22	2.22437	1.49143	2945.92	2152.19	5.19092	2.27836	2876.19
2149.26	2.25781	1.5026	2944.53	2152.22	5.22437	2.28569	2875.69
2149.29	2.29102	1.51361	2943.09	2152.26	5.25781	2.29299	2875.22
2149.32	2.32446	1.52462	2941.76	2152.29	5.29102	2.30022	2874.78
2149.36	2.35767	1.53547	2940.4	2152.32	5.32446	2.30748	2874.23
2149.39	2.39111	1.54632	2939.07	2152.36	5.35767	2.31466	2873.8
2149.42	2.42432	1.55702	2937.87	2152.39	5.39111	2.32188	2873.38
2149.46	2.45776	1.56773	2936.59	2152.42	5.42432	2.32902	2872.95
2149.49	2.49121	1.57836	2935.4	2152.46	5.45776	2.33619	2872.48
2149.52	2.52441	1.58884	2934.24	2152.49	5.49121	2.34333	2872.04
2149.56	2.55762	1.59926	2933.01	2152.52	5.52441	2.35041	2871.62
2149.59	2.59106	1.60968	2931.92	2152.56	5.55762	2.35746	2871.18
2149.62	2.62451	1.62003	2930.81	2152.59	5.59106	2.36454	2870.77
2149.66	2.65771	1.63025	2929.69	2152.62	5.62451	2.37161	2870.43
2149.69	2.69092	1.6404	2928.68	2152.66	5.65771	2.3786	2870.08
2149.72	2.72437	1.65057	2927.57	2152.69	5.69092	2.38556	2869.61
2149.76	2.75781	1.66067	2926.56	2152.72	5.72437	2.39256	2869.24
2149.79	2.79102	1.67063	2925.59	2152.76	5.75781	2.39954	2868.87
2149.82	2.82446	1.68061	2924.55	2152.79	5.79102	2.40645	2868.49
2149.86	2.85767	1.69046	2923.61	2152.82	5.82446	2.41339	2868.12
2149.89	2.89111	1.70033	2922.67	2152.86	5.85767	2.42026	2867.75
2149.92	2.92432	1.71006	2921.7	2152.89	5.89111	2.42716	2867.36
2149.96	2.95776	1.71982	2920.83	2152.92	5.92432	2.43399	2866.98
2149.99	2.99121	1.72951	2919.9	2152.96	5.95776	2.44085	2866.55
2150.02	3.02441	1.73908	2919.02	2152.99	5.99121	2.4477	2866.25
2150.06	3.05762	1.7486	2918.2	2153.02	6.02441	2.45447	2865.9

2150.09	3.09106	1.75814	2917.31	2153.06	6.05762	2.46122	2865.57
2150.12	3.12451	1.76763	2916.5	2153.09	6.09106	2.46801	2865.28
2150.16	3.15771	1.777	2915.68	2153.12	6.12451	2.47478	2864.97
2150.19	3.19092	1.78631	2914.8	2153.16	6.15771	2.48147	2864.67
2150.22	3.22437	1.79565	2914.04	2153.19	6.19092	2.48816	2864.35
2150.26	3.25781	1.80494	2913.21	2153.22	6.22437	2.49487	2863.99
2150.29	3.29102	1.81412	2912.39	2153.26	6.25781	2.50156	2863.73
2150.32	3.32446	1.82331	2911.65	2153.29	6.29102	2.50819	2863.33
2150.36	3.35767	1.83239	2910.82	2153.32	6.32446	2.51485	2863
2150.39	3.39111	1.8415	2910.06	2153.36	6.35767	2.52144	2862.69
2150.42	3.42432	1.85049	2909.28	2153.39	6.39111	2.52807	2862.45
2150.46	3.45776	1.85951	2908.47	2153.42	6.42432	2.53462	2862.32
2150.49	3.49121	1.86848	2907.71	2153.46	6.45776	2.54121	2862.08
2150.52	3.52441	1.87734	2906.91	2153.49	6.49121	2.54779	2861.74
2150.56	3.55762	1.88616	2906.13	2153.52	6.52441	2.55429	2861.53
2150.59	3.59106	1.89501	2905.4	2153.56	6.55762	2.56078	2862.24

Table C-2C G-function and diagnostic functions - case M2

$G(\Delta t_D, \alpha)$	P_w	$P_w FIT$	$X(n)$	$Y(n)$	$Y(n) FIT$
	Psi	Psi			
0	3545.5	3545.5	0.00	5.76E-01	5.76E-01
1.51462	3031.94	3026.24	3.07E-09	1.49759	1.42E+00
1.5204	3028.56	3024.26	3.80E-09	1.64654	1.63E+00
1.5261	3025.57	3022.3	4.12E-09	1.71745	1.72E+00
1.53181	3022.79	3020.34	4.56E-09	1.85967	1.84E+00
1.53745	3020.06	3018.41	5.03E-09	2.02461	1.97E+00
1.5431	3017.72	3016.48	5.23E-09	2.07558	2.02E+00
1.54867	3015.42	3014.56	5.63E-09	2.21881	2.13E+00
1.55426	3013.21	3012.65	5.80E-09	2.2676	2.18E+00
1.55981	3011.2	3010.74	5.90E-09	2.28526	2.21E+00
1.5653	3009.11	3008.86	6.16E-09	2.37398	2.28E+00
1.57076	3007.16	3006.99	6.05E-09	2.30947	2.25E+00
1.57623	3005.22	3005.12	6.17E-09	2.34043	2.28E+00
1.58167	3003.16	3003.25	6.32E-09	2.38462	2.32E+00
1.58705	3001.3	3001.41	6.14E-09	2.29539	2.27E+00

1.5924	2999.34	2999.57	6.33E-09	2.35574	2.33E+00
1.59777	2997.33	2997.73	6.26E-09	2.31508	2.31E+00
1.60311	2995.47	2995.9	6.15E-09	2.25552	2.28E+00
1.60839	2993.42	2994.09	6.32E-09	2.30594	2.32E+00
1.61368	2991.47	2992.28	6.09E-09	2.20187	2.26E+00
1.61891	2989.52	2990.48	6.20E-09	2.2276	2.29E+00
1.62416	2987.4	2988.69	6.51E-09	2.33094	2.38E+00
1.62934	2985.51	2986.91	6.37E-09	2.26627	2.34E+00
1.63454	2983.58	2985.13	6.50E-09	2.3033	2.37E+00
1.63972	2981.58	2983.35	6.57E-09	2.31764	2.39E+00
1.64484	2979.74	2981.6	6.60E-09	2.31891	2.40E+00
1.64994	2977.79	2979.85	6.98E-09	2.44935	2.51E+00
1.65505	2975.95	2978.09	6.88E-09	2.40576	2.48E+00
1.66015	2974.2	2976.35	6.95E-09	2.42309	2.50E+00
1.66519	2972.32	2974.62	7.34E-09	2.56024	2.61E+00
1.67021	2970.62	2972.9	7.24E-09	2.51707	2.58E+00
1.67524	2968.93	2971.17	7.38E-09	2.56006	2.62E+00
1.68026	2967.17	2969.45	7.50E-09	2.59828	2.65E+00
1.68522	2965.56	2967.75	7.49E-09	2.59058	2.65E+00
1.6902	2963.86	2966.05	7.87E-09	2.72288	2.75E+00
1.69512	2962.25	2964.36	7.81E-09	2.69759	2.74E+00
1.70006	2960.72	2962.66	8.00E-09	2.76018	2.79E+00
1.70495	2959.09	2960.99	8.41E-09	2.90378	2.90E+00
1.70985	2957.64	2959.31	8.07E-09	2.78014	2.81E+00
1.71474	2956.16	2957.63	8.24E-09	2.83673	2.85E+00
1.71958	2954.6	2955.97	8.36E-09	2.87817	2.89E+00
1.7244	2953.2	2954.32	8.12E-09	2.78505	2.82E+00
1.72923	2951.68	2952.66	8.42E-09	2.89142	2.91E+00
1.73406	2950.18	2951.01	8.41E-09	2.88305	2.90E+00
1.73882	2948.79	2949.37	8.46E-09	2.89562	2.92E+00
1.74358	2947.3	2947.75	8.76E-09	3.00268	3.00E+00
1.74835	2945.92	2946.11	8.54E-09	2.92043	2.94E+00
1.75311	2944.53	2944.48	8.71E-09	2.97565	2.98E+00
1.75781	2943.09	2942.86	8.94E-09	3.05561	3.05E+00
1.76254	2941.76	2941.24	8.92E-09	3.04775	3.04E+00
1.76722	2940.4	2939.64	9.44E-09	3.23236	3.19E+00
1.77191	2939.07	2938.03	9.60E-09	3.28837	3.23E+00
1.77656	2937.87	2936.44	9.64E-09	3.30514	3.24E+00
1.78122	2936.59	2934.84	1.01E-08	3.45303	3.36E+00

1.78587	2935.4	2933.24	9.82E-09	3.37407	3.29E+00
1.79048	2934.24	2931.67	1.01E-08	3.4795	3.38E+00
1.79507	2933.01	2930.09	1.01E-08	3.4795	3.38E+00
1.79968	2931.92	2928.51			
1.80427	2930.81	2926.94			
1.80882	2929.69	2925.38			

Table C-2D Net pressure during injection - case M2

Δt_{inj}	P_n	Δt_{inj}	P_n	Δt_{inj}	P_n
min	psi	min	psi	min	psi
0.016602	2654.35	2.81665	3189.82	5.616699	3171.08
0.050049	2878.4	2.850098	3188.8	5.649658	3170.54
0.083252	3113.15	2.883545	3188.62	5.68335	3171.01
0.116699	3136.7	2.916748	3188.52	5.716797	3171.17
0.149658	3113.92	2.949707	3187.68	5.75	3170.6
0.18335	3113.36	2.983398	3188.05	5.783203	3171.1
0.216797	3117.76	3.016602	3187.59	5.81665	3170.96
0.25	3120.1	3.050049	3187.69	5.850098	3171.09
0.283203	3119.77	3.083252	3187.42	5.883545	3170.4
0.31665	3118.44	3.116699	3186.86	5.916748	3170.83
0.350098	3119.02	3.149658	3187.24	5.949707	3170.13
0.383545	3120.45	3.18335	3185.9	5.983398	3170.48
0.416748	3119.68	3.216797	3184.93	6.016602	3171.41
0.449707	3117.71	3.25	3183.57	6.050049	3171.83
0.483398	3119.12	3.283203	3183.58	6.083252	3171.33
0.516602	3121.35	3.31665	3182.94	6.116699	3171.44
0.550049	3122.71	3.350098	3183.57	6.149658	3172.7
0.583252	3123.99	3.383545	3182.86	6.18335	3172.4
0.616699	3124.67	3.416748	3182.65	6.216797	3172.07
0.649658	3125.05	3.449707	3182.68	6.25	3173.25
0.68335	3125.29	3.483398	3182.83	6.283203	3173.14
0.716797	3125.64	3.516602	3182.39	6.31665	3172.35
0.75	3126.23	3.550049	3180.56	6.350098	3171.66
0.783203	3127.5	3.583252	3178.99	6.383545	3172.52
0.81665	3129.25	3.616699	3176.51	6.416748	3172.67
0.850098	3129.72	3.649658	3173.3	6.449707	3172.93
0.883545	3130.16	3.68335	3170.4	6.483398	3173.68
0.916748	3131.3	3.716797	3166.55	6.516602	3173.66

0.949707	3132.14	3.75	3163.25	6.550049	3173.77
0.983398	3133.38	3.783203	3160.18	6.583252	3173.11
1.016602	3135.01	3.81665	3159.37	6.616699	3173.5
1.050049	3136.12	3.850098	3160.75	6.649658	3173.96
1.083252	3136.49	3.883545	3161.58	6.68335	3173.85
1.116699	3137.76	3.916748	3161.52	6.716797	3173.75
1.149658	3140.38	3.949707	3161.27	6.75	3174.45
1.18335	3141.11	3.983398	3161.42	6.783203	3175.13
1.216797	3142.52	4.016602	3161.33	6.81665	3175.15
1.25	3142.95	4.050049	3161.45	6.850098	3175.37
1.283203	3143.77	4.083252	3160.44	6.883545	3175.47
1.31665	3144.3	4.116699	3160.37	6.916748	3175.77
1.350098	3145.11	4.149658	3162.22	6.949707	3176.41
1.383545	3145.98	4.18335	3163.89	6.983398	3175.75
1.416748	3147.16	4.216797	3164.35	7.016602	3175.93
1.449707	3149	4.25	3165.03	7.050049	3176.2
1.483398	3150.31	4.283203	3165.28	7.083252	3175.26
1.516602	3153.12	4.31665	3165.25	7.116699	3175.49
1.550049	3155.12	4.350098	3165.22	7.149658	3175.83
1.583252	3155.98	4.383545	3165.56	7.18335	3176.09
1.616699	3158.14	4.416748	3165.45	7.216797	3176.49
1.649658	3160.81	4.449707	3166.25	7.25	3176.93
1.68335	3162.14	4.483398	3166.52	7.283203	3177.07
1.716797	3163.56	4.516602	3166.66	7.31665	3178
1.75	3165.82	4.550049	3167.03	7.350098	3177.46
1.783203	3166.62	4.583252	3167.16	7.383545	3177.43
1.81665	3167.51	4.616699	3167.63	7.416748	3178.39
1.850098	3168.39	4.649658	3167.99	7.449707	3179.43
1.883545	3169.8	4.68335	3167.78	7.483398	3179.72
1.916748	3170.89	4.716797	3167.54	7.516602	3179.49
1.949707	3171.57	4.75	3168.17	7.550049	3180.76
1.983398	3170.99	4.783203	3167.62	7.583252	3181.49
2.016602	3172.33	4.81665	3167.83	7.616699	3181.19
2.050049	3173.89	4.850098	3169.12	7.649658	3182.04
2.083252	3175.15	4.883545	3169.02	7.68335	3181.72
2.116699	3176.7	4.916748	3168.78	7.716797	3182.69
2.149658	3177.85	4.949707	3168.93	7.75	3183.02
2.18335	3178.7	4.983398	3169.32	7.783203	3182.57
2.216797	3180.02	5.016602	3169.79	7.81665	3183.63
2.25	3181	5.050049	3169.38	7.850098	3184.58
2.283203	3181.8	5.083252	3170.4	7.883545	3183.54
2.31665	3183.14	5.116699	3170.17	7.916748	3184.26
2.350098	3184.85	5.149658	3170.58	7.949707	3184.36
2.383545	3185.45	5.18335	3170.8	7.983398	3184.82

2.416748	3186.75	5.216797	3170.45	8.016602	3185.34
2.449707	3187.77	5.25	3170.59	8.050049	3185.1
2.483398	3188.46	5.283203	3170.67	8.083252	3184.99
2.516602	3189.14	5.31665	3169.63	8.116699	3185.53
2.550049	3189.16	5.350098	3170.75	8.149658	3185.03
2.583252	3189.53	5.383545	3170.8	8.18335	3188.62
2.616699	3190.47	5.416748	3170.13	8.216797	3190.44
2.649658	3190.16	5.449707	3170.49	8.25	3186.15
2.68335	3188.88	5.483398	3171.34	8.283203	3189.12
2.716797	3189.3	5.516602	3171.28	8.31665	3182.55
2.75	3189.04	5.550049	3171.04	8.350098	3181.2
2.783203	3189.61	5.583252	3170.83	8.383545	3189.73

Table C-2E Synthesis of computed fluid and reservoir properties - case M2

S_p	c_f	R_f	\bar{w}	C_L	η	R_o	k_r
<i>ft</i>	<i>ft / psi</i>	<i>ft</i>	<i>in</i>	<i>ft / $\sqrt{\text{min}}$</i>	<i>%</i>	<i>(psi - min) / ft</i>	<i>md</i>
-3.31E-02	9.78E-05	66.6	5.53E-01	3.4E-02	23.65	3.88E+03	18.9

Table C-3A - Input parameters - case M3

Parameter	Description	Units	Value
ϕ	Reservoir porosity	fraction	0.43
c_t	reservoir total compressibility	1/psi	6.5e-6
μ_r	reservoir fluid viscosity	cp	1.4
μ_f	fracture fluid viscosity	cp	224
V_i	vol. of injected fluid	gal	28350
h_p	permeable height	ft	95
h_f	fracture height	ft	95
t_p	pumping time	min	22.5
t_c	fracture closure time	min	20.94
P_c	closure pressure	psi	6388
P_i	Initial reservoir pressure	psi	5500
$ISIP$	Initial shut-in pressure	psi	6694
E	Young's Modulus	psi	1.0E+06
ν	Poisson's ratio	fraction	0.27
E'	Plain-strain modulus	psi	1.1+06
	Fracture area - power law exponent		
α	RAD Model		8/9
n'	flow behavior index	fraction	0.5
K'	Ratio of shear stress to shear rate	Lbf s ^{0.5} /ft ²	0.0728
β_{RAD}	Average pressure ratio (wellbore-tip)		0.925

Table C-3B Fall off time - pressure data - case M3

t	$\Delta t_{fall-off}$	\sqrt{dt}	P_w	t	$\Delta t_{fall-off}$	\sqrt{dt}	P_w
min	min	$\sqrt{\text{min}}$	Psi	min	min	$\sqrt{\text{min}}$	Psi
119.083	0.0833	0.28861	6622.2	122.167	3.1666	1.77949	6590.15
119.167	0.1666	0.40816	6677.93	122.25	3.25	1.80278	6591.68
119.25	0.25	0.5	6728.13	122.333	3.3333	1.82573	6591.68
119.333	0.3333	0.57732	6660.69	122.417	3.4166	1.84841	6590.46
119.417	0.4166	0.64545	6642.19	122.5	3.5	1.87083	6590.46
119.5	0.5	0.70711	6666.83	122.583	3.5833	1.89296	6587.67
119.583	0.5833	0.76374	6661.6	122.667	3.6666	1.91484	6586.76
119.667	0.6666	0.81645	6644.36	122.75	3.75	1.93649	6586.45
119.75	0.75	0.86603	6644.67	122.833	3.8333	1.95788	6587.98
119.833	0.8333	0.91285	6647.15	122.917	3.9166	1.97904	6585.54
119.917	0.9166	0.95739	6638.52	123	4	2	6581.84
120	1	1	6634.82	123.083	4.0833	2.02072	6583.06
120.083	1.0833	1.04082	6633.56	123.167	4.1666	2.04122	6581.84
120.167	1.1666	1.08009	6633.26	123.25	4.25	2.06155	6579.05
120.25	1.25	1.11803	6631.12	123.333	4.3333	2.08166	6580.31
120.333	1.3333	1.15469	6627.42	123.417	4.4166	2.10157	6578.14
120.417	1.4166	1.19021	6623.42	123.5	4.5	2.12132	6580.31
120.5	1.5	1.22474	6622.5	123.583	4.5833	2.14086	6579.05
120.583	1.5833	1.25829	6616.02	123.667	4.6666	2.16023	6578.14
120.667	1.6666	1.29097	6618.5	123.75	4.75	2.17945	6576.61
120.75	1.75	1.32288	6613.88	123.833	4.8333	2.19848	6577.83
120.833	1.8333	1.35399	6611.1	123.917	4.9166	2.21734	6572.91
120.917	1.9166	1.38441	6612.32	124	5	2.23607	6574.13
121	2	1.41421	6606.17	124.083	5.0833	2.25462	6573.21
121.083	2.0833	1.44336	6608.92	124.167	5.1666	2.27301	6572.91
121.167	2.1666	1.47194	6605.26	124.25	5.25	2.29129	6571.65
121.25	2.25	1.5	6602.78	124.333	5.3333	2.30939	6571.99
121.333	2.3333	1.52751	6604	124.417	5.4166	2.32736	6566.73
121.417	2.4166	1.55454	6603.69	124.5	5.5	2.34521	6570.43
121.5	2.5	1.58114	6602.47	124.583	5.5833	2.3629	6567.03
121.583	2.5833	1.60726	6597.55	124.667	5.6666	2.38046	6568.29
121.667	2.6666	1.63297	6601.56	124.75	5.75	2.39792	6566.73
121.75	2.75	1.65831	6595.38	124.833	5.8333	2.41522	6568.29

121.833	2.8333	1.68324	6596.6	124.917	5.9166	2.43241	6563.33
121.917	2.9166	1.70781	6597.55	125	6	2.44949	6562.11
122	3	1.73205	6591.68	125.083	6.0833	2.46643	6564.29
122.083	3.0833	1.75593	6591.68	125.167	6.1666	2.48326	6563.03
125.25	6.25	2.5	6559.33	128.667	9.6666	3.10911	6525.15
125.333	6.3333	2.5166	6556.89	128.75	9.75	3.1225	6522.4
125.417	6.4166	2.5331	6557.19	128.833	9.83331	3.13581	6521.15
125.5	6.5	2.54951	6559.33	128.917	9.91658	3.14906	6523.93
125.583	6.5833	2.56579	6554.71	129	10	3.16228	6522.71
125.667	6.6666	2.58198	6559.67	129.083	10.0833	3.17542	6517.75
125.75	6.75	2.59808	6557.19	129.167	10.1666	3.18851	6517.44
125.833	6.8333	2.61406	6553.49	129.25	10.25	3.20156	6519.01
125.917	6.9166	2.62994	6553.49	129.333	10.3333	3.21455	6517.75
126	7	2.64575	6551.97	129.417	10.4166	3.22747	6516.53
126.083	7.0833	2.66145	6552.27	129.5	10.5	3.24037	6520.23
126.167	7.1666	2.67705	6553.49	129.583	10.5833	3.2532	6515.31
126.25	7.25	2.69258	6551.97	129.667	10.6666	3.26598	6515.31
126.333	7.3333	2.70801	6552.27	129.75	10.75	3.27872	6516.22
126.417	7.4166	2.72334	6546.09	129.833	10.8333	3.2914	6512.83
126.5	7.5	2.73861	6548.57	129.917	10.9166	3.30402	6512.83
126.583	7.5833	2.75378	6548.57	130	11	3.31662	6512.52
126.667	7.6666	2.76886	6547.01	130.083	11.0833	3.32916	6510.08
126.75	7.75	2.78388	6543.65	130.167	11.1666	3.34165	6511.61
126.833	7.8333	2.7988	6543.35	130.25	11.25	3.3541	6506.69
126.917	7.9166	2.81365	6542.39	130.333	11.3333	3.3665	6506.69
127	8	2.82843	6544.57	130.417	11.4166	3.37884	6505.43
127.083	8.0833	2.84311	6541.17	130.5	11.5	3.39116	6508.82
127.167	8.1666	2.85773	6538.39	130.583	11.5833	3.40343	6504.21
127.25	8.25	2.87228	6542.39	130.667	11.6666	3.41564	6504.21
127.333	8.3333	2.88675	6541.17	130.75	11.75	3.42783	6502.68
127.417	8.4166	2.90114	6536.25	130.833	11.8333	3.43996	6502.99
127.5	8.5	2.91548	6537.17	130.917	11.9166	3.45204	6501.42
127.583	8.5833	2.92973	6535.94	131	12	3.4641	6498.98
127.667	8.6666	2.94391	6535.03	131.083	12.0833	3.47611	6499.29
127.75	8.75	2.95804	6533.47	131.167	12.1666	3.48806	6500.51
127.833	8.8333	2.97209	6532.25	131.25	12.25	3.5	6500.51
127.917	8.9166	2.98607	6531.02	131.333	12.3333	3.51188	6496.81
128	9	3	6533.77	131.417	12.4166	3.52372	6494.36
128.083	9.08331	3.01385	6531.33	131.5	12.5	3.53553	6494.36

128.167	9.1666	3.02764	6529.77	131.583	12.5833	3.5473	6494.06
128.25	9.25	3.04138	6530.07	131.667	12.6666	3.55902	6495.59
128.333	9.33331	3.05505	6531.02	131.75	12.75	3.57071	6489.44
128.417	9.41658	3.06864	6526.06	131.833	12.8333	3.58236	6489.14
128.5	9.5	3.08221	6528.85	131.917	12.9166	3.59396	6486.66
128.583	9.58331	3.09569	6523.62	132	13	3.60555	6488.19
132.083	13.0833	3.61709	6490.67	135.5	16.5	4.06202	6448.78
132.167	13.1666	3.62858	6486.96	135.583	16.5833	4.07226	6442.6
132.25	13.25	3.64005	6486.66	135.667	16.6666	4.08247	6442.6
132.333	13.3333	3.65148	6481.74	135.75	16.75	4.09268	6439.85
132.417	13.4166	3.66286	6482.04	135.833	16.8333	4.10284	6438.59
132.5	13.5	3.67423	6484.18	135.917	16.9166	4.11298	6439.85
132.583	13.5833	3.68555	6480.82	136	17	4.12311	6439.85
132.667	13.6666	3.69684	6478.34	136.083	17.0833	4.1332	6439.85
132.75	13.75	3.7081	6479.56	136.167	17.1666	4.14326	6438.9
132.833	13.8333	3.71932	6477.12	136.25	17.25	4.15331	6433.98
132.917	13.9166	3.73049	6479.26	136.333	17.3333	4.16333	6432.45
133	14	3.74166	6478.34	136.417	17.4166	4.17332	6433.67
133.083	14.0833	3.75277	6475.86	136.5	17.5	4.1833	6431.23
133.167	14.1666	3.76385	6471.86	136.583	17.5833	4.19325	6432.76
133.25	14.25	3.77492	6470.94	136.667	17.6666	4.20316	6431.23
133.333	14.3333	3.78594	6473.12	136.75	17.75	4.21307	6427.84
133.417	14.4166	3.79692	6468.5	136.833	17.8333	4.22295	6426.58
133.5	14.5	3.80789	6470.94	136.917	17.9166	4.2328	6423.83
133.583	14.5833	3.81881	6469.72	137	18	4.24264	6426.27
133.667	14.6666	3.8297	6468.5	137.083	18.0833	4.25245	6427.84
133.75	14.75	3.84057	6464.8	137.167	18.1666	4.26223	6423.83
133.833	14.8333	3.8514	6463.54	137.25	18.25	4.272	6420.44
133.917	14.9166	3.8622	6466.94	137.333	18.3333	4.28174	6420.13
134	15	3.87298	6464.8	137.417	18.4166	4.29145	6421.66
134.083	15.0833	3.88372	6463.54	137.5	18.5	4.30116	6419.22
134.167	15.1666	3.89443	6459.84	137.583	18.5833	4.31084	6416.74
134.25	15.25	3.90512	6458.62	137.667	18.6666	4.32049	6417.96
134.333	15.3333	3.91578	6457.4	137.75	18.75	4.33013	6414.26
134.417	15.4166	3.9264	6458.62	137.833	18.8333	4.33974	6414.26
134.5	15.5	3.937	6459.84	137.917	18.9166	4.34932	6414.26
134.583	15.5833	3.94757	6453.4	138	19	4.3589	6413.95
134.667	15.6666	3.9581	6453.7	138.083	19.0833	4.36845	6412.73
134.75	15.75	3.96863	6452.17	138.167	19.1666	4.37797	6412.73

134.833	15.8333	3.97911	6452.17	138.25	19.25	4.38748	6409.03
134.917	15.9166	3.98956	6454.92	138.333	19.3333	4.39697	6408.11
135	16	4	6453.7	138.417	19.4166	4.40642	6409.34
135.083	16.0833	4.0104	6452.48	138.5	19.5	4.41588	6406.59
135.167	16.1666	4.02077	6450.92	138.583	19.5833	4.4253	6405.64
135.25	16.25	4.03113	6448.47	138.667	19.6666	4.4347	6401.63
135.333	16.3333	4.04145	6447.22	138.75	19.75	4.4441	6401.94
135.417	16.4166	4.05174	6445.08	138.833	19.8333	4.45346	6400.71
138.917	19.9166	4.4628	6400.71	142.333	23.3333	4.83046	6362.53
139	20	4.47214	6401.94	142.417	23.4166	4.83907	6362.23
139.083	20.0833	4.48144	6399.49	142.5	23.5	4.84768	6361
139.167	20.1666	4.49072	6395.49	142.583	23.5833	4.85627	6360.05
139.25	20.25	4.5	6395.79	142.667	23.6666	4.86483	6360.05
139.333	20.3333	4.50925	6394.57	142.75	23.75	4.8734	6361
139.417	20.4166	4.51847	6397.01	142.833	23.8333	4.88194	6358.83
139.5	20.5	4.52769	6393.31	142.917	23.9166	4.89046	6358.83
139.583	20.5833	4.53688	6392.09	143	24	4.89898	6358.83
139.667	20.6666	4.54605	6388.39	143.083	24.0833	4.90748	6356.35
139.75	20.75	4.55522	6393.01	143.167	24.1666	4.91595	6356.35
139.833	20.8333	4.56435	6390.87	143.25	24.25	4.92443	6352.69
139.917	20.9166	4.57346	6387.17	143.333	24.3333	4.93288	6356.04
140	21	4.58258	6388.39	143.417	24.4166	4.94131	6354.82
140.083	21.0833	4.59166	6383.47	143.5	24.5	4.94975	6351.12
140.167	21.1666	4.60072	6384.69	143.583	24.5833	4.95816	6352.69
140.25	21.25	4.60977	6385.95	143.667	24.6666	4.96655	6353.91
140.333	21.3333	4.6188	6383.17	143.75	24.75	4.97494	6348.68
140.417	21.4166	4.62781	6382.25	143.833	24.8333	4.9833	6348.99
140.5	21.5	4.63681	6378.25	143.917	24.9166	4.99165	6352.34
140.583	21.5833	4.64578	6379.77	144	25	5	6346.51
140.667	21.6666	4.65474	6378.25	144.083	25.0833	5.00832	6346.2
140.75	21.75	4.66369	6376.99	144.167	25.1666	5.01663	6347.42
140.833	21.8333	4.67261	6375.77	144.25	25.25	5.02494	6348.99
140.917	21.9166	4.68151	6378.55	144.333	25.3333	5.03322	6346.51
141	22	4.69042	6377.29	144.417	25.4166	5.04149	6344.98
141.083	22.0833	4.69929	6377.29	144.5	25.5	5.04975	6344.98
141.167	22.1666	4.70814	6374.85	144.583	25.5833	5.05799	6344.03
141.25	22.25	4.71699	6370.85	144.667	25.6666	5.06622	6342.81
141.333	22.3333	4.72581	6374.55	144.75	25.75	5.07445	6341.59
141.417	22.4166	4.73462	6369.63	144.833	25.8333	5.08265	6339.11

141.5	22.5	4.74342	6370.85	144.917	25.9166	5.09083	6339.11
141.583	22.5833	4.75219	6368.37	145	26	5.09902	6340.37
141.667	22.6666	4.76094	6367.15	145.083	26.0833	5.10718	6338.8
141.75	22.75	4.7697	6371.15	145.167	26.1666	5.11533	6337.58
141.833	22.8333	4.77842	6369.93	145.25	26.25	5.12348	6337.58
141.917	22.9166	4.78713	6368.67	145.333	26.3333	5.1316	6337.89
142	23	4.79583	6368.37	145.417	26.4166	5.13971	6337.89
142.083	23.0833	4.80451	6367.45	145.5	26.5	5.14782	6337.58
142.167	23.1666	4.81317	6367.15	145.583	26.5833	5.1559	6334.19
142.25	23.25	4.82183	6361	145.667	26.6666	5.16397	6333.88
145.75	26.75	5.17204	6335.1	149.167	30.1666	5.49241	6305.84
145.833	26.8333	5.18009	6332.66	149.25	30.25	5.5	6304.32
145.917	26.9166	5.18812	6332.66	149.333	30.3333	5.50757	6300.62
146	27	5.19615	6334.19	149.417	30.4166	5.51512	6303.1
146.083	27.0833	5.20416	6328.96	149.5	30.5	5.52268	6304.62
146.167	27.1666	5.21216	6330.49	149.583	30.5833	5.53022	6298.44
146.25	27.25	5.22015	6330.49	149.667	30.6666	5.53774	6300.92
146.333	27.3333	5.22813	6329.27	149.75	30.75	5.54527	6298.14
146.417	27.4166	5.23608	6326.79	149.833	30.8333	5.55278	6300.62
146.5	27.5	5.24404	6326.48	149.917	30.9166	5.56027	6296.92
146.583	27.5833	5.25198	6326.79	150	31	5.56776	6299.7
146.667	27.6666	5.2599	6325.26	150.083	31.0833	5.57524	6297.22
146.75	27.75	5.26783	6325.56	150.167	31.1666	5.5827	6299.7
146.833	27.8333	5.27573	6325.56	150.25	31.25	5.59017	6299.7
146.917	27.9166	5.28361	6325.56	150.333	31.3333	5.59762	6294.48
147	28	5.2915	6321.56	150.417	31.4166	5.60505	6294.48
147.083	28.0833	5.29937	6321.56	150.5	31.5	5.61249	6296
147.167	28.1666	5.30722	6324.34	150.583	31.5833	5.6199	6293.52
147.25	28.25	5.31507	6321.86	150.667	31.6666	5.62731	6292.3
147.333	28.3333	5.3229	6320.34	150.75	31.75	5.63471	6292
147.417	28.4166	5.33072	6320.34	150.833	31.8333	5.6421	6294.48
147.5	28.5	5.33854	6321.56	150.917	31.9166	5.64948	6289.82
147.583	28.5833	5.34634	6315.42	151	32	5.65685	6292
147.667	28.6666	5.35412	6315.72	151.083	32.0833	5.66421	6290.77
147.75	28.75	5.3619	6319.08	151.167	32.1666	5.67156	6291.08
147.833	28.8333	5.36967	6316.64	151.25	32.25	5.67891	6289.52
147.917	28.9166	5.37741	6315.72	151.333	32.3333	5.68624	6286.12
148	29	5.38516	6316.64	151.417	32.4166	5.69356	6289.82
148.083	29.0833	5.39289	6314.46	151.5	32.5	5.70088	6289.82

148.167	29.1666	5.40061	6312.94	151.583	32.5833	5.70818	6287.38
148.25	29.25	5.40833	6314.46	151.667	32.6666	5.71547	6284.9
148.333	29.3333	5.41602	6310.46	151.75	32.75	5.72276	6282.15
148.417	29.4166	5.42371	6309.54	151.833	32.8333	5.73004	6287.07
148.5	29.5	5.43139	6309.24	151.917	32.9166	5.7373	6284.6
148.583	29.5833	5.43905	6308.02	152	33	5.74456	6282.15
148.667	29.6666	5.4467	6309.24	152.083	33.0833	5.75181	6282.46
148.75	29.75	5.45436	6308.32	152.167	33.1666	5.75904	6283.37
148.833	29.8333	5.46199	6309.24	152.25	33.25	5.76628	6281.2
148.917	29.9166	5.46961	6309.54	152.333	33.3333	5.7735	6281.2
149	30	5.47723	6305.84	152.417	33.4166	5.78071	6281.2
149.083	30.0833	5.48483	6304.32	152.5	33.5	5.78792	6279.67
152.583	33.5833	5.79511	6277.5	156	37	6.08276	6257.51
152.667	33.6666	5.80229	6278.76	156.083	37.0833	6.08961	6256.56
152.75	33.75	5.80948	6279.98	156.167	37.1666	6.09644	6254.12
152.833	33.8333	5.81664	6277.5	156.25	37.25	6.10328	6259.04
152.917	33.9166	5.82379	6277.19	156.333	37.3333	6.1101	6258.73
153	34	5.83095	6279.98	156.417	37.4166	6.11691	6255.34
153.083	34.0833	5.83809	6276.28	156.5	37.5	6.12372	6255.03
153.167	34.1666	5.84522	6275.06	156.583	37.5833	6.13052	6255.03
153.25	34.25	5.85235	6275.97	156.667	37.6666	6.13731	6255.03
153.333	34.3333	5.85946	6275.97	156.75	37.75	6.1441	6254.12
153.417	34.4166	5.86656	6273.49	156.833	37.8333	6.15088	6254.12
153.5	34.5	5.87367	6275.06	156.917	37.9166	6.15764	6251.64
153.583	34.5833	5.88076	6271.05	157	38	6.16441	6253.81
153.667	34.6666	5.88783	6273.84	157.083	38.0833	6.17117	6250.42
153.75	34.75	5.89491	6273.49	157.167	38.1666	6.17791	6250.42
153.833	34.8333	5.90198	6272.58	157.25	38.25	6.18466	6248.85
153.917	34.9166	5.90903	6268.88	157.333	38.3333	6.19139	6250.11
154	35	5.91608	6271.05	157.417	38.4166	6.19811	6247.63
154.083	35.0833	5.92312	6271.05	157.5	38.5	6.20484	6250.11
154.167	35.1666	5.93014	6271.36	157.583	38.5833	6.21155	6249.19
154.25	35.25	5.93717	6268.57	157.667	38.6666	6.21825	6247.63
154.333	35.3333	5.94418	6266.13	157.75	38.75	6.22495	6249.19
154.417	35.4166	5.95118	6267.66	157.833	38.8333	6.23164	6247.63
154.5	35.5	5.95819	6265.18	157.917	38.9166	6.23832	6246.41
154.583	35.5833	5.96518	6268.88	158	39	6.245	6243.01
154.667	35.6666	5.97215	6267.66	158.083	39.0833	6.25166	6243.01
154.75	35.75	5.97913	6263.65	158.167	39.1666	6.25832	6244.23

154.833	35.8333	5.98609	6267.66	158.25	39.25	6.26498	6245.49
154.917	35.9166	5.99304	6263.96	158.333	39.3333	6.27163	6247.63
155	36	6	6265.18	158.417	39.4166	6.27826	6241.79
155.083	36.0833	6.00694	6265.18	158.5	39.5	6.2849	6241.49
155.167	36.1666	6.01387	6259.95	158.583	39.5833	6.29153	6240.53
155.25	36.25	6.0208	6261.17	158.667	39.6666	6.29814	6241.49
155.333	36.3333	6.02771	6262.74	158.75	39.75	6.30476	6238.09
155.417	36.4166	6.03462	6262.74	158.833	39.8333	6.31136	6240.53
155.5	36.5	6.04152	6262.74	158.917	39.9166	6.31796	6239.31
155.583	36.5833	6.04841	6259.04	159	40	6.32456	6240.23
155.667	36.6666	6.05529	6257.82	159.083	40.0833	6.33114	6239.01
155.75	36.75	6.06218	6260.26	159.167	40.1666	6.33771	6238.09
155.833	36.8333	6.06905	6260.26	159.25	40.25	6.34429	6235.61
155.917	36.9166	6.0759	6259.95	159.333	40.3333	6.35085	6236.57
159.417	40.4166	6.3574	6234.39	162.833	43.8333	6.62067	6219.59
159.5	40.5	6.36396	6237.79	162.917	43.9166	6.62696	6216.85
159.583	40.5833	6.3705	6236.57	163	44	6.63325	6219.59
159.667	40.6666	6.37704	6236.87	163.083	44.0833	6.63953	6216.85
159.75	40.75	6.38357	6236.87	163.167	44.1666	6.6458	6214.37
159.833	40.8333	6.39009	6235.31	163.25	44.25	6.65207	6218.07
159.917	40.9166	6.39661	6233.17	163.333	44.3333	6.65833	6218.07
160	41	6.40312	6235.61	163.417	44.4166	6.66458	6214.67
160.083	41.0833	6.40963	6234.09	163.5	44.5	6.67083	6214.37
160.167	41.1666	6.41612	6232.87	163.583	44.5833	6.67707	6215.93
160.25	41.25	6.42262	6234.39	163.667	44.6666	6.68331	6214.67
160.333	41.3333	6.4291	6231.91	163.75	44.75	6.68954	6215.93
160.417	41.4166	6.43557	6233.17	163.833	44.8333	6.69577	6214.37
160.5	41.5	6.44205	6229.47	163.917	44.9166	6.70198	6214.67
160.583	41.5833	6.44851	6230.69	164	45	6.7082	6212.23
160.667	41.6666	6.45497	6234.09	164.083	45.0833	6.71441	6215.93
160.75	41.75	6.46142	6231.91	164.167	45.1666	6.72061	6213.45

Table C-3C G-function and diagnostic functions - case M3

$G(\Delta t_D, \alpha)$	P_w	$P_w FIT$	$X(n)$	$Y(n)$	$Y(n) FIT$
	Psi	psi			
0	6.96E+03	6.96E+03	0	0.267164	0.267164
1.3968	6.67E+03	6.65E+03	4.74E-10	0.59032	0.5827846
1.403172	6.67E+03	6.65E+03	6.38E-10	0.656819	0.6915174
1.409452	6.66E+03	6.64E+03	7.32E-10	0.71551	0.7542616
1.415658	6.66E+03	6.64E+03	8.12E-10	0.768329	0.8072574
1.421783	6.66E+03	6.64E+03	8.82E-10	0.816438	0.8541919
1.427843	6.65E+03	6.64E+03	9.46E-10	0.860906	0.896801
1.43385	6.65E+03	6.64E+03	1.01E-09	0.902366	0.9360617
1.439793	6.65E+03	6.64E+03	1.06E-09	0.940885	0.972342
1.445684	6.64E+03	6.64E+03	1.11E-09	0.977368	1.0064393
1.451531	6.64E+03	6.63E+03	1.16E-09	1.011757	1.0384601
1.457324	6.64E+03	6.63E+03	1.2E-09	1.044122	1.0685602
1.463073	6.64E+03	6.63E+03	1.25E-09	1.075213	1.0973271
1.468786	6.64E+03	6.63E+03	1.29E-09	1.10479	1.1246505
1.47445	6.63E+03	6.63E+03	1.33E-09	1.132936	1.1506421
1.480076	6.63E+03	6.63E+03	1.36E-09	1.159866	1.1754823
1.48567	6.63E+03	6.63E+03	1.4E-09	1.185957	1.1994773
1.49122	6.63E+03	6.63E+03	1.44E-09	1.210819	1.2223715
1.496735	6.63E+03	6.62E+03	1.47E-09	1.23484	1.244459
1.502223	6.62E+03	6.62E+03	1.5E-09	1.257899	1.265676
1.50767	6.62E+03	6.62E+03	1.53E-09	1.27992	1.2859811
1.513086	6.62E+03	6.62E+03	1.56E-09	1.301477	1.3058111
1.518476	6.62E+03	6.62E+03	1.59E-09	1.32261	1.3252025
1.52383	6.62E+03	6.62E+03	1.62E-09	1.342683	1.3436914
1.529154	6.62E+03	6.62E+03	1.64E-09	1.36198	1.3614981
1.534456	6.61E+03	6.62E+03	1.67E-09	1.380727	1.3788064
1.539723	6.61E+03	6.61E+03	1.7E-09	1.399205	1.3958337
1.544963	6.61E+03	6.61E+03	1.72E-09	1.417219	1.4124285
1.550182	6.61E+03	6.61E+03	1.74E-09	1.434271	1.4282199
1.555368	6.61E+03	6.61E+03	1.77E-09	1.450803	1.4435628
1.560529	6.61E+03	6.61E+03	1.79E-09	1.466981	1.4585775
1.565671	6.61E+03	6.61E+03	1.81E-09	1.483463	1.4737713
1.570783	6.60E+03	6.61E+03	1.83E-09	1.498473	1.4877811
1.57587	6.60E+03	6.61E+03	1.86E-09	1.513665	1.5018887

1.58094	6.60E+03	6.61E+03	1.88E-09	1.528847	1.5159437
1.585981	6.60E+03	6.60E+03	1.9E-09	1.54232	1.5286384
1.590999	6.60E+03	6.60E+03	1.91E-09	1.556257	1.5416664
1.596001	6.60E+03	6.60E+03	1.93E-09	1.570032	1.5545341
1.600976	6.60E+03	6.60E+03	1.95E-09	1.583194	1.5668927
1.605929	6.60E+03	6.60E+03	1.97E-09	1.596463	1.5793045
1.610867	6.59E+03	6.60E+03	1.99E-09	1.608843	1.5909928
1.615778	6.59E+03	6.60E+03	2.01E-09	1.620877	1.602393
1.620669	6.59E+03	6.60E+03	2.02E-09	1.632982	1.6138284
1.625546	6.59E+03	6.59E+03	2.04E-09	1.644827	1.6250362
1.630397	6.59E+03	6.59E+03	2.06E-09	1.65652	1.6361049
1.63523	6.59E+03	6.59E+03	2.07E-09	1.667451	1.6465534
1.640049	6.59E+03	6.59E+03	2.09E-09	1.678578	1.6571429
1.644843	6.59E+03	6.59E+03	2.1E-09	1.689079	1.6672233
1.649619	6.58E+03	6.59E+03	2.12E-09	1.699636	1.6773349
1.654383	6.58E+03	6.59E+03	2.13E-09	1.710304	1.6875178
1.659123	6.58E+03	6.59E+03	2.15E-09	1.720135	1.6970225
1.663846	6.58E+03	6.59E+03	2.16E-09	1.730017	1.7065591
1.668557	6.58E+03	6.59E+03	2.18E-09	1.73916	1.7154988
1.673245	6.58E+03	6.58E+03	2.19E-09	1.748812	1.7248404
1.677917	6.58E+03	6.58E+03	2.2E-09	1.758045	1.7338339
1.682577	6.58E+03	6.58E+03	2.22E-09	1.767388	1.742904
1.687216	6.58E+03	6.58E+03	2.23E-09	1.776612	1.7518696
1.691838	6.57E+03	6.58E+03	2.24E-09	1.784407	1.7596844
1.69645	6.57E+03	6.58E+03	2.26E-09	1.792886	1.768051
1.70104	6.57E+03	6.58E+03	2.27E-09	1.801754	1.7767218
1.705615	6.57E+03	6.58E+03	2.28E-09	1.809662	1.7846098
1.710181	6.57E+03	6.58E+03	2.29E-09	1.817682	1.7925851
1.714725	6.57E+03	6.57E+03	2.3E-09	1.82594	1.8007487
1.719255	6.57E+03	6.57E+03	2.32E-09	1.833206	1.808105
1.723775	6.57E+03	6.57E+03	2.33E-09	1.84068	1.815631
1.728276	6.57E+03	6.57E+03	2.34E-09	1.847866	1.8229241
1.732761	6.57E+03	6.57E+03	2.35E-09	1.855133	1.8302797
1.737239	6.56E+03	6.57E+03	2.36E-09	1.862535	1.8377405
1.741696	6.56E+03	6.57E+03	2.37E-09	1.868922	1.8443773
1.74614	6.56E+03	6.57E+03	2.38E-09	1.876544	1.8520132
1.750575	6.56E+03	6.57E+03	2.39E-09	1.88326	1.8589062
1.754991	6.56E+03	6.57E+03	2.4E-09	1.888953	1.864972
1.759394	6.56E+03	6.56E+03	2.41E-09	1.896514	1.8725586
1.763789	6.56E+03	6.56E+03	2.42E-09	1.902462	1.8788221
1.768166	6.56E+03	6.56E+03	2.43E-09	1.907799	1.8845963
1.772529	6.56E+03	6.56E+03	2.44E-09	1.91446	1.8914561
1.776885	6.56E+03	6.56E+03	2.45E-09	1.920789	1.8980357
1.781223	6.56E+03	6.56E+03	2.46E-09	1.926538	1.9041388

1.785547	6.55E+03	6.56E+03	2.47E-09	1.931795	1.9098439
1.789866	6.55E+03	6.56E+03	2.48E-09	1.937867	1.9162198
1.794166	6.55E+03	6.56E+03	2.49E-09	1.943833	1.9225039
1.798454	6.55E+03	6.56E+03	2.5E-09	1.948674	1.9278636
1.802736	6.55E+03	6.55E+03	2.5E-09	1.953807	1.9334721
1.807	6.55E+03	6.55E+03	2.51E-09	1.958864	1.9390228
1.811252	6.55E+03	6.55E+03	2.52E-09	1.964749	1.945251
1.815498	6.55E+03	6.55E+03	2.53E-09	1.969536	1.9505721
1.819726	6.55E+03	6.55E+03	2.54E-09	1.974101	1.9557154
1.823944	6.55E+03	6.55E+03	2.55E-09	1.97952	1.9615676
1.828155	6.55E+03	6.55E+03	2.55E-09	1.983926	1.9665785
1.832349	6.54E+03	6.55E+03	2.56E-09	1.988835	1.972012
1.836533	6.54E+03	6.55E+03	2.57E-09	1.993259	1.9770442
1.84071	6.54E+03	6.55E+03	2.58E-09	1.997939	1.9822907
1.844872	6.54E+03	6.55E+03	2.58E-09	2.002295	1.987271
1.849023	6.54E+03	6.54E+03	2.59E-09	2.006869	1.9924323
1.853167	6.54E+03	6.54E+03	2.6E-09	2.011124	1.9973314
1.857296	6.54E+03	6.54E+03	2.61E-09	2.014373	2.0013999
1.861414	6.54E+03	6.54E+03	2.61E-09	2.019274	2.0068501
1.865528	6.54E+03	6.54E+03	2.62E-09	2.023053	2.0113618
1.869625	6.54E+03	6.54E+03	2.63E-09	2.027133	2.0161285
1.873713	6.54E+03	6.54E+03	2.63E-09	2.030712	2.0204818
1.877795	6.54E+03	6.54E+03	2.64E-09	2.03473	2.0252019
1.881861	6.53E+03	6.54E+03	2.65E-09	2.039853	2.0308437
1.885918	6.53E+03	6.54E+03	2.66E-09	2.042244	2.0341967
1.88997	6.53E+03	6.53E+03	2.66E-09	2.044986	2.0378639
1.894007	6.53E+03	6.53E+03	2.67E-09	2.049459	2.0429866
1.898035	6.53E+03	6.53E+03	2.67E-09	2.052872	2.0472142
1.902057	6.53E+03	6.53E+03	2.68E-09	2.056401	2.0515382
1.906065	6.53E+03	6.53E+03	2.69E-09	2.059436	2.055457
1.910063	6.53E+03	6.53E+03	2.69E-09	2.062554	2.0594476
1.914057	6.53E+03	6.53E+03	2.7E-09	2.066785	2.0643753
1.918037	6.53E+03	6.53E+03	2.71E-09	2.069391	2.0679333
1.922005	6.53E+03	6.53E+03	2.71E-09	2.072081	2.0715719
1.925972	6.53E+03	6.53E+03	2.72E-09	2.074934	2.0753529
1.929924	6.53E+03	6.53E+03	2.72E-09	2.079103	2.080246
1.933866	6.52E+03	6.52E+03	2.73E-09	2.081764	2.0838592
1.937804	6.52E+03	6.52E+03	2.73E-09	2.083191	2.0864422
1.941729	6.52E+03	6.52E+03	2.74E-09	2.086905	2.0909713
1.945644	6.52E+03	6.52E+03	2.75E-09	2.089911	2.094894
1.949556	6.52E+03	6.52E+03	2.75E-09	2.092322	2.0983116
1.953455	6.52E+03	6.52E+03	2.76E-09	2.09601	2.1028173
1.957343	6.52E+03	6.52E+03	2.76E-09	2.098152	2.106008
1.961229	6.52E+03	6.52E+03	2.77E-09	2.0999	2.1088745

1.965102	6.52E+03	6.52E+03	2.77E-09	2.102248	2.1122668
1.968964	6.52E+03	6.52E+03	2.78E-09	2.104717	2.1157589
1.972824	6.52E+03	6.52E+03	2.78E-09	2.108319	2.1202127
1.976672	6.52E+03	6.52E+03	2.79E-09	2.110609	2.1235458
1.98051	6.52E+03	6.51E+03	2.79E-09	2.11217	2.1262626
1.984345	6.52E+03	6.51E+03	2.8E-09	2.114228	2.1294153
1.988167	6.51E+03	6.51E+03	2.8E-09	2.116835	2.1330398
1.99198	6.51E+03	6.51E+03	2.81E-09	2.11871	2.1360421
1.995791	6.51E+03	6.51E+03	2.81E-09	2.12092	2.1393326
1.999589	6.51E+03	6.51E+03	2.82E-09	2.123458	2.1429066
2.003378	6.51E+03	6.51E+03	2.82E-09	2.125264	2.1458503
2.007165	6.51E+03	6.51E+03	2.83E-09	2.127629	2.1492792
2.010939	6.51E+03	6.51E+03	2.83E-09	2.128704	2.1516086
2.014704	6.51E+03	6.51E+03	2.84E-09	2.130823	2.1548398
2.018468	6.51E+03	6.51E+03	2.84E-09	2.133333	2.1584092
2.022219	6.51E+03	6.50E+03	2.85E-09	2.134312	2.160658
2.025962	6.51E+03	6.50E+03	2.85E-09	2.136353	2.1638354
2.029702	6.51E+03	6.50E+03	2.86E-09	2.139015	2.1675438
2.03343	6.51E+03	6.50E+03	2.86E-09	2.140286	2.1700503
2.037149	6.51E+03	6.50E+03	2.86E-09	2.140806	2.1719184
2.040868	6.50E+03	6.50E+03	2.87E-09	2.142685	2.174974
2.044574	6.50E+03	6.50E+03	2.87E-09	2.144777	2.1782099
2.048271	6.50E+03	6.50E+03	2.88E-09	2.147053	2.1816022
2.051966	6.50E+03	6.50E+03	2.88E-09	2.148138	2.1839615
2.055651	6.50E+03	6.50E+03	2.88E-09	2.149599	2.1866577
2.059326	6.50E+03	6.50E+03	2.89E-09	2.151243	2.1895129
2.063	6.50E+03	6.50E+03	2.89E-09	2.152449	2.1919887
2.066663	6.50E+03	6.49E+03	2.9E-09	2.153802	2.1946036
2.070318	6.50E+03	6.49E+03	2.9E-09	2.1544	2.1965657
2.07397	6.50E+03	6.49E+03	2.9E-09	2.156676	2.1999899
2.077612	6.50E+03	6.49E+03	2.91E-09	2.158319	2.2028591
2.081244	6.50E+03	6.49E+03	2.91E-09	2.158243	2.2042368
2.084877	6.50E+03	6.49E+03	2.91E-09	2.159678	2.2069435
2.088498	6.50E+03	6.49E+03	2.92E-09	2.162182	2.2105794
2.092111	6.50E+03	6.49E+03			
2.095722	6.49E+03	6.49E+03			
2.099323	6.49E+03	6.49E+03			
2.102914	6.49E+03	6.49E+03			

Table C-3D Net pressure during injection - case M3

Δt_{inj}	P_n	Δt_{inj}	P_n	Δt_{inj}	P_n
min	psi	min	psi	min	psi
0.016602	2654.35	2.81665	3189.82	5.616699	3171.08
0.009972	6983.486	7.926598	7149.807	15.8433	7133.785
0.0933	6990.581	8.010002	7142.102	15.9266	7133.479
0.176636	6977.307	8.0933	7151.027	16.01	7132.564
0.259972	7008.129	8.176605	7147.327	16.0933	7131.344
0.3433	7018.887	8.260002	7154.728	16.17661	7129.779
0.426628	7063.251	8.3433	7153.507	16.26	7133.785
0.509972	7070.957	8.426598	7148.281	16.3433	7133.785
0.5933	7118.717	8.510002	7154.423	16.4266	7133.785
0.676636	7118.717	8.5933	7159.648	16.51	7128.559
0.759972	7110.401	8.676605	7151.981	16.5933	7130.085
0.8433	7127.337	8.760002	7149.502	16.67661	7128.864
0.926628	7131.344	8.8433	7151.981	16.76	7133.785
1.009972	7132.259	8.926598	7153.507	16.8433	7127.644
1.0933	7138.706	9.010002	7150.723	16.9266	7131.038
1.176636	7143.322	9.0933	7148.586	17.01	7131.344
1.259972	7147.022	9.176605	7149.502	17.0933	7119.938
1.3433	7153.202	9.260002	7148.586	17.17661	7123.638
1.426628	7155.644	9.3433	7148.281	17.26	7128.864
1.509972	7153.507	9.426598	7150.723	17.3433	7129.779
1.5933	7158.428	9.510002	7147.327	17.4266	7131.344
1.676636	7167.965	9.5933	7142.406	17.51	7122.685
1.759972	7171.665	9.676605	7146.106	17.5933	7122.685
1.8433	7169.528	9.760002	7145.802	17.67661	7127.644
1.926628	7168.308	9.8433	7143.322	17.76	7129.779
2.009972	7179.371	9.926598	7143.665	17.8433	7132.564
2.0933	7183.071	10.01	7141.186	17.9266	7128.559
2.176636	7177.845	10.0933	7148.281	18.01	7126.385
2.259972	7181.851	10.17661	7139.965	18.0933	7121.464
2.3433	7183.071	10.26	7139.965	18.17661	7124.857
2.426628	7184.292	10.3433	7135.958	18.26	7125.164
2.509972	7189.251	10.4266	7143.665	18.3433	7127.644
2.5933	7185.551	10.51	7151.027	18.4266	7118.717
2.676636	7187.992	10.5933	7148.281	18.51	7129.779
2.759972	7187.992	10.67661	7139.66	18.5933	7126.079
2.8433	7184.292	10.76	7142.406	18.67661	7122.685
2.926628	7189.251	10.8433	7143.665	18.76	7125.164
3.009972	7185.551	10.9266	7144.886	18.8433	7123.943
3.0933	7189.251	11.01	7135.958	18.9266	7122.685

3.176636	7186.466	11.0933	7138.706	19.01	7124.857
3.259972	7188.907	11.17661	7136.265	19.0933	7123.943
3.3433	7188.907	11.26	7143.665	19.17661	7126.385
3.426628	7182.766	11.3433	7137.485	19.26	7119.022
3.509972	7181.851	11.4266	7135.006	19.3433	7120.243
3.5933	7192.913	11.51	7133.785	19.4266	7119.022
3.676636	7183.986	11.5933	7136.265	19.51	7120.243
3.759972	7182.766	11.67661	7144.581	19.5933	7122.378
3.8433	7187.992	11.76	7142.406	19.67661	7129.779
3.926628	7184.292	11.8433	7135.006	19.76	7132.564
4.009972	7184.292	11.9266	7137.485	19.8433	7125.164
4.0933	7181.851	12.01	7137.18	19.9266	7127.337
4.176636	7180.286	12.0933	7143.322	20.01	7124.857
4.259972	7181.851	12.17661	7135.958	20.0933	7127.644
4.3433	7178.15	12.26	7133.785	20.17661	7128.559
4.426628	7180.592	12.3433	7132.564	20.26	7123.638
4.509972	7178.15	12.4266	7139.965	20.3433	7122.685
4.5933	7176.624	12.51	7141.186	20.4266	7124.857
4.676636	7174.145	12.5933	7139.965	20.51	7127.644
4.759972	7175.671	12.67661	7136.265	20.5933	7125.164
4.8433	7176.624	12.76	7135.958	20.67661	7119.022
4.926598	7178.15	12.8433	7139.66	20.76	7124.857
5.010002	7170.444	12.9266	7141.186	20.8433	7122.378
5.0933	7171.97	13.01	7136.265	20.9266	7128.864
5.176605	7170.749	13.0933	7138.706	21.01	7116.237
5.260002	7171.97	13.17661	7138.706	21.0933	7121.464
5.3433	7169.224	13.26	7138.706	21.17661	7115.017
5.426598	7168.308	13.3433	7136.265	21.26	7121.158
5.510002	7164.607	13.4266	7133.785	21.3433	7121.158
5.5933	7170.749	13.51	7137.485	21.4266	7123.638
5.676605	7171.97	13.5933	7137.485	21.51	7122.378
5.760002	7166.744	13.67661	7138.706	21.5933	7115.017
5.8433	7164.303	13.76	7140.881	21.67661	7119.022
5.926598	7166.744	13.8433	7135.958	21.76	7122.378
6.010002	7162.128	13.9266	7138.706	21.8433	7120.243
6.0933	7161.823	14.01	7133.785	21.9266	7125.164
6.176605	7165.523	14.0933	7134.7	22.01	7119.938
6.260002	7163.044	14.17661	7134.7	22.0933	7116.543
6.3433	7154.728	14.26	7138.706	22.17661	7116.543
6.426598	7149.807	14.3433	7140.881	22.26	7122.685
6.510002	7148.281	14.4266	7133.785	22.3433	7123.943
6.5933	7154.423	14.51	7132.259	22.4266	7123.943
6.676605	7149.502	14.5933	7133.479	22.51	7115.322
6.760002	7143.322	14.67661	7135.006	22.5933	7115.322

6.8433	7142.406	14.76	7136.265	22.67661	7112.843
6.926598	7143.322	14.8433	7136.265	22.76	7115.322
7.010002	7138.706	14.9266	7135.006	22.8433	7111.622
7.0933	7146.106	15.01	7131.038	22.9266	7115.322
7.176605	7147.022	15.0933	7135.006	23.01	7108.836
7.260002	7142.406	15.17661	7134.7	23.0933	7107.922
7.3433	7135.958	15.26	7130.085	23.17661	7103
7.426598	7142.102	15.3433	7133.479	23.26	7103
7.510002	7143.665	15.4266	7127.644	23.3433	7099.3
7.5933	7141.186	15.51	7129.779	23.4266	7098.995
7.676605	7144.581	15.5933	7130.085	23.51	7094.378
7.760002	7143.665	15.67661	7132.259		
7.8433	7148.586	15.67661	7132.259		
7.926598	7149.807	15.76	7137.485		

Table C-3E Synthesis of computed fluid and reservoir properties - case M3

S_p	c_f	R_f	\bar{w}	C_L	η	R_o	k_r
<i>ft</i>	<i>ft / psi</i>	<i>ft</i>	<i>in</i>	<i>ft / $\sqrt{\text{min}}$</i>	<i>%</i>	<i>(psi - min) / ft</i>	<i>md</i>
-7.6E-02	2.04E-05	143	7.61E-01	1.36E-02	45.7	1.71E+04	11.2

Table C-4A - Input parameters - case M4

Parameter	Description	Units	Value
ϕ	Reservoir porosity	fraction	0.23
c_t	reserve total compressibility	1/psi	5.6e-6
μ_r	reservoir fluid viscosity	cp	1.6
μ_f	fracture fluid viscosity	cp	202
V_i	vol. of injected fluid	gal	21315
h_p	permeable height	ft	120
h_f	fracture height	ft	120
t_p	pumping time	min	35
t_c	fracture closure time	min	42
P_c	closure pressure	psi	5225
P_i	Initial reservoir pressure	psi	3685
$ISIP$	Initial shut-in pressure	psi	5995
E	Young's Modulus	psi	5.56E+06
ν	Poisson's ratio	fraction	0.27
E'	Plain-strain modulus	psi	6.0E+06
	Fracture area - power law exponent		
α	RAD Model		8/9
n'	flow behavior index	fraction	0.5
K'	Ratio of shear stress to shear rate	Lbf s ^{0.5} /ft ²	0.064
β_{RAD}	Average pressure ratio (wellbore-tip)		0.925

Table C-4B Fall off time - pressure data - case M4

$\Delta t_{fall-off}$	\sqrt{dt}	P_w
min	$\sqrt{\text{min}}$	Psi
0.9	0.948683	5963
3.7	1.923538	5882
6.5	2.54951	5811
9.2	3.03315	5748
12	3.464102	5694
13.8	3.714835	5659
15.7	3.962323	5626
17.5	4.1833	5594
19.4	4.404543	5564
21.2	4.604346	5534
23	4.795832	5504
24.9	4.98999	5474
26.7	5.167204	5447
28.6	5.347897	5418
30.4	5.51362	5392
32.3	5.683309	5364
34.1	5.839521	5338
36	6	5314
37.8	6.14817	5291
39.6	6.292853	5269
41.5	6.442049	5247
43.3	6.580274	5228
46.1	6.789698	5200
48.9	6.992853	5174
51.6	7.183314	5148
54.4	7.375636	5126
57.2	7.563068	5106
59.9	7.739509	5087

Table C-4C G-function and diagnostic functions - case M4

$G(\Delta t_D, \alpha)$	P_w	$P_w FIT$	$X(n)$	$Y(n)$	$Y(n) FIT$
	Psi	psi			
0	6745.498	6745.498	0	1.828608	46508570
1.37689	5989.999	5960.788	1.00E-09	2.303078	46508570
1.421438	5963.001	5935.4	1.47E-09	2.41817	46508570
1.542574	5882	5866.363	1.68E-09	2.504679	46508570
1.650304	5811	5804.966	1.79E-09	2.479944	46508570
1.746017	5748	5750.417	1.93E-09	2.538408	46508570
1.838923	5693.999	5697.469	2.09E-09	2.659932	46508570
1.895852	5659	5665.024	2.28E-09	2.78311	46508570
1.953901	5626	5631.941	2.42E-09	2.849542	46508570
2.007165	5594	5601.585	2.48E-09	2.810671	46508570
2.061743	5564	5570.481	2.66E-09	2.951774	46508570
2.112029	5533.999	5541.822			
2.161051	5504	5513.883			
2.211533	5474	5485.113			
2.258248	5447	5458.489			
2.306472	5418	5431.006			

Table C-4D Pressure derivative data – case M4

$F(t)$	$F(t)^2$	$P'_D \cdot F(t)^2$	$F(t)$	$F(t)^2$	$P'_D \cdot F(t)^2$
0.85242	0.72662	-22.116	0.43499	0.18921	-6.0366
0.72639	0.52765	-17.759	0.42602	0.18149	-5.6786
0.65796	0.43291	-15.159	0.41803	0.17475	-5.3635
0.61107	0.37341	-13.295	0.41009	0.16818	-5.0538
0.57328	0.32865	-11.754	0.40299	0.1624	-4.7802
0.55288	0.30567	-10.911	0.39625	0.15702	-4.5243
0.53381	0.28495	-10.118	0.38951	0.15172	-4.2716
0.51764	0.26795	-9.4443	0.38344	0.14703	-4.0475
0.50221	0.25221	-8.8008	0.37455	0.14029	-3.7257
0.48889	0.23901	-8.2466	0.36626	0.13415	-3.4332
0.47666	0.2272	-7.739	0.35878	0.12873	-3.1759
0.46475	0.216	-7.2477	0.3515	0.12355	-2.9321
0.45431	0.2064	-6.8195	0.34466	0.11879	-2.7092
0.44405	0.19718	-6.4023	0.33843	0.11453	-2.5122

Table C-4E Synthesis of computed fluid and reservoir properties - case M4

S_p	c_f	R_f	\bar{w}	C_L	η	R_o	k_r
<i>ft</i>	<i>ft / psi</i>	<i>ft</i>	<i>in</i>	<i>ft / $\sqrt{\text{min}}$</i>	<i>%</i>	<i>(psi - min) / ft</i>	<i>md</i>
-1.01E-02	4.24E-05	175	3.64E-01	2.01E-02	48.48	3.05E+05	17.7

Table C-5A - Input parameters - case M5

Parameter	Description	Units	Value
ϕ	Reservoir porosity	fraction	0.41
c_t	reservoir total compressibility	1/psi	6.1e-6
μ_r	reservoir fluid viscosity	cp	1.6
μ_f	fracture fluid viscosity	cp	208
V_i	vol. of injected fluid	gal	23000
h_p	permeable height	ft	95
h_f	fracture height	ft	95
t_p	pumping time	min	18
t_c	fracture closure time	min	19.26
P_c	closure pressure	psi	5816
P_i	Initial reservoir pressure	psi	4930
$ISIP$	Initial shut-in pressure	psi	6040
E	Young's Modulus	psi	6.0E+05
ν	Poisson's ratio	fraction	0.27
E'	Plain-strain modulus	psi	6.5+05
	Fracture area - power law exponent		
α	KGD Model		2/3
n'	flow behavior index	fraction	0.55
K'	Ratio of shear stress to shear rate	Lbf s ^{0.5} /ft ²	0.0618
β_{KGD}	Average pressure ratio (wellbore-tip)		0.9

Table C-5B Fall off time - pressure data - case M5

t	$\Delta t_{fall-off}$	\sqrt{dt}	P_w	t	$\Delta t_{fall-off}$	\sqrt{dt}	P_w
min	min	$\sqrt{\text{min}}$	Psi	min	min	$\sqrt{\text{min}}$	Psi
196.078	0.07843	0.28005	5970.25	220.085	24.0851	4.90766	5742.93
196.25	0.25009	0.50009	6030.99	220.245	24.2451	4.92393	5740.41
196.412	0.41174	0.64167	6105.07	220.417	24.4168	4.94133	5737.75
196.583	0.58347	0.76385	6056.7	220.577	24.5767	4.95749	5735.14
196.743	0.74342	0.86222	6034.18	220.749	24.7485	4.97479	5732.29
196.915	0.91509	0.9566	6030.75	220.918	24.9185	4.99184	5729.75
197.087	1.08675	1.04247	6019.69	221.078	25.0785	5.00784	5731.45
197.247	1.24676	1.11659	6017.2	221.25	25.2501	5.02495	5726.48
197.418	1.41843	1.19098	6020.38	221.41	25.4101	5.04084	5724.33
197.578	1.57845	1.25636	6014.13	221.582	25.5818	5.05784	5720.86
197.75	1.75011	1.32292	6010.1	221.73	25.7301	5.07249	5718.7
197.912	1.91174	1.38266	6006.58	221.913	25.9134	5.09052	5716.39
198.083	2.08345	1.44342	6003.38	222.085	26.0851	5.10736	5713.49
198.255	2.25511	1.5017	6000.27	222.245	26.2451	5.123	5710.86
198.415	2.41507	1.55405	5998.52	222.417	26.4168	5.13972	5708.2
198.587	2.58673	1.60833	5994.41	222.577	26.5768	5.15527	5705.89
198.747	2.74675	1.65733	5992.17	222.748	26.7484	5.17189	5705.68
198.918	2.91841	1.70834	5991.39	222.918	26.9184	5.1883	5701.45
199.078	3.07845	1.75455	5987.37	223.078	27.0784	5.20369	5698.99
199.238	3.23846	1.79957	5985.2	223.25	27.2501	5.22016	5695.94
199.41	3.41013	1.84665	5983.27	223.41	27.4101	5.23547	5692.88
199.582	3.58179	1.89256	5981.13	223.582	27.5818	5.25184	5694.87
199.743	3.74342	1.93479	5979.22	223.753	27.7534	5.26815	5688.71
199.915	3.91508	1.97866	5976.95	223.913	27.9135	5.28332	5686.78
200.087	4.08675	2.02157	5974.8	224.085	28.0851	5.29954	5682.97
200.247	4.24676	2.06077	5973.12	224.245	28.2451	5.31461	5680.29
200.418	4.41843	2.10201	5971.15	224.417	28.4167	5.33074	5677.65
200.578	4.57843	2.13973	5969.44	224.587	28.5868	5.34666	5674.71
200.75	4.75009	2.17947	5967.52	224.747	28.7467	5.3616	5671.87
200.91	4.91011	2.21588	5965.41	224.918	28.9184	5.37759	5669.85
201.082	5.08177	2.25428	5963.55	225.078	29.0784	5.39244	5670.86
201.253	5.25343	2.29204	5961.72	225.25	29.2501	5.40833	5666.32
201.413	5.41345	2.32668	5960.39	225.41	29.4101	5.42311	5663.45
201.587	5.58673	2.36363	5958.09	225.582	29.5817	5.43891	5659.93

201.747	5.74676	2.39724	5955.85	225.753	29.7534	5.45467	5657.12
201.918	5.91843	2.43278	5953.82	225.913	29.9135	5.46932	5654.81
202.078	6.07844	2.46545	5951.92	226.083	30.0834	5.48484	5651.06
202.25	6.25011	2.50002	5949.91	226.255	30.2551	5.50046	5647.79
202.41	6.41013	2.53182	5948.37	226.415	30.4151	5.51499	5645.03
202.582	6.58179	2.5655	5946.15	226.587	30.5868	5.53053	5642.23
202.753	6.75345	2.59874	5944.14	226.747	30.7468	5.54498	5641.77
202.913	6.91347	2.62935	5942.22	226.918	30.9184	5.56044	5640.08
203.085	7.08513	2.66179	5942.48	227.078	31.0785	5.57481	5636.23
203.245	7.24509	2.69167	5938.75	227.248	31.2484	5.59003	5633.45
203.417	7.41675	2.72337	5936.85	227.42	31.4201	5.60536	5630.52
203.578	7.57843	2.7529	5934.91	227.58	31.5801	5.61962	5627.75
203.75	7.75009	2.7839	5932.77	227.752	31.7518	5.63487	5626.71
203.922	7.92175	2.81456	5930.79	227.912	31.9117	5.64905	5622.8
204.082	8.08177	2.84285	5928.8	228.083	32.0835	5.66423	5620.73
204.253	8.25343	2.87288	5926.6	228.243	32.2434	5.67833	5617.85
204.413	8.41345	2.9006	5924.7	228.413	32.4135	5.69328	5615.8
204.585	8.58512	2.93004	5924.71	228.585	32.5851	5.70834	5613.41
204.745	8.74507	2.95721	5921.37	228.745	32.7451	5.72233	5611.11
204.917	8.91673	2.98609	5919.13	228.917	32.9167	5.73731	5608.57
205.077	9.07676	3.01277	5917.15	229.077	33.0768	5.75124	5607.25
205.248	9.24841	3.04112	5914.63	229.248	33.2484	5.76615	5608.32
205.42	9.42007	3.06921	5912.57	229.418	33.4185	5.78087	5605.32
205.58	9.58011	3.09518	5913.89	229.578	33.5784	5.79469	5603.31
205.752	9.75175	3.12278	5908.54	229.75	33.7501	5.80948	5600.88
205.913	9.91346	3.14856	5907.37	229.91	33.9101	5.82324	5598.8
206.085	10.0851	3.17571	5905.29	230.082	34.0818	5.83796	5596.41
206.245	10.2451	3.2008	5903.42	230.253	34.2534	5.85264	5594.67
206.417	10.4167	3.2275	5901.39	230.413	34.4134	5.8663	5592.84
206.577	10.5768	3.25219	5899.89	230.583	34.5834	5.88077	5590.56
206.748	10.7484	3.27848	5899.02	230.743	34.7434	5.89436	5588.76
206.92	10.9201	3.30455	5896.74	230.915	34.9151	5.9089	5586.32
207.08	11.0801	3.32868	5894.85	231.087	35.0868	5.92341	5584.58
207.252	11.2518	3.35436	5892.58	231.247	35.2468	5.9369	5585.34
207.412	11.4118	3.37813	5890.63	231.417	35.4167	5.9512	5582.18
207.583	11.5834	3.40345	5888.8	231.577	35.5768	5.96463	5580.63
207.755	11.7551	3.42857	5887.42	231.748	35.7485	5.979	5578.45
207.903	11.9034	3.45013	5885.63	231.92	35.9201	5.99334	5576.21
208.087	12.0868	3.4766	5883.77	232.08	36.0801	6.00668	5574.71

208.247	12.2467	3.49953	5881.8	232.252	36.2518	6.02095	5572.84
208.407	12.4068	3.52232	5880.08	232.41	36.4101	6.03408	5571.16
208.578	12.5784	3.54661	5877.97	232.582	36.5818	6.04829	5569.22
208.75	12.7501	3.57073	5876.27	232.753	36.7534	6.06246	5568.24
208.922	12.9217	3.59468	5876.07	232.913	36.9135	6.07565	5566.08
209.083	13.0834	3.61711	5873.64	233.085	37.0851	6.08976	5564.85
209.243	13.2435	3.63916	5871.79	233.243	37.2435	6.10274	5563.38
209.415	13.4151	3.66267	5869.73	233.415	37.4151	6.11679	5561.9
209.587	13.5868	3.68602	5867.91	233.587	37.5868	6.13081	5560.13
209.747	13.7468	3.70766	5866.83	233.747	37.7467	6.14384	5558.69
209.918	13.9185	3.73075	5864.66	233.918	37.9185	6.1578	5557.01
210.078	14.0784	3.75212	5863.09	234.077	38.0767	6.17064	5555.82
210.25	14.2501	3.77493	5860.8	234.248	38.2485	6.18454	5553.99
210.41	14.4101	3.79606	5860.65	234.42	38.4201	6.1984	5552.71
210.582	14.5818	3.81861	5858.05	234.58	38.5801	6.21129	5551.25
210.753	14.7534	3.84102	5855.97	234.752	38.7517	6.22509	5549.76
210.913	14.9134	3.86179	5853.86	234.91	38.9101	6.2378	5548.39
211.085	15.0851	3.88395	5852.02	235.082	39.0818	6.25154	5546.84
211.245	15.2451	3.9045	5849.77	235.253	39.2535	6.26526	5545.5
211.417	15.4168	3.92642	5848.21	235.413	39.4134	6.27801	5544.17
211.577	15.5767	3.94674	5850.62	235.585	39.5851	6.29167	5542.67
211.748	15.7485	3.96843	5845.1	235.743	39.7434	6.30424	5541.3
211.92	15.9201	3.99	5843.75	235.915	39.9151	6.31784	5540.11
212.08	16.0801	4.01	5841.89	236.087	40.0867	6.33141	5538.62
212.252	16.2517	4.03134	5839.3	236.247	40.2468	6.34403	5537.28
212.412	16.4118	4.05114	5837.56	236.417	40.4167	6.35741	5535.76
212.583	16.5834	4.07228	5835.41	236.577	40.5768	6.36999	5534.26
212.743	16.7434	4.09188	5833.47	236.748	40.7484	6.38345	5532.75
212.915	16.9151	4.1128	5835	236.92	40.9201	6.39688	5531.48
213.087	17.0868	4.13361	5830.4	237.08	41.0801	6.40938	5530.04
213.247	17.2468	4.15293	5828.84	237.25	41.2502	6.42263	5528.8
213.418	17.4184	4.17354	5826.61	237.398	41.3985	6.43416	5527.02
213.578	17.5785	4.19267	5824.52	237.582	41.5818	6.4484	5525.98
213.75	17.7501	4.21309	5823.42	237.753	41.7534	6.46169	5524.6
213.91	17.9101	4.23203	5820.3	237.913	41.9135	6.47406	5523.3
214.082	18.0817	4.25226	5818.37	238.072	42.0718	6.48628	5522.15
214.253	18.2535	4.27241	5816.53	238.243	42.2434	6.4995	5520.81
214.413	18.4134	4.29109	5814.16	238.415	42.4151	6.51269	5519.7
214.585	18.5851	4.31104	5812.21	238.587	42.5868	6.52585	5518.16

214.745	18.7451	4.32956	5809.93	238.745	42.7452	6.53798	5517.03
214.917	18.9167	4.34934	5808.96	238.917	42.9167	6.55109	5515.63
215.077	19.0768	4.3677	5811.22	239.077	43.0768	6.56329	5514.4
215.248	19.2484	4.3873	5806.54	239.248	43.2484	6.57636	5513.08
215.42	19.4201	4.40682	5804.75	239.418	43.4184	6.58927	5511.77
215.58	19.5801	4.42494	5802.78	239.567	43.5667	6.60051	5510.65
215.752	19.7518	4.4443	5800.39	239.75	43.7501	6.61439	5509.17
215.912	19.9117	4.46226	5800.57	239.91	43.9102	6.62648	5508.07
216.083	20.0835	4.48146	5795.3	240.08	44.0801	6.63929	5506.4
216.243	20.2434	4.49927	5793.27	240.252	44.2518	6.6522	5505.5
216.415	20.4151	4.51831	5790.65	240.412	44.4118	6.66422	5504.25
216.587	20.5867	4.53726	5787.9	240.583	44.5834	6.67708	5503.18
216.747	20.7468	4.55486	5787.57	240.743	44.7434	6.68905	5501.99
216.918	20.9184	4.57367	5783.93	240.913	44.9135	6.70175	5500.66
217.078	21.0784	4.59113	5781.82	241.085	45.0852	6.71455	5499.62
217.25	21.2501	4.60978	5779.23	241.245	45.2452	6.72645	5498.48
217.41	21.4101	4.62711	5777.09	241.415	45.4151	6.73907	5497.33
217.582	21.5818	4.64562	5774.45	241.587	45.5868	6.7518	5496
217.753	21.7534	4.66406	5773.12	241.747	45.7468	6.76364	5495.02
217.913	21.9135	4.68118	5770.29	241.918	45.9185	6.77632	5493.94
218.083	22.0834	4.6993	5767.95	242.079	46.0785	6.78812	5492.88
218.243	22.2435	4.7163	5765.66	242.248	46.2484	6.80062	5491.44
218.415	22.4151	4.73446	5763.21	242.42	46.4201	6.81323	5490.51
218.587	22.5868	4.75256	5762.48	242.58	46.5801	6.82496	5488.85
218.747	22.7467	4.76935	5760.31	242.75	46.7501	6.8374	5488.05
218.918	22.9185	4.78732	5758.2	242.91	46.9101	6.8491	5486.98
219.078	23.0784	4.804	5755.95	243.082	47.0818	6.86162	5485.83
219.25	23.2501	4.82183	5753.37	243.253	47.2534	6.87411	5484.46
219.41	23.4101	4.8384	5751.23	243.412	47.4118	6.88562	5483.54
219.582	23.5818	4.85611	5748.79	243.583	47.5835	6.89808	5482.39
219.753	23.7534	4.87375	5747.39	243.744	47.7435	6.90967	5481.36
219.913	23.9134	4.89014	5745.29	243.915	47.9151	6.92208	5480.07

Table C-5C G-function and diagnostic functions - case M5

$G(\Delta t_D, \alpha)$	P_w	$P_w FIT$	$X(n)$	$Y(n)$	$Y(n) FIT$
	Psi	psi			
0	0	6346.16	0	0	0.87115
1.4685	6055.22	6037.32	6.76238E-10	1.91699	1.77113
1.48302	6049.69	6034.27	8.76065E-10	2.0353	2.03706
1.49633	6044.88	6031.47	9.75881E-10	2.13874	2.16991
1.51038	6040.03	6028.52	1.0558E-09	2.23553	2.27626
1.52423	6035.45	6025.6	1.12917E-09	2.32789	2.37391
1.53696	6031.38	6022.93	1.19091E-09	2.40825	2.45607
1.55044	6027.21	6020.09	1.25113E-09	2.4886	2.53621
1.56285	6023.48	6017.48	1.3035E-09	2.55953	2.60592
1.576	6019.62	6014.72	1.35531E-09	2.63093	2.67487
1.58824	6016.11	6012.14	1.40258E-09	2.69589	2.73778
1.6011	6012.51	6009.44	1.44651E-09	2.7584	2.79624
1.61382	6009.02	6006.76	1.48919E-09	2.81865	2.85304
1.62554	6005.86	6004.3	1.52721E-09	2.87266	2.90364
1.638	6002.55	6001.68	1.56573E-09	2.92768	2.95491
1.6495	5999.55	5999.26	1.59984E-09	2.97636	3.0003
1.66172	5996.41	5996.69	1.63361E-09	3.02547	3.04524
1.67301	5993.55	5994.31	1.66587E-09	3.07135	3.08818
1.68421	5990.75	5991.96	1.69666E-09	3.11507	3.12915
1.69611	5987.81	5989.46	1.72648E-09	3.15854	3.16884
1.7079	5984.93	5986.98	1.75561E-09	3.20055	3.20761
1.71892	5982.27	5984.66	1.78269E-09	3.23912	3.24364
1.73052	5979.5	5982.22	1.80909E-09	3.27774	3.27877
1.74203	5976.78	5979.8	1.83501E-09	3.3152	3.31327
1.75268	5974.29	5977.56	1.85846E-09	3.34905	3.34449
1.76401	5971.66	5975.18	1.88236E-09	3.38344	3.3763
1.77449	5969.25	5972.97	1.90394E-09	3.41437	3.40501
1.78566	5966.7	5970.62	1.92659E-09	3.44706	3.43516
1.79599	5964.36	5968.45	1.94733E-09	3.47636	3.46275
1.807	5961.89	5966.13	1.96764E-09	3.50571	3.48979
1.81793	5959.45	5963.84	1.98805E-09	3.53488	3.51694
1.82805	5957.21	5961.71	2.0066E-09	3.5614	3.54163
1.83894	5954.82	5959.42	2.02578E-09	3.5888	3.56717

1.84892	5952.64	5957.32	2.04286E-09	3.61293	3.5899
1.85957	5950.33	5955.08	2.06069E-09	3.63814	3.61362
1.86942	5948.2	5953.01	2.07679E-09	3.66075	3.63505
1.87993	5945.95	5950.8	2.09352E-09	3.68423	3.65732
1.88967	5943.87	5948.75	2.10902E-09	3.70552	3.67795
1.90005	5941.67	5946.57	2.12482E-09	3.72794	3.69897
1.91037	5939.49	5944.4	2.14043E-09	3.74973	3.71974
1.91993	5937.49	5942.39	2.15451E-09	3.76923	3.73848
1.93012	5935.36	5940.24	2.16902E-09	3.7892	3.75779
1.93957	5933.39	5938.25	2.18221E-09	3.80719	3.77535
1.94965	5931.31	5936.13	2.19605E-09	3.82609	3.79376
1.9591	5929.36	5934.15	2.20894E-09	3.84333	3.81093
1.96906	5927.31	5932.05	2.22187E-09	3.86108	3.82813
1.97898	5925.29	5929.97	2.2348E-09	3.87857	3.84533
1.98817	5923.42	5928.03	2.24629E-09	3.89386	3.86063
1.99798	5921.43	5925.97	2.25813E-09	3.90947	3.87639
2.00707	5919.6	5924.06	2.26972E-09	3.92504	3.89182
2.01678	5917.64	5922.02	2.28105E-09	3.93985	3.90689
2.02578	5915.84	5920.12	2.29198E-09	3.9543	3.92143
2.03538	5913.92	5918.1	2.30299E-09	3.96863	3.93609
2.0443	5912.15	5916.23	2.31241E-09	3.98008	3.94862
2.05381	5910.26	5914.23	2.32345E-09	3.99483	3.96332
2.06327	5908.39	5912.24	2.33372E-09	4.00795	3.97699
2.07206	5906.66	5910.39	2.34285E-09	4.0193	3.98914
2.08143	5904.82	5908.42	2.35294E-09	4.03213	4.00257
2.09022	5903.1	5906.57	2.36174E-09	4.04299	4.01427
2.0995	5901.28	5904.62	2.3711E-09	4.05457	4.02673
2.10812	5899.6	5902.81	2.3799E-09	4.06549	4.03845
2.11732	5897.82	5900.87	2.38888E-09	4.07643	4.05039
2.12586	5896.16	5899.08	2.39705E-09	4.08595	4.06127
2.13498	5894.4	5897.16	2.40573E-09	4.09668	4.07281
2.14405	5892.65	5895.25	2.41407E-09	4.10656	4.08391
2.15248	5891.04	5893.48	2.42154E-09	4.11519	4.09386
2.16147	5889.31	5891.59	2.42942E-09	4.12427	4.10435
2.16983	5887.71	5889.83	2.43679E-09	4.13242	4.11415
2.17875	5886.01	5887.95	2.44514E-09	4.14295	4.12526
2.18763	5884.32	5886.09	2.45254E-09	4.15096	4.13512
2.19527	5882.87	5884.48	2.45852E-09	4.15702	4.14308
2.20468	5881.09	5882.5	2.46698E-09	4.16746	4.15433

2.21286	5879.54	5880.78	2.47337E-09	4.17401	4.16284
2.221	5878.01	5879.07	2.47938E-09	4.17984	4.17084
2.2297	5876.37	5877.24	2.48675E-09	4.18806	4.18065
2.23837	5874.74	5875.41	2.49336E-09	4.19523	4.18944
2.247	5873.12	5873.6	2.49988E-09	4.2023	4.19812
2.2551	5871.6	5871.9	2.5061E-09	4.20856	4.2064
2.26308	5870.11	5870.22	2.51217E-09	4.21455	4.21448
2.27161	5868.52	5868.42	2.51812E-09	4.22062	4.22239
2.28011	5866.94	5866.64	2.52403E-09	4.22633	4.23025
2.288	5865.47	5864.98	2.53016E-09	4.23274	4.23842
2.29643	5863.91	5863.2	2.53564E-09	4.23773	4.24571
2.30426	5862.46	5861.56	2.54117E-09	4.24307	4.25306
2.31263	5860.91	5859.8	2.54722E-09	4.24907	4.26113
2.32041	5859.48	5858.16	2.55174E-09	4.25237	4.26714
2.32872	5857.95	5856.41	2.55742E-09	4.25797	4.27469
2.33699	5856.43	5854.67	2.56288E-09	4.26292	4.28196
2.34468	5855.02	5853.06	2.56752E-09	4.26675	4.28814
2.3529	5853.51	5851.33	2.57322E-09	4.27211	4.29572
2.36054	5852.11	5849.72	2.57811E-09	4.27638	4.30223
2.3687	5850.62	5848	2.58298E-09	4.28033	4.30872
2.37628	5849.24	5846.41	2.5871E-09	4.28296	4.3142
2.38439	5847.76	5844.71	2.59224E-09	4.28762	4.32103
2.39246	5846.29	5843.01	2.59698E-09	4.29132	4.32734
2.39996	5844.93	5841.43	2.60074E-09	4.29363	4.33235
2.40798	5843.47	5839.74	2.60568E-09	4.29767	4.33892
2.41544	5842.12	5838.18	2.61021E-09	4.30129	4.34495
2.4234	5840.68	5836.5	2.61431E-09	4.3039	4.35041
2.43081	5839.34	5834.94	2.61835E-09	4.30638	4.35578
2.43872	5837.91	5833.28	2.62279E-09	4.30983	4.36169
2.44661	5836.49	5831.62	2.62662E-09	4.31197	4.36679
2.45394	5835.16	5830.08	2.63108E-09	4.31545	4.37272
2.46178	5833.75	5828.43	2.63512E-09	4.31795	4.3781
2.46906	5832.45	5826.9	2.63872E-09	4.31998	4.38289
2.47685	5831.05	5825.26			
2.48408	5829.75	5823.74			
2.49182	5828.36	5822.11			
2.49954	5826.98	5820.49			

Table C-5D Net pressure during injection - case M5

Δt_{inj}	P_n	Δt_{inj}	P_n	Δt_{inj}	P_n
min	psi	min	psi	min	psi
0.075012	1004.56	6.405014	1000.6	12.90001	977.5801
0.235031	959.3398	6.565033	1005.9	13.06003	980.7695
0.406693	944.5996	6.736694	1001.01	13.23337	980.2998
0.568329	969.8398	6.898315	999.2495	13.40503	981.5498
0.73999	970.0498	7.069977	996.8696	13.56667	980.5898
0.899994	968.7598	7.241638	997.8496	13.73833	982
1.071655	972.3799	7.403351	992.6094	13.89835	979.3696
1.233368	968.9697	7.575012	991.1494	14.07169	980.1094
1.405029	966.8999	7.735031	990.4697	14.23166	982.0498
1.564987	961.9199	7.908356	988.4497	14.40337	982.3198
1.736649	968.8599	8.068329	990.3296	14.565	983.9497
1.898346	973.48	8.23999	986.3999	14.73666	982.6694
2.070007	979.48	8.401688	988.5801	14.89838	988.1494
2.241669	983.4399	8.573349	987.2695	15.07004	983.96
2.401688	991.1494	8.733368	986.9097	15.23166	986.4897
2.575027	990.8599	8.906647	985.6094	15.40332	983.04
2.734985	994.1797	9.066666	986.9297	15.57498	986.7295
2.906647	997.4697	9.238327	987.02	15.73669	986.0801
3.066666	993.3198	9.400024	987.5898	15.90834	986.3896
3.240005	997.0298	9.571686	988.2695	16.06999	986.6094
3.40004	1003.22	9.731644	986.6494	16.24165	987.5698
3.571686	999.9199	9.904984	987.46	16.40167	991.2896
3.733322	1000.2	10.065	989.8296	16.575	995.2197
3.904984	997.48	10.23666	990.1895	16.73503	991.3696
4.065002	993.98	10.39836	987.8198	16.90837	990.2798
4.236664	986.02	10.57002	983.52	17.06833	996.3096
4.398376	982.54	10.74168	985.1196	17.24167	995.7397
4.570023	975.5698	10.90332	983.8198	17.40169	996.4697
4.741684	970.6797	11.07498	981.8799	17.57333	993.4297
4.901642	966.6494	11.235	977.6494	17.73499	997.2197
5.074997	960.1494	11.40836	978.0698	17.90665	997.8599
5.235016	958.1396	11.56838	977.1797	18.06834	999.4697
5.406677	955.4297	11.74004	980.2798	18.24001	994.8398
5.566681	961.3896	11.90166	977.5801	18.40166	995.2397
5.740021	972.1494	12.06168	973	18.57336	997.3496
5.899979	978.7695	12.23503	976.1597	18.735	991.9297
6.07164	985.54	12.40669	979.98	18.90666	992.9697
6.233353	992.3096	12.56665	977.0098	19.06838	993.2998
6.405014	1000.6	12.73999	980.1597	19.24004	986.1597

Table C-5E Synthesis of computed fluid and reservoir properties - case M3

S_p	c_f	x_f	\bar{w}	C_L	η	R_o	k_r
gal/100 ft	ft/psi	ft	in	ft/ $\sqrt{\text{min}}$	%	(psi - min)/ft	md
SPURT LOSS IDENTIFIED							
4.4	2.83 E-04	139	6.62 E-01	8.21 E-03	42.2	1.03 E+05	1.03
NO SPURT LOSS ASSUMPTION							
0.0	2.83 E-04	144	6.86 E-01	8.51 E-03	47.2	9.98 E+04	1.11

Table C-5F Synthesis and comparison of computed fluid and reservoir properties obtained from the old and new model

S_p	c_f	x_f	\bar{w}	C_L	η	R_o	k_r
gal/100 ft ²	ft/psi	ft	in	ft/ $\sqrt{\text{min}}$	%	(psi - min)/ft	md
Case M1 - New Model							
NO SPURT LOSS ASSUMPTION							
-6.8E-03	8.99 E-05	66.2	2.81 E-01	1.18 E-02	61.6	6.95E+03	19.5
Case M1 - Old Model							
NO SPURT LOSS ASSUMPTION							
0	9.72 E-05	52.5	2.24 E-01	6.46 E-03	61.5	< 0	6.9
Case M2 - New Model							
NO SPURT LOSS ASSUMPTION							
-3.31E-02	9.05 E-05	66.6	5.53E-01	3.4E-02	23.7	3.88E+03	18.9
Case M2 - Old Model							
NO SPURT LOSS ASSUMPTION							
0	9.78 E-05	52.8	4.4 E-01	1.49 E-02	23.5	4.13 E +04	10.3
Case M3 - New Model							
NO SPURT LOSS ASSUMPTION							
-7.6E-02	2.83 E-04	143	7.61E-01	1.36 E-02	45.7	1.71E+04	11.2
Case M3 - Old Model							
NO SPURT LOSS ASSUMPTION							
0	2.68 E-04	120	6.56 E-01	1.25 E-02	34.6	< 0	6.3
Case M4 - New Model							
NO SPURT LOSS ASSUMPTION							
-1.01E-02	4.53 E-05	175	3.64E-01	2.01E-02	48.4	3.05E+05	17.7
Case M4 - Old Model							
NO SPURT LOSS ASSUMPTION							
0	4.77 E-05	127	3.4 E-01	4.12 E-03	58.4	1.3 E+6	20
Case M5 - New Model							
SPURT LOSS IDENTIFIED							
4.4	3.02 E-04	139	6.62 E-01	8.21 E-03	42.2	1.03 E+05	1.03
NO SPURT LOSS ASSUMPTION							
0	3.13 E-04	144	6.86 E-01	8.51 E-03	45.7	9.98 E+04	1.11
Case M5 - Old Model							
NO SPURT LOSS ASSUMPTION							
0	3.14 E-04	108	5.47 E-01	9.86 E-03	41.7	13.6 E+5	1.45

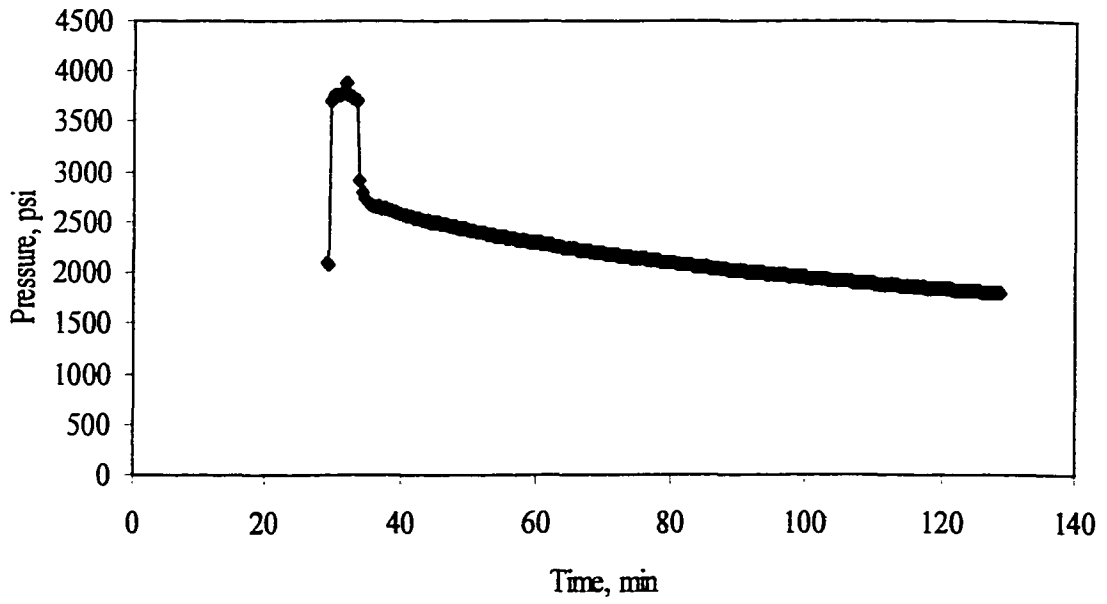


Fig. C-1 Injection and fall-off of a minifrac - Case M1

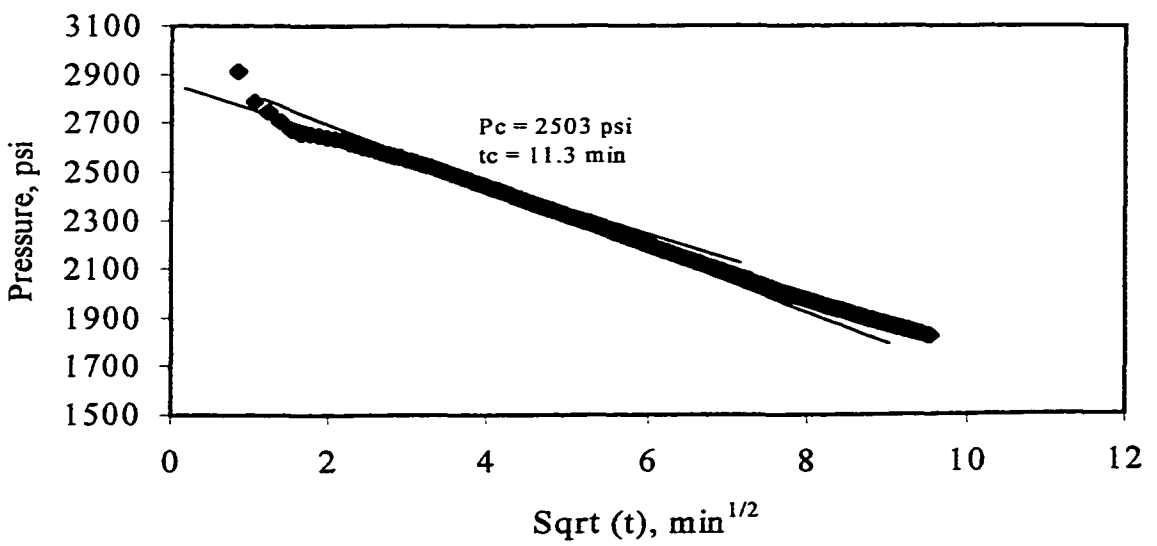


Fig. C-2 Identification of closure from the fall-off of a minifrac - Case M1

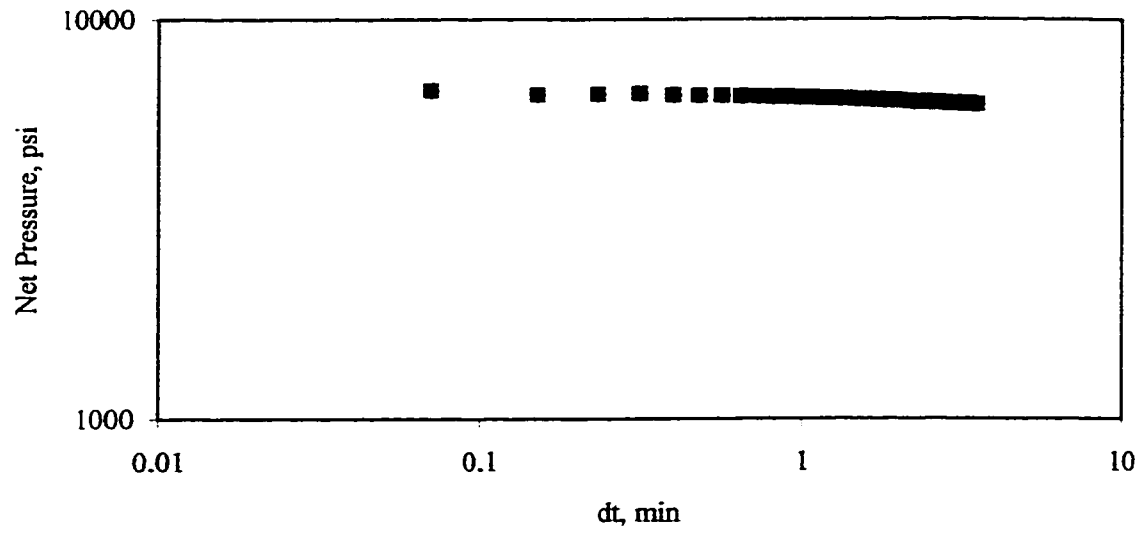


Fig. C-3 Net pressure versus time – Case M1

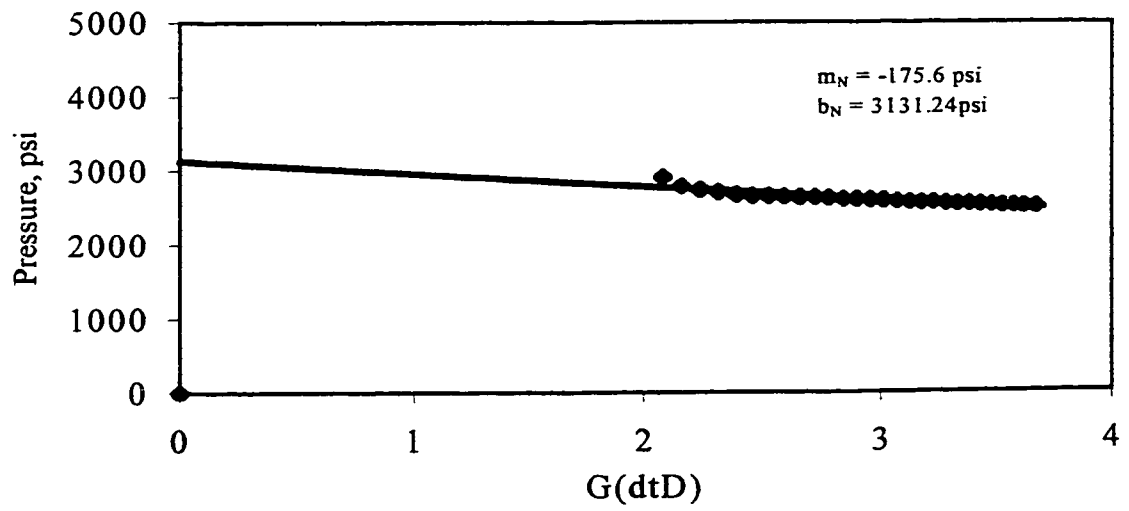


Fig. C-4 G-function of a minifrac test – Case M1

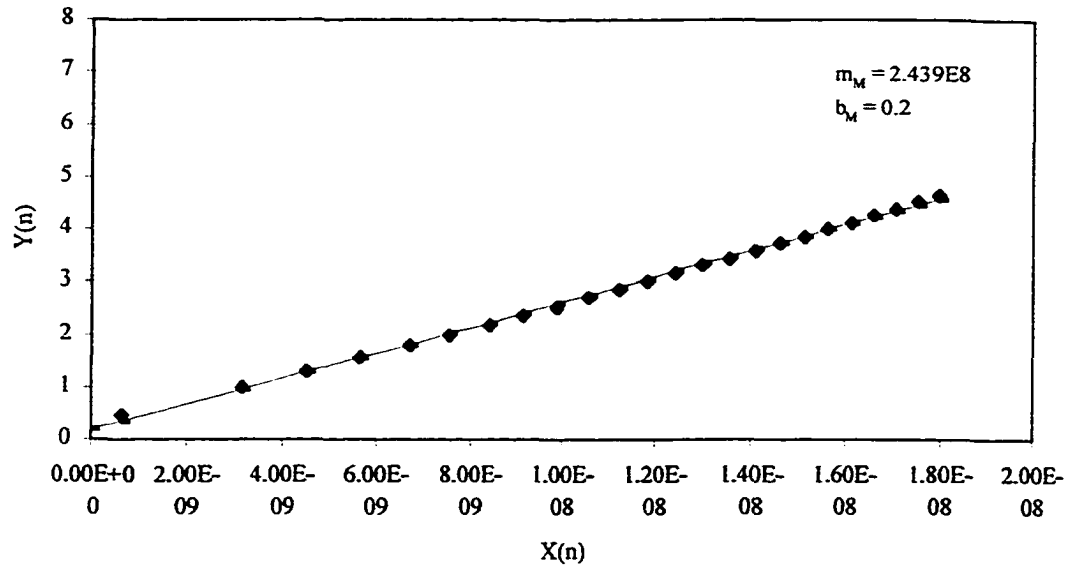


Fig. C-5 Filtercake-reservoir flow diagnostic plot – Case M1

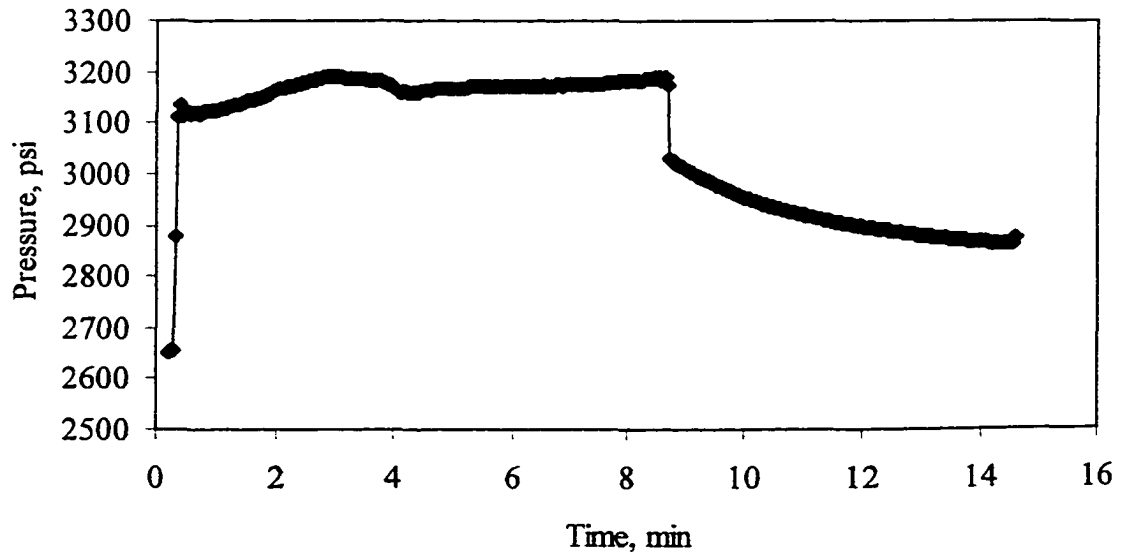


Fig. C-6 Injection and fall-off of a minifrac - Case M2

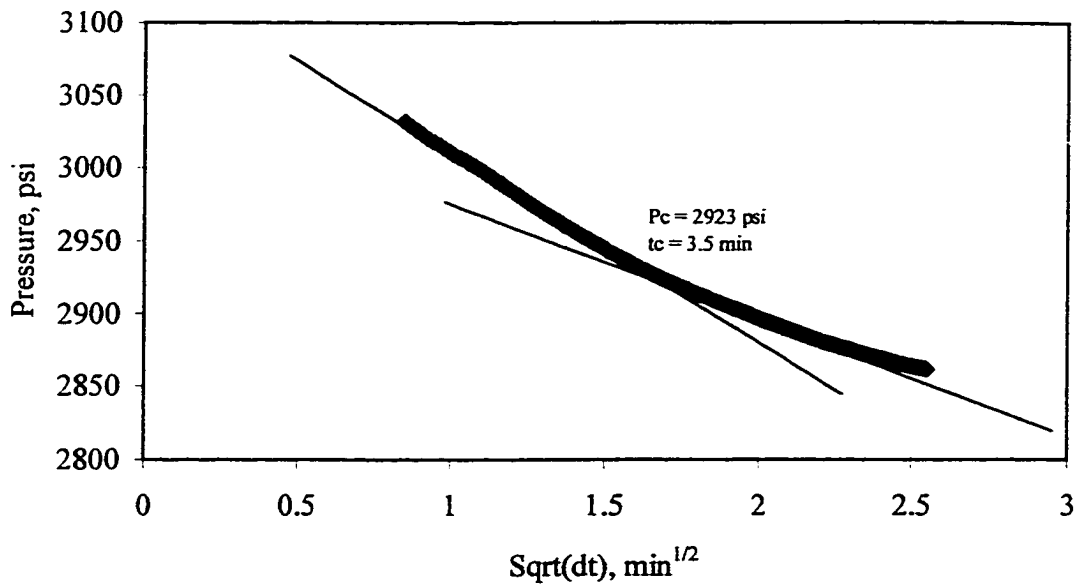


Fig. C-7 Identification of closure from the fall-off of a minifrac - Case M2

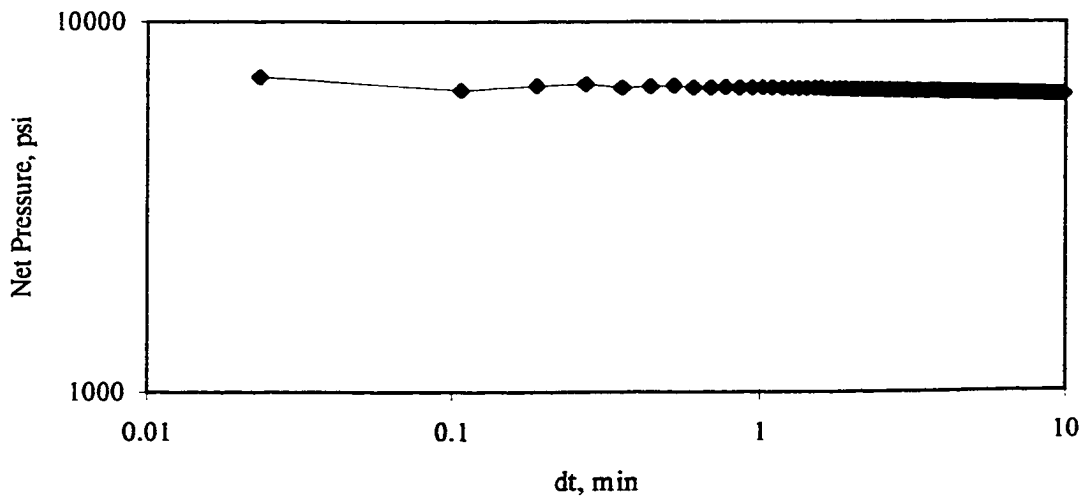


Fig. C-8 Net pressure versus time – Case M2

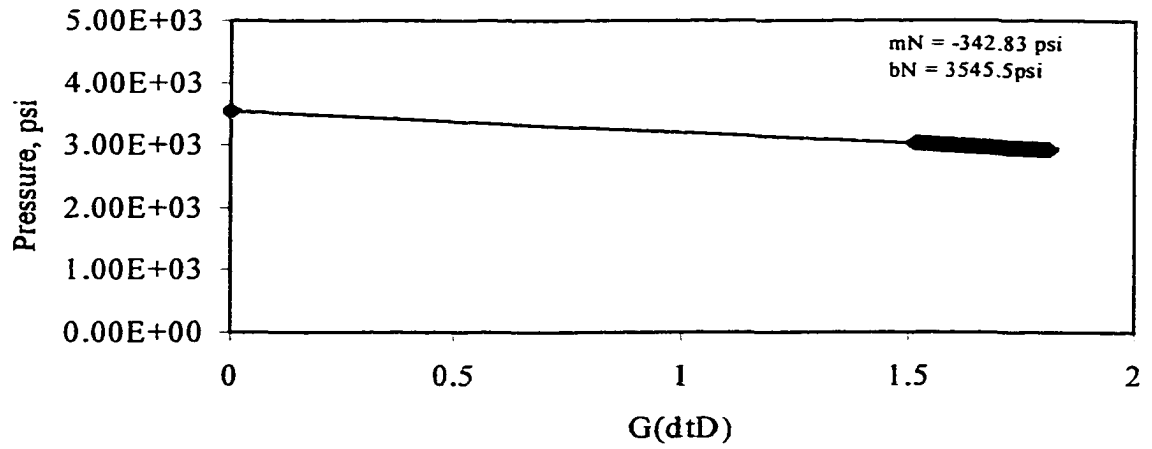


Fig. C-9 G-function of a minifrac test – Case M2

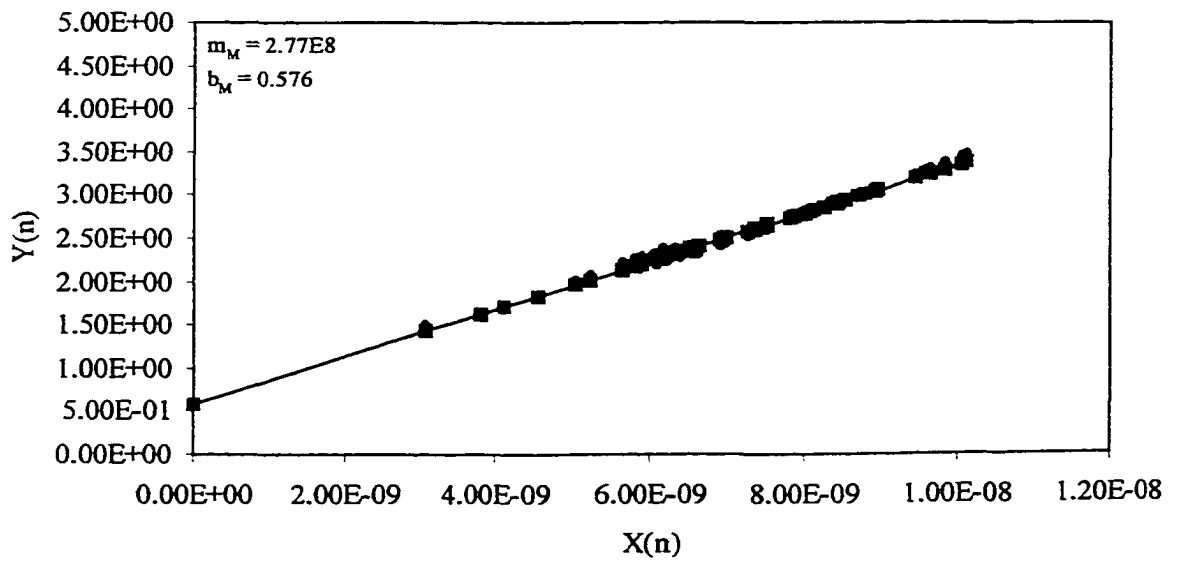


Fig. C-10 Filtercake –reservoir flow diagnostic plot – Case M2

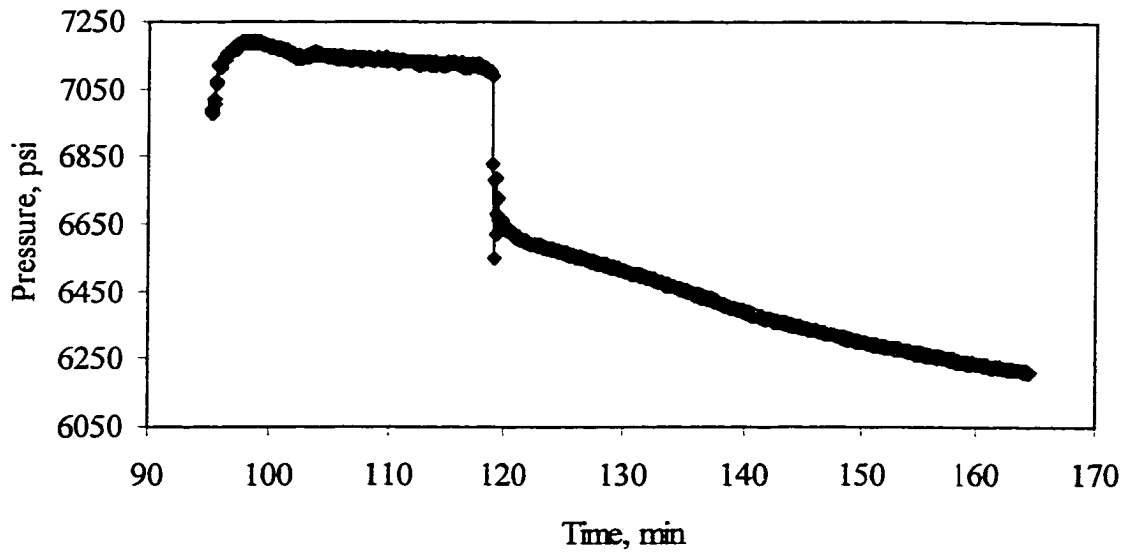


Fig. C-11 Injection and fall-off of a minifrac - Case M3

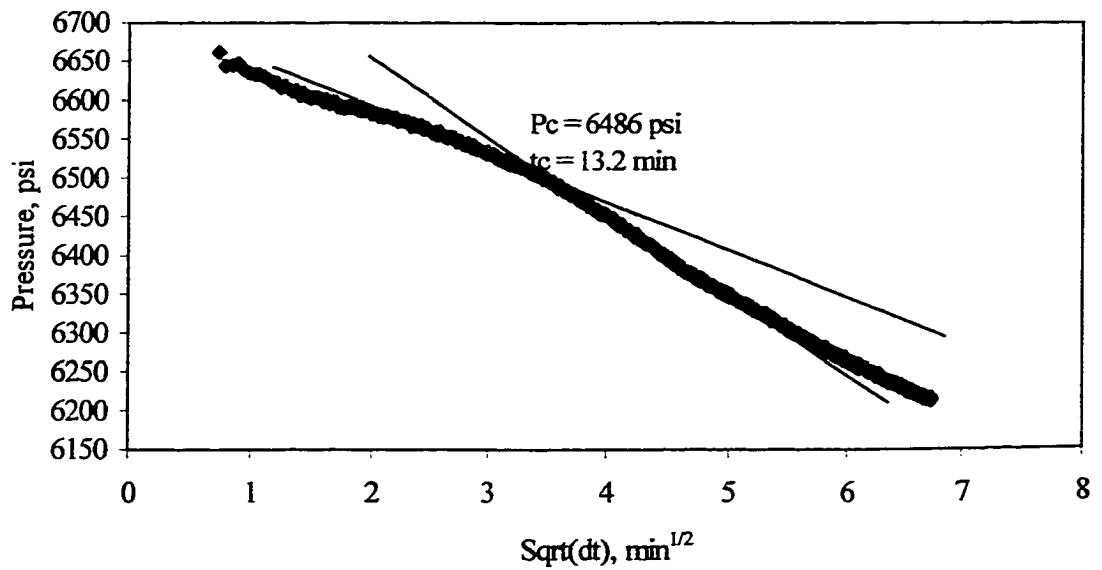


Fig. C-12 Identification of closure from the fall-off of a minifrac - Case M3

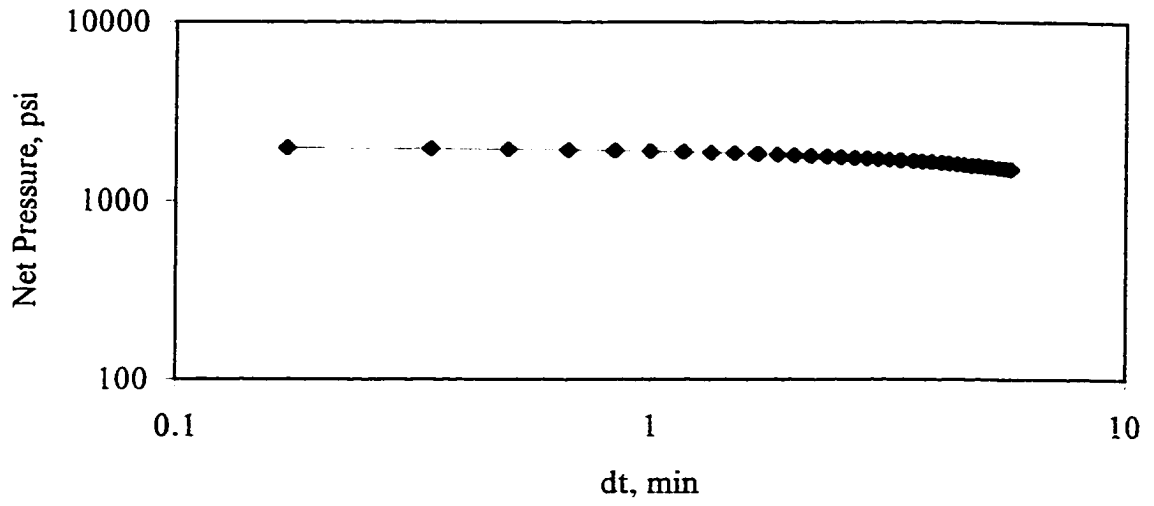


Fig. C-13 Net pressure versus time – Case M3

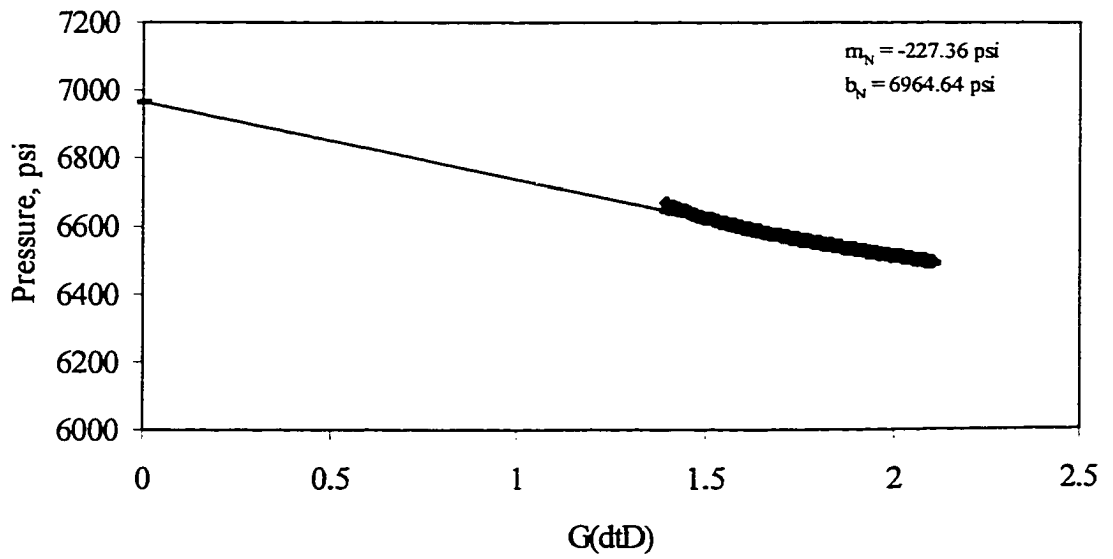


Fig. C-14 G-function of a minifrac test – Case M3

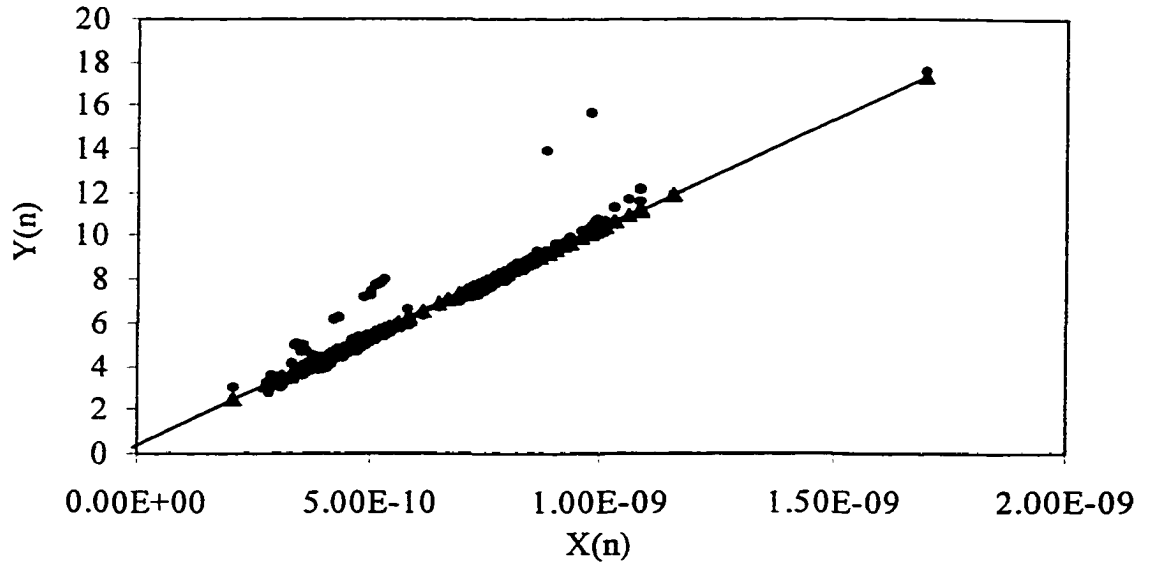


Fig. C-15 Filtercake –reservoir flow diagnostic plot (significant noise)– Case M3

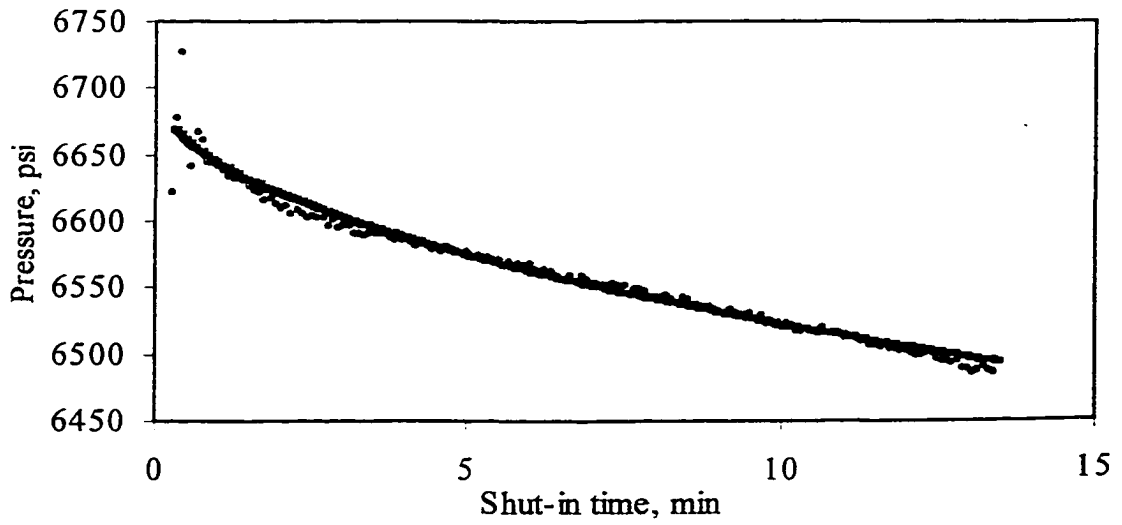


Fig. C-16 Filter cake –reservoir flow diagnostic plot (data filtering)– Case M3

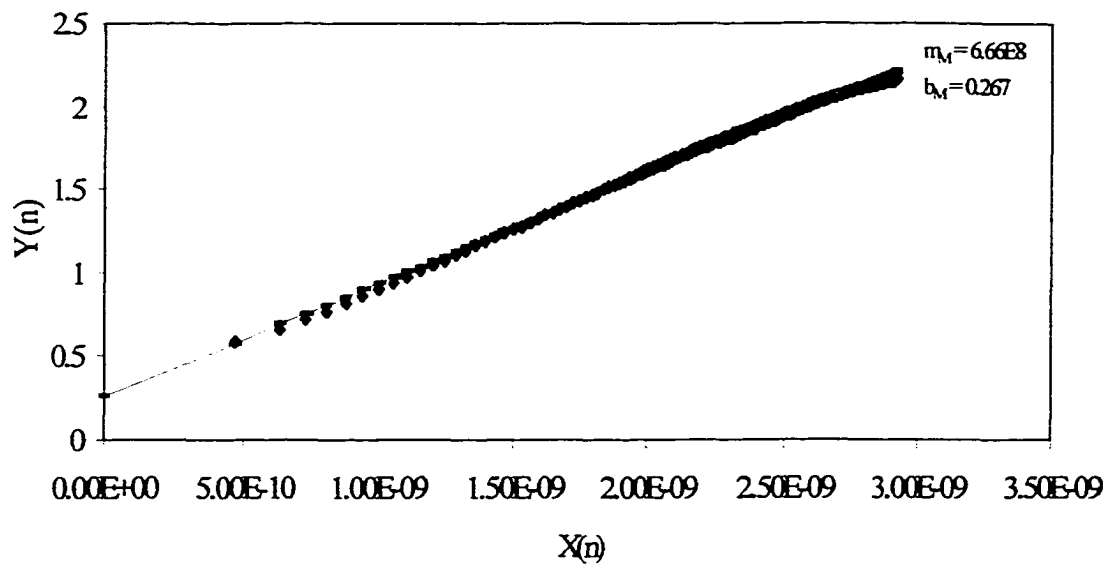


Fig. C-17 Filter cake-reservoir flow diagnostic plot (after data filtering)- Case M3

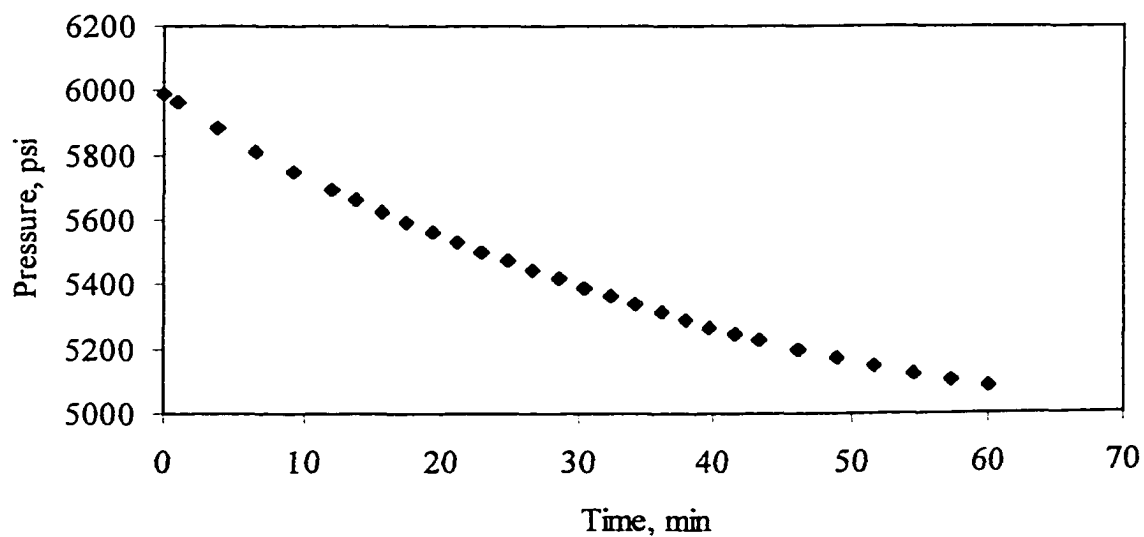


Fig. C-18 Fall-off of a minifrac test - Case M4

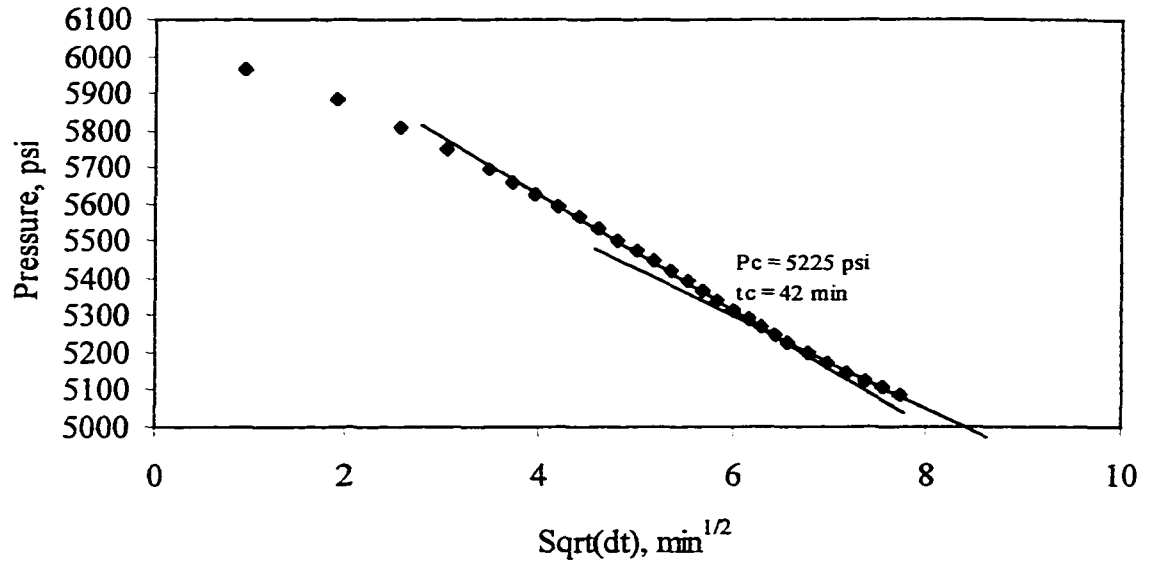


Fig. C-19 Identification of closure from the fall-off of a minifrac - Case M4

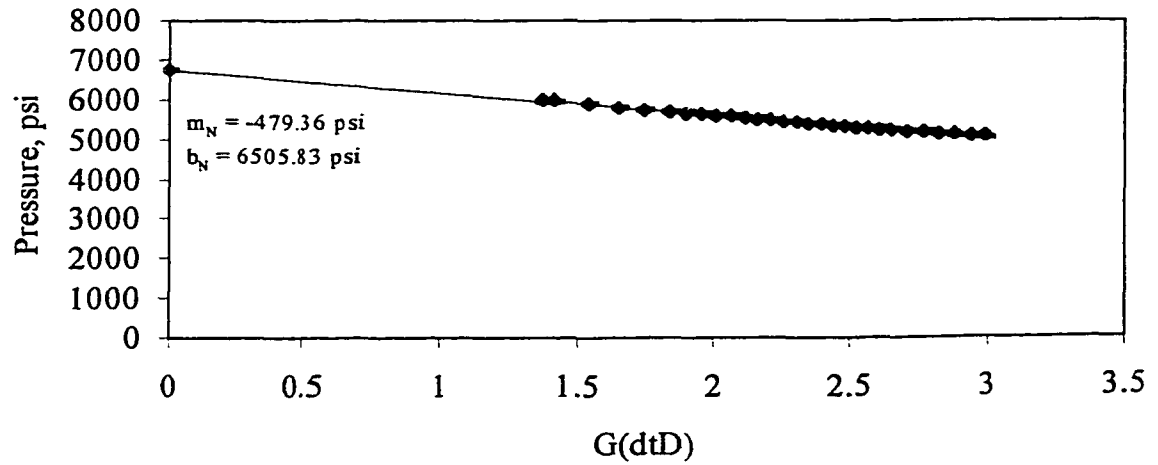


Fig. C-20 G-function of a minifrac test - Case M4

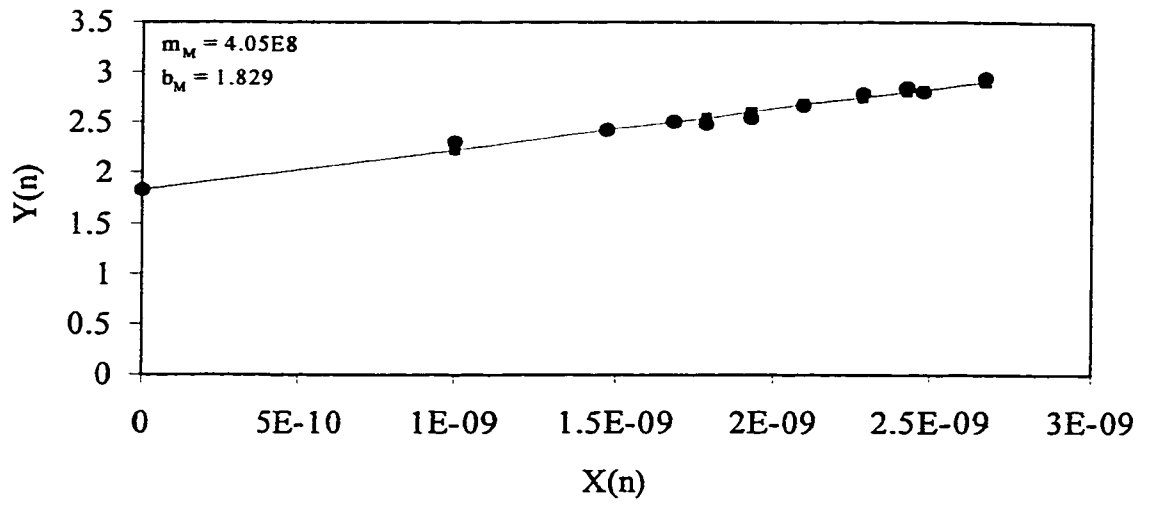


Fig. C-21 Filter cake-reservoir flow diagnostic plot - Case M4

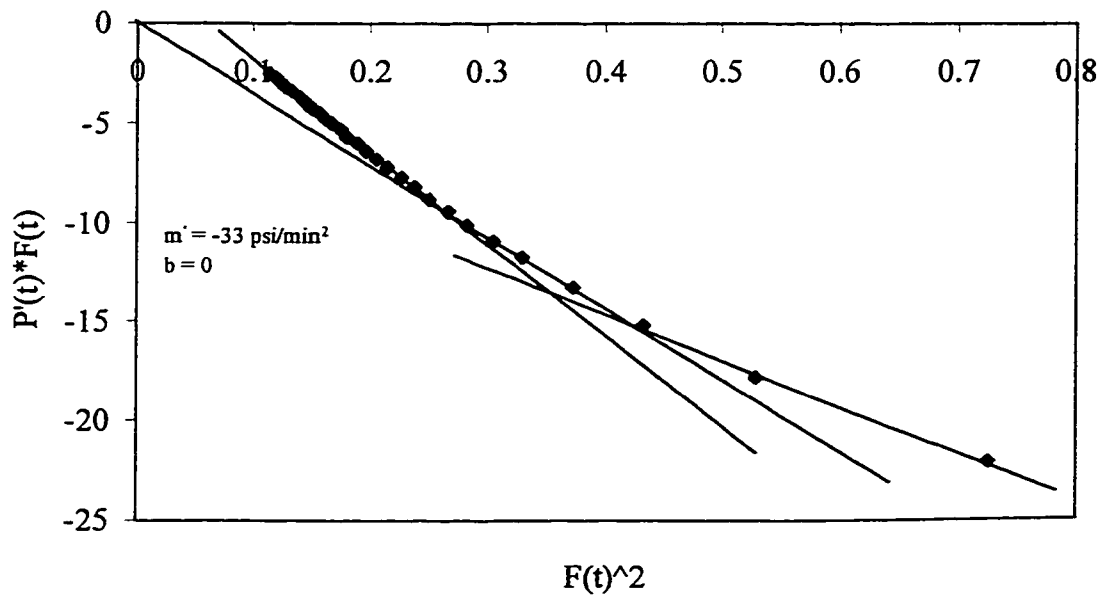


Fig. C-22 Pressure derivative - Case M4

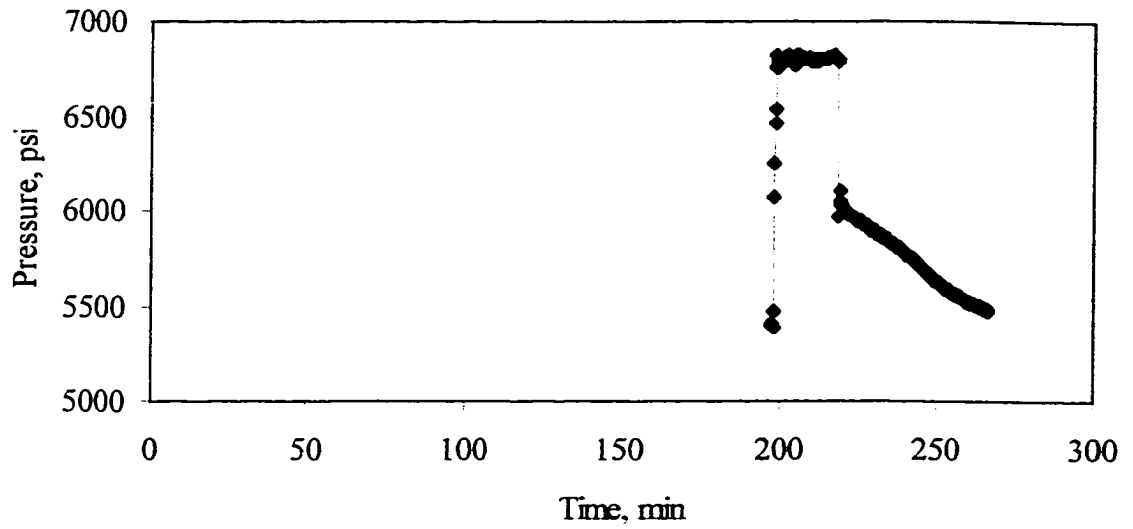


Fig. C-23 Injection and fall-off of a minifrac - Case M5

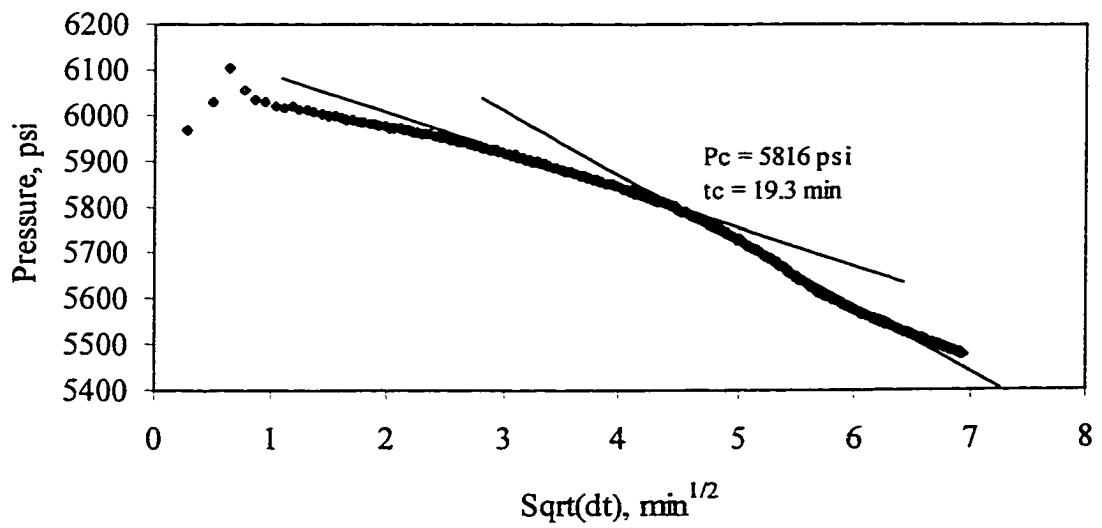


Fig. C-24 Identification of closure from the fall-off of a minifrac - Case M5

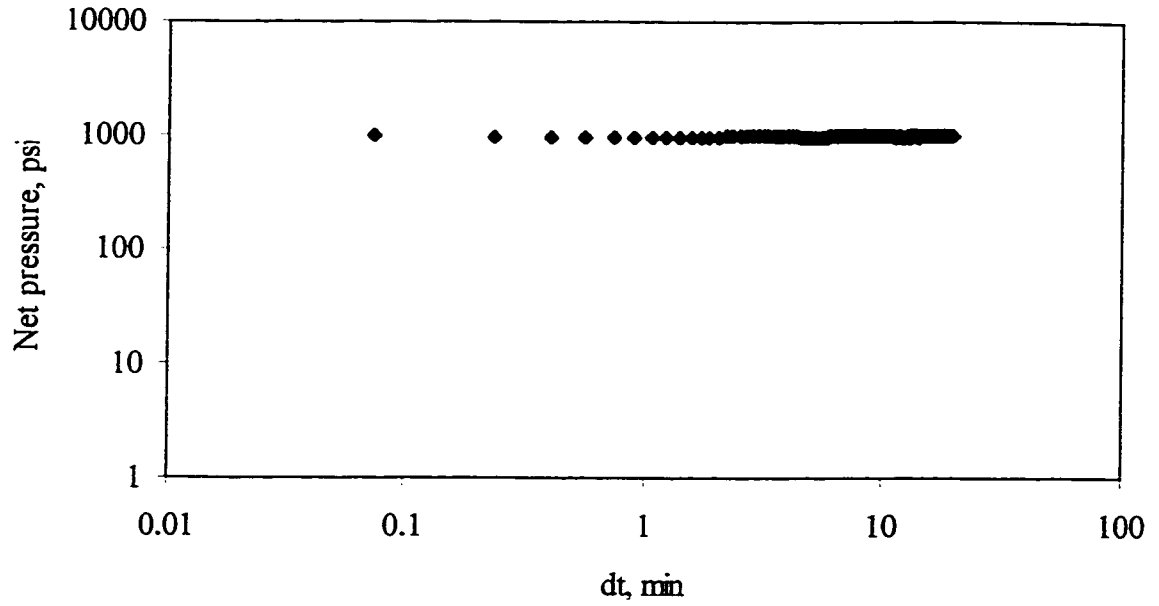


Fig. C-25 Net pressure versus time – Case M5

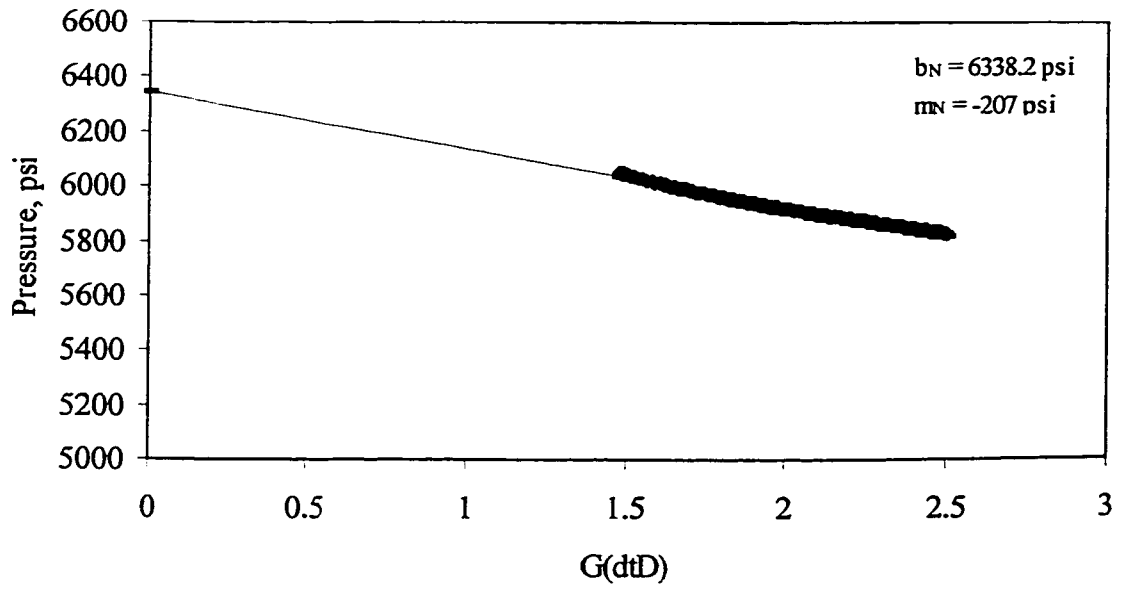


Fig. C-26 G-function of a minifrac test - Case M5

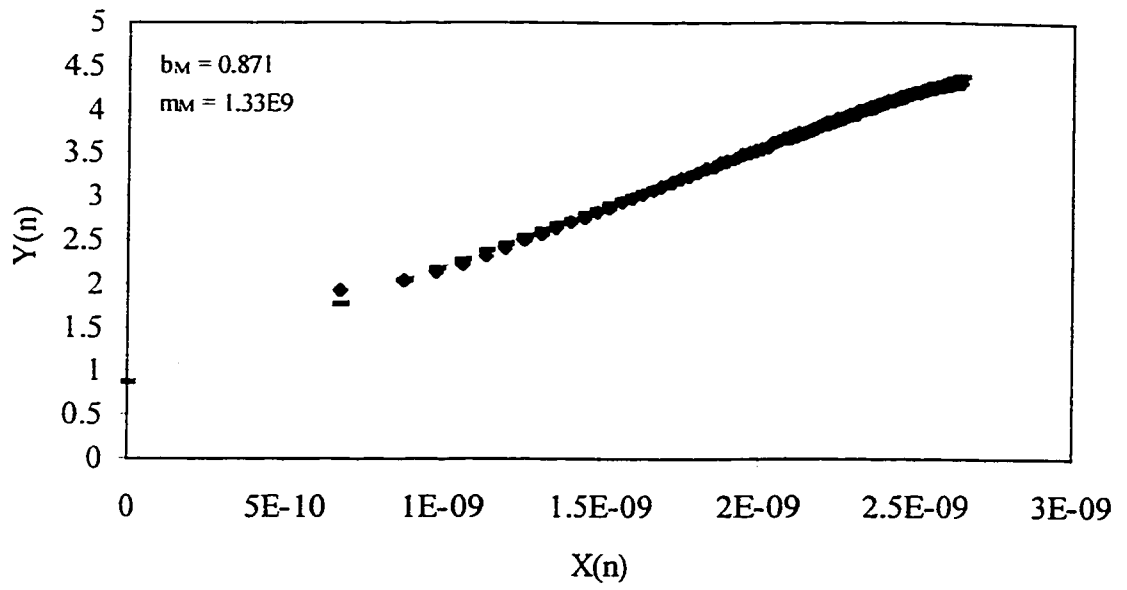


Fig. C-27 Filter cake –reservoir flow diagnostic plot (after data filtering)– Case M5

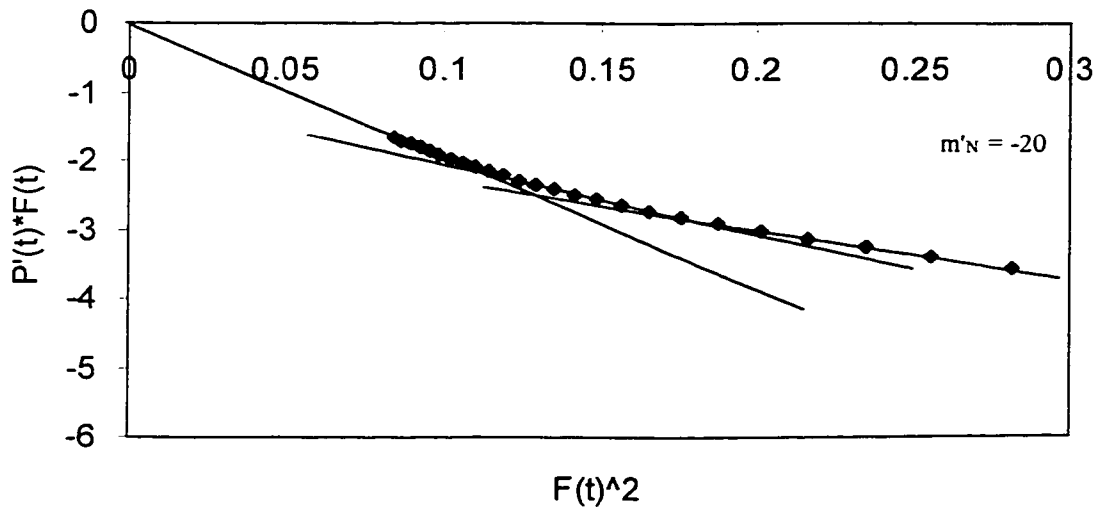


Fig. C-28 Pressure derivative – Case M1

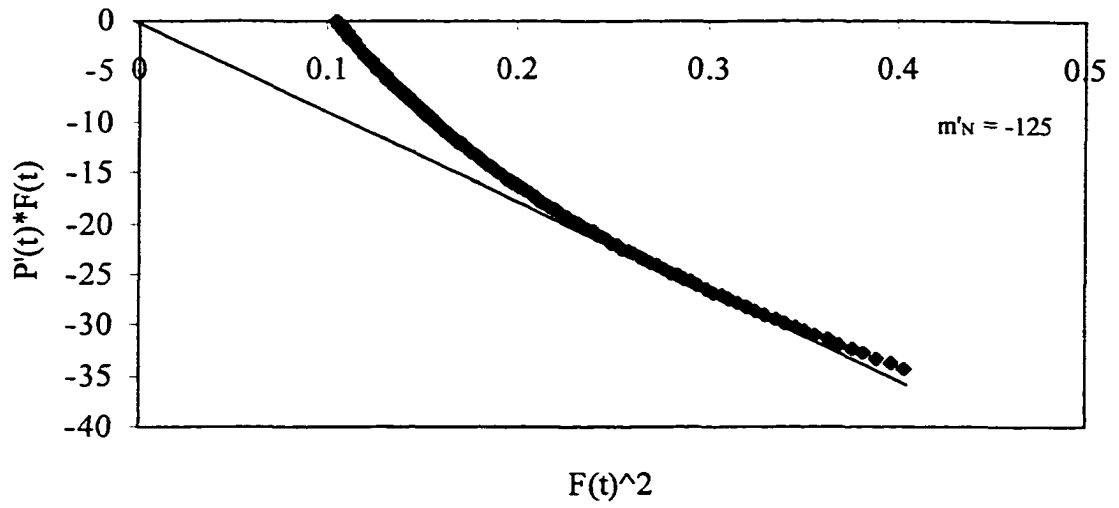


Fig. C-29 Pressure derivative – Case M2

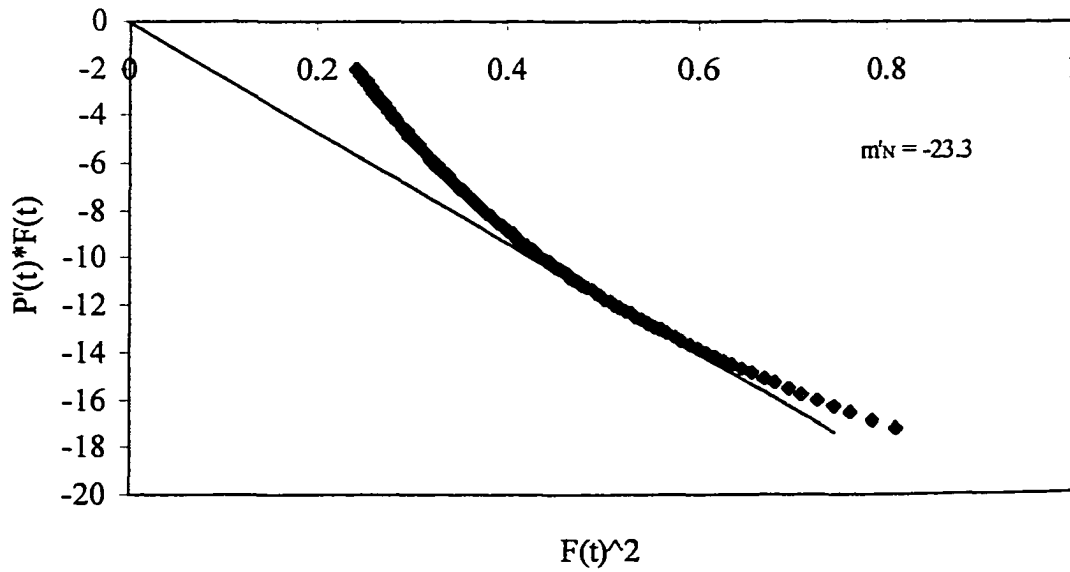


Fig. C-30 Pressure derivative – Case M3

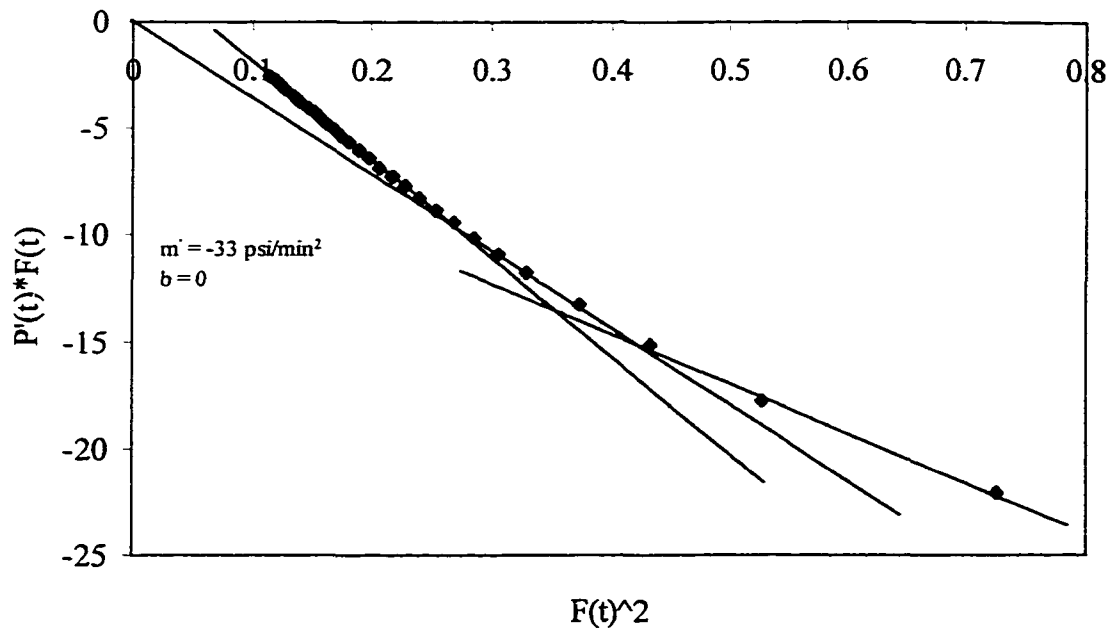


Fig. C-31 Pressure derivative – Case M4

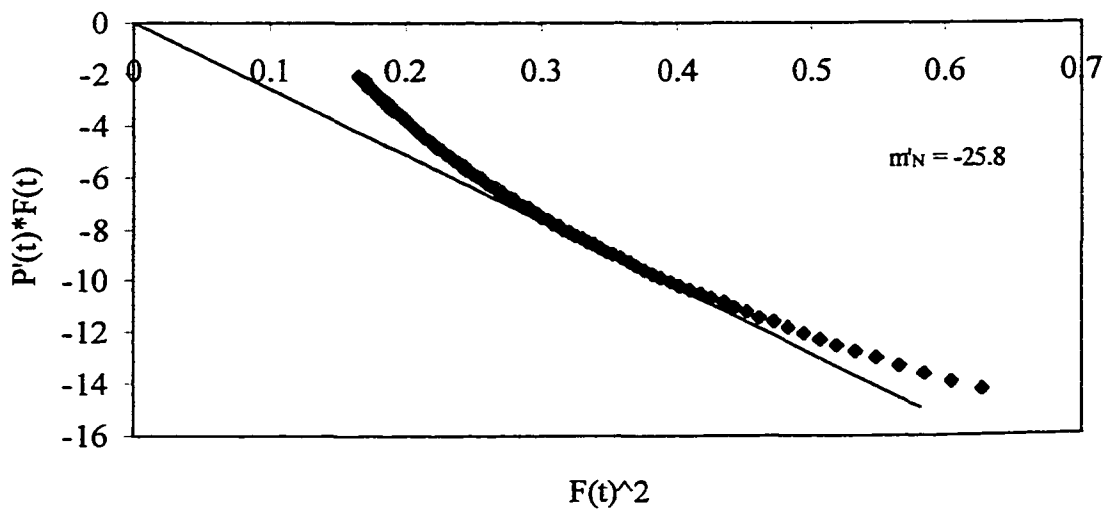


Fig. C-32 Pressure derivative – Case M5

Leak-off coefficient from pressure derivative analysis

Using the slope, m'_N , from the pressure derivative plot, Figs. C-28 – C32 and Eq. (4.105), the leak-off coefficient, C_L , can be calculated for each data set as follows:

Case M1

$$C_L = -\frac{c_f t_p m'_N}{4(r_p)(\sqrt{t_p})} = -\frac{(9.72E-05)(4.76)(-20)}{4(0.356)\sqrt{4.76}} = 2.97 E-03 \text{ ft}/\sqrt{\text{min}}$$

Case M2

$$C_L = -\frac{c_f t_p m'_N}{4(r_p)(\sqrt{t_p})} = -\frac{(9.78E-05)(3.3)(-125)}{4(0.288)\sqrt{3.3}} = 1.93 E-02 \text{ ft}/\sqrt{\text{min}}$$

Case M3

$$C_L = -\frac{c_f t_p m'_N}{4(r_p)(\sqrt{t_p})} = -\frac{(2.04E-04)(22.5)(-23.3)}{4(0.388)\sqrt{22.5}} = 1.45 E-02 \text{ ft}/\sqrt{\text{min}}$$

Case M4

$$C_L = -\frac{c_f t_p m'_N}{4(r_p)(\sqrt{t_p})} = -\frac{(4.24E-05)(35)(-33)}{4(1)\sqrt{35}} = 2.06 E-03 \text{ ft}/\sqrt{\text{min}}$$

Case M5

$$C_L = -\frac{c_f t_p m_N'}{4(r_p)(\sqrt{t_p})} = -\frac{(2.83E-04)(18)(-25.8)}{4(1)\sqrt{18}} = 7.74 E-03 \text{ ft}/\sqrt{\text{min}}$$

Table - 5G

Evaluation of the leak-off coefficient obtained from pressure and pressure derivative analysis

Case	Pressure	Pressure derivative
	C_L	C_L
	$\text{ft}/\sqrt{\text{min}}$	$\text{ft}/\sqrt{\text{min}}$
M1	1.18E-02	2.97E-03
M2	3.40E-02	1.93E-02
M3	1.36E-02	1.45E-02
M4	2.01E-03	2.06E-03
M5	8.21E-03	7.74E-03

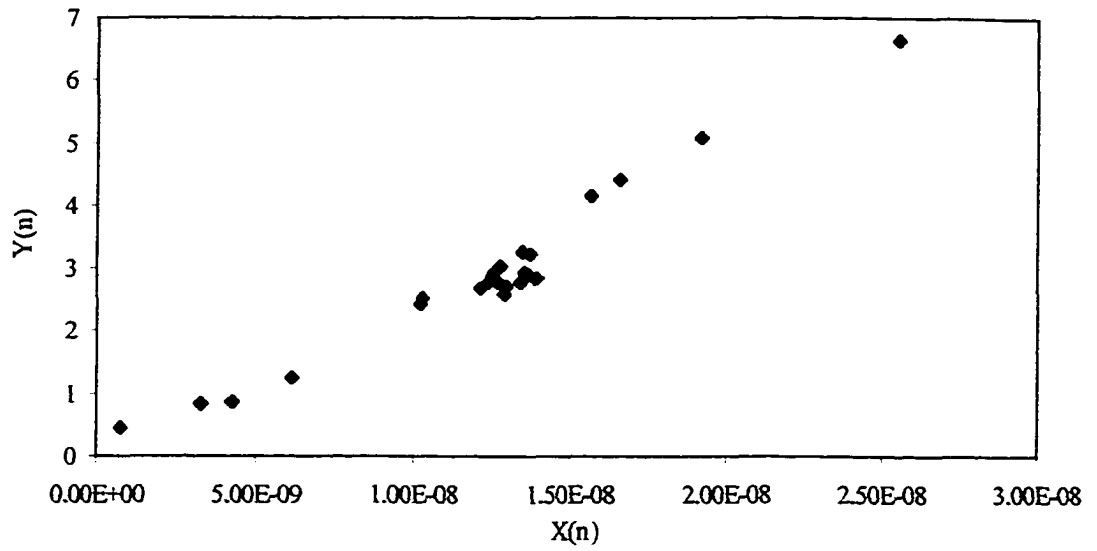


Fig. C-33 Old filtercake – reservoir flow model - Case M1

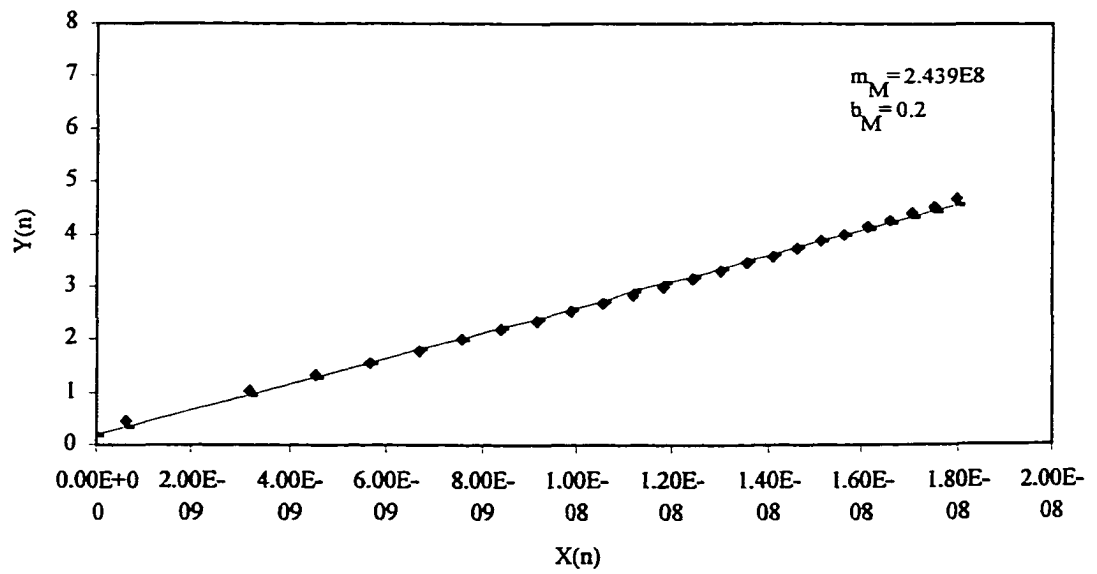


Fig. C-34 New filtercake – reservoir flow model - Case M1

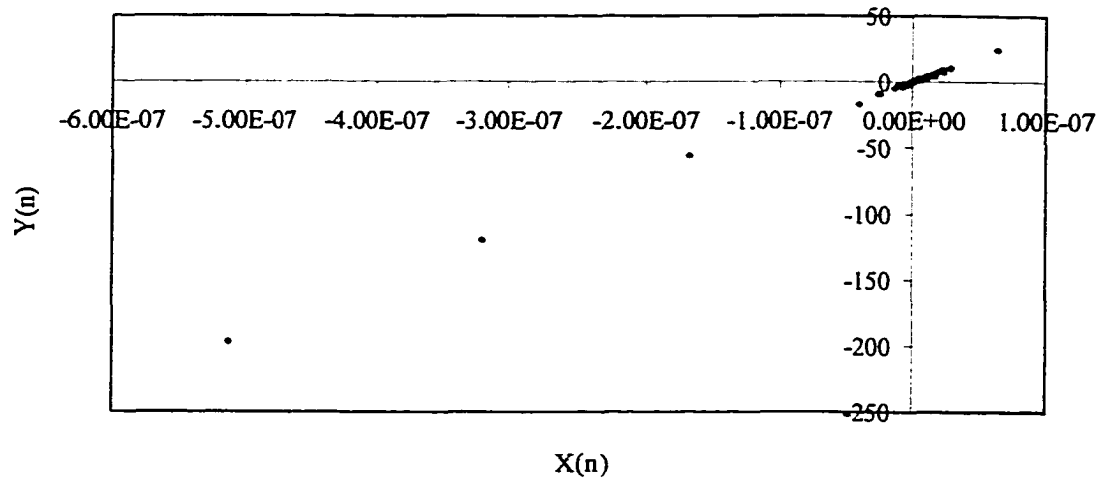


Fig. C-35 Old filtercake – reservoir flow model - Case M2

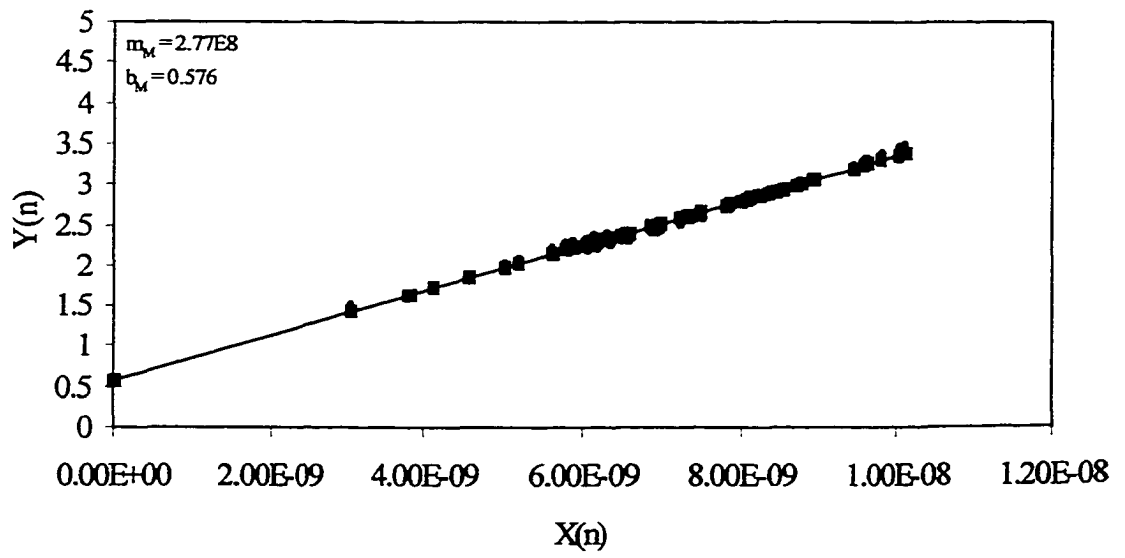


Fig. C-36 New filtercake – reservoir flow model – Case M2

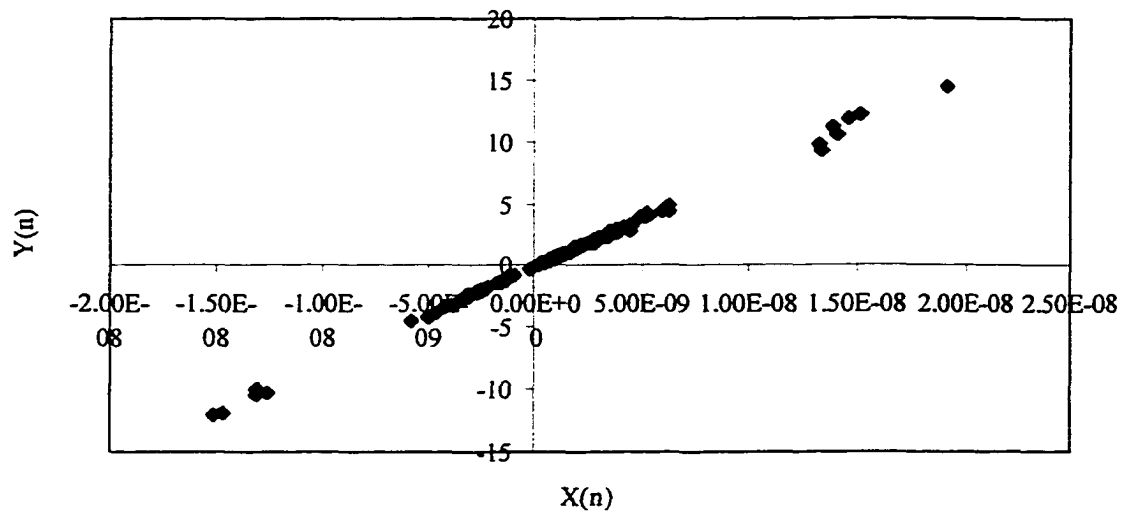


Fig. C-37 Old filtercake – reservoir flow model - Case M3

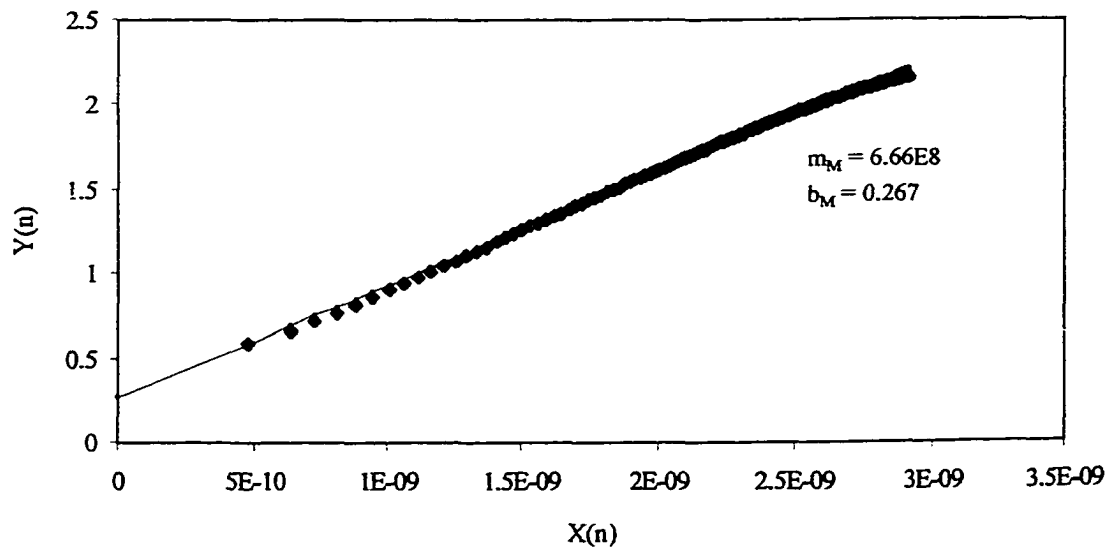


Fig. C-38 New filtercake – reservoir flow model – Case M3

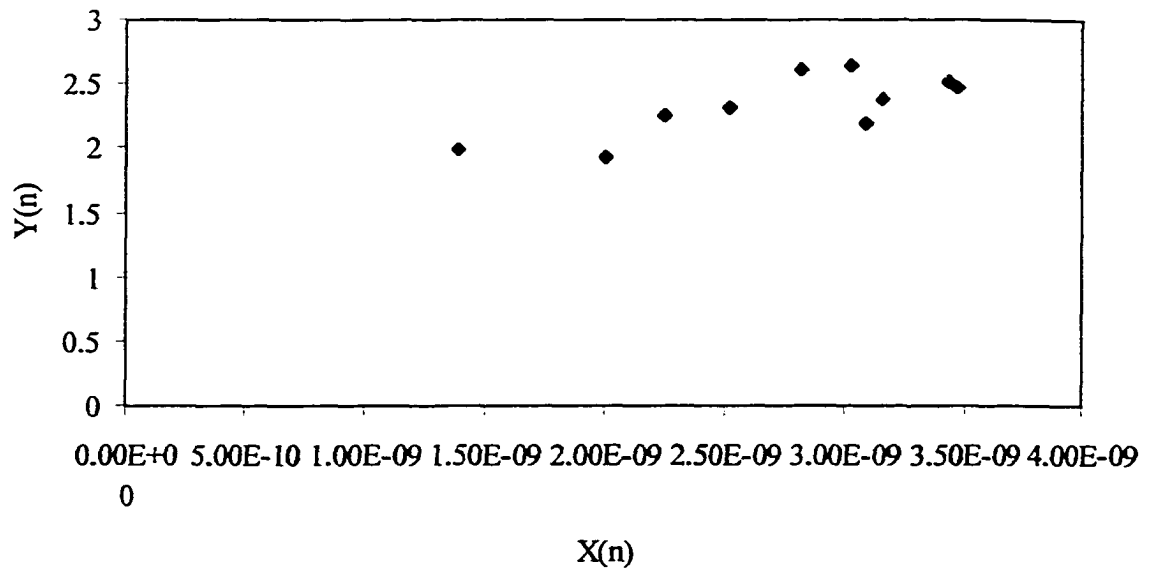


Fig. C-39 Old filtercake – reservoir flow model - Case M4

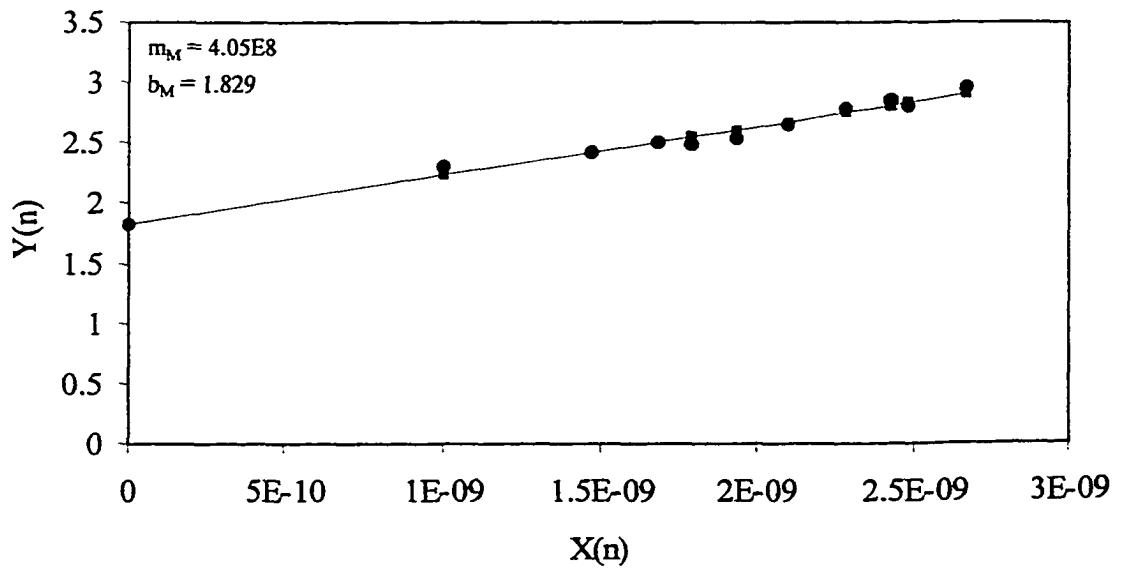


Fig. C-40 New filtercake – reservoir flow model – Case M4

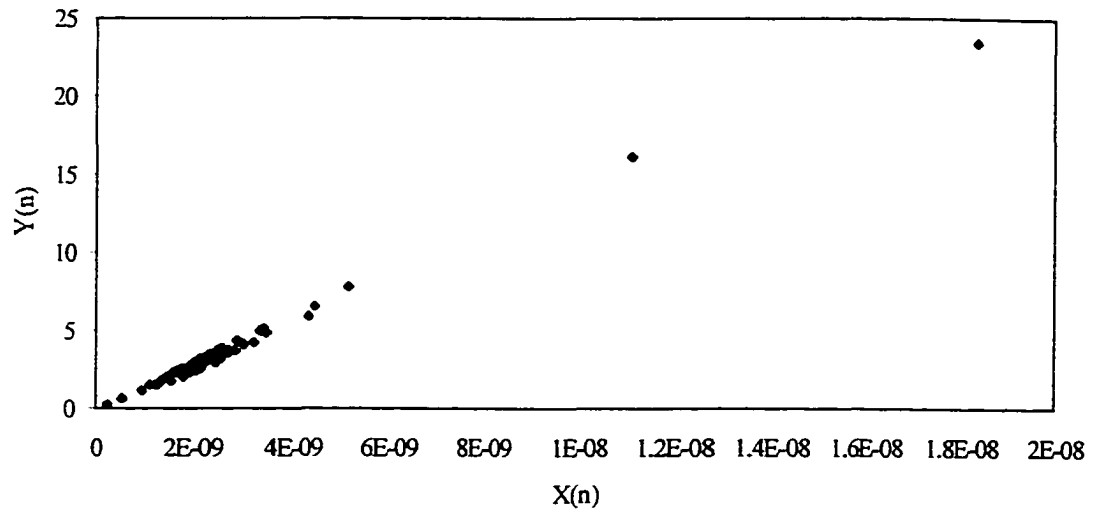


Fig. C-41 Old filtercake – reservoir flow model - Case M5

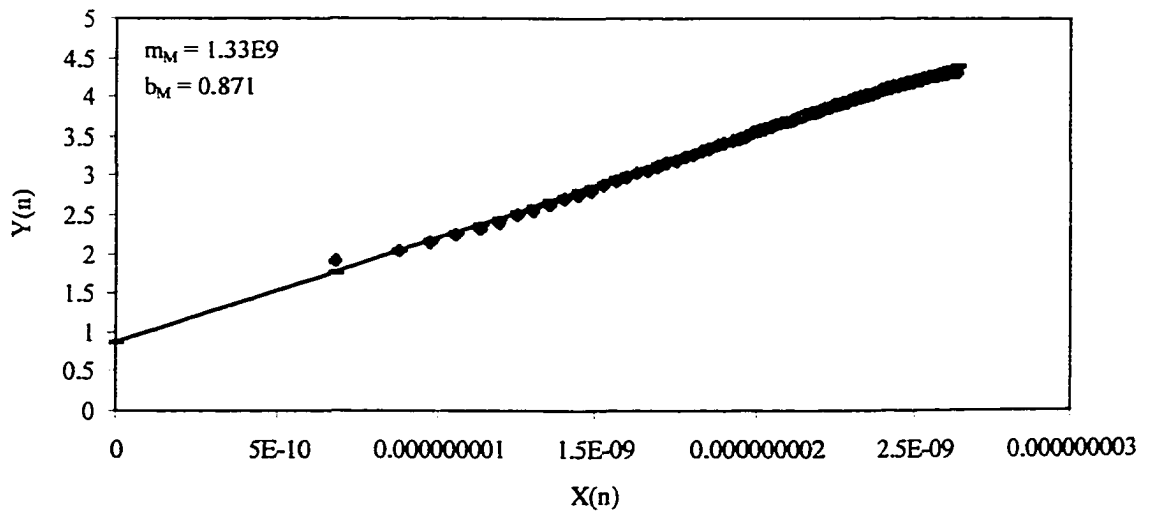


Fig. C-42 New filtercake – reservoir flow model – Case M5

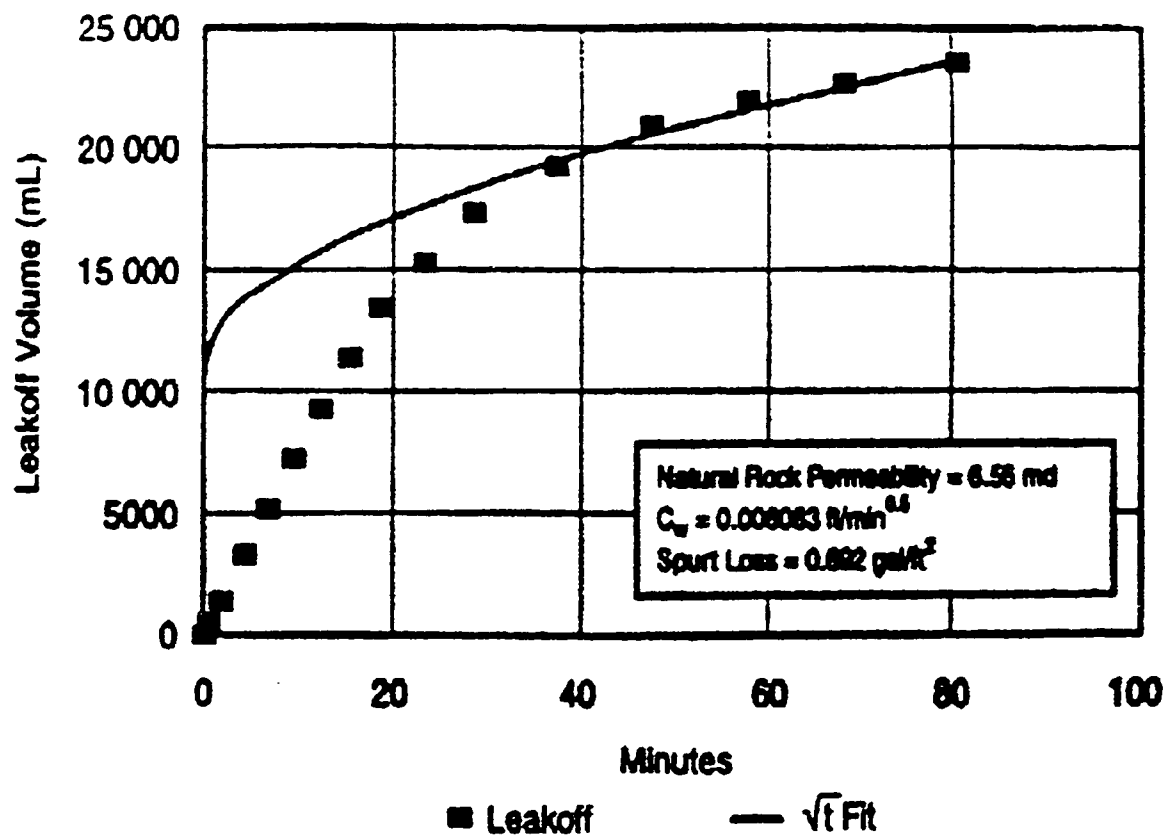


Fig. C-43 Dynamic fluid-loss test (adapted from Lord et al⁷³)

Appendix D

Sensitivity Analysis

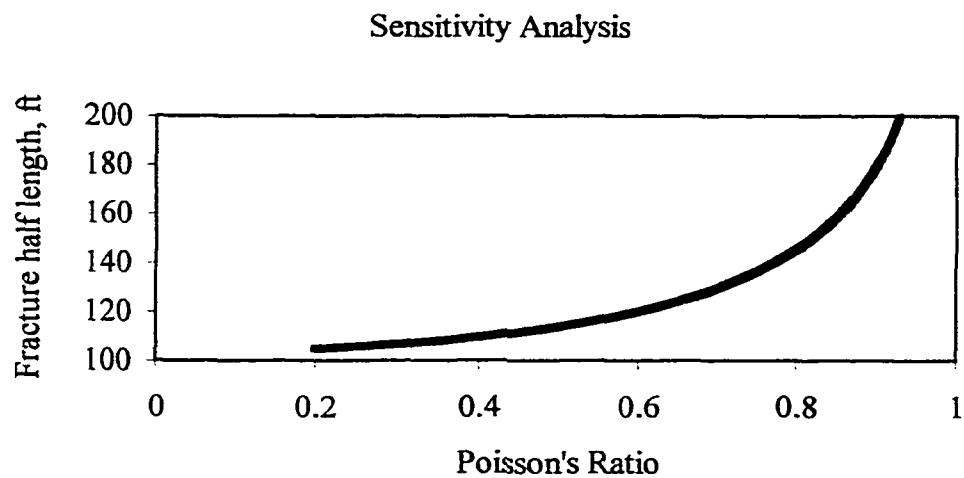


Fig. D-1 Fracture half-length – Poisson's Ratio

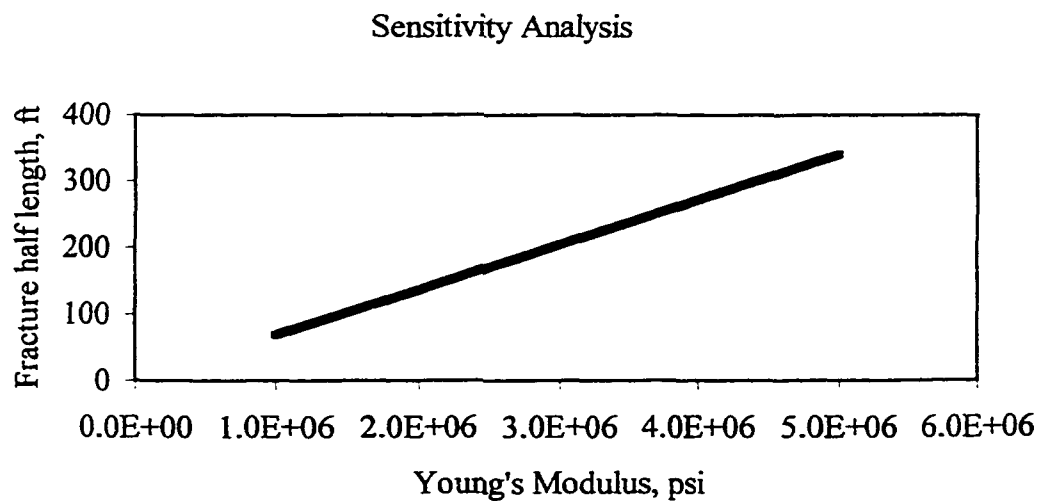


Fig. D-2 Fracture half-length – Young's Modulus

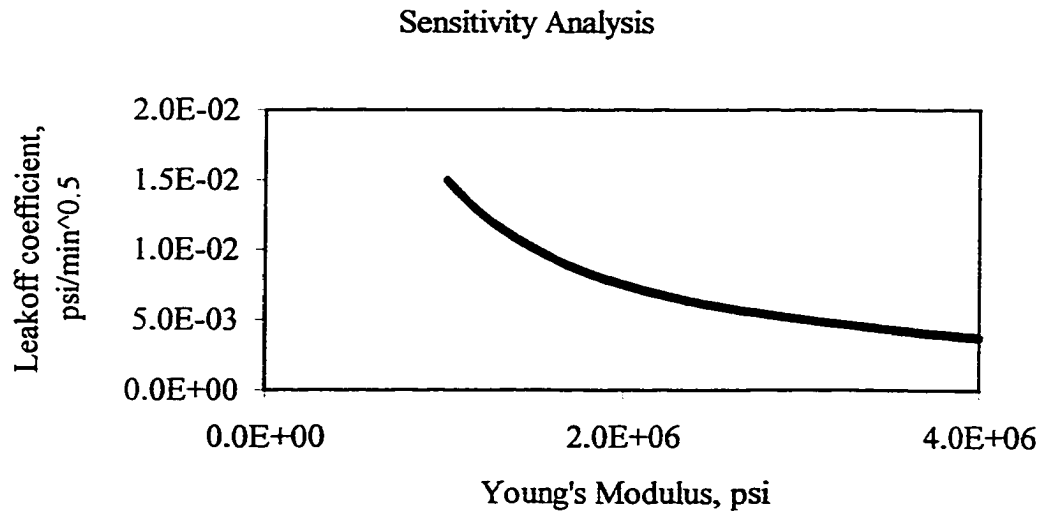


Fig. D-3 Leak-off coefficient – Young's Modulus

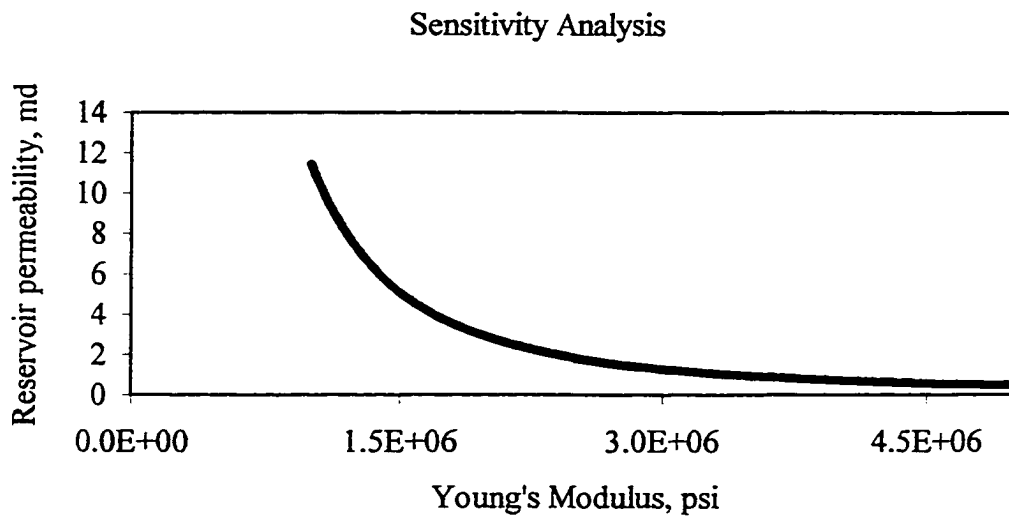


Fig. D-4 Reservoir permeability – Young's Modulus

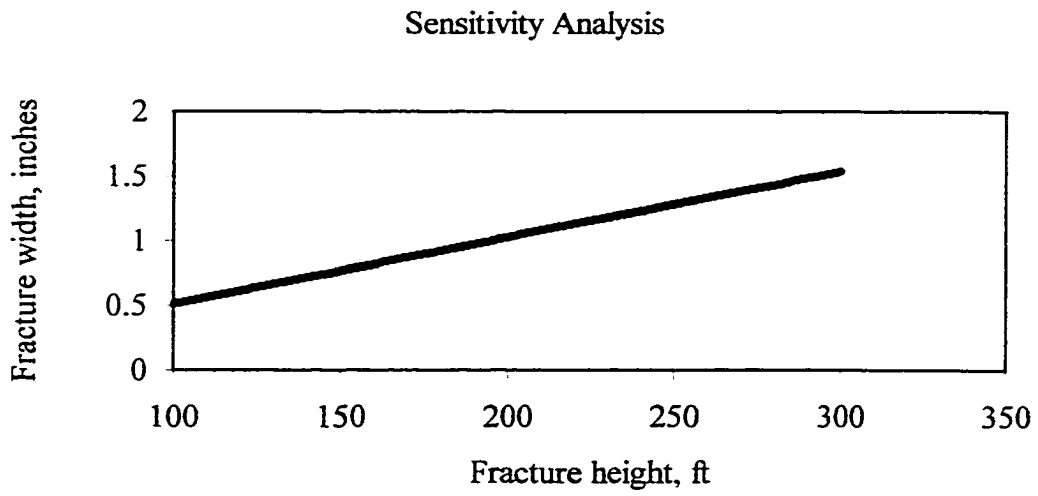


Fig. D-5 Fracture width – fracture height

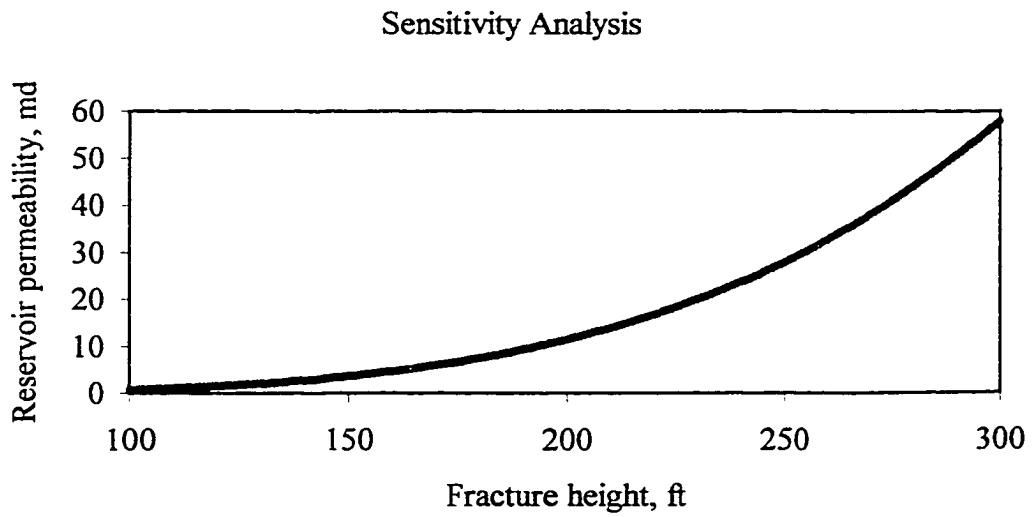


Fig. D-6 Reservoir permeability – fracture height

Sensitivity Analysis

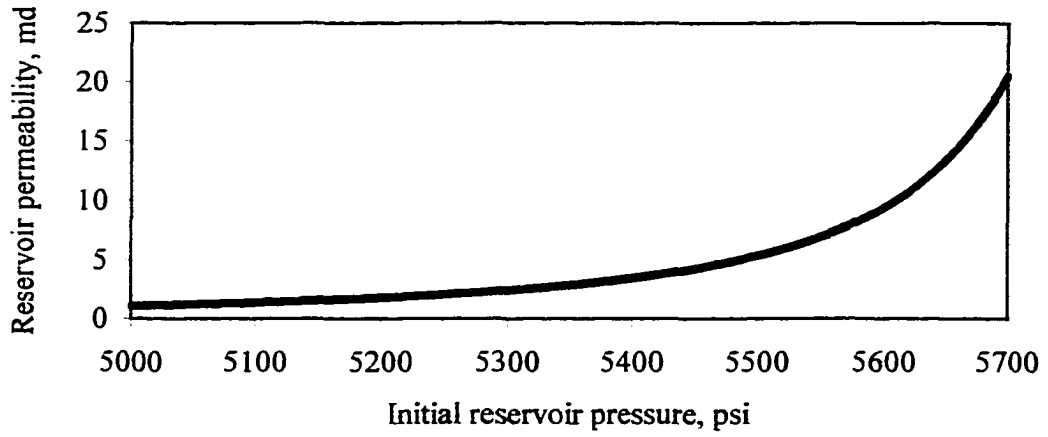


Fig. D-7 Reservoir permeability – initial reservoir pressure

Sensitivity Analysis

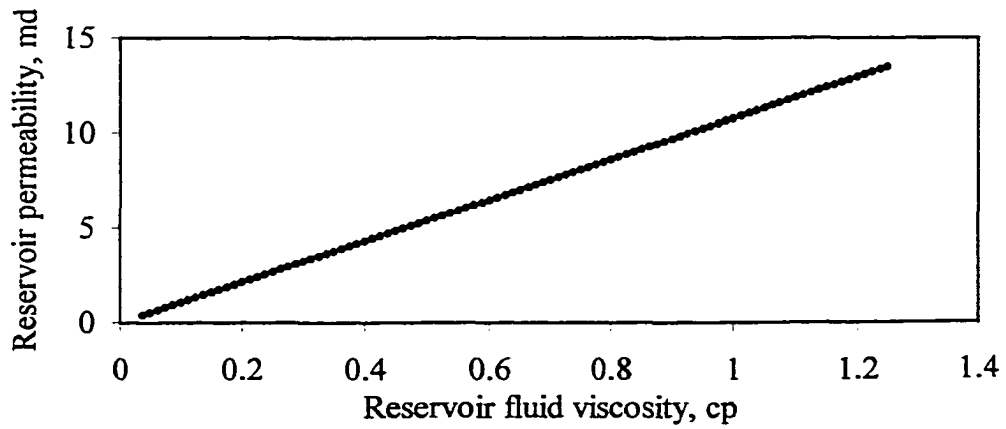
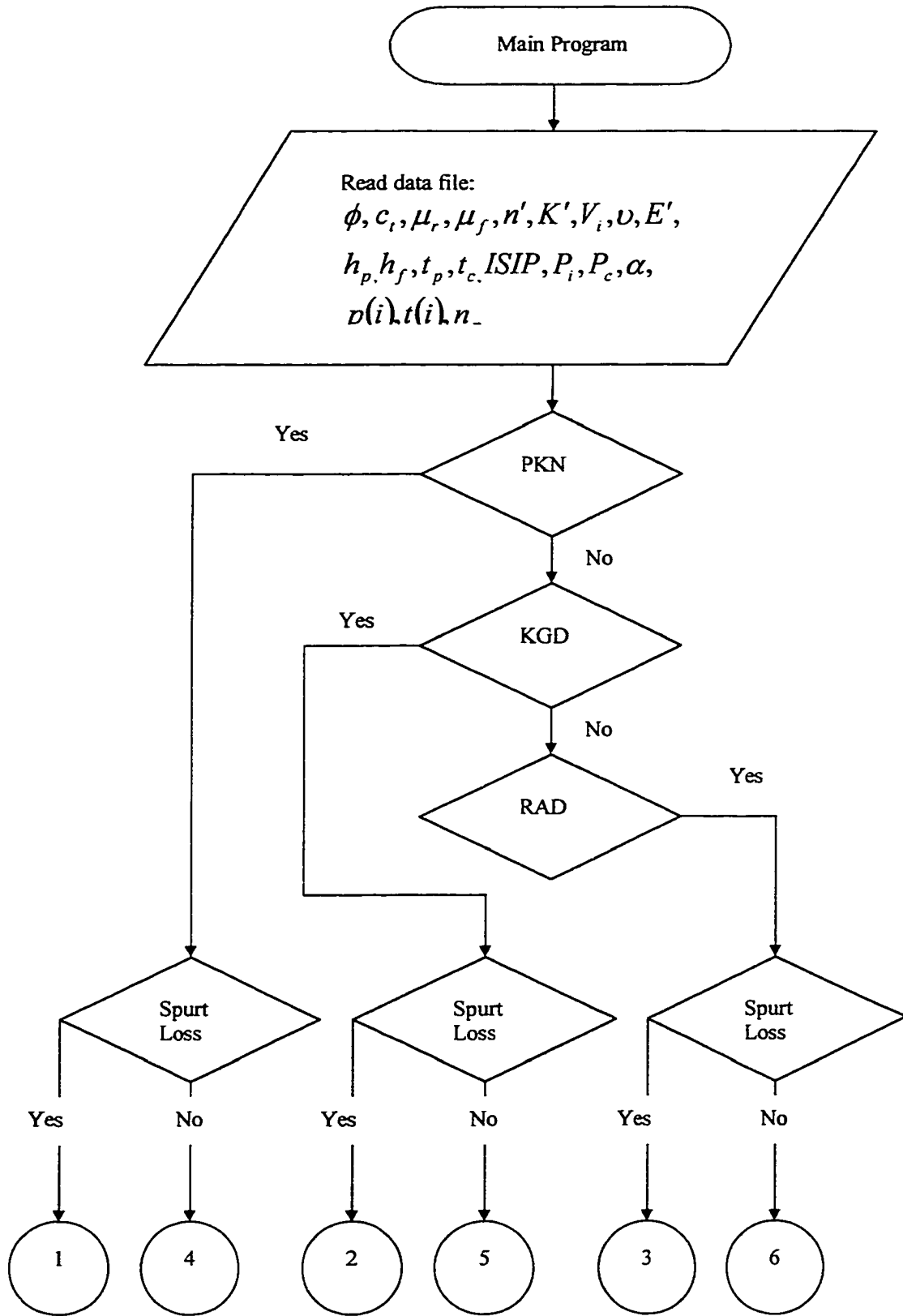
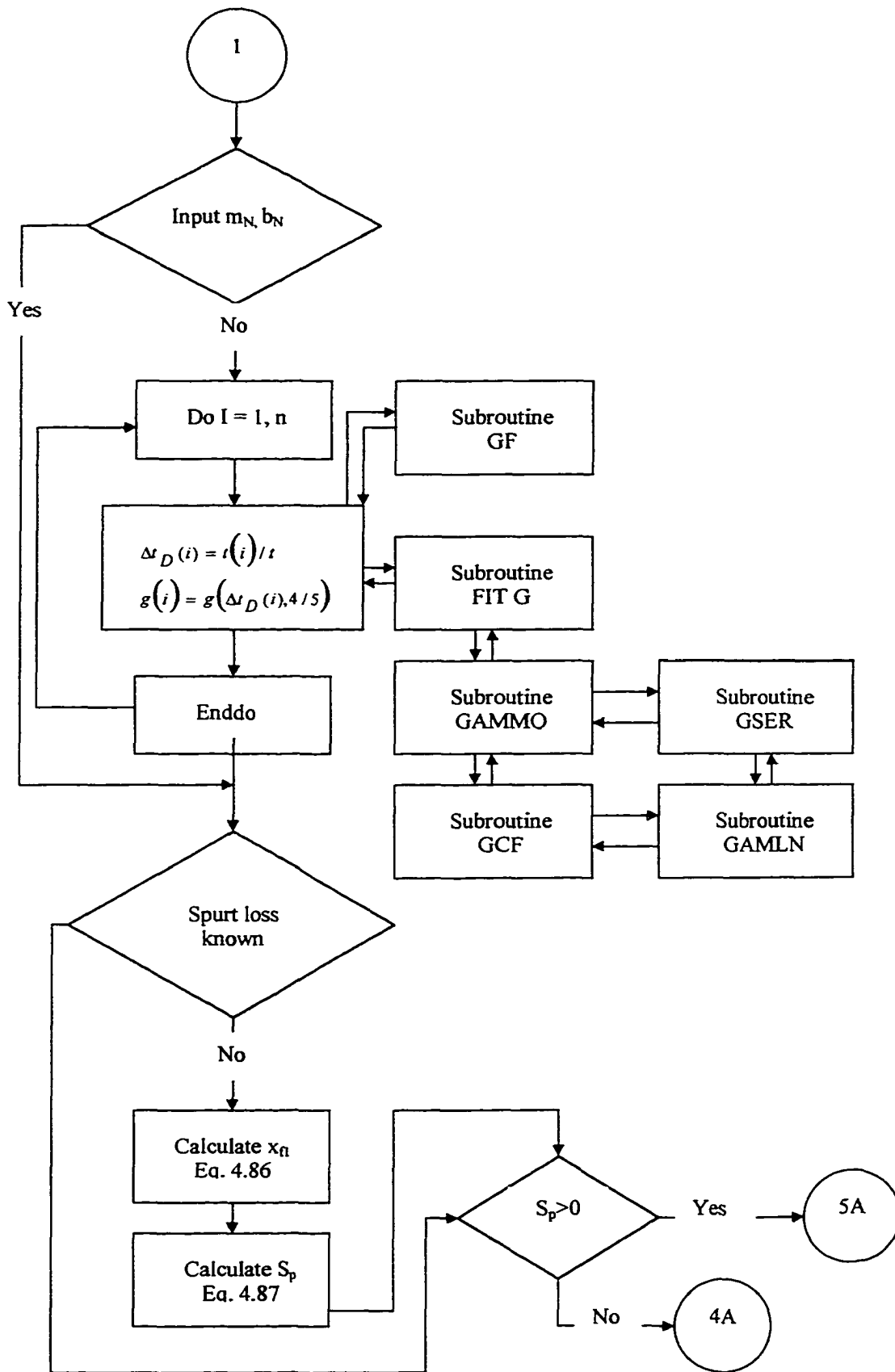
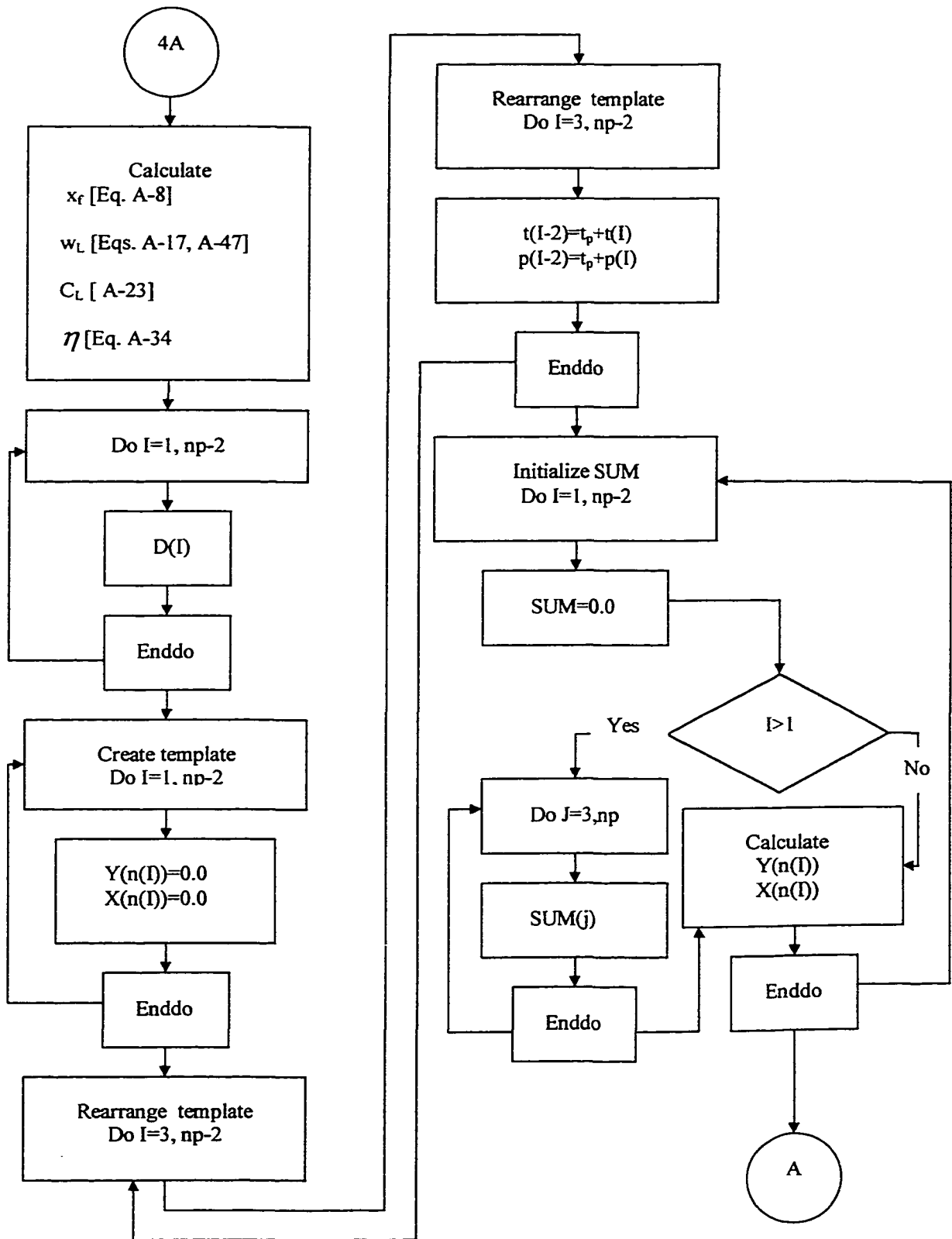


Fig. D-8 Reservoir permeability – reservoir fluid viscosity

Appendix E







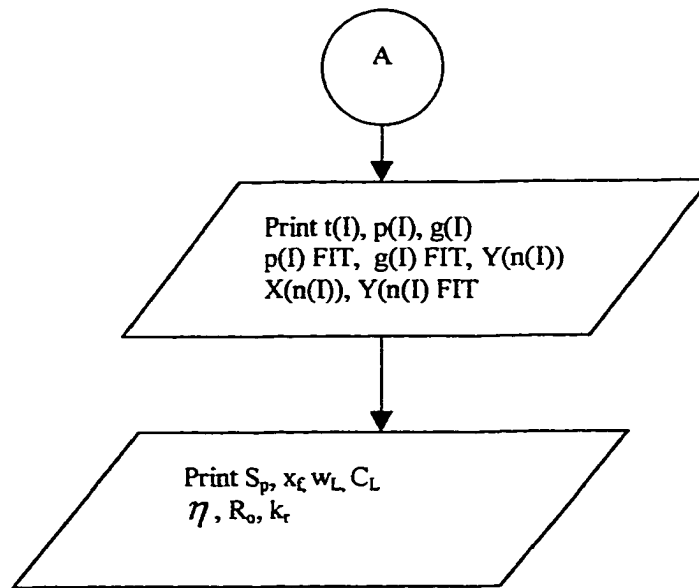


Fig. E-1 Flow chart of the modeling program

The above flow chart is for a PKN geometry. For the other two geometries, KGD and Radial, the flow chart is the same.